Report No. IITRI-U6003-19
(Final Report)

INVESTIGATION OF LIGHT SCATTERING
IN HIGHLY REFLECTING PIGMENTED COATINGS

Volume 3

National Aeronautics
and Space Administration

Report No. IITRI-U6003-19
(Final Report)

INVESTIGATION OF LIGHT SCATTERING
IN HIGHLY REFLECTING PIGMENTED COATINGS

Volume 3
MONTE CARLO AND OTHER STATISTICAL INVESTIGATIONS

May 1, 1963, through September 30, 1966

Contract No. NASr-65(07)
IITRI Project U6003

B. H. Kaye, M. Jackson, and G. A. Zerlaut

of

IIT RESEARCH INSTITUTE
Technology Center
Chicago, Illinois 60616

for

National Aeronautics and Space Administration
Office of Advanced Research and Technology
Washington 25, D.C.

November 1966

FOREWORD

This is Volume 3 of three volumes of Report No. IITRI-U6003-19 (Final Report) of IITRI Project U6003, Contract No. NASr-65(07), entitled "Investigation of Light Scattering in Highly Reflecting Pigmented Coatings." This report covers the period from May 1, 1963, to September 30, 1966.

The following Quarterly Reports were issued:

IITRI-C6018-3	October 11, 1963
IITRI-C6018-6	January 29, 1964
IITRI-C6018-8	May 5, 1964
IITRI-C6018-11	September 5, 1964
IITRI-C6018-12	December 21, 1964
IITRI-C6018-13	March 10, 1965
IITRI-C6018-14	May 13, 1965
IITRI-C6018-15	August 9, 1965
IITRI-U6003-16	November 9, 1965
IITRI-U6003-17	February 28, 1966
IITRI-U6003-18	May 3, 1966

Because of a divisional reorganization and the accompanying administrative changes, the IITRI number designating this project was changed from C6018 to U6003 on September 1, 1965. The Quarterly Report issued on November 9, 1965, was the first report to bear the new number. Project administration and technical organization were not affected in this change.

The project was under the technical direction of the Research Projects Laboratory of the George C. Marshall Space Flight Center, and Mr. Daniel W. Gates was the cognizant technical manager. The contract was administered by Mr. James J. Gangler of the Office of Advanced Research and Technology, National Aeronautics and Space Administration.

Major contributors to the program were G. A. Zerlaut, project leader, and (alphabetically): T. Church, shape factor analysis; H. Iglarsh, preparation of random models; M. R. Jackson, experimental studies and statistical analyses; Dr. B. H. Kaye, theoretical Monte Carlo and statistical studies; Dr. S. Katz, theoretical (classical) light-scattering studies; V. Raziunas, experimental (classical) studies on silver

bromide suspensions; and J. Stockham, preparation of suspensions. Administrative supervision was provided by Dr. T. H. Meltzer, Manager, Polymer Research.
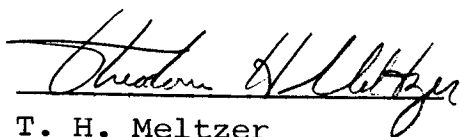
Experimental data are recorded in Logbooks C13906, C14085, C14644, C16369, and C16765.

<div style="text-align: right;">

Respectfully submitted,

IIT RESEARCH INSTITUTE

G. A. Zerlaut
Group Leader
Polymer Research

</div>

Approved by:

T. H. Meltzer
Manager
Polymer Research

ABSTRACT

INVESTIGATION OF LIGHT SCATTERING
IN HIGHLY REFLECTING PIGMENTED COATINGS
Volume 3
MONTE CARLO AND OTHER STATISTICAL INVESTIGATIONS

This search for a theory to predict the reflectance properties of paint films revealed that several aspects of current descriptive terminology are insidious barriers to progress. For example, the term "highly reflective paint" can only be defined within a specific context of requirements. Also, false concepts encouraged a search for a technique for applying Mie scattering theory to pigment optics.

An introduction to the report is given in Section I. The relevance of Mie theory to paint technology is discussed in Section II. The semantic problems of paint reflectance studies are explored in Section III; it is shown that until randomness, diffuse light, pigment shape, and pigment size are understood better development of paint technology will be accomplished by empirical exploration, which is qualitatively justified a posteriori rather than predicted theoretically.

Some developmental work on the concepts and the techniques of particle shape measurement was carried out. A computer program for investigating the potential use of statistical diameters in shape factor analysis was developed. The shape factor experiments are reported in Section IV.

Possible techniques for simulating particle packing are presented in Section V, and a general discussion of Monte Carlo techniques as applied to reflectance studies is given in Section VI. General considerations concerning the development of a random-walk model for studying energy penetration of a paint film are presented in Section VII.

To study cluster growth in a paint film, a Monte Carlo experiment in two dimensions was developed. From the properties of the model, a statistical derivation of the Lambert-Beer law has been proposed. By use of the model, the possible

mechanism by which extender particles can increase the opacity of a given amount of pigment was explored. From statistical reasoning alone, the existence of a critical pigment volume concentration for efficient use of pigment was predicted. The simulated data are given and their implications discussed in Section VIII.

Early in the development of a possible random-walk model for paint reflectance studies, it was thought that the very small interparticle distances within the paint film would place severe restrictions on any model of this type. Therefore a random screen model was explored. The various aspects of a random screen model are discussed in Section IX.

Various aspects of general studies of technologies such as filtration theory are discussed in Sections X and XI.

TABLE OF CONTENTS

LIST OF TABLES

LIST OF FIGURES

INVESTIGATION OF LIGHT SCATTERING
IN HIGHLY REFLECTING PIGMENTED COATINGS
Volume 3
MONTE CARLO AND OTHER STATISTICAL INVESTIGATIONS

I. INTRODUCTION

The principal objective of this program was to apply
light-scattering theory to polydisperse, highly reflecting,
highly pigmented coatings. The program was aimed at an eluci-
dation of the light-scattering parameters associated with the
multiple scattering events that operate in highly pigmented
systems. Definition of these parameters should facilitate the
eventual development of pigmented coatings that reflect maximum
solar radiation.

This report, which is Volume 3 of the three-volume final
report on the subject program, is concerned with concepts of
statistical approaches and random-walk techniques with which
to treat the problem of multiple scattering. This report and
Volume 2, "Classical Investigations; Theoretical and Experi-
mental," are summarized in Volume 1, "Summary Report."

The work reported in this volume consists of: (1) a
discussion of the relevance of Mie theory to highly pigmented
coatings, (2) discussion of some of the semantic problems
of defining various concepts associated with paint technology,
(3) analysis and discussion of the significance of par-
ticle shape factors, (4) discussion of pigment packing and
simulation of packing, (5) results of the development of Monte
Carlo concepts that can be applied to the field of paint tech-
nology and of the development of a model for studying energy
penetration through pigmented films, (6) discussion of Monte
Carlo techniques for studying growth in scattering centers
as a function of increasing pigment concentration, and
(7) application of Monte Carlo techniques to fibrous filters
and other problem areas.

II. RELEVANCE OF MIE THEORY FOR PREDICTING REFLECTIVE PROPERTIES OF PAINT FILMS

The scattering power of a single smooth spherical particle placed in the path of a plane parallel beam of noncoherent monochromatic light can be studied by the theory developed by Mie (ref. 1). The variations in scattering power of a single sphere with refractive index and particle diameter/wavelength ratio has been computed from the Mie theory, and this curve is often used to justify the claim that optimum opacity is obtained with a pigment-particle size of about 1/5 the wavelength of the incident light. When the relevance of the Mie theory to the physical phenomena occurring within the paint film is considered, it is found that even if the maximum-opacity pigment size eventually proves to be 1/5 of the wavelength, this fact cannot possibly be deduced from the Mie theory. Any agreement between fact and speculation stimulated by considering Mie theory can only be fortuitous.

The relationship between Mie theory and phenomena occurring within a paint film can be understood by considering several aspects of interference and Frauenhoffer diffraction patterns of long single slits for plane parallel beams of monochromatic noncoherent light. First consider the Frauenhoffer diffraction pattern of single slits of various widths. These patterns are shown in Figure 1. These patterns are observed on a screen at infinity (by using simulated lenses). Now consider that the screens are replaced by a photoelectric device that receives all scattered light. We are not concerned with the spatial distribution of the energy, and we observe that the total energy from the three slits is simply proportional to the slit widths, i.e., 1:5:10. From this point of view, we are not troubled by the fact that geometric optics does not apply to the system.

Next consider the diffraction pattern of a set of slits each 5 wavelengths wide but 50 wavelengths apart. The resultant
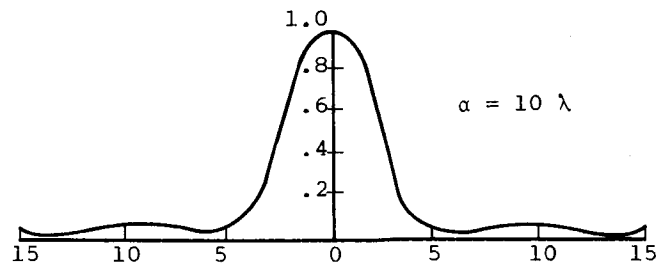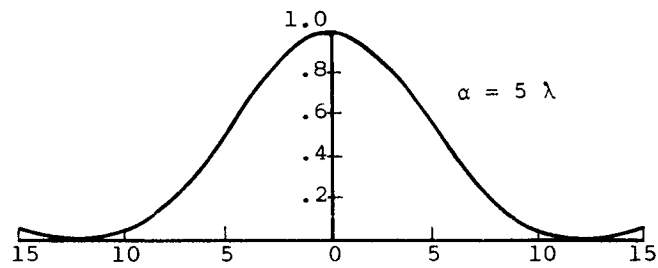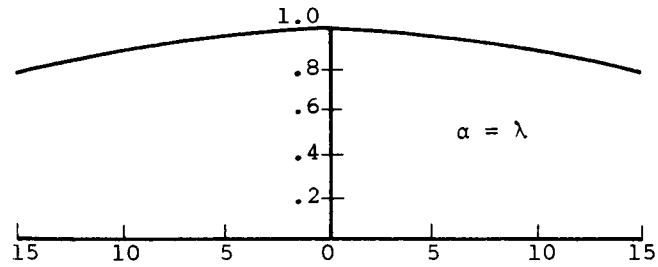
λ = Slit width

Figure 1

RELATIVE INTENSITY IN SINGLE-SLIT DIFFRACTION
FOR THREE VALUES OF SLIT WIDTH OF THE RATIO α/λ
(Reproduced from Physics for Students and Engineers,
by D. Halliday and R. Resnick, John Wiley and Sons)

pattern is shown in Figure 2. The interference fringes lie
within the envelope of the diffraction pattern for the single
slit. Familiarity with these diagrams in school textbooks on
optics tends to obscure the important point. Although the
relative intensity pattern is dominated by the system pre-
dicted from the single slit, the total energy passing through
the slits is proportional to the number of slits. Again, if
the screen is replaced by a photoelectric detector capable of
receiving all the diffracted light, the measurement device
would not be able to differentiate between 20 slits 2 wave-
lengths wide or 40 slits 1 wavelength wide, even though the
spatial distribution of the energy for the two systems would
be very different.

1.0

Envelope to
interference
fringes

$\alpha = 5\ \lambda$
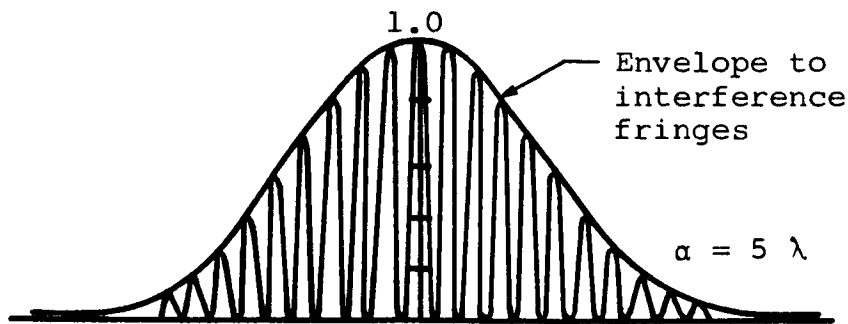
Figure 2

COMBINED INTERFERENCE AND DIFFRACTION PATTERN
FOR SLITS 5 WAVELENGTHS WIDE AND 50 WAVELENGTHS APART
(Reproduced from Physics for Students and Engineers,
by D. Halliday and R. Resnick, John Wiley and Sons)

Now consider what would happen if we had 50 parallel slits each 5 wavelengths wide but spaced randomly across the diffraction screen. Any pair of lines would produce an interference pattern modulated by the diffraction envelope, but the peaks for each pattern would be separated by a factor related to the separation of the two slits. The argument holds for any pair of slits, so that the peak for each pair would fall at different points within the same diffraction envelope. Averaged out for the 50 lines, the net effect would be relatively uniform illumination modulated by the diffraction pattern for the single slit width. This results in the important observation that the diffraction pattern for 50 randomly spaced slits is undistinguishable from that of 1 slit if the power of the beam for the single slit is 50 times that of the beam passing through the 50 random slits. Physically what happens is that the random positioning of the lines obscures the fine structure of the combined interference diffraction pattern.

So far, we have considered only the effect of a single beam. If two beams at two different angles pass through the same slit, the system will be as outlined in Figure 3. A screen placed on the axis of the first beam would show the diffraction for the specific slit width.[*] If a second beam at an angle θ is passed through the screen, a screen placed on the axis of this second beam would have a slightly different pattern, since the effective slit width is now $\alpha \cdot \sin \theta$, so the prime diffraction lobe will be somewhat wider than that for the first beam. If, however, the screens are replaced by a semicircular photoconductive device, the power received by the device will be proportional to $\alpha + \alpha \sin \theta$ if the beams are of equal strength.

---

[*]The distances in Figure 3 are not to scale. Either the screen is placed at a relatively great distance from the screen, or lenses have to be used to produce the pattern.

α = Slit width
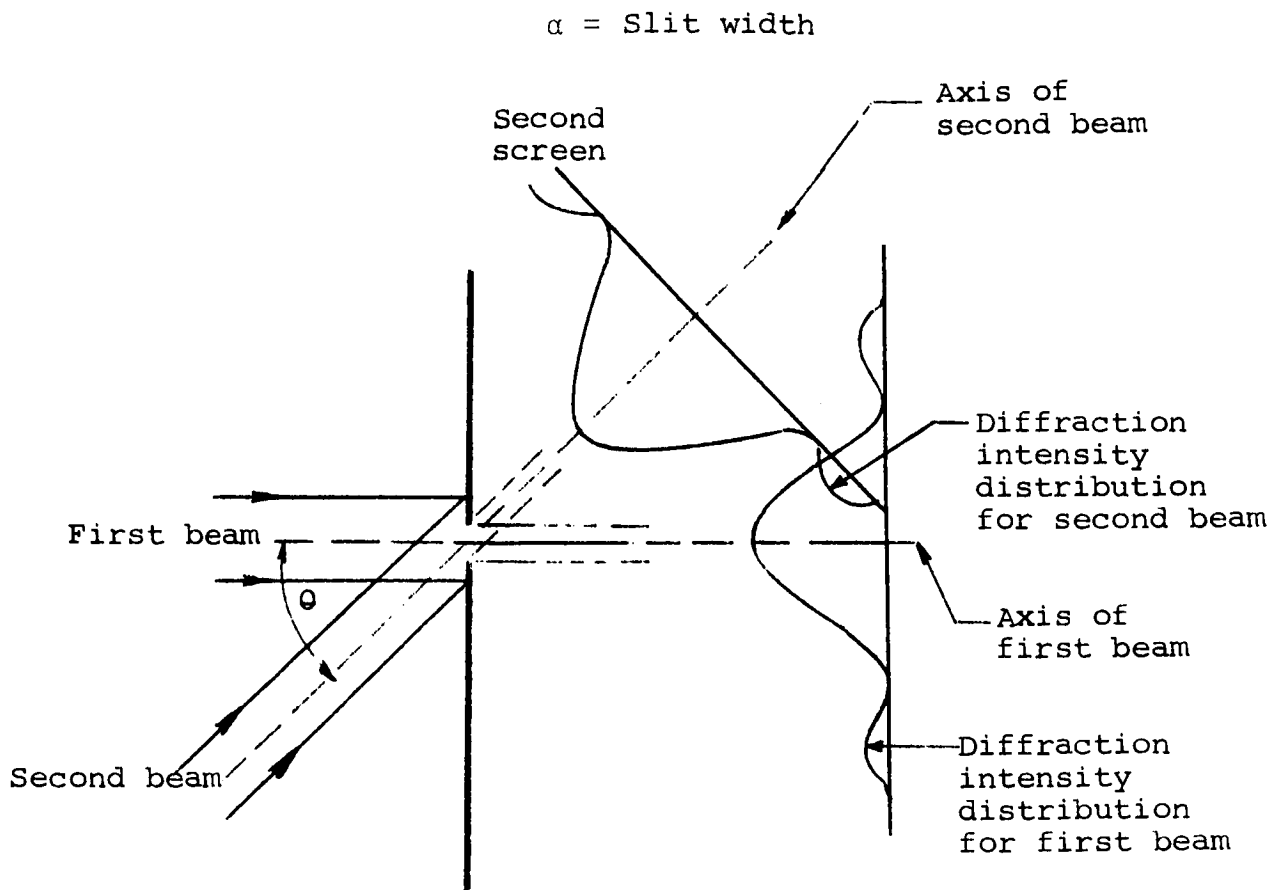
Figure 3

DIFFRACTION PATTERNS FOR TWO BEAMS PASSING THROUGH THE SAME SLIT

If there are beams at a whole range of equally spaced values of θ, the calculation of the diffraction pattern on a screen perpendicular to the axis of the prime beam would be very complicated. Again, if the screen were moved so that it would be only several wavelengths from the slit, the simplified theory of Frauenhoffer would no longer apply and the calculation of resultant diffraction patterns would be exceedingly complex.

If the system is extended to consist of randomly spaced parallel slits of the same width and if all the beams are polychromatic, the calculation of diffraction patterns is, in practice, impossible. However, the power penetrating the screen is still a function of the available area in the diffracting screen, and if the width of the screen is of the order of the wavelength of light, it is probable that we could treat each hole as a source of light.

Now consider screens as shown in Figure 4. Consider that the 14 slits shown are a wavelength wide and that the portion between the slits is painted with a completely absorbing black paint. Again, if one screen were placed in the path of a plane parallel beam of monochromatic light, the diffraction pattern observed on a screen placed at a distance large compared to the wavelength of light is the diffraction pattern of a single slit and the power is 14 times that for a single slit.

Now, however, consider the problem of studying the passage of diffuse white light through 100 of these screens placed three slit widths apart when the surface of the screen between the slits is 80% reflective. From one point of view, the diffuse light can be considered to be a multiplex of parallel equipowered beams of light at equally spaced units of solid angles in space. By considering the complications arising from the combined effects of multiple-wavelength light and multidirectional beams, it is obvious that knowledge of the Frauenhoffer diffraction pattern of a single screen containing randomly spaced slits will be of very little use in solving the partially reflecting multi-screen problem involving diffuse white light.
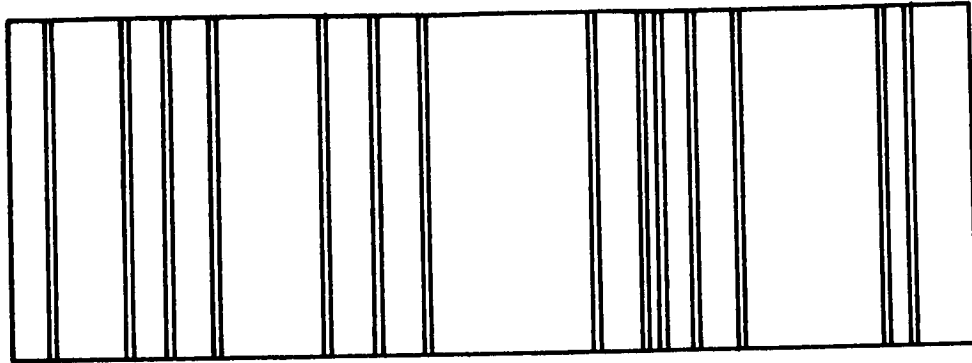
(a)
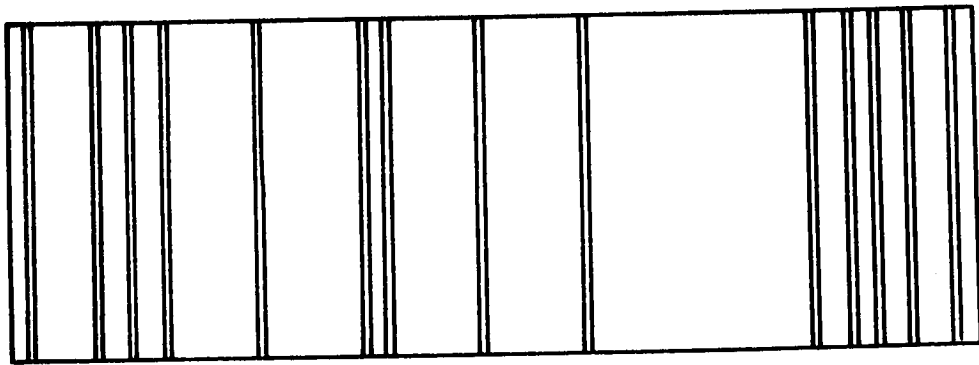
(b)

Figure 4

SCREENS CONTAINING RANDOMLY SPACED PARALLEL SLITS OF EQUAL WIDTH

However, it can be shown that the Mie theory studies are related to paint film phenomena in approximately the same manner as the Frauenhoffer pattern of a single screen containing randomly positioned slits is related to the multiscreen problem.

In order to gain an appreciation of the relevance of some of the published studies of the optical properties of pigment particles to the general problem of paint reflectance, it is necessary to extend the discussion of diffraction phenomena to the case of a screen containing randomly positioned regular apertures. This problem has been discussed by Andrews (ref. 2). He considered Frauenhoffer diffraction of monochromatic noncoherent radiation for the screen shown in Figure 5. He states: "If a very large number of identical rectangular apertures with identical orientation in a plane screen are randomly scattered about on the screen, the interference pattern of the combination will be smoothed out to constant intensity, but the diffraction pattern will be the same as that for a single rectangular aperture." The bright spots of the Frauenhoffer pattern for the single aperture are shown in Figure 5. The screen in Figure 5 is, in fact, a two-dimensional extension of the essentially one-dimensional case of the randomly spaced slits discussed earlier, and the considerations leading to the conclusions given by Andrews are, in fact, extensions of those given for the random slits to two dimensions.

Andrews also points out that the same type of result is obtained for the diffraction pattern produced by random spheres located in one plane perpendicular to the forward direction of the forward beam. Thus, if human blood corpuscles are placed on a glass slide and the Frauenhoffer diffraction pattern is studied, a series of concentric rings typical of the diffraction pattern of the single spheres is obtained (ref. 3). In fact, the structure of the rings is sufficiently well defined that the average diameter of the blood corpuscles can be deduced from the dimensions of the diffraction rings. A clinical device that makes use
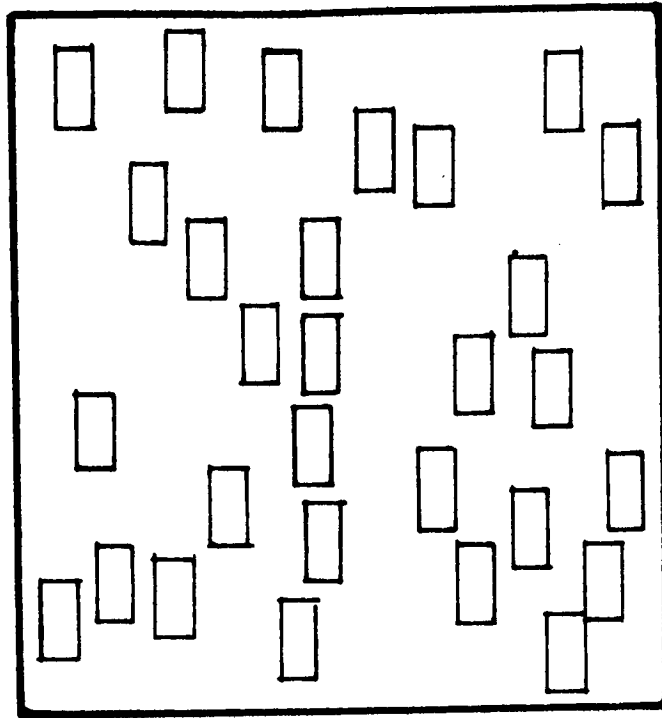
Randomly distributed identical apertures
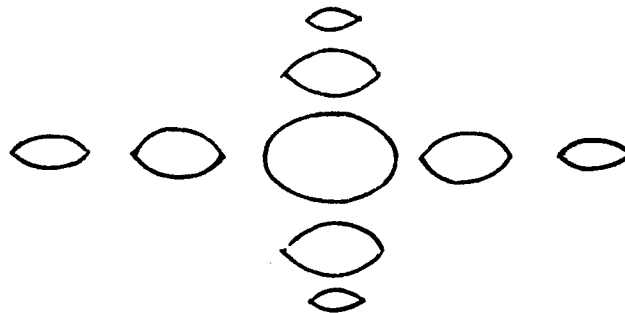
Schematic of light regions in Frauenhoffer
diffraction patterns of a rectangular aperture

Figure 5

DIFFRACTION BY RECTANGULAR APERTURES

of this phenomenon is called Young's eriometer. Thus, a random array of uniform spheres confined to a single plane should have a Frauenhoffer diffraction pattern the same as that for a single sphere (ref. 4).

Mie theory represents a general solution for the scattering properties of a single sphere. When the sphere is very small compared to the wavelength of light, the scattering is symmetrical in front of and behind the particle. This type of scattering is known as Rayleigh scattering. Although Mie theory covers all scattering phenomena, the term "Mie scattering" is usually restricted to the description of scattering by particles in the size range of 0.25 to 10 λ. In fact, Mie scattering is the growing tendency toward forward scattering with increasing particle size (ref. 5). The boundary between classical diffraction theory and the restricted Mie theory is not well defined, and in one sense the pattern of scattered light produced by particles in the range of 0.25 to 10 λ can still be called a diffraction pattern.

The Mie theory is based upon two explicit conditions. First, the incident beam is a plane parallel beam of noncoherent monochromatic light. Second, the radiation detector used to explore the scattering pattern is at infinity, i.e., at a distance large compared to the wavelength of light. In a sense, therefore, the Mie theory corresponds to Frauenhoffer diffraction.

Experiments on a thin (1 or 2 particles thick) array of pigment particles have been conducted (ref. 6) with a spectrophotometer and monochromatic radiation. Optical equipment of this kind satisfies the condition of plane parallel incident radiation with the detector at a large distance. In is not surprising that these experiments demonstrated maximum scattering power for a given particle size at wavelengths predicted from the Mie theory, since it is a general principle that the diffraction pattern produced by a thin random array of identical particles perpendicular to the beam is the same as that produced by a single particle.

To conclude from this type of observation that the scattering power of the pigment in a paint film is optimum at this size is to attempt to extrapolate from (a) monochromatic single scattering from a plane parallel beam studied at infinity to (b) the behavior in diffuse polychromatic light studied at a distance of two or three wavelengths, i.e., from the next pigment particle. This is no more logical than trying to predict the behavior of the series of screens shown in Figure 4 when placed in diffuse white light at separations of a few wavelengths from Frauenhoffer diffraction patterns of a single slit.

We suggested in earlier reports (ref. 7,8) that a multilayer system may prove to be an efficient paint surface for preventing penetration of white light.* This suggestion was based on reasoning which extrapolated Mie theory results to the complex interactions occurring in a paint film. If radiation from diffuse light falls on the particle from all directions, any diffraction pattern rotated through 360° yields the same pattern. Therefore, with diffuse radiation, it is the fact that the radiation interacts with the surface that is important, not the specific diffraction pattern for a single particle in a specific direction. Should a multilayer system prove to have important properties, the properties of the system cannot be regarded as predictable from Mie theory.

---

*See also discussion and Figure 44 in Section IIID of Report No. IITRI-U6003-19, Volume 2.

III. SEMANTIC PROBLEMS IN STUDYING REFLECTIVE PROPERTIES OF PAINT FILMS

A. Introduction

In an essay on the meaning of time, Millikan (ref. 9) states that the beginnings of science are nearly always found in the first steps taken toward refining natural but inaccurately defined concepts and making them more precise. When considering problems associated with the development of highly reflective paints, we find that as we extend our desire to control and predict the properties of paint films many of the words used in paint technology are not defined precisely enough. Thus the first stage in developing a new technology is elaboration of a new terminology.

In developing and planning the studies carried out under this contract, many difficulties arose from an inability to give definite meaning to the concepts and terms used in discussing properties of paint systems. Inaccurately defined terms that have hindered efficient prosecution of the research program are: random, diffuse, size of particle, scattering power, highly reflective, boundary, Fresnel coefficient, and reflection.

B. Highly Reflecting Paint Films

When attempting to construct various models of paint films, it was realized that in the early reports the concept "highly reflecting paint films" was not defined. One cannot define a highly reflecting paint film without reference to the boundary conditions of the system being studied. For example, does one attempt to maximize radiative properties with respect to unit weight or unit volume of the film? To define reflectance of the paint, it is necessary to specify the radiation concerned.

In these studies we were concerned with an environment in which the energy is direct radiation from the sun (in a vacuum), but this fact was not explicit in early definitions of high reflectivity. Because of the changes brought about by absorbed

radiation, it may also be necessary to take into account a time integral of the radiation effects on the paint film for the required time interval. In studies concerned with paint for spacecraft, a highly reflective paint film should be optimized with respect to unit weight of film. In cannot be stated too strongly that the general concept "highly reflective paint" has no meaning unless it is applied in the operational context in which the paint film is to be used.

C. Specification of Pigment Size

In an excellent review article on the relationship between the particle size of pigments and the properties of the paint made from them. Newman (ref. 10) made these comments. "If one wishes to make a scientific correlation between pigment particle size and paint properties, it is necessary to be able to measure with some reasonable degree of accuracy quantities involved in the proposed correlation. Unfortunately, the scientific acceptable knowledge both of the pigment particle sizes and of really significant paint properties still leaves much to be desired."

Although these remarks were made almost 20 years ago, they are relevant to the current state of knowledge and practice in the paint industry. In particular, there is not sufficient awareness that the precision with which a particle size can be defined may be the limiting factor in applying light-scattering theory to the study of the optical behavior of paints. For example, consider the curve shown in Figure 6. In the literature, this type of curve has been suggested as an effective universal curve to be used in studying pigment optics (ref. 11). The merits of this curve as a valid measure of optical scattering power in a paint film need to be examined as a result of our criticisms of the use of the Mie theory and optical experiments made with parallel beams of light on dilute dispersed suspensions (see Section IIIC, Volume 2, of this final report). Leaving the question of its validity open at this stage of the discussion,

let us consider the difficulties of applying it even if it were established as the operative, effective function.
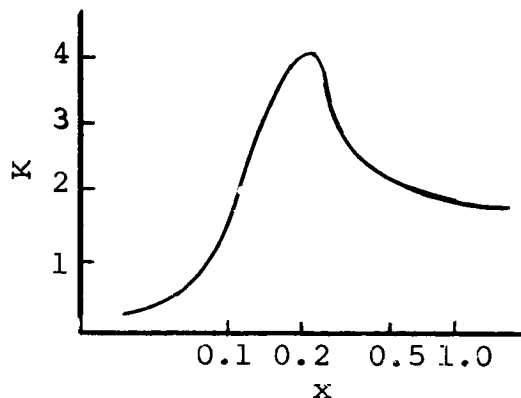
K = extinction coefficient

$x = d\dfrac{m^2-1}{m^2+2}$, where m is relative refractive index

Figure 6

CLAIMED UNIVERSAL EFFECTIVE EXTINCTION CURVE
FOR PIGMENT PARTICLES

Consider the problem of predicting the performance of a pigment by using this curve. In the July 16, 1963, issue of Chemical Processing it was claimed that hydrated alumina can be used as a pigment or filler in paint systems. The measured characteristics of the powder were quoted as:

Average Particle Size, μ	Method
0.12	BET
0.39	Fisher subsieve sizes
0.60	MSA centrifuge
0.30	Electron microscope

In applying the light-scattering curve of Figure 6 (even making the daring assumption that the average particle size can be used to calculate the overall properties of the paint), which value of the diameter should be used? The two extreme estimates differ by a factor of 5, and the four estimates would locate at very different regions on the scattering curve.

The other aspect of this problem is the difficulty of correlating reported data on the light-scattering properties of small particles. It is common practice to report data by drawing graphs of some measured quantity such as extinction coefficient versus particle diameter. However, the significance of the measured diameter quoted is not always apparent. For example, consider the curves in Figure 7. These curves represent data from light-transmission data reported by Andreasen and coworkers (ref. 12) from their studies of barium sulfate suspensions. The variable $\bar{\varepsilon}$ is defined as the specific extinction and is related to the extinction coefficient.

The significance of these transmission data will be discussed when the transmission measurements reported for suspensions are reviewed (Section IIIC, Volume 2, of this report). The important point is that only a careful reading of the text of the Andreasen paper reveals that the particle-size parameter used in plotting the data is the length of the cube volume equal to that of the sphere of equal Stokes' diameter. Let this length be k. By definition,

$$k^3 = \frac{1}{6} \pi d^3$$

$$\frac{k}{d} = \sqrt[3]{\frac{\pi}{6}} = \sqrt[3]{0.525} = 0.807$$

Therefore, without a full realization of the exact definition of particle size used, a superficial location of the peak of the transmission could have been 20% off if the Stokes' diameter had been used as the parameter.

Curve A: λ = 7500 A
Curve B: λ = 5300 A
Curve C: $\lambda \tau$ 4300 A
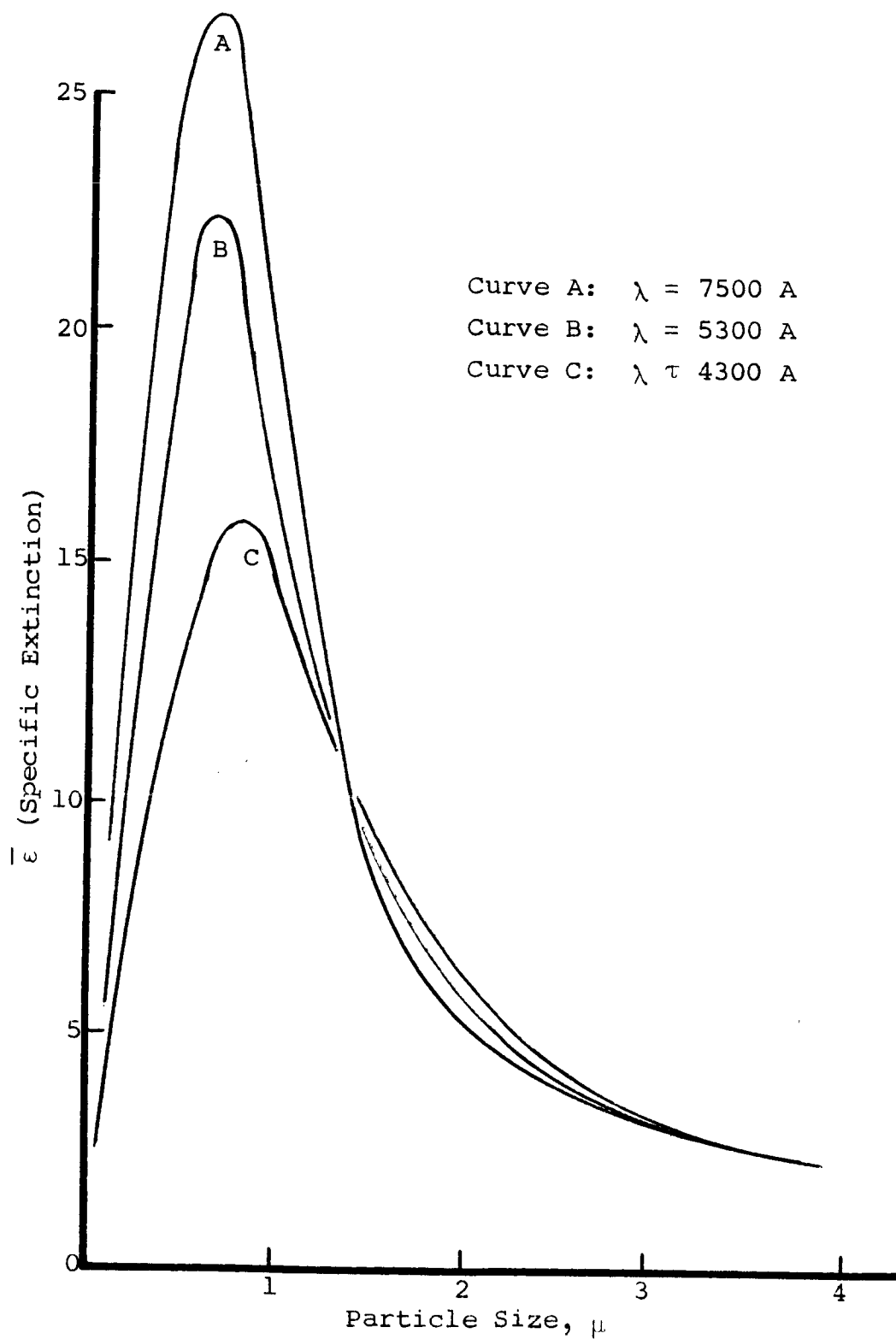
Figure 7

LIGHT-SCATTERING PROPERTIES OF BARIUM SULFATE PRECIPITATES

Even if we developed an ideal, foolproof method for analyzing the size distribution of raw pigment before it was used in paint films and even if all remaining difficulties were avoided, one important problem still remains: What is the operative size distribution of the pigment when it is dispersed in the film?

Studies of sections through paint films by analytical techniques for determining state of dispersion and spatial configuration of pigment locations are almost nonexistent. To understand the importance of the question, consider the systems in Figure 8, in which the dispersion rate in a paint film is considered from a simplified two-dimensional system. In Figure 8a a number of circles are set at random; in Figure 8b these are collected into random clusters.

The grouping of the particles has a twofold effect. First, it reduces the area of the film in which pigment particles are available for scattering interaction. Even a very crude estimate of interaction area, made by projecting interaction areas along the base line, shows that the clusters are less effective. It is not sufficient to regard a cluster as a formation of particles of larger diameter. A cluster has a higher effective absorption coefficient, because its internal porosity tends to oscillate the light back and forth, whereas a single particle has a lower absorption coefficient, because of the probability of a shorter path length within its boundaries.

A filler may improve the opacity of an active white pigment, since random mixing of the larger inert filler particles prevents large clusters of pigment from forming by filling in the interstitial spaces available. One way to improve the performance of paint may be a mechanical process for ensuring random efficient dispersion within the film. In testing the performance of any film from any theory, however, the exact nature of the distribution within the film must be known.

Section IIIG discusses problems associated with determination of particle size by examining sections through a paint film. Section VIII describes Monte Carlo studies of the distribution of scattering centers formed by clustered particles in a paint film.

Incident radiation

Projected
action
areas

(a) Random dispersion

Incident radiation

Projected
action
areas

(b) Flocculated dispersion
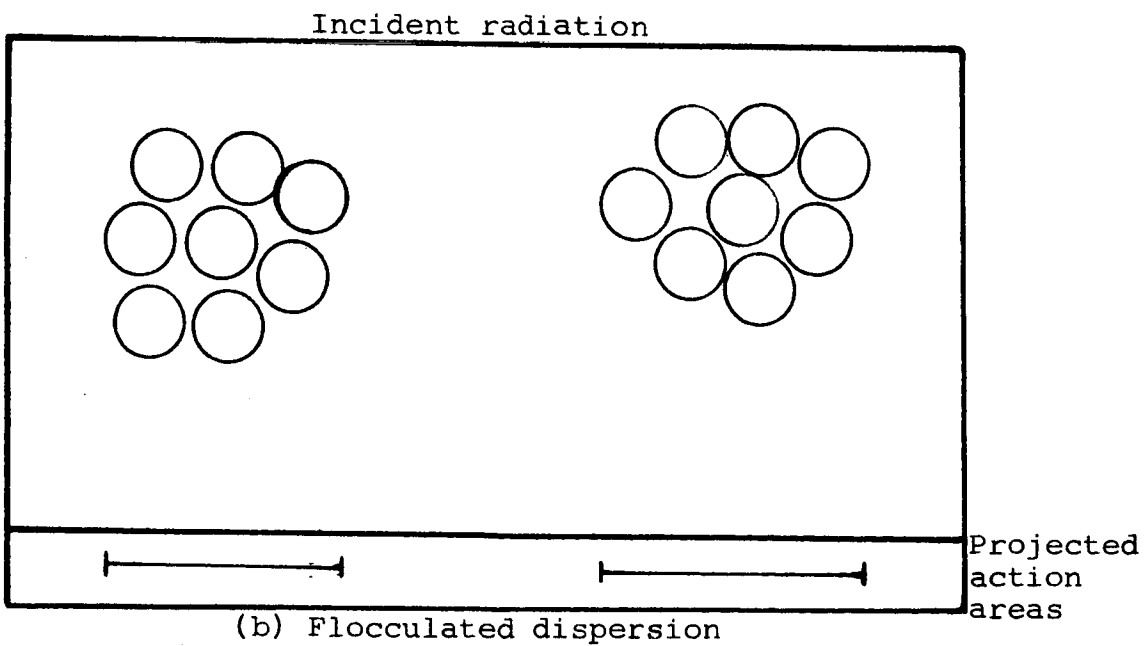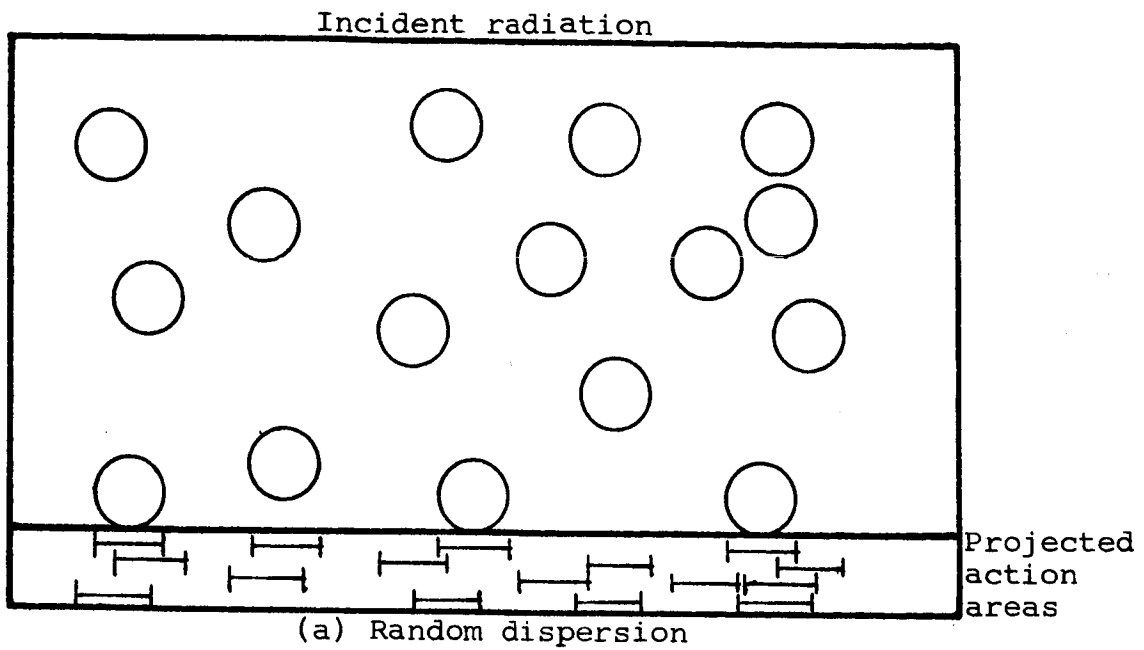
Figure 8

DIFFERENT DISPERSION STATES WITHIN A PIGMENT FILM

D. The Concept of Randomness

The term "random" as used in everyday speech describes a system that is not uniform or is nonsystematic. When the term is used to describe a system that has finite dimensions in space, it is necessary to be specific about the exact nature of the randomness of the system considered. Two similar systems can both be random in the technical sense and yet have different physical properties. This fact can be illustrated by considering the problem of drawing random lines across a circle. This situation arises in the study of the light-scattering behavior of paint films, since the average length of intercepts of a circle could represent the average path of photons through a spherical pigment particle.

One method of constructing random intercepts of circles is to draw a circle on a piece of paper and then toss thin wires onto the paper in a random manner. The record of the different positions in which the wires fall provides a set of random intercepts. However, it can be shown that this kind of randomness is not necessarily a true simulation of the random paths through a spherical object.

There are four possible mathematical procedures for constructing random intercepts. In the first method, the perimeter is divided into a convenient set of intervals. Each interval is then allocated a number. To construct a random intercept, two numbers within the appropriate range are selected from random-number tables, and a line is drawn between the two corresponding points on the perimeter. This method is illustrated in Figure 9a, and an example of this type of random intercept is shown in Figure 10. Circular graph paper with the perimeter divided into 360 intervals (polar graph paper) was used. Random numbers between 1 and 360 were selected, and then 20 random lines were drawn to construct the system of random intercepts given in Figure 10.
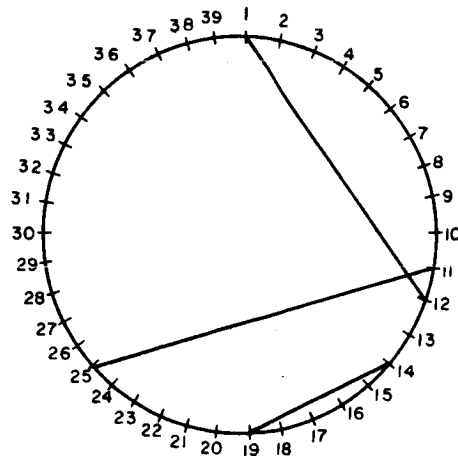
Method 1: Intercept drawn between two randomly
selected points on the perimeter.

Figure 9a
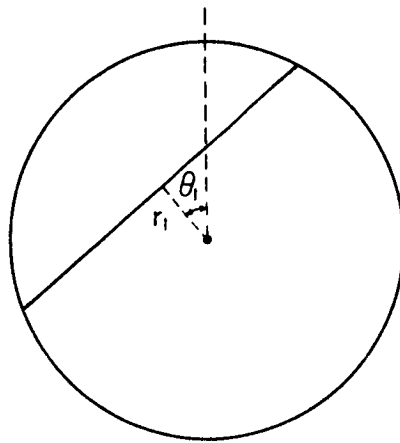
Method 2: Line drawn perpendicular to radius r_1 at angle θ_1
to fixed direction; r_1 and θ selected randomly.

Figure 9b
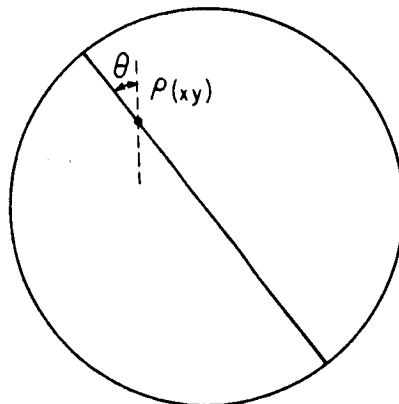
Method 3: Line drawn through point P of coordinates x,y in
a direction θ. The coordinates x and y are on a
rectangular grid; x,y and θ selected randomly.

Figure 9c

Figure 9

THREE METHODS OF DRAWING RANDOM INTERCEPTS IN A CIRCLE
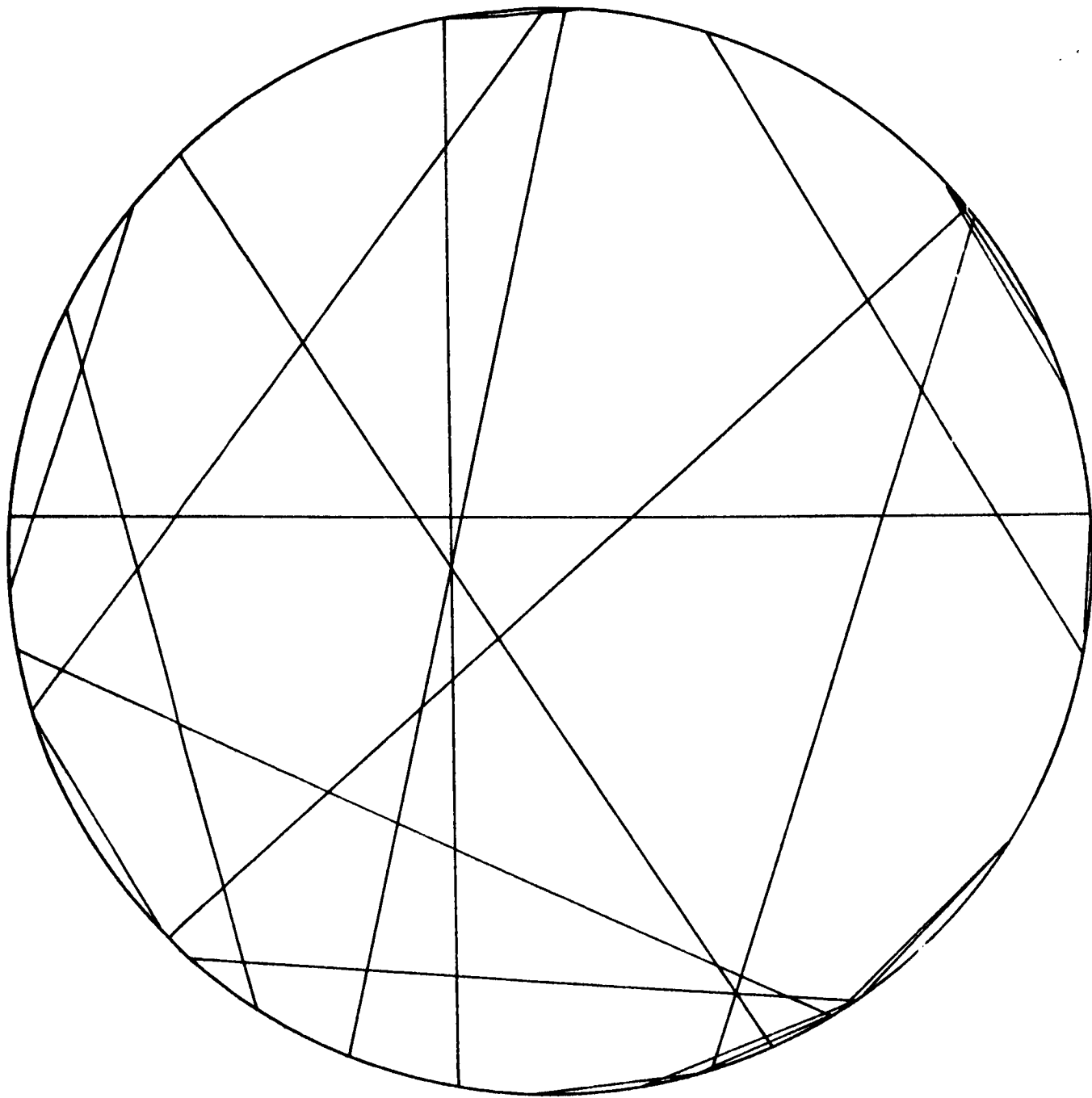
Figure 10

LINES DRAWN BETWEEN TWO RANDOM NUMBERS SELECTED ON THE PERIMETER OF A CIRCLE

In the second method, the length of a radial line r_1 is chosen from random-number tables, and the direction of this line with respect to some fixed direction, θ, is also chosen at random. Then the intercept is drawn perpencircular to this radius. The method is illustrated in Figure 9b. An example of the system is given in Figure 11. Figures 10 and 11 show that shorter intercepts are more probable in method 1, and for that kind of randomness, the average intercept length is smaller in method 1 than in method 2.

In the third method, a point is specified by using a rectangular grid system superimposed upon the circle. Then the direction of the line at this point is selected at random. This method is illustrated in Figure 9c. Method 3 is equivalent to method 2, since in method 2 all values of direction are equally probable and all values of P are equally probable. This fact can be deduced from the following reasoning.

Consider the families of intercepts for a given direction of various values of r. Since each value of r is equally probable, a set of parallel lines will be obtained. Therefore, all possible intercepts are formed by rotating a set of parallel lines about the center point. As the lines come closer and closer together, at any point in space there will be a group of intersecting lines that are spread uniformly through 360°. This result is also obtained when many intercepts are drawn by method 3. An alternative viewpoint is that x and y specify a value, P, and that corresponding values of r and θ_1 in method 2 result in an intercept of the same length and direction as if x, y, and θ were chosen.

In the fourth method, a point on the perimeter is chosen by using random-number tables and the direction is chosen in the same manner. This method is mathematically equivalent to method 1. Therefore, methods 1 and 4 and methods 2 and 3 are equivalent. In subsequent discussions methods 1 and 4 will be called method A, and methods 2 and 3 will be called method B.
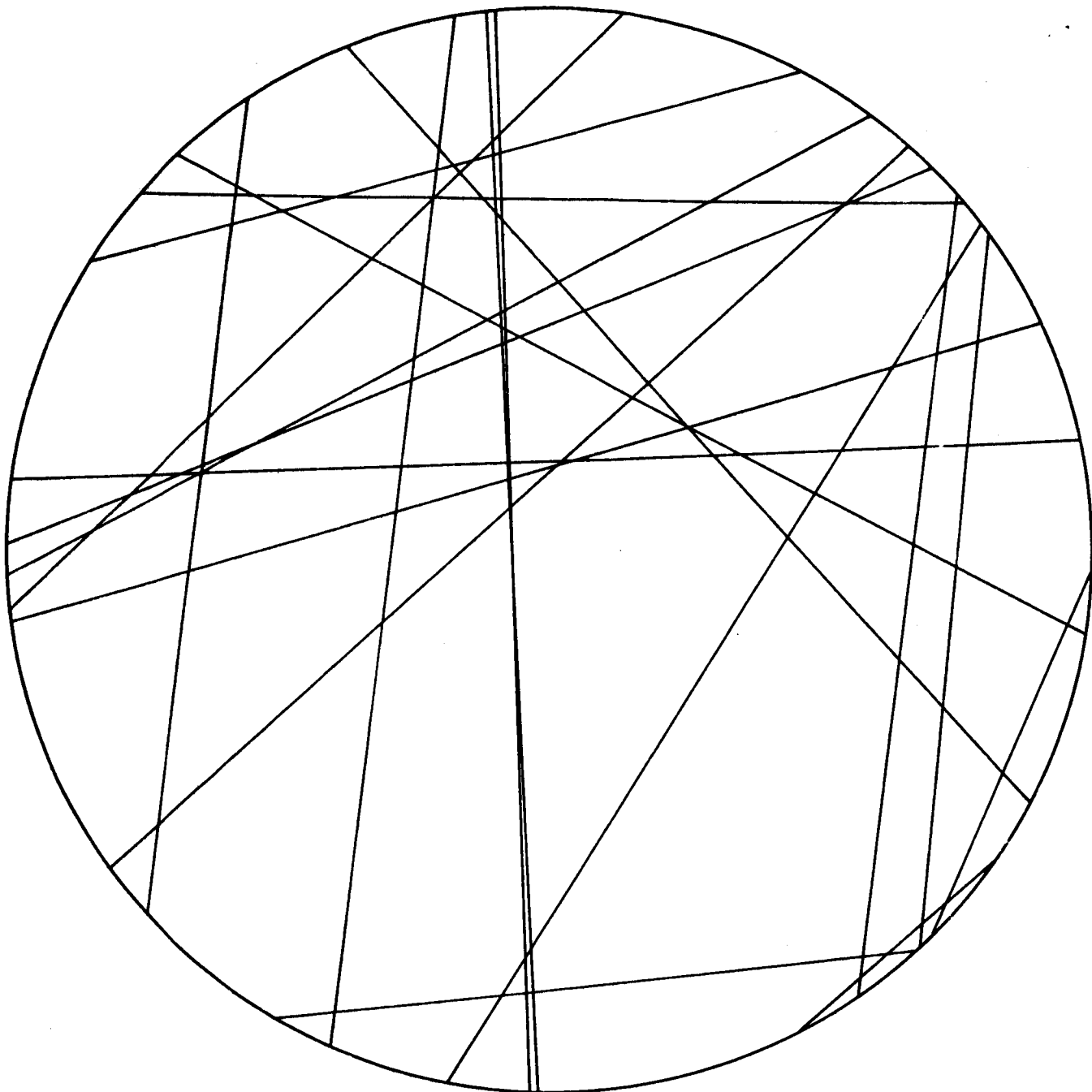
Figure 11

LINES DRAWN PERPENDICULAR TO RADIUS
FOR RANDOMLY SELECTED ANGLES TO A FIXED DIRECTION

The physical method of constructing random intercepts described at the beginning of this section corresponds to method B. That is, if we consider the midpoint of the wire tossed onto the paper, the probability of finding this point at any point within the circle is the same for all possible points. This is equivalent to saying that all possible x and y coordinates for this fixed reference point on the wire are equally probable. On landing, all possible orientations of the wire are equally probable. Therefore the tossing of the wire onto the cirlce is physically equivalent to method B.

Therefore the wire-tossing method yields average intercept lengths that correspond to those obtained graphically by using method B. It can be seen that the apparently simple concept of randomness is not simple when we try to define a random system.

E. Diffuse Light

A search was made of standard optical textbooks for a definition of diffuse light. It was not possible to find a precise definition, since normally the term is used in the sense of "nondirected light" rather than in the sense of a particular spatial distribution of radiant energy. In order to begin the development of the theory of diffuse light penetration, we defined diffuse light as follows.

Diffuse light is light in which the density of photons per unit volume is the same at any location in space with all directions for the photon tracks being equally probable. By this definition, the density of photon entries at any point of the pigment perimeter is equal at all points on the perimeter. This is equivalent to saying that all points of entry for any specified photon are equally probable. The probability of directions permissible for the photon after it crosses the pigment boundary is difficult to assess, since we cannot talk about refraction phenomena unless we have an extended wave front. If equal probabilities for all possible directions can be assumed, the possible tracks correspond to the intercepts constructed by method A.

If gas molecules instead of photons are considered, the effect of collisions would have to be considered. The effect of collisions would be to bring the density of particles per unit volume to the same value for all regions of the system for which track lengths are being considered. This would tend to make track lengths equivalent to those constructed by method B, since in this technique the density of intersection of tracks is more uniform over the area considered.

It may be possible to deduce the correct type of randomness for diffuse light by using the fact that the average branch as considered by method A is shorter than that as considered by method B. Therefore, the absorption of a colored pigment that is related to path length through the pigment particle should be related to the type of random track that occurs.

F. Boundary Conditions of Paint Films

To enable any postulated optical theory of paint behavior to be applied to any paint-film system, the boundary conditions of the paint film must be known. The important boundary conditions are:

(a) Surface finish and reflectivity of the boundary between the incident energy and the pigment-vehicle matrix

(b) Surface finish and reflectivity of the boundary between the pigment-vehicle and the body to which the paint film is applied

(c) Extent and spatial configuration of the paint film.

The surface finish of the boundary surfaces is important because it affects the energy entry, energy escape, and directional properties of radiation within the paint film. The paint industry is concerned with the surface finish of a paint, but only gross qualitative properties such as the gloss or matt nature of a surface are measured.

In studies of the interaction of waves with a boundary, it is generally recognized that the surface is smooth if irregularities are small compared to the wavelength of light. However, there is little information on how surface irregularities affect radiation incident on a surface or on how large a smooth area must be before regular reflection occurs.

Strong (ref. 13) quotes data for infrared reflection from brass plates of various roughnesses. Figure 11 shows that the energy entering the brass plate depended greatly on the surface finish. On a superficial level it can be argued that, since a smooth surface rejects a higher amount of energy than a rough one, the aim should be to have a smooth surface finish. In this manner the pigment-vehicle reflecting matrix will have less energy to cope with.

However, a brief examination shows that this argument is too simple. All the energy returned to the surface by the pigment particles has to pass through this surface to be expelled from the system. The very fact that the smooth surface is an efficient barrier to incident energy means that scattered energy returning from the pigment particles encounters an efficient radiation barrier. It is conceivable that a rough surface may be more effective when averaged over many radiation-transfer events.

A second property of a rough surface that could increase the overall reflectivity of the surface is that directional properties of the incident radiation would be changed; i.e., part of the incident radiation would become diffuse and would be spread over a greater area of the pigment film, which therefore would be utilized more efficiently. Without quantitative information on the reflectance of directed and diffuse light from rough surfaces and also on the reflective power of smooth surfaces for incident diffuse radiation, it is not possible to develop quantitatively the statistical models for a paint film.

G. Size Distribution of Pigment Particles Dispersed in Paint Films

Analytical techniques for studying the particle-size distribution of a three-dimensional system from two-dimensional sections are almost nonexistent. The work described in this section was initiated to examine the feasibility of developing techniques for measuring the size distribution of a pigment from sections through a paint film. There are some geometric probability theories that can be used as a basis for analytical procedures for deducing the particle-size distribution of a pigment embedded in a paint film.

Let there be n particles of arbitary shape embedded in a unit volume. We define the average surface, a, as:

$$a = \frac{\sum\limits_{i=s}^{i=} n_i a_i}{n} \tag{1}$$

where

n_i is the number of particles of area a_i

i=s and i= are the smallest and largest particles present.

We define the average volume as:

$$v = \frac{\sum\limits_{i=s}^{i=} n_i v_i}{n} \tag{2}$$

where n_i is the number of particles of volume v_i.

Let a plane section be taken at random through the pigmented matrix. Let n_p be the number of sections exposed in the plane per unit area, and let P_a be the average perimeter of these sections defined by:

$$P_a = \frac{\sum\limits_{i=s}^{i=} n_i P_i}{n_p} \tag{3}$$

. where there are n_i particles of perimeter P_i. We define the average area of the exposed sections as:

$$A_p = \frac{\sum\limits_{i=s}^{i=\ell} n_i A_i}{n_p} \qquad (4)$$

where there are n_i exposed sections of area A_i.

Now let a random line be drawn on the exposed section. Let there be n_ℓ intersections with the exposed portions of pigment per unit length of the random line. We define the average length of the sections of the random line in the pigment particles as:

$$L_\ell = \frac{\sum\limits_{i=s}^{i=\ell} n_i L_i}{n_\ell} \qquad (5)$$

All the above definitions assume that the summation is averaged over many unit areas and many unit lengths. It can be shown (ref. 14) that the above-defined quantities are linked by the relationship:

$$n_p A_p = n_\ell L_\ell = nv \qquad (6)$$

From this relationship it follows that since nv is the volume fraction of pigment α, from the definition of A_p and L_p,

$$\alpha = \sum\limits_{i=s}^{i=\ell} n_i A_i = \text{surface of exposed pigment per unit area} \qquad (7)$$

$$\alpha = \sum\limits_{i=s}^{i=\ell} n_i L_i = \text{fractional density of exposed pigment on any random line drawn in the section} \qquad (8)$$

Since the relationships in Equations 7 and 8 would apply separately to different pigments present, it follows that the relative proportions of the different substances can be deduced by repeated application of the relationship. This fact is already being used in grain analysis of metal sections and in

evaluation of ores. Usually Relationship 8 is used. The same
relationship is also used to evaluate from aerial photographs
the proportion of different kinds of trees in a forest.

It can be shown that the total perimeter per unit area, $n_p P_a$,
is:

$$n_p P_a = \frac{2n}{\pi} \qquad (9)$$

when averaged over many events. This relationship was first
derived by Cauchy (ref. 15). From a second theory of Cauchy's
it can be shown that:

$$na = 4n \quad \text{unit length units} \qquad (10)$$

(This at first appears to be dimensionally incorrect, but it
should be recalled that a is the average area per unit volume
and dimensionally is measured in length units.) From Relations
10 and 6 it follows that:

$$\frac{na}{nv} = \frac{4n}{n\,L} = \frac{4}{L}$$

In a more useful form this relation is written:

$$\frac{S}{V} = \frac{4}{\beta} \qquad (11)$$

"The ratio of volume to surface per unit volume of a pigment
is the average fractional length within the pigment of a random
line drawn across a section through the paint film." As far as
we are aware, this relationship has never been suggested in this
form for application to the study of paint films. It has been
used by Bates and Pillow (ref. 16), who showed that the average
path of a sound wave in an auditorium is $4VS^{-1}$. This relation-
ship would seem to have great potential in the study of random
paths through nonhomogeneous systems.

Although we are proposing currently to use the relationship
to find the surface/volume ratio for a pigment, it can be used
in reverse to predict the average path through a given phase in
a nonhomogeneous system if the surface/volume ratio is known.
For instance, consider the path of a drill through a sintered

metal body. If the surface/mass ratio of the sintered metal particles were known, the average depth of actual metal in any drilled hole could be predicted.

Except for the work of Bates and Pillow (ref. 16), we are not aware of any experimental proof of Equation 11; we could use a simulated system to test the relationship, however.

Again, from Relation 6:

$$A_p = \frac{n_\lambda L_\ell}{n_p}$$

But, from Relation 9:

$$n_\ell = n_p P_a \cdot \frac{\pi}{2}$$

Therefore,

$$A_p = P_a \cdot L_\ell \cdot \frac{\pi}{2} \tag{12}$$

As far as we are aware, this is the first time that this relationship has been deduced. It is difficult to be certain, because the information for abstractions of this kind has to be searched over such a broad range of literature.

Again, using the symbol β for the average length of the random intercept and using γ as the average perimeter per unit section, Equation 12 is written in the consise form (since, from Equation 7, the volume fraction of pigment is numerically the same as the area exposed per unit section):

$$\alpha = \gamma\beta \cdot \frac{\pi}{2} \tag{13}$$

H. Discussion

Some interesting general equations related to the problems of deducing the properties of a three-dimensional disperse system from a study of two-dimensional sections were developed. Possible limitations of the general validity of the equations for the case of reentrant figures have to be explored. No general theory of the prediction of the light-scattering properties of a paint from a consideration of the particle-size distributions of the pigment can be tested until good methods are available for physically studying sections of paint films.

IV. MEASUREMENT OF SHAPE OF PARTICLES

A. Analysis

In the literature on particle-size analysis the term
"shape factor" has been used in the following manners. First,
it has been applied to factors used to convert linear dimensions
of individual particles to corresponding particle surfaces and
volumes. Since powder usually contains at least a small range
of shapes, these shape factors are usually averaged values for
several particles.

Second, the term has been used to describe the ratio of
the mean diameters measured by two different techniques. For
instance, if d_s is the mean diameter determined by sieving and
d_m is the mean diameter determined by microscopic examination,
d_s/d_m would be a measure of the shape effects that have contri-
buted to the difference between the diameters. Neither of these
types of shape factors is appropriate to the problem of defining
the shape of a particle dispersed in a paint film, particularly
since the shape of a cluster is sometimes of interest to the
technologist.

One other type of shape factor has been briefly mentioned
in the literature. This is the use of the ratio of two statis-
tical diameters, which have been measured by microscope count,
to characterize shape. Two statistical diameters that have
been used are Martin's diameter and Feret's diameter. Martin's
diameter is the mean length of a line intercepting a profile
boundary of the image of the particle and dividing the image
into two portions of equal area. The bisecting line is always
taken parallel to the direction of traverse. Feret's diameter
is the mean length of the distance between two tangents on
opposite sides of the image of the particle. The tangents are
drawn perpendicular to the direction of traverse.

These definitions show that statistical diameters are
mathematical conventions used to describe readily measured
averages and not actual physical dimensions of individual

particles. An apparent advantage of this type of shape factor is that the use of statistical diameters removes the need for constant realignment of the eyepiece graticule to measure a particular dimension of a particle. The use of the ratio of statistical diameters to define shape is an attempt to define a shape factor in terms of parameters that can be measured readily.

The lack of information on the number of particles to be counted to obtain a given confidence of a measured statistical diameter probably accounts for the fact that ratios of statistical diameters have not been used widely to describe the shape of the particles. The potential use of this type of shape factor was explored for a simplified set of particle profiles by investigating the relationship between the Martin's and the Feret's diameters for a given type of profile. In the theoretical investigation reported here, we considered the case of particles having either elliptical cross sections or projected areas that are elliptical.

In the following discussion the major and minor axes of the elliptical profile are referred to as 2a and 2b, respectively (see Figure 12). There is no particular reason to choose an ellipse, except that it is a definite, familiar shape and its analytical geometry is moderately tractable. For the first stages in developing a theory of statistical shape factors analysis, we shall assume a monosized population of particle profiles in random array.

The equation of the ellipse in the x'-y' coordinate system is:

$$\frac{x'^2}{a^2} + \frac{y'^2}{b^2} = 1$$

By rotating coordinates to the x-y system, the transformed equation is:

$$Ax^2 + 2Bxy + Cy^2 = 1 \tag{14}$$

where
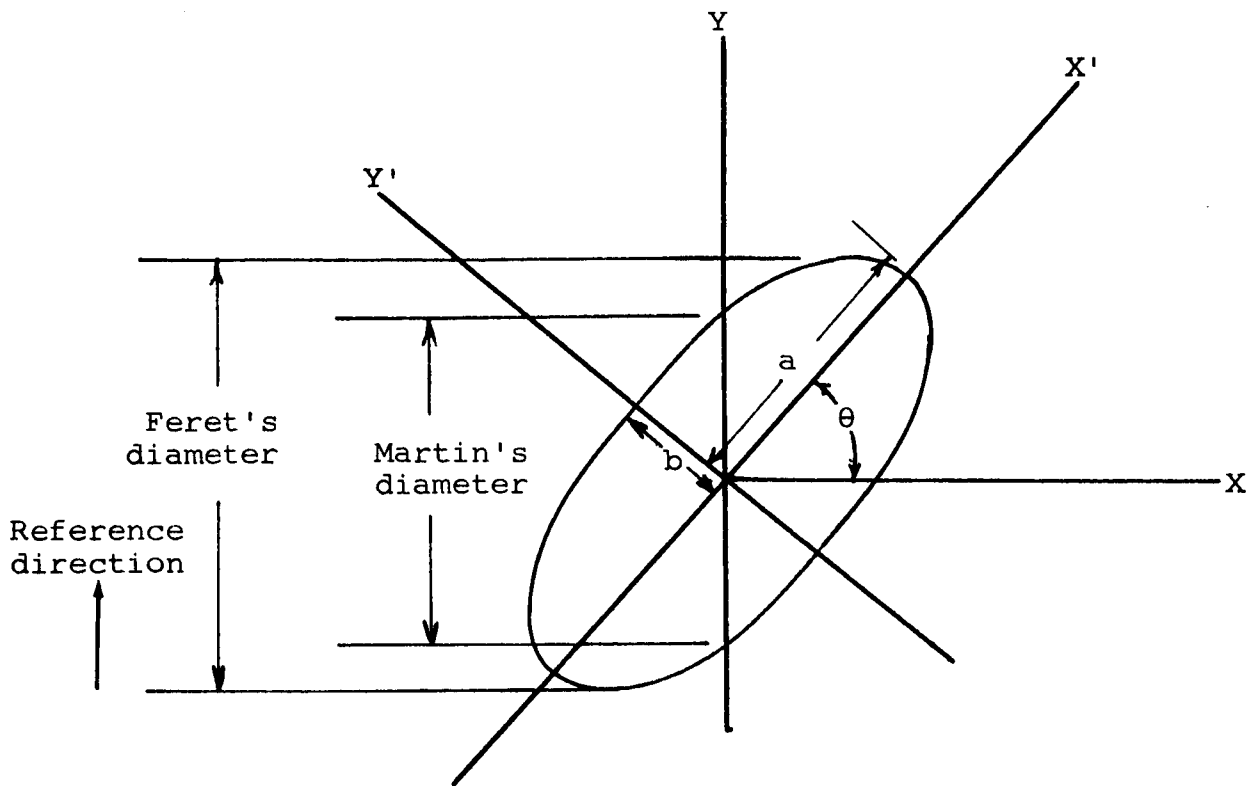
Figure 12

STATISTICAL DIAMETERS (SHOWING COORDINATE SYSTEM)
FOR ELLIPSOIDAL PARTICLE

$$A = \frac{\cos^2 \Theta}{a^2} + \frac{\sin^2 \Theta}{b^2}$$

$$B = \sin \Theta \cos \Theta \left(\frac{1}{a^2} - \frac{1}{b^2} \right)$$

$$C = \frac{\sin^2 \Theta}{a^2} + \frac{\cos^2 \Theta}{b^2}$$

It is necessary to define Feret's diameter, d_f, and Martin's diameter, d_m, explicitly as functions of a, b, and Θ. Feret's diameter is equal to twice that value of y for which dy/dx equals zero. Calculating dy/dx yields:

$$\frac{dy}{dx} = - \frac{Ax + By}{Bx + Cy} = 0$$

or the equivalent:

$$Ax + By = 0$$

This equation, together with Equation 14, determine x and y at the point where the tangent to the ellipse is horizontal. By solving simultaneously, it is found that:

$$y = \sqrt{A/(AC - B^2)}$$

Eliminating A, B, and C and doubling the result gives:

$$d_f(a,b;\Theta) = 2 \sqrt{b^2 \cos^2 \Theta + a^2 \sin^2 \Theta} \qquad (15)$$

Martin's diameter is equal to twice that value of y obtained when x equals zero. That is,

$$y = \sqrt{1/C}$$

or

$$d_m(a,b;\Theta) = \frac{2ab}{\sqrt{b^2 \sin^2 \Theta + a^2 \cos^2 \Theta}} \qquad (16)$$

Next it is desired to average out the dependence on the random variable Θ so as to get expected values for d_f and d_m. As before, a and b are fixed. The desired quantities are given by:

$$E[d_f] = \frac{2}{\pi} \int_0^{\pi/2} 2\sqrt{b^2 \cos^2\theta + a^2 \sin^2\theta}\, d\theta \qquad (17)$$

and

$$E[d_m] = \frac{2}{\pi} \int_0^{\pi/2} \frac{2ab}{\sqrt{b^2 \sin^2\theta + a^2 \cos^2\theta}}\, d\theta \qquad (18)$$

These expressions already assume that θ is distributed uniformly on $[0, \pi/2]$. Because of symmetry, it is only necessary to consider the first quadrant.

Expressions 17 and 18 are elliptic integrals. The next step is to convert them to standard form. Eliminating $\cos^2\theta$ and dividing suitably yields:

$$E[d_f] = \frac{4b}{\pi} \int_0^{\pi/2} \sqrt{1 - \frac{(b^2 - a^2)}{b^2} \sin^2\theta}\, d\theta \qquad (19)$$

and

$$E[d_m] = \frac{4b}{\pi} \int_0^{\pi/2} \frac{d\theta}{\sqrt{1 - \frac{(a^2 - b^2)}{a^2} \sin^2\theta}} \qquad (20)$$

In Equation 19 it is convenient to interchange a and b. This is permissible. It is equivalent to relabeling the axes for the Feret's diameter; the expected value is not affected. The result is:

$$E[d_f] = \frac{4a}{\pi} \int_0^{\pi/2} \sqrt{1 - \frac{(a^2 - b^2)}{a^2} \sin^2\theta}\, d\theta \qquad (21)$$

Next assume that a is greater than or equal to b. Set

$$k^2 = \frac{a^2 - b^2}{a^2}$$

Expressions 20 and 21 become:

$$E\left[d_m\right] = \frac{4b}{\pi} \int_0^{\pi/2} \frac{d\Theta}{\sqrt{1 - k^2 \sin^2 \Theta}}$$

and

$$E\left[d_f\right] = \frac{4a}{\pi} \int_0^{\pi/2} \sqrt{1 - k^2 \sin^2 \Theta} \, d\Theta$$

The complete elliptic integrals of first and second kind are defined, respectively, by:

$$K(k) = \int_0^{\pi/2} \frac{d\Theta}{\sqrt{1 - k^2 \sin^2 \Theta}}$$

and

$$E(k) = \int_0^{\pi/2} \sqrt{1 - k^2 \sin^2 \Theta} \, d\Theta$$

For present purposes, it is more suitable to regard K and E as functions of b/a. This leads to:

$$E\left[d_m\right] = \frac{4b}{\pi} K(b/a) \tag{22}$$

and

$$E\left[d_f\right] = \frac{4a}{\pi} E(b/a) \tag{23}$$

Next, divide Equation 23 by Equation 23:

$$\frac{E\left[d_m\right]}{E\left[d_f\right]} = \frac{b}{a} \cdot \frac{K(b/a)}{E(b/a)} \tag{24}$$

The quotient on the left is a shape factor, since it is dimensionless, and it characterizes the particle population. The same is true of the ratio b/a. Thus Equation 24 is a relation between these two shape factors. Figure 13 is a plot of one shape factor against the other.
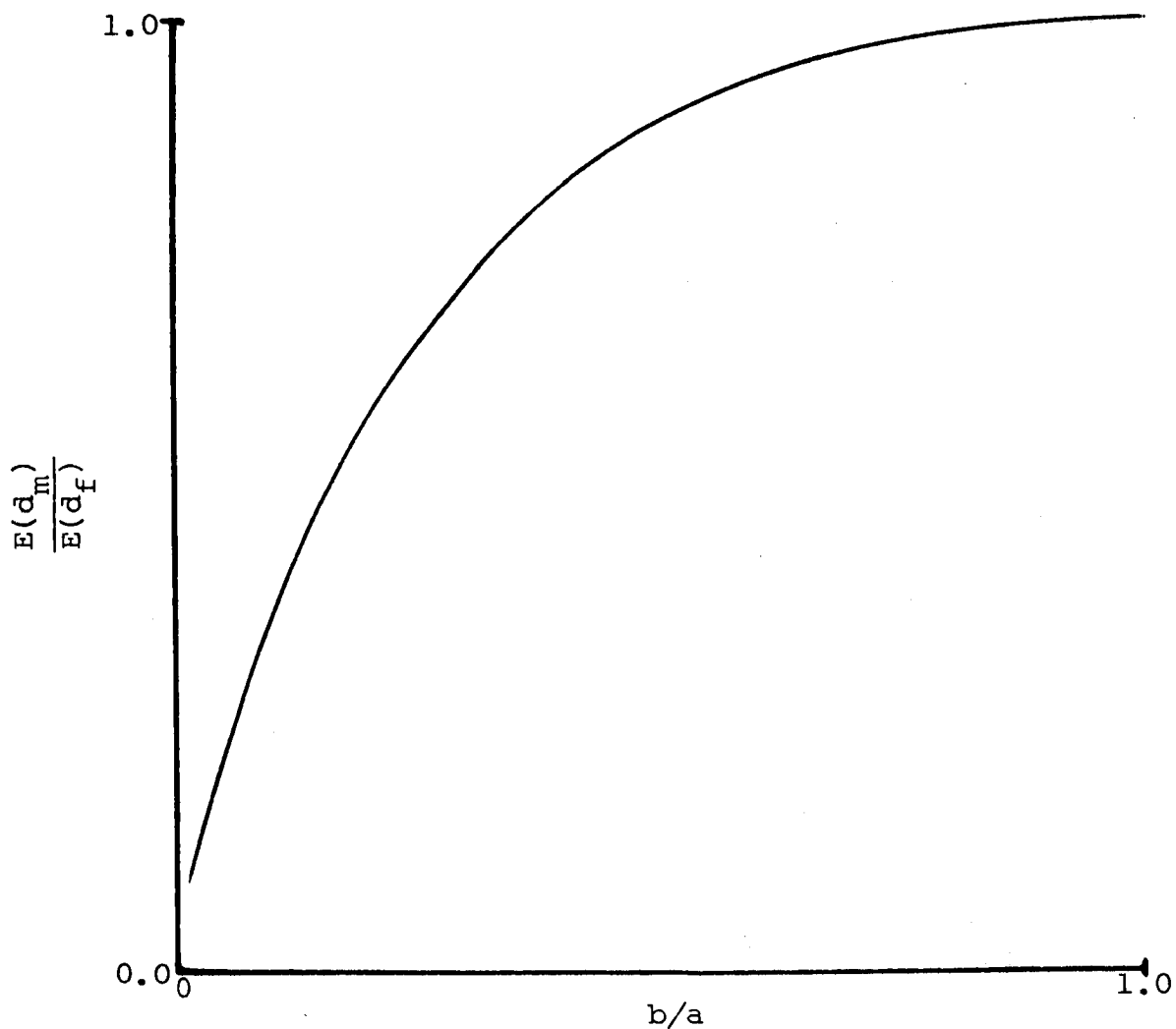
Figure 13

SHAPE FACTOR CONVERSION

Equations 22, 23, and 24 are all that are necessary to obtain from $E\left[d_m\right]$ and $E\left[d_f\right]$ the values of a and b. Alternatively, $E\left[d_m\right]$ and $E\left[d_f\right]$ can be found from a and b. In order to simplify this calculation, a tabulation of b/a, K(b/a), and E(b/a) has been prepared along with the values of the right-hand side of Equation 24. These parameters are presented in Table 1.

If a and b are given, Feret's and Martin's diameters can be found from Equations 22 and 23 once D and E are extracted from the table. An example of the reverse procedure might be useful. Suppose that the following values of the two diameters are given.

$$\bar{d}_m = 5.3499$$

and

$$\bar{d}_f = 8.1918$$

Bars are used on these quantities, which presumably were obtained experimentally, to distinguish them from the theoretically expected values.

Next, calculate the ratio:

$$\frac{\bar{d}_m}{\bar{d}_f} = 0.65308$$

By taking this value to column 4 of Table 1 and interpolating to columns 1, 2, and 3, it is found that:

$$\frac{\bar{b}}{\bar{a}} = 0.25012$$

$$K(\bar{b}/\bar{a}) = 2.8004$$

$$E(\bar{b}/\bar{a}) = 1.0723$$

Finally, by transposing Equations 22 and 23 and replacing the expected values by the measured values, it is found that:

Table 1

TABULATION OF DATA REQUIRED TO DETERMINE SHAPE FACTOR (Equation 24)

b/a	K(b/a)	E(b/a)	$\left(\dfrac{b}{a}\right)\dfrac{K}{E}$
1.00000	1.5708	1.5708	1.00000
0.98163	1.5854	1.5564	0.99992
0.96126	1.6020	1.5405	0.99963
0.93358	1.6252	1.5191	0.99878
0.89879	1.6557	1.4924	0.99714
0.88295	1.6701	1.4803	0.99616
0.86603	1.6858	1.4675	0.99486
0.83867	1.7119	1.4469	0.99227
0.80902	1.7415	1.4248	0.98885
0.77715	1.7748	1.4013	0.98429
0.75471	1.7992	1.3849	0.98048
0.71934	1.8396	1.3594	0.97344
0.69466	1.8691	1.3418	0.96765
0.65606	1.9180	1.3147	0.95712
0.62932	1.9539	1.2963	0.94857
0.58779	2.0133	1.2681	0.93320
0.55919	2.0571	1.2492	0.92084
0.52992	2.1047	1.2301	0.90669
0.50000	2.1565	1.2111	0.89031
0.48481	2.1842	1.2015	0.88133
0.46947	2.2132	1.1920	0.87167
0.45399	2.2435	1.1826	0.86126
0.43837	2.2754	1.1732	0.85021
0.42262	2.3088	1.1638	0.83841
0.40674	2.3439	1.1545	0.82577
0.39073	2.3809	1.1453	0.81227
0.37461	2.4198	1.1362	0.79782
0.35837	2.4610	1.1272	0.78242
0.34202	2.5046	1.1184	0.76594
0.32557	2.5507	1.1096	0.74841
0.30902	2.5998	1.1011	0.72962
0.29237	2.6521	1.0927	0.70961
0.27564	2.7081	1.0844	0.68836
0.25882	2.7681	1.0764	0.66559
0.24192	2.8327	1.0686	0.64129
0.22495	2.9026	1.0611	0.61534
0.20791	2.9786	1.0538	0.58766
0.19081	3.0617	1.0468	0.55808
0.17365	3.1534	1.0401	0.52648
0.15643	3.2553	1.0338	0.49258
0.13917	3.3699	1.0278	0.45630
0.12187	3.5004	1.0223	0.41729
0.10453	3.6519	1.0172	0.37528
0.08716	3.8317	1.0127	0.32978
0.06976	4.0528	1.0086	0.28031
0.05234	4.3387	1.0053	0.22589
0.03490	4.7427	1.0026	0.16509
0.01745	5.4349	1.0008	0.09476

$$\bar{a} = \frac{\pi \overline{d_f}}{4E(\overline{b/a})} = 6.000$$

and

$$\bar{b} = \frac{\pi \overline{d_m}}{4K(\overline{b/a})} = 1.500$$

In most cases values of $\overline{d_f}$ and $\overline{d_m}$ will be obtained from measurements of a fixed number, say n, of particles. It will be assumed from now on that both measurements are obtained from the same set of particles, rather than two independent sets. It will be seen that it is desirable to meet this condition. Now, in order for $\overline{d_f}$ and $\overline{d_m}$ to be consistent with Equations 17 and 18, it is required that they be obtained from arithmetic averages of the observed values.

Equations 17 and 18 assume that Θ is uniformly distributed on $\left[0, \pi/2\right]$. When a finite sample is taken, this condition will seldom be met exactly. Suppose in a particular experiment that large values of Θ occur slightly more often than small values. Then, from Figure 12, it is seen that both $\overline{d_f}$ and $\overline{d_m}$ will be larger than their expected values. However, in the ratio $\overline{d_m}/\overline{d_f}$ the effect of these two errors cancels to a certain extent, so that the value of the ratio should be somewhat more accurate than either $\overline{d_f}$ or $\overline{d_m}$. Similarly, since the shape factor $\overline{b/a}$ is a function only of the shape factor $\overline{d_m}/\overline{d_f}$, its value should be more accurate than either $\bar{a}$ or $\bar{b}$ alone.

The next result consists of an attempt to estimate the variances of $\overline{d_f}$ and $\overline{d_m}$. This attempt is successful to the extent that exact theoretical expressions for the variances can be found. However, to evaluate these expressions requires a knowledge of a and b, or of $E\left[d_f\right]$ and $E\left[d_m\right]$. Since these quantities are not known, certain simplifications are made.

Analogous to Equations 14 and 18 for the expected values are two integrals for the variances:

$$\sigma_f^2(a,b) = \frac{2}{\pi} \int_0^{\pi/2} d_f^2(a,b;\Theta) \, d\Theta - E^2 \lfloor d_f \rfloor$$

Similarly,

$$\sigma_m^2(a,b) = \frac{2}{\pi} \int_0^{\pi/2} d_m^2(a,b;\Theta) \, d\Theta - E^2 \lfloor d_m \rfloor$$

Equations 15 and 16 can be substituted into these, and the integrals can be found in closed form:

$$\sigma_f^2(a,b) = 2(a^2 + b^2) - E^2 \lfloor d_f \rfloor \tag{25}$$

$$\sigma_m^2(a,b) = 4ab - E^2 \lfloor d_m \rfloor \tag{26}$$

The use to be made of these results is as follows. Under certain regularity conditions of the underlying population distribution and when n is sufficiently large, the Central Limit Theorem asserts:

$$\text{Var} \, (\bar{d}_f) = \frac{1}{n} \sigma_f^2 \tag{27}$$

$$\text{Var} \, (\bar{d}_m) = \frac{1}{n} \sigma_m^2 \tag{28}$$

Equations 25 and 26 cannot be applied in an experimental case, since a and b are not known exactly. One approach is to estimate them by using observed sample variances:

$$s_f^2 = \frac{1}{n-1} \sum_{n-1}^{n} \left\{ d_f(\Theta_i) - \bar{d}_f \right\}^2$$

A similar calculation is made for s_m^2.

As an alternative, the following approach is proposed. Let $\bar{a}$ and $\bar{b}$ be quantities obtained from $\bar{d}_f$ and $\bar{d}_m$ as described above. In Equations 25 and 26 replace the four theoretical parameters by their observed values. The following estimates of σ_f^2 and σ_m^2 are obtained.

$$c_f^2 = 2(\bar{a}^2 + \bar{b}^2) - \bar{d}_f^2 \tag{29}$$

$$c_m{}^2 = 4\bar{a}\bar{b} - \overline{d_m}{}^2 \tag{30}$$

These estimates can be justified in part in the following way. If, by chance, $\overline{d_f}$ and $\overline{d_m}$ are exactly equal to $E\left[d_f\right]$ and $E\left[d_m\right]$, then $c_f{}^2$ and $c_m{}^2$ are exactly equal to $\sigma_f{}^2$ and $\sigma_m{}^2$. The same cannot be said of $s_f{}^2$ and $s_m{}^2$.

In order to illustrate the use of these quantities, consider again the numerical example. By using the previous values, Equations 29 and 30 yield:

$$c_f{}^2 = 9.4$$

$$c_m{}^2 = 7.4$$

Again, from the Central Limit Theorem as expressed by Equations 27 and 28, we can assert that the following inequalities hold approximately 68% of the time, provided that n is sufficiently large.

$$-\frac{\sigma_f}{\sqrt{n}} \stackrel{\sim}{<} \overline{d_f} - E\left[d_f\right] \stackrel{\sim}{<} \frac{\sigma_f}{\sqrt{n}}$$

$$-\frac{\sigma_m}{\sqrt{n}} \stackrel{\sim}{<} \overline{d_m} - E\left[d_m\right] \stackrel{\sim}{<} \frac{\sigma_m}{\sqrt{n}}$$

Assuming a sample size of twenty for the example leads to:

$$7.507 \stackrel{\sim}{<} E\left[d_f\right] \stackrel{\sim}{<} 8.877$$

$$4.740 \stackrel{\sim}{<} E\left[d_m\right] \stackrel{\sim}{<} 5.960$$

By proceeding in the same way, estimates can be made for the variances of $\bar{a}$ and $\bar{b}$. Rewrite Equations 22 and 23 in the form:

$$\bar{a} = \frac{\pi}{4E(\overline{b/a})} \, \overline{d_f}$$

$$\bar{b} = \frac{\pi}{4K(\overline{b/a})} \, \overline{d_m}$$

In view of previous remarks, assume that $\overline{b/a}$ is known very accurately compared to $\overline{d_f}$ and $\overline{d_m}$. Accordingly, $E(\overline{b/a})$ and $K(\overline{b/a})$ can be considered constants. This gives:

$$\text{Var }(\bar{a}) \approx \left\{ \frac{\pi}{4E(\bar{b}/\bar{a})} \right\}^2 \text{Var }(\overline{d_f})$$

$$\text{Var }(\bar{b}) \approx \left\{ \frac{\pi}{4K(\bar{b}/\bar{a})} \right\}^2 \text{Var }(\overline{d_m})$$

Again assuming a sample of twenty for the example, it is found that:

$$\text{Var }(\bar{a}) \approx 0.25$$

$$\text{Var }(\bar{b}) \approx 0.029$$

Finally, the true population parameters, a and b, will satisfy the following inequalities approximately 68% of the time.

$$5.5 \lesssim a \lesssim 6.5$$

$$1.33 \lesssim b \lesssim 1.67$$

To conclude, it is worthwhile to discuss the interpretation of the results and also the possibilities for extending them. Suppose a sample of particles is drawn from a population of arbitrary nonuniform particles, not necessarily ellipses. All the measurements and calculations described above can still be performed. The values of $\bar{a}$ and $\bar{b}$ obtained can be thought of as the semiaxes of a reference ellipse that characterizes the particle population in some sense. This is exactly analogous to the way in which the Stokes' diameter is used.

One possible generalization of the results would be to permit a and b to possess probability distributions of their own. In the present case of two parameters, a joint distribution should be chosen. Assuming one can be selected, the analytic calculations become enormous. All the single integrals become double or triple integrals. In order to get estimates of variance in the present case, certain approximations had to be made; these were not entirely satisfactory. For the extended problem, even this step would probably not be possible at all. The most promising approach for this larger problem appears to be the use of large-scale sampling experiments on a digital computer.

B. Possible Developments in Shape Factor Analysis Techniques

From the studies reported in Section A on the possibility of using the ratio of Martin's to Ferret's diameter to characterize shape factors of irregularly shaped particles, it is obvious that any method of measuring that takes into account orientation by seeking to make many measurements of a magnitude projected into a fixed direction is an inefficient measuring technique. In the following discussion, possible techniques for measuring shape factors independent of orientation are outlined.

The ratio of the radii of two circles that encircle some paramaters of the particle profile could be a very useful shape factor. One possible shape factor of this type would be the ratio of the radius of the circumscribing circle whose center is on the center of gravity of the particle profile to the radius of the circle of equal area. This shape factor we define as the extension shape factor. This shape factor would be independent of the orientation of the particle and would not involve estimating the position of tangents with regard to a fixed direction. It would have the disadvantages that two operator decisions would be required: (1) the location of the appropriate center and (2) the judgment of equal areas.

It is probable that the first judgment would not be too difficult and that the second would be an easier judgment than estimating Martin's diameter, but this would have to be investigated experimentally by conducting a series of tests with a team of operators and a set of test profiles. This measurement could be carried out very rapidly by using a variable-iris diaphragm and photomicrographs. The use of the circle of equal area is suggested because this would facilitate isolation of particles of the same size but with different shapes. This shape factor would have a value of 1 for a spherical particle, and the value would increase for an elongated particle.

Another shape factor of the same type we can call an extremity shape factor. The extremity shape factor would be defined as the ratio of the radius of the circumscribing circle to the inscribed circle when the center of both circles is on the center of gravity of the particle profile. This shape factor would also be equal to unity for a spherical particle but would increase more rapidly than the extension shape factor as the particle profile became elongated. It would reduce operator decisions to location of the particle center and to recognition of intersections. It is anticipated that these operator decisions would be relatively free from bias and cause little fatigue. However, the isolation of differently shaped particles and concurrent sizing of the particles would be more difficult.

It is probable that the extension shape factor could be measured easily by photoelectric means. The particle profile could be placed in a light beam with its center on the axis of the beam and a diaphragm opened. The radius of the circumscribing circle is the value of r at which the received light intensity begins to increase in proportion to $2\pi r dr$. It should be possible to visually display gain against expected gain or to have a meter indicate when this situation is reached.

To measure the circle of equal area, the particle profile is moved and the diaphragm reduced until the intensity without the particle has dropped to that with the particle. Alternatively, the optical system could be altered, and an increasing black circle could be used to measure the obscuring power of the particle. It should be possible to gain high precision for a relatively small amount of work with these shape factors, since they are independent of the orientation of the particles.

This type of shape factor could be very useful in the analysis of photomicrographs. With improved methods of obtaining photomicrographs, such as the use of Polaroid film, these types of shape factor could acquire important technical meaning.

A different type of shape factor that may have important properties is the ratio of the perimeter of the particle to the square root of the area. This shape factor would have a minimum of $2\sqrt{\pi}$ for a circle and would increase with increasing departures from the circular shape. Probably this type of shape factor has not been used in the past because of the difficulties associated with the measurement of the perimeter.

V. SIMULATION OF PACKING OF PIGMENT PARTICLES IN PAINT FILMS

In order to obtain a satisfactory model for studying the penetration of light through a pigmented film, it is necessary to study the structure of a randomly packed paint film. Direct studies of the packing of powders of different shape and size distributions have been reported by various workers (ref. 17-20).

The experiments described in this section were carried out to explore the possibility of using a new technique for simulating the packing properties of small particles. This preliminary discussion will be limited to monosized spheres assembled in a random manner.

Consider sections taken at random through a sphere. All sections are equally probable. It can be shown that the fractional area of solids exposed by a section taken through a random packing is numerically equal to the volume fraction of solids in the three-dimensional packing. Therefore, it should be possible to simulate the appearance of a section through a three-dimensional packing by using the probability distribution of particle sections that can be in the plane of the section and by using some appropriate plotting technique for locating the particle sections in the plane of the section.

To carry out a trial set of experiments, we considered the packing of spheres of 2.5-in. diameter. To simulate sections through this sphere, a circle of 2.5-in. diameter was thrown at random onto a set of parallel lines 0.25 in. apart. The diameters of the 10 sections formed by the straight lines were as follows.

Section No.	Diameter, in.
1	1.40
2	1.95
3	2.25
4	2.45
5	2.50
6	2.49
7	2.35
8	2.10
9	1.65
10	0.80

A set of circles with these diameters was prepared. The first plotting schedule tried was as follows. A large circle of 15-in. diameter was drawn on a graph paper having rectangular coordinates. A profile was selected at random by selecting an integer between 1 and 10. The profile selected was placed at the center of the large circle. A series of profiles was selected at random from random-number tables. When a profile was added to the system being built up in the large circle, it was allowed to touch the profile nearer the center and the last profile was added. The buildup of profiles proceeded in a clockwise manner. The procedure was repeated until the large circle was full of profiles.

As the cluster of circular profiles approached the perimeter of the containing circle, it was not always possible to place the selected profile and a second choice had to be made. Eventually, when the plotting was completed, the region in the vicinity of the perimeter was deficient in profiles with respect to the regions near the center of the system, because of the impossibility of plotting circles that intersected the perimeter. The low density in the region of the perimeter of the system is termed "edge effect" in this discussion.

To measure the local porosity of a selected region within the system of profiles, a circle of 10 in., i.e., 4 sphere diameters, was placed on top of the system. In the first experiments the position of the center of the circle was chosen by choosing two random coordinates from a random-number table such that the superimposed circle did not come within 1 in. of the perimeter of the 15-in. circle. The porosity of the 10-in. circle was measured by tracing out the equivalent solid portions onto the 10-in.-diameter disc. These portions were then cut away. The residual fractional weight of the disc was numerically equal to the porosity, if uniform thickness of the paper is assumed.

By arranging for the test circle of 10 in. to be well within the simulated packing field, edge effects were excluded.

Table 2 reports the data for eight experiments. These porosities were lower than those reported for random packing.

Table 2

MEASURED POROSITIES FOR SIMULATED PACKING
OF MONOSIZED SPHERES WITHOUT END EFFECTS

Trial	Density Packing	Porosity
1	0.816	0.184
2	0.831	0.169
3	0.829	0.171
4	0.825	0.175
5	0.819	0.181
6	0.830	0.170
7	0.806	0.194
8	0.823	0.177

The experiments were repeated, and the search circle was allowed to touch the perimeter of the simulated packing. In this way, edge effects were included. The porosity was measured, and these data are given in Table 3. The porosity was higher and was closer to that of real random packings, which normally involve edge effects.

Table 3

MEASURED POROSITIES FOR SIMULATED PACKING
OF MONOSIZED SPHERES WITH END EFFECTS

Trial	Density Packing	Porosity
1	0.740	0.260
2	0.764	0.236
3	0.755	0.245
4	0.772	0.228
5	0.756	0.244
6	0.761	0.239
7	0.759	0.241
8	0.760	0.240

A figure often quoted for randomly packed monosized spheres is 39.5% (ref. 20). The simple simulated model described here obviously does not adequately take into account the competition for space by adjacent spheres.

In Section IIIG it was shown that the average track density across a field of view is numerically equal to the porosity. The formula was tested by drawing lines at random on the simulated field of view and measuring the track density per unit line, but the line was terminated 1 in. from the perimeter, so that edge effects were eliminated. The results for 20 measurements are shown in Table 4. From this distribution of results, plotted in Figure 14, it can be seen that the measured porosities are distributed according to the Gaussian equation with a mean value of 81%. This value compares well with the porosity measurements made by the search-circle-weighing technique.

Table 4

MEASURED POROSITIES FOR PACKING OF RANDOMLY CHOSEN LINES
ENDING 1 IN. FROM EDGE

Trial	Density Packing	Porosity
1	0.905	0.095
2	0.863	0.137
3	0.751	0.249
4	0.869	0.131
5	0.816	0.184
6	0.813	0.187
7	0.722	0.278
8	0.869	0.131
9	0.857	0.143
10	0.827	0.173
11	0.768	0.232
12	0.882	0.118
13	0.764	0.236
14	0.853	0.147
15	0.815	0.185
16	0.746	0.254
17	0.775	0.225
18	0.840	0.110
19	0.849	0.151
20	0.747	0.253
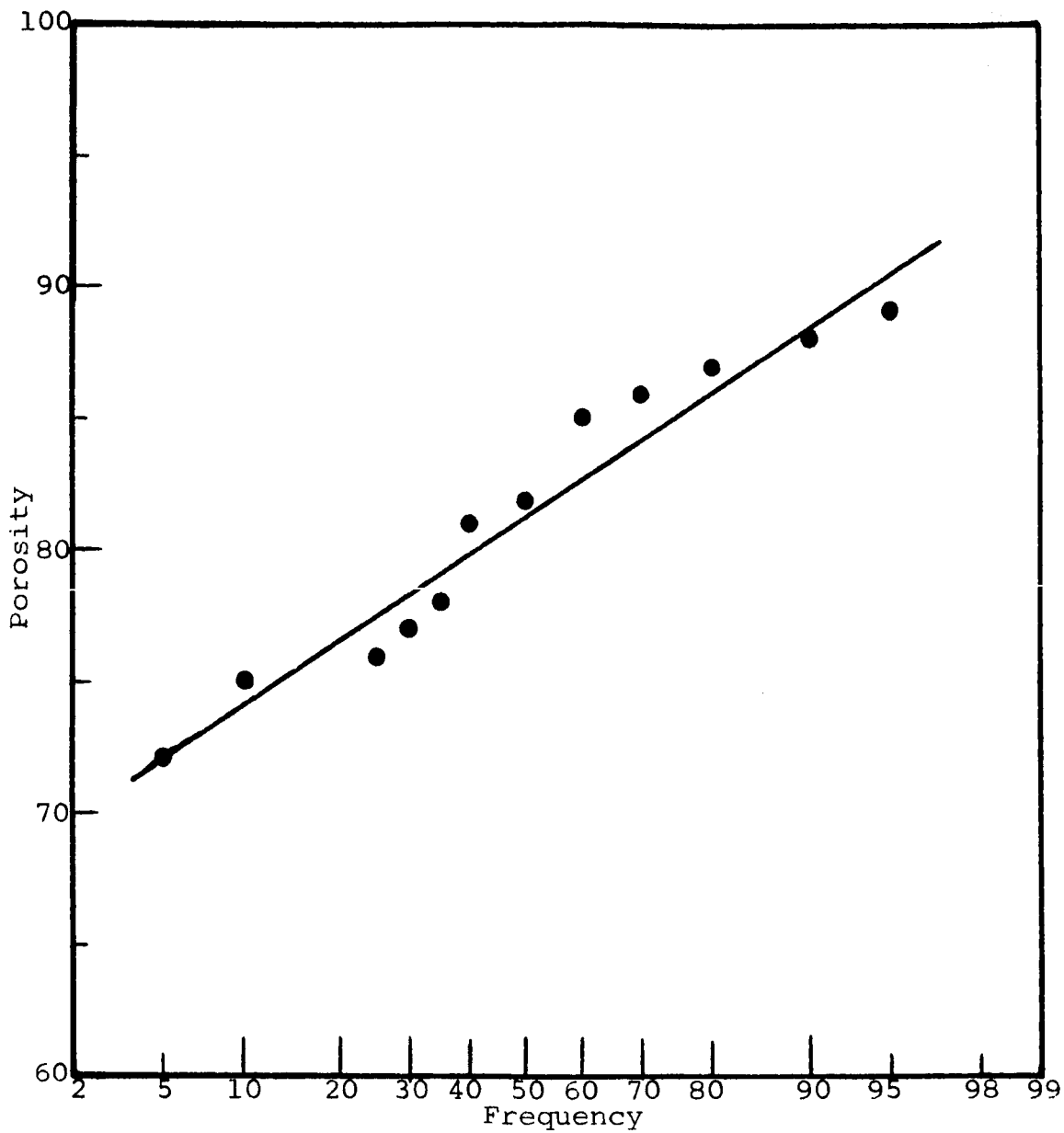
Figure 14

FREQUENCY OF OCCURRENCE OF POROSITIES LESS THAN STATED SIZE

VI. USE OF MONTE CARLO METHODS IN PAINT TECHNOLOGY

The Monte Carlo technique for solving complex physical problems has received considerable attention since it was used by Von Neuman and Ulam to solve the problems of neutron shielding associated with the design of atomic reactors. McCracken (ref. 21) has given an excellent introduction to the theory of Monte Carlo techniques. He points out that the basic procedure in a Monte Carlo method for solving problems is to construct a statistical model of a complex physical problem. The behavior of the physical system is then simulated by studying the behavior of the statistical model. McCracken discusses the problem of a neutron traveling through matter; and he points out that we can write mathematical formulas for the probabilities at each collision, but we are often not able to write anything useful for the probabilities of an entire sequence of collisions.

The problems associated with the study of light transmission through a paint film are somewhat analogous to the problems associated with radiation penetration through a paint film. Because the pigment particles are randomly distributed through the paint film and because their size is of the same order as the wavelength of light, we cannot use macroscopic optic theory with its associated concepts of reflection and refraction. The radiation penetration problem involves the solution of many random interactions between randomly directed photons and randomly distributed particles.

For a system of interaction of this kind, we construct probability equations; but, as in the case of neutron shielding discussed by McCracken, it is virtually impossible at the present stage of technology to write anything useful for the probability of an entire sequence of interactions.

From a study of the literature of paint film research, it appears that too many scientists have been preoccupied with studying to a high degree of precision isolated physical properties of individual constituents of the paint film and

that little research has been directed toward the interaction between physical variables within the paint film.

In an attempt to elucidate the complex phenomena occurring within a paint film, we have explored the possibility of constructing several statistical models of a paint film. The properties of these statistical models have been investigated to determine whether anything concerning the properties of real paint systems can be deduced from the models. In justification of this novel approach to solving problems of paint technology, it should be noted that Van de Hulst (ref. 23) has recently criticized current attempts to solve multiple-scattering problems. He states that "too much emphasis has been placed upon redoing with better accuracy and more refined mathematical methods the problems for which rough answers are already available." He also points to the encouraging fact that "usually, the intuitively chosen solution turns out to be the correct one." By implication, he exhorts the scientist to seek intuitive solutions to some of the more complex interaction problems.

VII. RANDOM-WALK MODEL FOR STUDYING ENERGY PENETRATION THROUGH PAINT FILMS

A. Theoretical Considerations

In an initial attempt to construct a statistical model of a paint film we considered the possibility of studying the interaction of radiation in a cloud of particles many diameters apart. It was postulated that a study of the variation in properties of the scattering behavior of a well-dispersed cloud as the solids concentration increased could give some indication of the behavior of a paint film.

The initial idea consisted of considering the interaction between a beam of light and a particle by using Mie theory and then calculating the secondary scattering events from a knowledge of the probability distribution of particles in the cloud. This successive study of energy events cascading through the cloud is, in effect, a random-walk study.

A regular array of particles in the cloud would at first sight appear to be the simplest model for studying interaction phenomena. A regular array of particles is shown in Figure 15. In a cloud of this type the density of scattering centers is not independent of the direction of the incident radiation. In fact, a random array of particles is the simplest model to treat, since the properties of the array on the average (averaged over a sufficient distance) are independent of the direction of travel. The only effect of nonnormal incidence is that a given thickness of film appears thicker. These effects are illustrated in Figure 16. It may therefore be possible to study several random walks through a random array and average them for an average effect.

To investigate penetration of radiation through a cloud of particles, consider radiation incident on a particle. After interaction, the energy will be radially distributed about the center of the particle. Then consider possible locations of the next sphere encountered and determine how the energy is distributed.
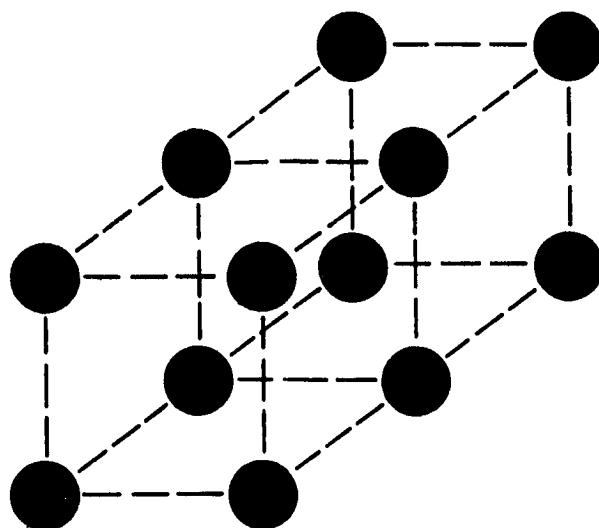
Regular array of
particles in a cloud
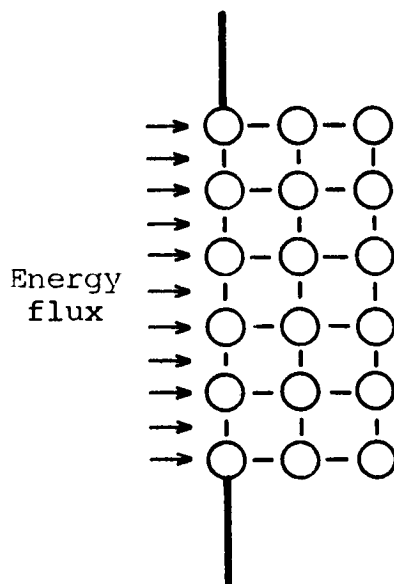
Energy
flux

Two-dimensional representation of
energy penetration of the array

Figure 15

PROPERTIES OF A CLOUD OF PARTICLES IN REGULAR ARRAY
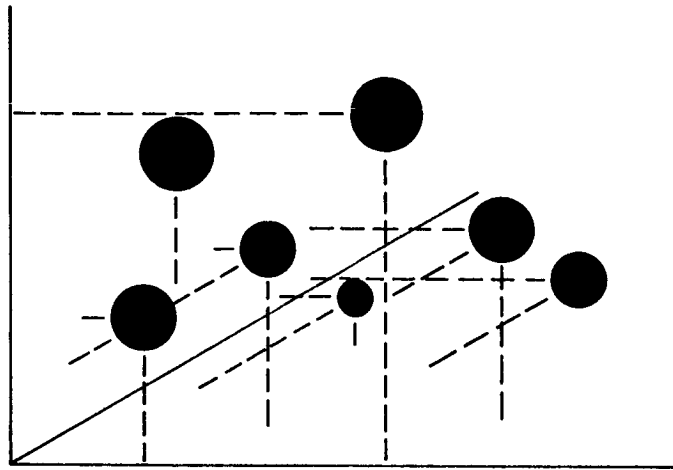
Three-dimensional array
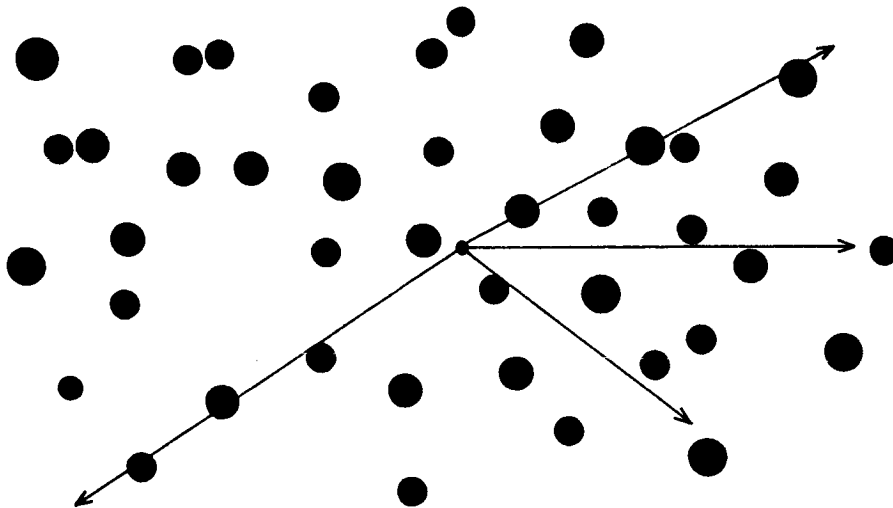
Two-dimensional array

Figure 16

RANDOM ARRAYS

A random array has properties independent of the
direction studied if averaged over a sufficient
distance; i.e., on the average, a line drawn in
any direction intercepts the same number of particles.

For instance, in Figure 17 the center of the prime scattering is denoted by O. The arrow AO denotes vectorially the direction and magnitude of the incident radiation and is not intended to represent the physical nature of the interaction between the particle and the light beam. The other arrows, OB, OC, OD, etc., denote the magnitude and direction of the scattered radiation in the various angular bands delineated by the dotted lines. The distance to the next sphere encountered in any direction will vary according to the solids concentration of the array and to random fluctuations in position.

Initially, let us study the direction parallel to the incident radiation. Let G be the center of the second scattering sphere when the scattering spheres touch and H the center at the greatest probable distance. For any given concentration of solids it should be possible to calculate the probability distribution of the second scattering centers between G and H. For each position of the scattering center along GH the solid angle subtended by the second sphere can be calculated, and the energy in this case can be considered to interact with the second sphere. By averaging for all possible locations and by weighting the average to allow for the probability of occurrence, the average energy occurring at I (the edge of the sphere of influence of the second interaction) can be calculated.

The next stage of development is calculation of the probability distribution of particle centers within the cloud. Let

ε = volume fraction of empty space in the particle cloud

= volume fraction of vehicle in collapsed cloud, i.e., a paint film

n = number of particles per unit volume of system

V_p = volume of particle

α = $1 - E$ = volume fraction of particles in a cloud (note α/V_p = n)

ϕ = solid angle that the second particle subtends with respect to the center of the prime scattering particle

Prime scatterers

Possible location of
secondary scattering center
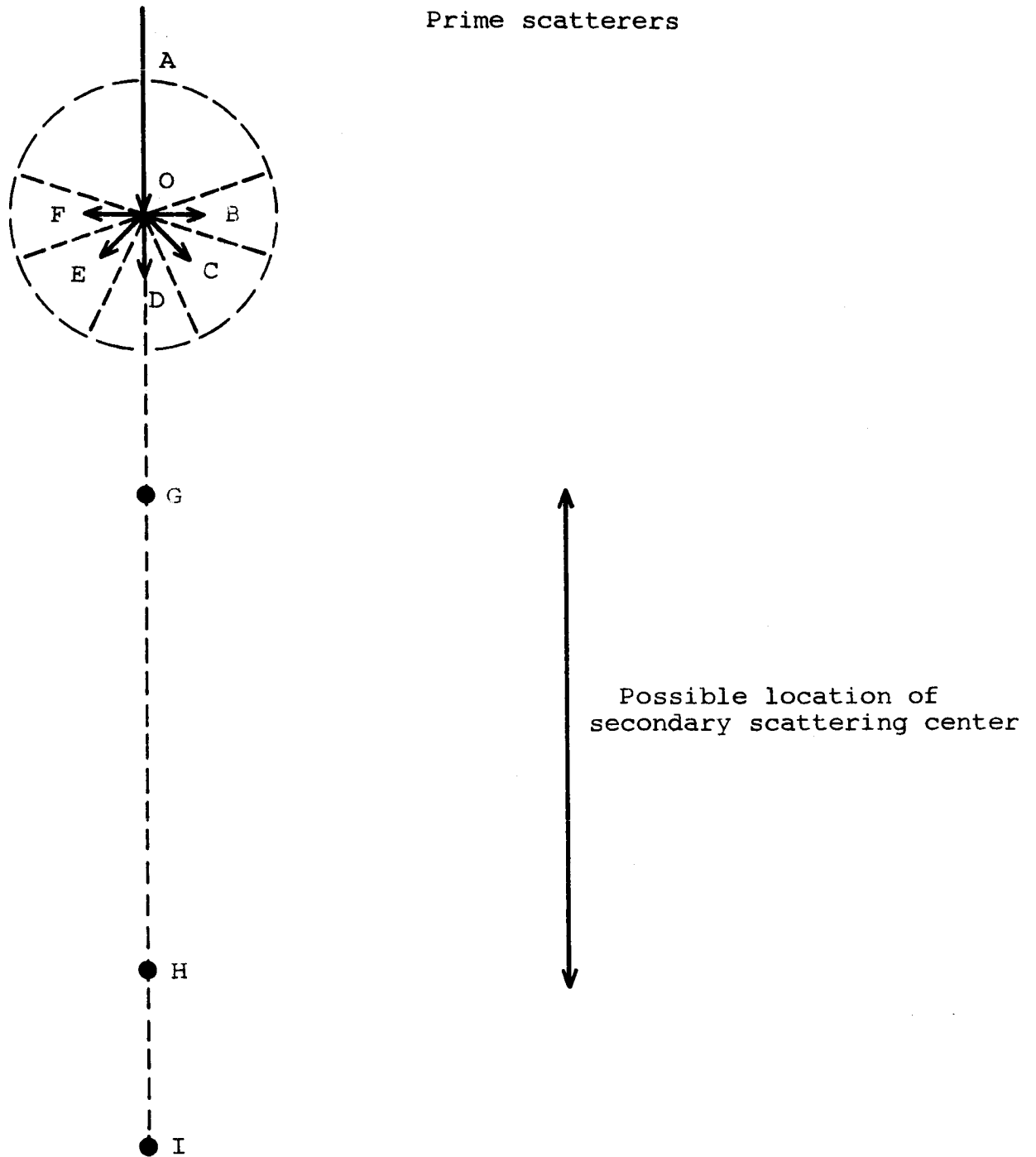
Figure 17

SCHEMATIC DIAGRAM OF INTERACTION OF RADIATION WITH A PARTICLE

σ = extension factor used to take into account that a particle exerts an influence over a greater area than its physical projected area

$F(\phi)_{xyz}$ = function defining the energy entering a solid angle ϕ that has as its axis the line joining the centroid of the area defining the solid angle ϕ, the coordinates of the centroid being x, y, and z

V_s = volume of cloud studied.

The simplest average interparticle distance that can be calculated for a monosized system of spheres is that for a system in which the particles are assembled in a symmetrical, cubic array. This simple average is a useful average even when considering the properties of a random array, because from it we can calculate the order of magnitude of particle separation within a given cloud. Such a system is shown in Figure 18.

Let x be the distance between centers. It follows from the symmetry of Figure 18 that each particle occupies a volume x^3 of the array. Therefore

$$\frac{1}{n} = x^3$$

where n is the number of particles per unit volume. Now

$$V_p = \frac{1}{6}\pi d^3$$

where d is the diameter of the particle. Then

$$n = \frac{\alpha}{V_p} = \frac{\alpha}{\frac{1}{6}\pi d^3} = \frac{6\alpha}{\pi d^3}$$

where α is the volume fraction of particles. Therefore

$$x^3 = \frac{\pi d^3}{6\alpha}$$

and

$$x = d\sqrt[3]{\frac{\pi}{6\alpha}}$$

Let y be the number of particle diameters between particle centers.
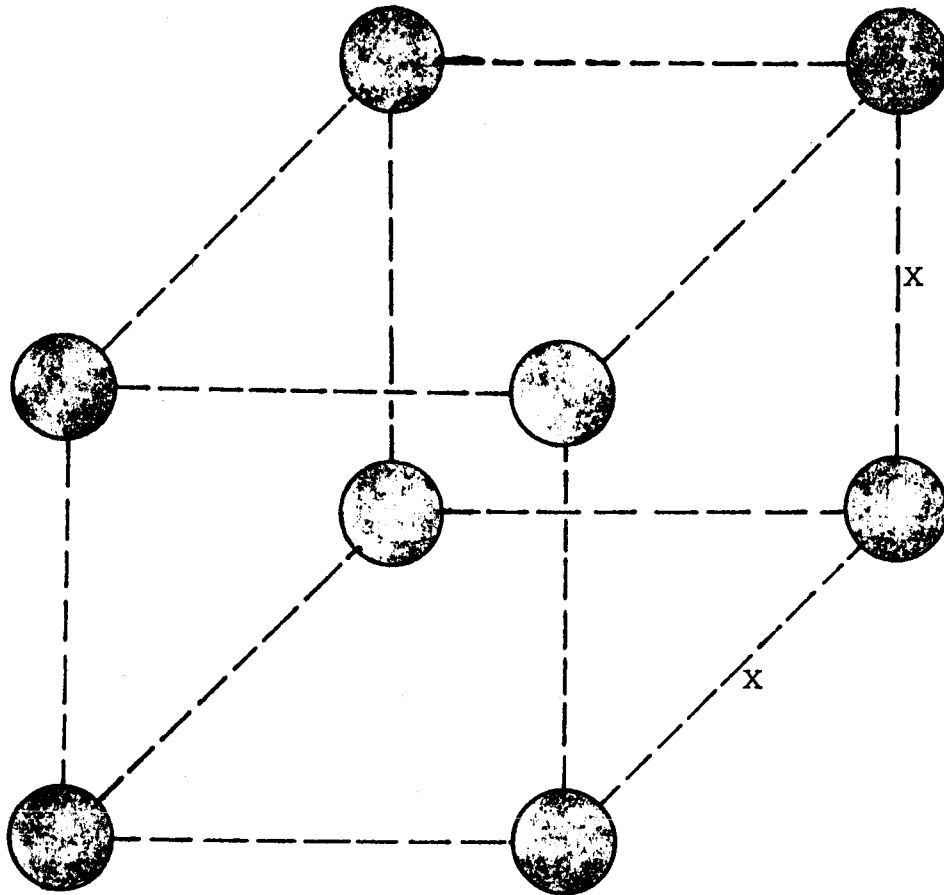
Figure 18

INTERPARTICLE DISTANCE IN A MAXIMUM SEPARATION UNIFORM ARRAY

$$y = \frac{x}{d} = \sqrt[3]{\frac{\pi}{6\alpha}} = 0.806 \sqrt[3]{\frac{1}{\alpha}} \tag{31}$$

From this relation we see that the average interparticle distance in a symmetrical array is a function of the volume concentration only.

A graph of the relationship in Equation 31 is shown in Figure 19. The volume concentration at which the particles touch is that for $y = 1$. For nonspherical particles in random array, the values read from the curve in Figure 19 are not exact but do indicate the order of magnitude for intersurface separation.

B. Solid Angles Subtended in Multiple-Particle Systems

The discussion here is limited to spherical particles. An important factor determining the effects of multiple scattering within a cloud of particles is the distance between the particles. Since the scattered light from a particle is non-homogeneous in space, the interaction with a particle at a given distance varies with its orientation in space with respect to the direction of the incident beam and the center of the prime scattering particle.

A general relationship concerning the position of the second particle can be expressed as follows. For a plane wave incident on a spherical particle as shown in Figure 20, the second particle shown subtends a solid angle ϕ defined by:

$$\phi = \frac{\text{projected area of particle}}{R^2} = \frac{(\pi/4)d^2}{R^2} \tag{32}$$

If the x,y,z coordinates of the system shown in Figure 20 are defined by the fact that the y-z plane is perpendicular to the direction of the incident radiation, it follows that

$$R^2 = x^2 + y^2 + z^2 \tag{33}$$

Therefore

$$\phi = \frac{\pi}{4} \frac{d^2}{x^2 + y^2 + z^2} \tag{34}$$
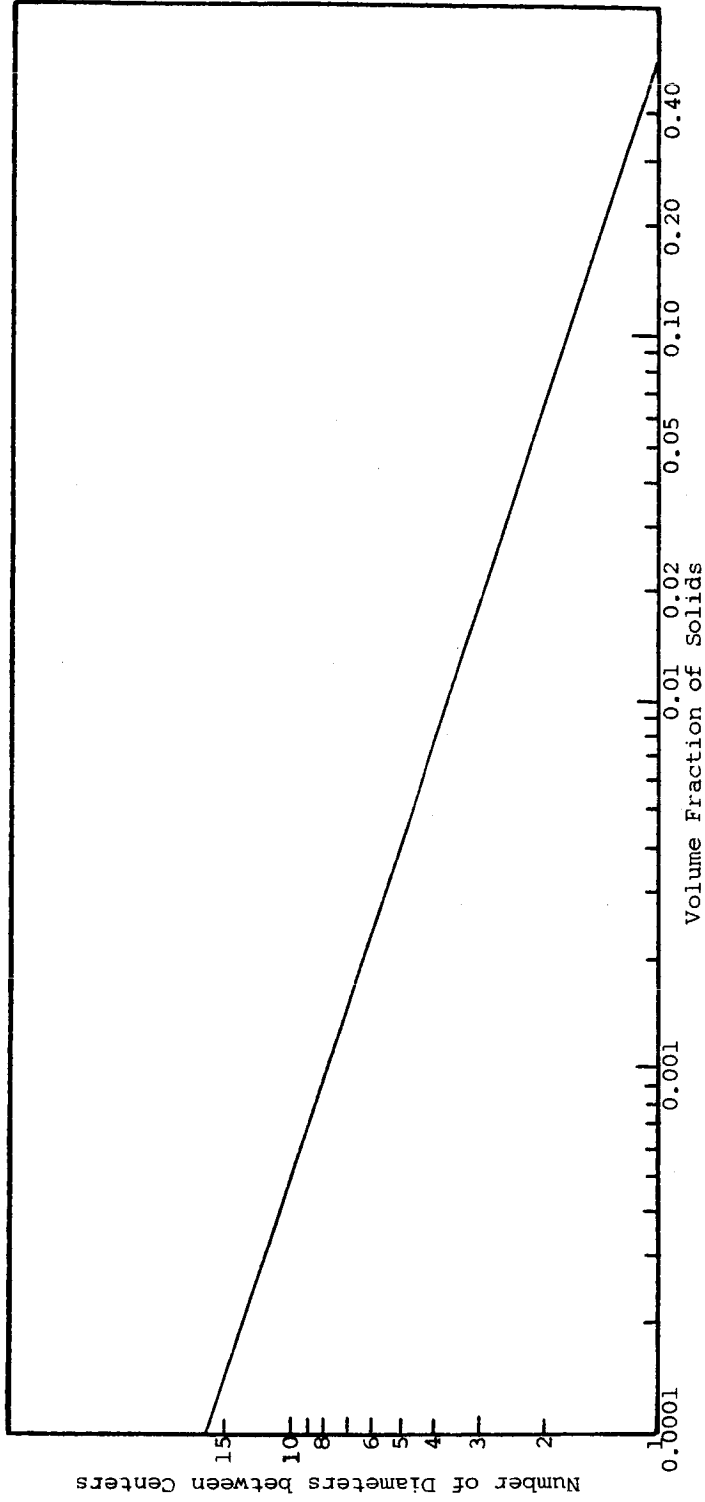
Figure 19

RELATIONSHIP BETWEEN VOLUME FRACTION OF SOLIDS AND INTERPARTICLE DISTANCE
IN A MONOSIZED MAXIMUM INTERPARTICLE DISTANCE ARRAY
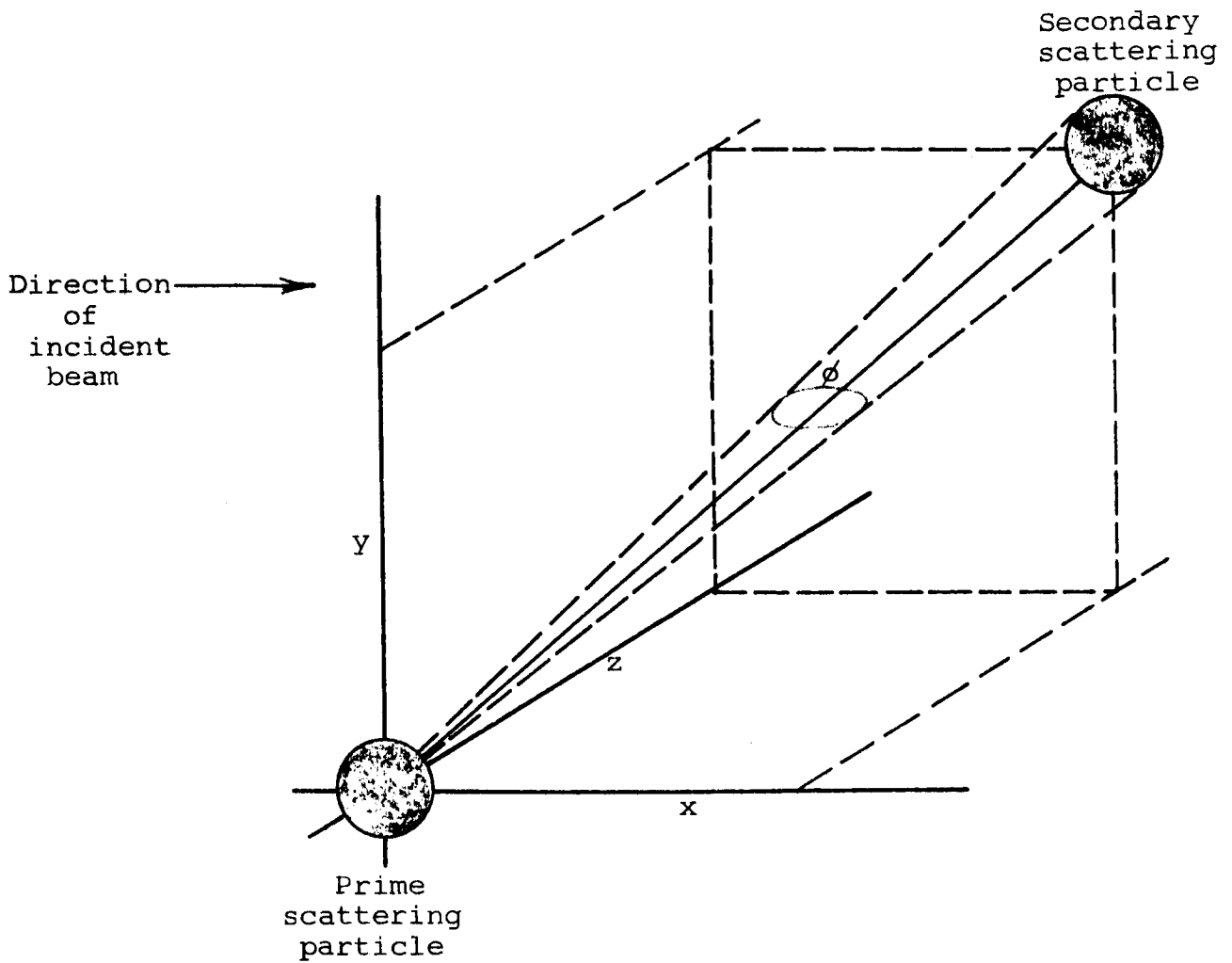
Figure 20

RELATION OF PRIME TO SECONDARY SCATTERING PARTICLES

Let the general function for the distribution of the scattered energy from the prime scattering particle be $F(\phi)_{xyz}$, where $F(\phi)$ denotes a general function of ϕ and x,y,z are the coordinates of the line joining the center of the particle to the centroid of the area defining the solid angle ϕ. The solid angle of influence of the second scattering particle is greater than its nominal solid angle, since radiation adjacent to the perimeter is also affected by the particle.

Let σ be an extension parameter such that $\phi\sigma$ is the area over which the particle influences the incident radiation. At the present stage of development of the theory we assume that σ is a function both of d/λ, the ratio of the particle diameter, and of S, the direction; λ is the wavelength of the radiation considered.

An important quantity in predicting the effects of multiple interaction is the solid angle subtended by a particle that is a specified number of diameters away from secondary particles; i.e., R is expressed as a number of diameters.

Let R $= $ yd. The solid angle subtended is:

$$\phi = \frac{\pi d^2}{4} \frac{1}{y^2 d^2}$$

$$\phi = \frac{\pi}{y^2 4} \tag{35}$$

Now the scattered energy is distributed into 4π steradians. The numerical fraction of scattered energy intercepted by a particle y diameters from the first particle is:

$$(f)_y = \frac{\pi}{y^2 4} \frac{1}{4\pi}$$

$$(f)_y = \frac{1}{y^2 16} \tag{36}$$

A plot of the relationship in Equation 36 is given in Figure 21.
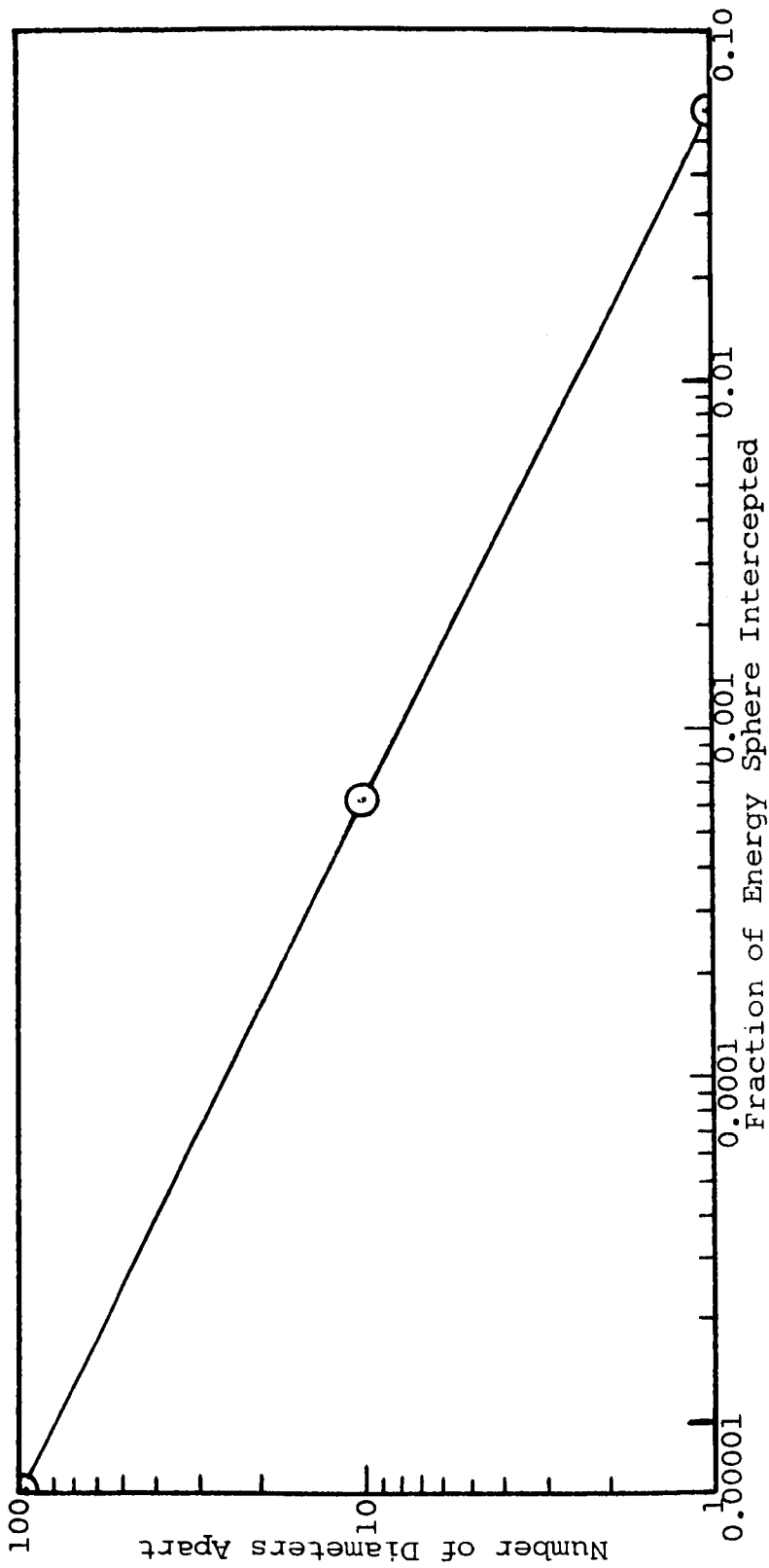
Figure 21

FRACTION OF ENERGY SPHERE INTERCEPTED AT ANY GIVEN DIAMETER SEPARATION
OF TWO EQUAL SPHERES

C. Probability Distribution of Interparticle Distances within a Dilute Cloud of Particles

An approximation to the interparticle distance within a cloud of particles in which the particles are randomly distributed can be obtained in the following manner.

Consider a single reference sphere as shown in Figure 22. At the closest approach of a second sphere to the first sphere the center of the second sphere lies on a sphere of radius 2r. Let us consider a portion of the cloud defined by the radius S, and let this be termed the sphere of study. Now let the sphere of study be divided into x spherical shells of thickness ρ. The volume of the mth spherical shell is $4\pi(2r + m\rho)^2$. The volume of the sphere of study is $4\pi(2rtp)^2$. Therefore the probability that the second sphere center lies within the mth shell is:

$$P_m = \frac{4\pi(2r + m\rho)^2\rho}{\sum\limits_{i=0}^{i=n} 4\pi(2r + i\rho)^2\rho} \tag{37}$$

Now

$$\sum\limits_{i=0}^{i=n} 4\pi(2r + i\rho)^2\rho = \text{volume of shell that can contain the particle center}$$

$$= \frac{4}{3}\pi\left(s^3 - d^3\right)$$

Therefore

$$P_m = 3\frac{(d + m\rho)^2}{s^3 - d^3} \tag{38}$$

If we consider a certain volume of the cloud, on the average the number of particles in this portion of the cloud is:

$$(N)_V = Vn = \frac{\alpha V}{V_p}$$

where V is the volume of the cloud selected.
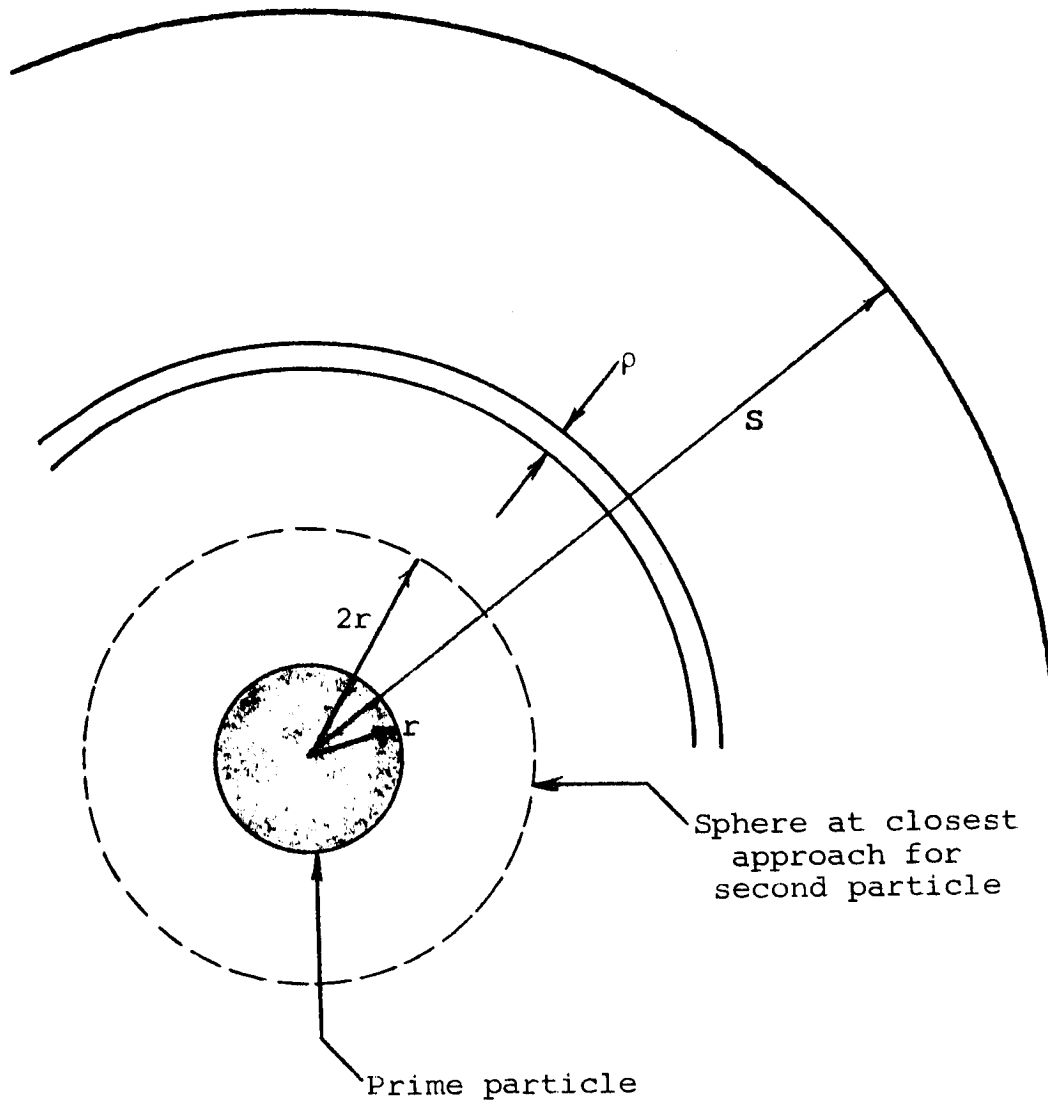
Figure 22

REFERENCE SPHERE FOR DETERMINING PROBABILITY DISTRIBUTION
OF INTERPARTICLE DISTANCES WITHIN A DILUTE CLOUD

If N is very large, then to the first order of magnitude any sample of cloud of volume V isolated from the cloud would have N particles. As the absolute value of N decreased, the actual number within the isolated portion would fluctuate at random. It is generally recognized that if N is approximately 25, random fluctuations in the sampled volume are relatively small.

If N is greater than 25 and the volume of the cloud studied is the same as the study volume of the earlier derivation, $N/\alpha = V_s/V_p$. Since $V_s/V_p = s^3/d^3$,

$$\frac{N}{\alpha} = \frac{s^3}{d^3} \tag{39}$$

Now let $\rho = d/\beta$, where β is some convenient number. Then the number of shells of thickness ρ in the study volume is:

$$\gamma = \frac{S - d}{\rho} = \frac{S - d}{d} \beta$$

$$\gamma = \left[\frac{N}{\alpha}^{1/3} - 1 \right] \beta \tag{40}$$

By substituting for S, d, and ρ in Equation 38,

$$P_m = \frac{3}{\beta} \left[\frac{1 + m\beta}{(N/\alpha) - 1} \right] \tag{41}$$

for $m = 1 \rightarrow \gamma$

By expressing all distances in fractions of a diameter, an expression that is independent of the particle diameter has been attained. (A check on the validity of the equation is provided by the fact that all relationships are dimensionally correct.)

Another general relationship that is useful in discussing multiple interaction is the value of P_m in terms of P_1, the probability that the first shell is occupied. We note that

$$\frac{P_m}{P_1} = \frac{3}{\beta} \left[\frac{1 + m\beta}{(n/\alpha) - 1} \right] \cdot \frac{\beta}{3} \left[\frac{(N/\alpha) - 1}{1 + \beta} \right]$$

$$\frac{P_m}{P_1} = \frac{1 + m\beta}{1 + \beta} \qquad (42)$$

With the aid of these general equations, we can draw up a descriptive array in two dimensions of a three-dimensional cloud.

The relationships developed in this section apply to the geometric relationship of particles in a cloud. They have not been used intensively to study paint theory because the implications of Equation 31 were that in a paint film the particles are too close for the cloud model to be valid. For instance, it can be seen from Figure 19 that at the average distances between particle centers to be expected in normal paint films of about 40% by volume solids concentration, there is a high probability that many of the surfaces of the particles will be in contact. This physically resembles the situation that occurs when the cloud is completely collapsed. The special features of a collapsed cloud are loss of identity by individual particles that are in intimate contact and high density of scatterers per unit volume.

In view of these special features of a closely packed pigment particle system, it was decided that a random walk consisting of a series of discrete particle/energy encounters was not an appropriate model for current high-pigment-density paint systems. Therefore, studies of random walks through dilute cloud systems were discontinued.

VIII. MONTE CARLO STUDIES OF GROWTH IN SCATTERING CENTERS AT VARIOUS CONCENTRATIONS OF PIGMENT

A. Simple Model of Monosized Cubic Pigment without Extender

1. Construction of the Monte Carlo Plot

The penetration of radiation into a dispersed particle system and the probabilities of secondary scattering within the system were previously discussed with specific reference to clouds of particles (Report No. IITRI-C6018-13). For a complete random-walk treatment of energy penetration through a paint film comprising particles distributed randomly in a vehicle, the probabilities of the persistence of the forward beam have to be known. When these probabilities have been determined, the energy flux at any surface perpendicular to the direction of the original energy flow at a certain depth can be described by the equation:

$$E_T = E_0 P_x + E_D \qquad (43)$$

where

E_T is the total energy

E_0 is the original energy in the parallel forward beam

P_x is the probability of persistence at depth x

E_D is the diffuse energy flux.

Several problems arise in predicting the decay of the forward energy beam. Although formulas for light-scattering phenomena are useful in predicting the total energy removed from the forward direction, it is not easy (sometimes it is impossible) to determine the area of the wave front disturbed by the particle. Another major problem is prediction of the statistics of persistence of the forward beam, e.g., the number of particles that are effective scattering centers and the probability that particles along the direction of traverse will occur in line with particles nearer to the source. The following experimental system was devised to study this type of problem.

Consider a rectangular grid. Along the x-axis let there be N_x units, and along the y-axis, N_y units. Therefore, within the major grid there are $N_x N_y$ small squares. If we now consider the path of a plane parallel beam of light passing through the plane of the grid, the z-axis perpendicular to the plane of the grid represents the direction of travel. If an observer looks along the z-axis and if dispersed particles are placed between the observer and the source of light, the observer is not aware of the z coordinate of the particles. The projected representation of the particles on the x-y plane represents their appearance to the distant observer. Also, the fraction of open area seen by the observer represents the fraction of the initial forward beam penetrating the system if diffraction effects are negligible.

Therefore a series of experiments was conducted to simulate the appearance of a dispersed monosize-particle system. A piece of graph paper with 70 units along the x-axis and 100 units along the y-axis was selected. A pair of coordinates was selected from random-number tables, and the appropriate square on the grid was filled with black ink. This blacked-out square represents the shadow of the particles. If the particles are small, the square represents their effective area.[*] If the particles are large, the square represents their geometric shadow.

It can be argued that the use of square particles that cannot partially overlap (only completely, or not at all) is an artificial system. It is, but the generalizations obtained from this study are very informative and probably qualitatively correct. After all, the simple kinetic theory of gases is artificial, but it served as a useful tool in the development of the physical sciences.

---

[*]The exact meaning of "effective" depends upon the system considered and is not defined further.

In this study we consider particles larger than the wave-length of light, so that only the geometric shadow needs to be considered. To simulate the light-obscuring behavior of particles, the appropriate number of particles is plotted on the grid. Typical sets of coordinates selected from random-number tables are given in Table 5. When coordinates occur for a position that is already occupied, this represents a particle that is ineffective in destroying the forward beam. The fact that an overlapped particle has occurred is recorded, and plotting continues. The number of particle coordinates plotted represents the concentration of particles in the beam, and the number of spaces remaining represents the open area persisting. Therefore, a record of the two numbers simulates the efficiency with which the forward beam is diverted.

Table 5

TYPICAL SETS OF COORDINATES USED IN MONTE CARLO SIMULATION OF PARTICLE-SCATTERING PHENOMENA

x Coordinate	y Coordinate
7	33
71	21
30	24
75	21
76	47
14	18
47	53
67	29
80	61
94	43

At measured particle concentrations, the grid was examined visually for squares that were touching, and the number of squares within any cluster of profiles is recorded in Table 6. The total number of separate clusters was determined from the data and is presented in Table 7 (separate single particles were classed as a cluster). Figures 23 through 27 show the grid at 20, 30, 35, 45, and 50% coverage. Figures 28 through 32 show development of typical clusters with increasing particle coverage.

Number of Units in Cluster	.020	.030	.039	.048	.058	.067	.075	.085	.094	.103	.112	.121	.131	.138	.147
1	128	172	207	246	263	270	281	301	316	323	315	313	316	313	311
2	8	16	29	38	52	65	76	77	82	82	86	90	97	98	105
3		1	3	6	7	16	21	23	31	38	43	46	49	54	56
4					3	3	5	5	4	9	15	21	24	20	20
5					1	2	0	4	5	3	7	8	8	11	13
6							2	2	5	8	6	5	5	10	6
7								1	2	3	4	4	2	2	5
8											0	2	6	3	4
9											1	1	2	4	5
10												1	0	1	3
11													1	2	1
12														1	0
13															1
14															1
15															
16															
17															
18															
19															
20															
21															
22															
23															
24															
25															
26															
27															
28															
29															
30															
31															
32															
33															
34															
35															
36															
37															
38															
39															
40															
41															
42															
43															
44															
45															
46															
47															
48															
49															
50															
51															
52															
53															
54															
55															
56															
57															
58															
59															
60															
61															
62															
63															
64															
65															
66															
67															
68															
69															
70															
71															
72															

Number of Clusters at

ed Fractional Concentration

.161	.172	.179	.188	.195	0.20	0.21	0.22	0.23	0.24	0.25	0.26	0.27	0.28	0.29	0.30
302	298	289	270	262	243	239	228	213	191	174	155	151	146	135	121
100	96	95	90	92	93	89	83	84	82	83	76	73	65	66	56
55	58	57	64	65	58	56	55	56	57	52	49	52	52	47	38
27	28	25	23	23	23	21	22	31	22	22	21	20	23	25	23
18	19	21	13	15	21	20	21	16	15	17	19	17	16	15	14
10	15	15	19	19	18	15	14	16	18	19	14	11	12	9	9
6	8	12	17	16	16	16	13	12	10	10	10	12	9	7	6
3	3	3	2	2	4	10	12	15	14	13	14	15	13	10	13
6	6	7	7	9	10	8	10	9	10	11	8	4	6	8	8
4	2	2	7	5	5	7	10	10	9	11	16	11	9	6	6
3	3	3	3	7	4	6	8	8	7	5	1	3	3	5	4
0	1	1	1	2	2	3	2	3	6	4	5	5	3	4	3
0	1	0	0	0	0	1	2	4	3	6	3	2	3	3	3
1	1	2	3	1	2	3	2	2	1	1	5	3	3	1	1
1	0	2	2	3	2	2	1	2	1	3	3	4	3	3	5
	1	1	1	2	3	1	2	1	3	1	3	2	5	5	3
					1	0	1	2	1	1	2	2	3	0	2
					0	0	0	0	2	2	1	1	1	0	0
					0	0	1	0	0	1	3	2	1	1	0
					0	0	0	1	2	1	0	4	0	1	0
					1	0	0	0	0	0	0	1	2	2	0
						1	0	0	0	0	0	1	3	4	4
						0	1	1	1	0	1	0	0	1	4
						1	1	1	0	2	0	0	0	0	0
									0	0	0	1	0	2	1
									1	1	0	0	0	0	1
									0	0	0	0	1	0	0
									0	0	1	0	0	0	0
									2		1	0	1	1	1
									0		0	1	1	2	1
											0	1	1	0	0
											0	0	0	0	0
											0	1	0	0	1
											1	0	0	0	0
											0	1	1	1	0
											0	0	0	0	0
											0	0	0	0	0
											1	0	0	0	0
											1	0	0	0	1
												1	0	0	0
												0	0	0	0
												0	1	0	1
												0	0	0	0
												0	0	1	1
												1	0	0	0
													0	0	0
													0	0	0
													0	0	0
													0	1	1

Table 7

NUMBER OF INDEPENDENT SCATTERING CENTERS

Plotted Fraction	Number of Centers
0.020	136
.029	189
.039	239
.049	292
.058	325
.067	356
.075	385
.085	415
.093	445
.103	466
.112	477
.121	491
.131	509
.139	518
.147	529
.155	528
.161	536
.172	540
.180	534
.188	520
.195	523
.200	510
.210	501
.220	491
.230	481
.240	459
.250	443
.260	412
.270	403
.280	390
.290	374
.300	340
.350	220
0.400	123
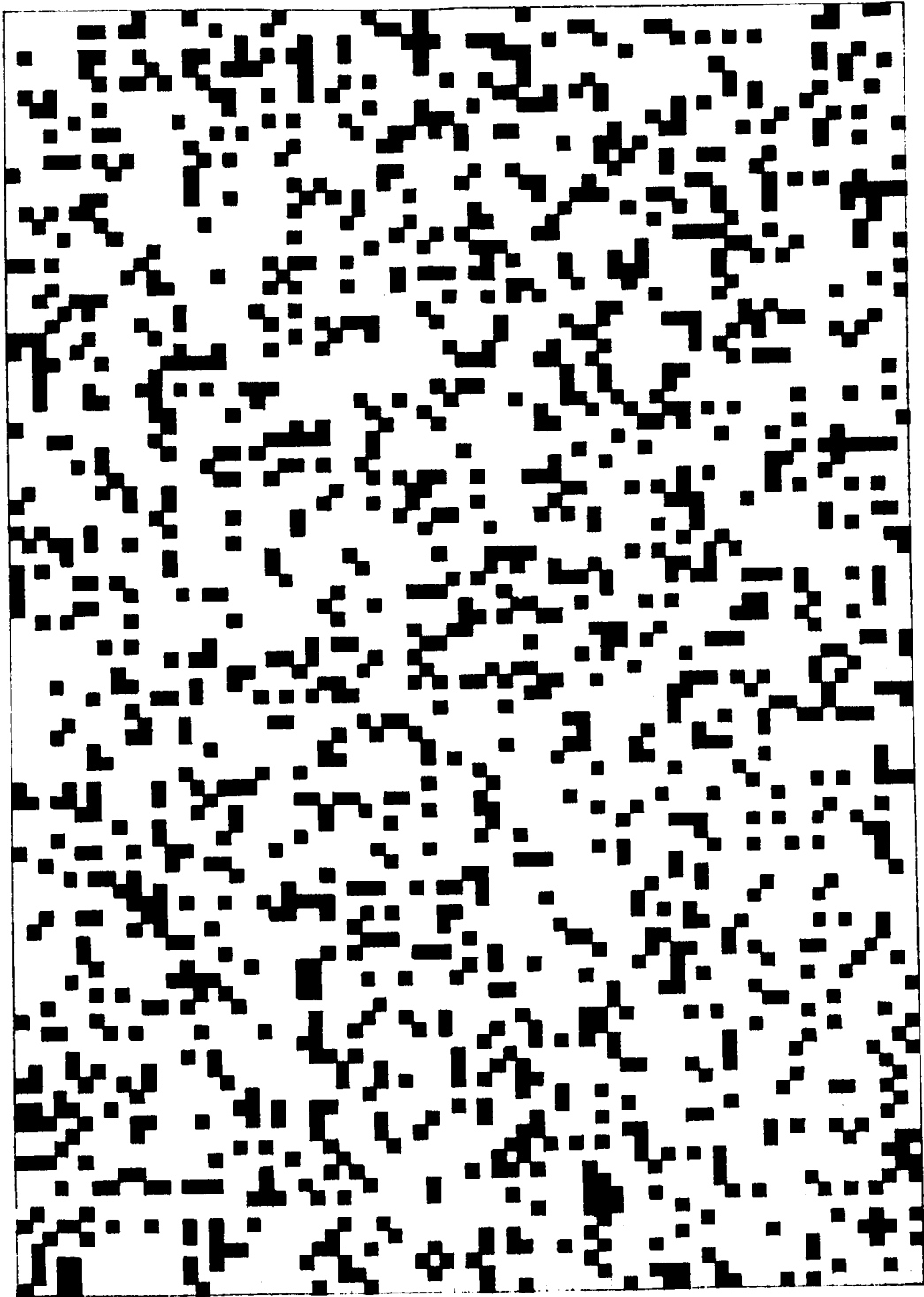
Figure 23

MONTE CARLO BLOCK PLOTTING EXPERIMENT AT 20% CONCENTRATION
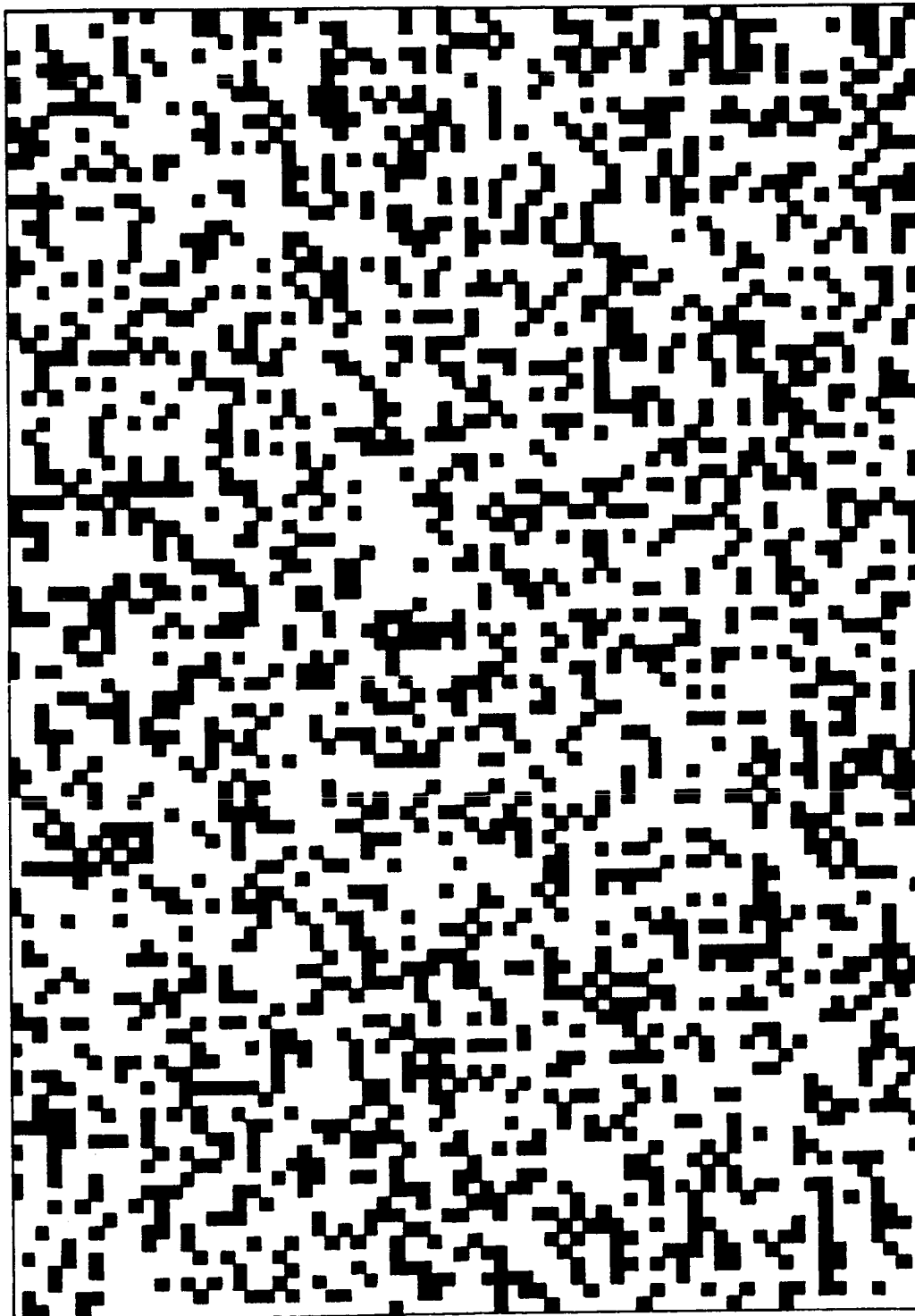
Figure 24

MONTE CARLO BLOCK PLOTTING EXPERIMENT AT 30% CONCENTRATION

Figure 25

MONTE CARLO BLOCK PLOTTING EXPERIMENT AT 35% CONCENTRATION

Figure 26

MONTE CARLO BLOCK PLOTTING EXPERIMENT AT 45% CONCENTRATION

Figure 27

MONTE CARLO BLOCK PLOTTING EXPERIMENT AT 50% CONCENTRATION
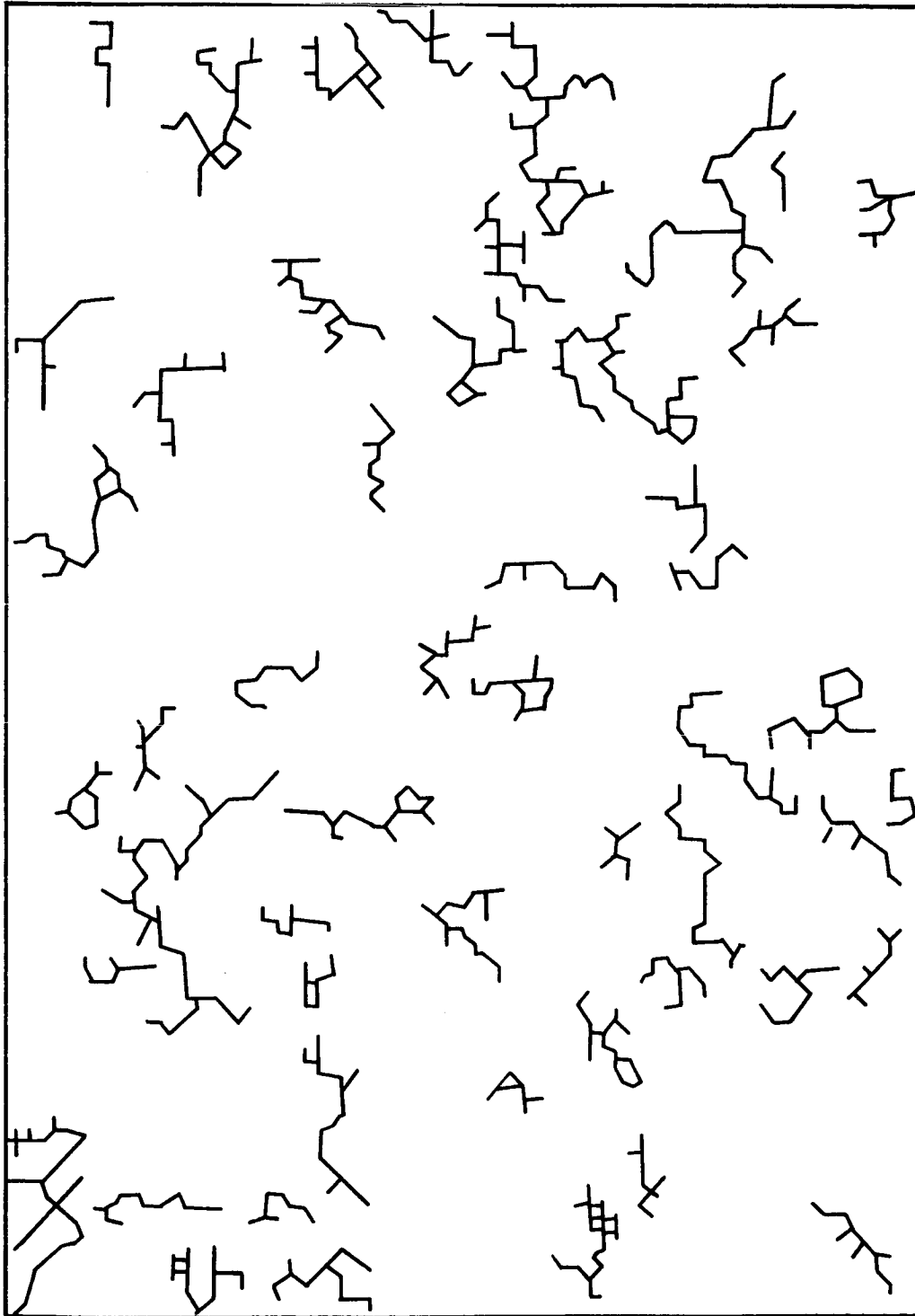
Figure 28

CLUSTERS DEVELOPED AT 27% VOLUME CONCENTRATION
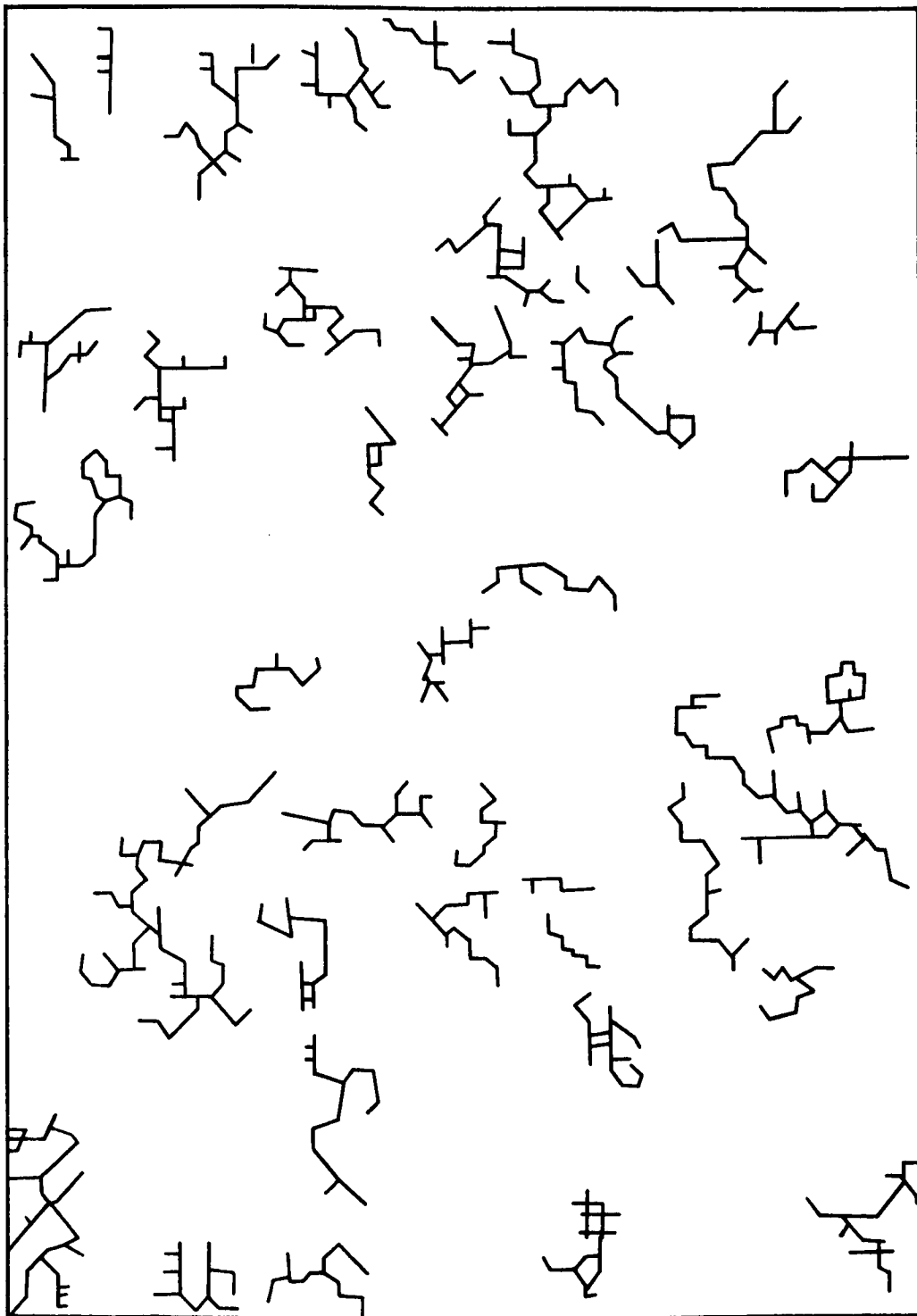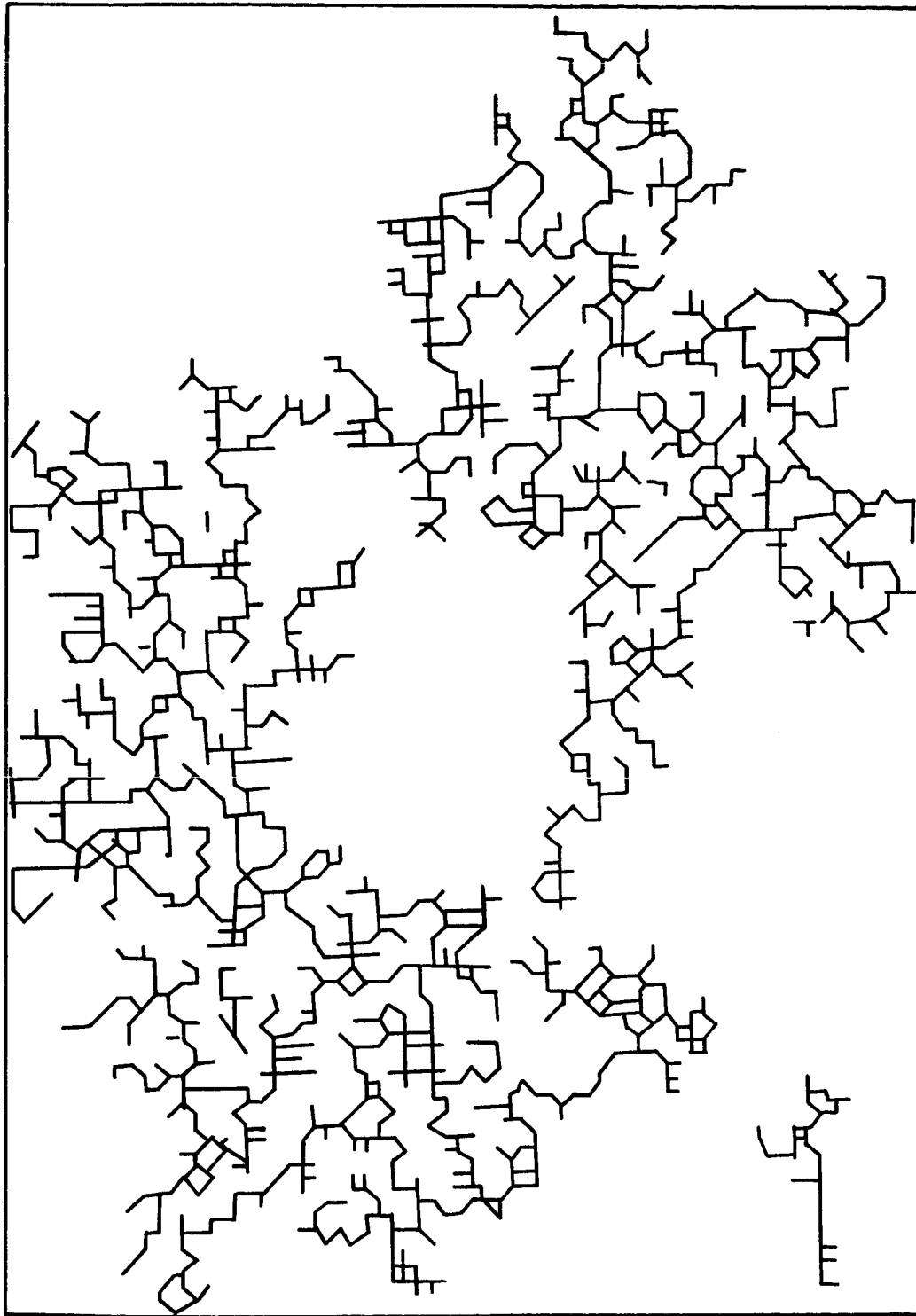
Figure 29

CLUSTERS DEVELOPED AT 28% VOLUME CONCENTRATION
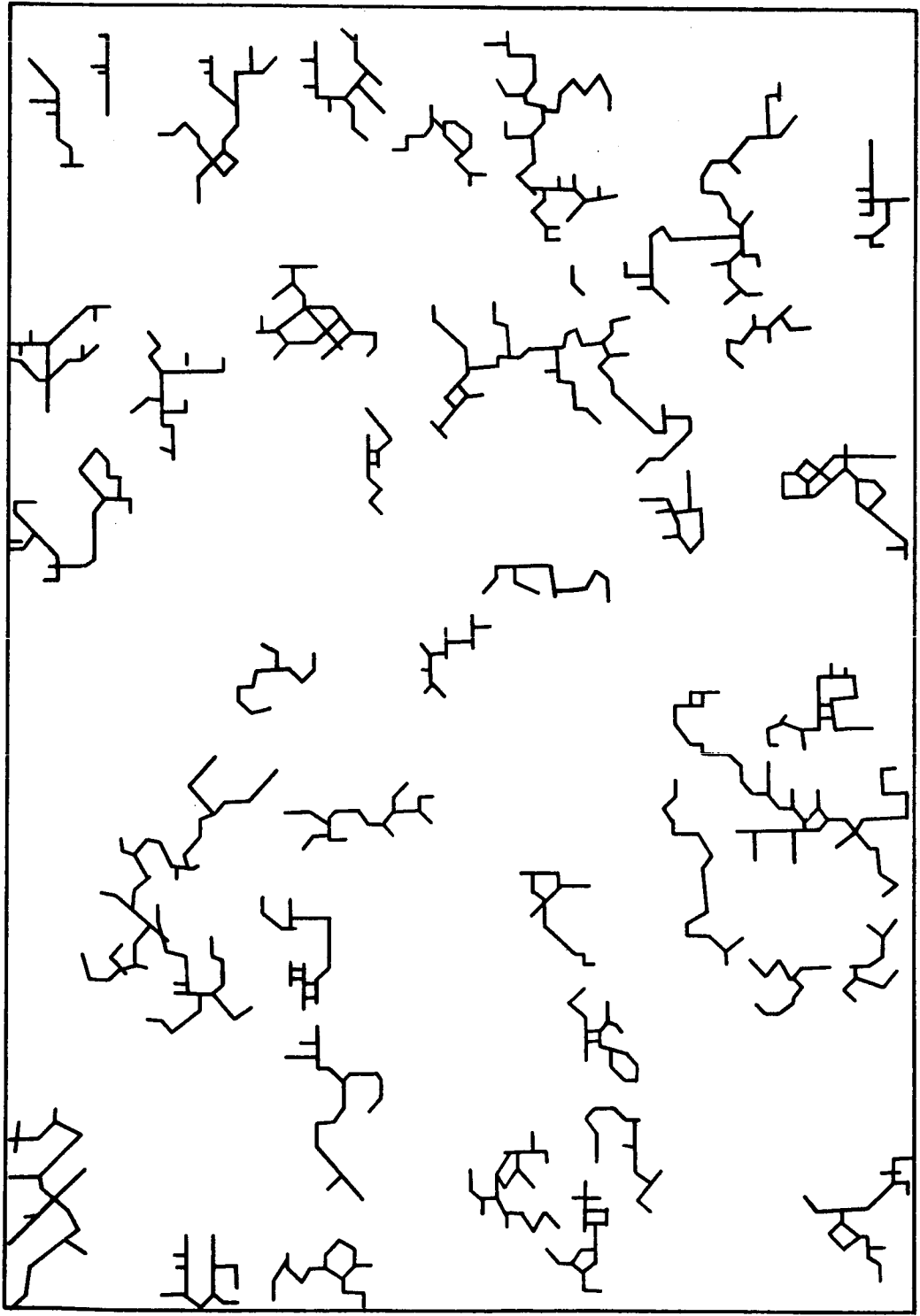
Figure 30

CLUSTERS DEVELOPED AT 29% VOLUME CONCENTRATION
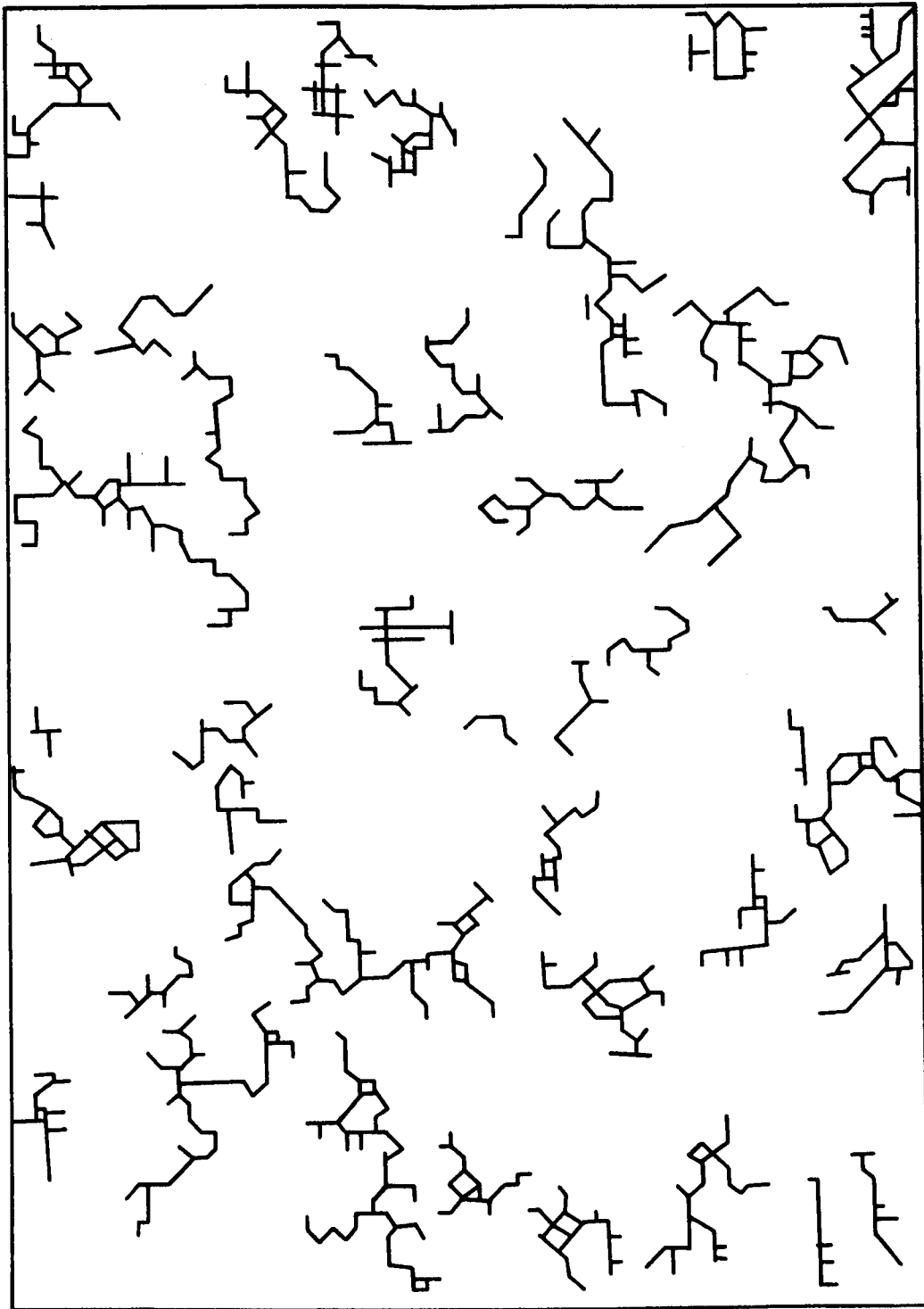
Figure 31

CLUSTERS DEVELOPED AT 30% VOLUME CONCENTRATION

Figure 32

CLUSTERS DEVELOPED AT 40% VOLUME CONCENTRATION

The implications and importance of these data are discussed below.

2. Rate of Overlapping within a Paint Film (Simulation of Lambert-Beer Law)

Increasing the number of pairs of coordinates considered for plotting on the master grid is equivalent to two physical procedures. Either it is equivalent to studying the changes in attenuation for a unit volume of the beam as the concentration increases, or it is equivalent to studying the increased attenuation caused by increasing the path length through a film of constant pigment volume concentration.

Consider what happens when N pairs of coordinates are selected; this is equivalent to considering the effect of N particles. Let there be ϕ unit squares at the commencement of the plotting experiment. Let β be the number of particles that have overlapped. The original energy of the beam is $\phi \cdot E$, where E is the energy per unit square. The energy passing through the film is given by $[\phi - (N - \beta)]E$. Let the incident energy be denoted by I_0 and the transmitted energy by I_T. Then:

$$\frac{I_T}{I_0} = \frac{(\phi - N + \beta)}{\phi} = \delta \tag{44}$$

where δ is the fractional area remaining open.

It has been established empirically that the ratio of the incident to the transmitted energy for light passing through a dilute dispersed particle system is given by the Lambert-Beer law. This law can conveniently be written in the form:

$$\log \frac{I_T}{I_0} = \exp(-KCL) \tag{45}$$

where

> K is a constant dependent on the size and the geometry of the particle
>
> L is the length of the beam's path
>
> C is the concentration of a unit volume of the cloud.

The product CL represents the total number of particles in a unit area.

Therefore the Lambert-Beer law can be written in the form:

$$\log \frac{I_T}{I_0} = A + N \qquad (46)$$

where A is a constant.

If the simulation experiment is in agreement with empirically determined knowledge, then, from Equations 44 and 46,

$$\log \delta = B + N \qquad (47)$$

where B is an arbitrary constant.

That is, a plot of the logarithm of δ against N should be a straight line. The relevant information obtained during the plotting experiment is presented in Table 8 and plotted in Figure 33. These data follow the predicted pattern and demonstrate that a Lambert-Beer equation for attenuation of a light beam can be deduced from statistical reasoning alone.

3. Cluster Configuration

For verification of the Lambert-Beer law, the basic grid of the Monte Carlo experiment can be considered to be an end-on view through a paint film in which monosized particles are dispersed. Now consider the plot to be a slice of a paint film one unit thick and the particles to be located exactly in the plane of the section. Again, although this is an idealized paint system, the information derived from it is qualitatively in accord with measured properties of actual paint systems. For this interpretation of the plotting experiments, the over-lapped particles are regarded as particles that try to occupy positions already filled. They are not considered in studying the distribution of particles or the configuration of clusters in the film section, since they represent nonpermissible particles.

Therefore, the important parameter is N', the number of spaces occupied. It seems reasonable to regard the cluster as the scattering unit. In fact, it has generally been assumed in paint technology that a badly dispersed pigment has low scattering efficiency because the effective pigment particles are larger and therefore less effective in scattering light.

Table 8

OVERLAPPED PARTICLES IN MONTE CARLO EXPERIMENT

Number of Pairs of Coordinates	Overlapping Particles	Fraction Plotted	Fractional Open Space
70	0	0.010	0.990
140	0	.020	.980
210	3	.029	.971
280	6	.039	.961
350	10	.049	.951
420	15	.058	.942
490	20	.067	.933
560	32	.075	.925
630	35	.085	.915
700	42	.093	.907
770	49	.103	.897
840	56	.112	.888
910	62	.121	.879
980	66	.131	.869
1050	76	.139	.861
1120	90	.147	.853
1190	105	.155	.845
1260	113	.164	.836
1330	127	.172	.828
1400	145	.180	.820
1470	156	.188	.812
1540	172	.195	.805
1580	180	.200	.800
1669	199	.210	.790
1758	218	.220	.780
1841	231	.230	.770
1924	244	.240	.760
2012	262	.250	.750
2110	290	.260	.740
2210	320	.270	.730
2317	357	.280	.720
2417	387	.290	.710
2552	422	.300	.700
3075	629	.350	.650
3780	950	.410	.590
4368	1216	.450	.550
5065	1565	0.500	0.500
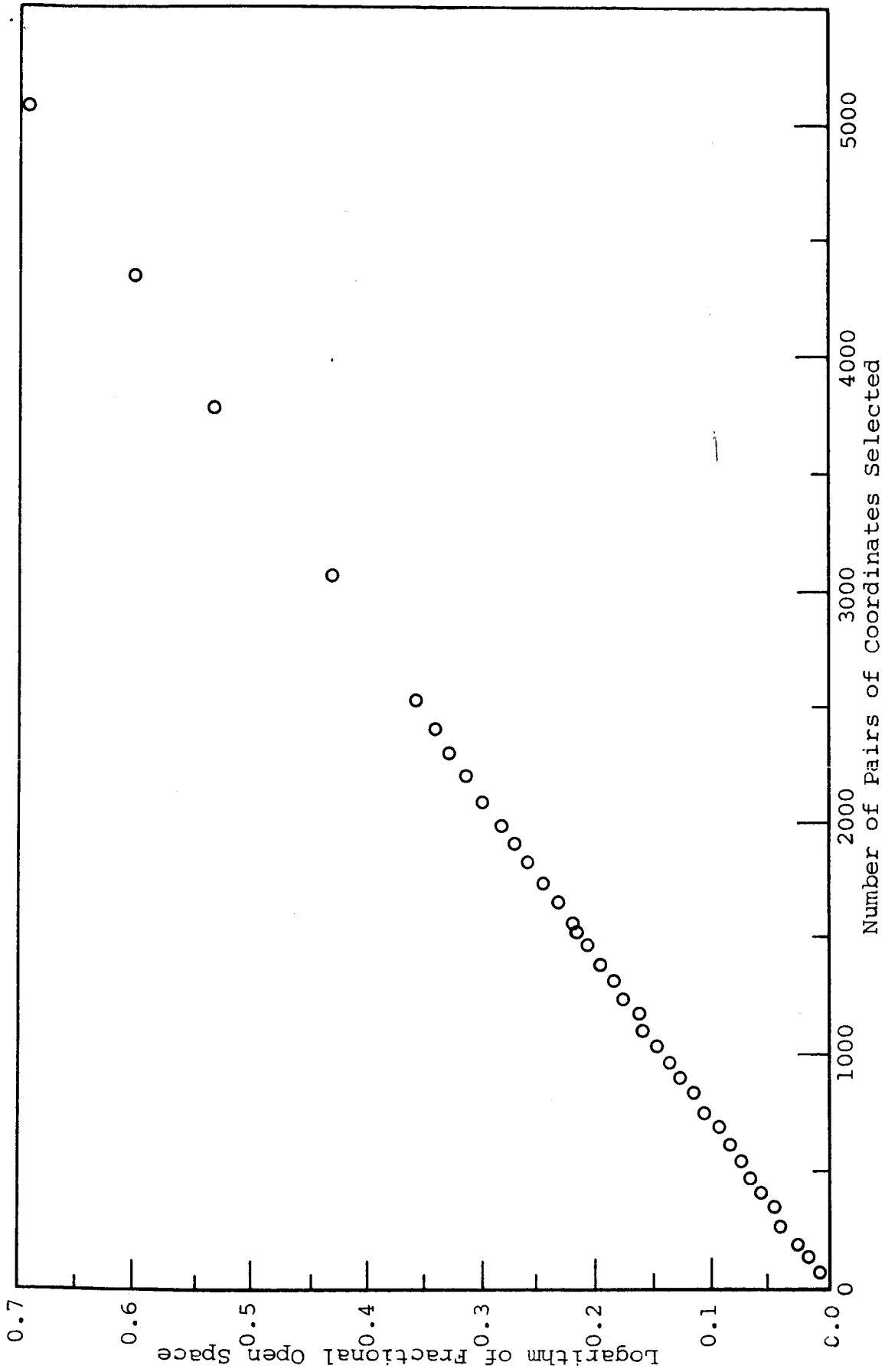
Figure 33

LOGARITHM OF FRACTIONAL OPEN SPACE AGAINST TOTAL NUMBER OF PARTICLES

If we treat a cluster as the scattering unit, we can calculate S, which is the total number of scatterers in the paint film at each volume concentration. We note that the volume concentration and surface exposed are numerically equal. The data in this form are summarized in Table 6. In Figure 34 the number of scatterers achieved is expressed as a fraction of the number of particles placed in the section. This curve offers a statistical explanation of the fact that a higher volume concentration of pigment dispersion yields a lower hiding power of a given amount of pigment.

If, instead of plotting percentage scattering centers, we plot the absolute number of scattering units per unit volume at various volume concentrations, the data appear as shown in Figure 35. Note that at 17% volume concentration there is an absolute maximum of scattering centers and that further additions of pigment particles only serve to create larger clusters. This suggests the possibility that there is an optimum pigment volume concentration at which maximum numbers of scatters per unit volume are achieved. A survey of the literature indicates that this statistical reasoning may explain the experimentally determined peak in the scattering power/PVC relationships of paints discussed by several investigators (ref. 23-25).

If the growth of clusters of different size is plotted (Figure 36), the reason for the drop in the scattering centers achieved with rising concentration is confirmed; i.e., further addition of particles creates bigger clusters and fewer scattering centers. Thus the number of doublets initially increases at a rapid rate and then declines as further single particles convert doublets into triplets.

Another cluster property of a randomly dispersed monosize pigmented paint film was demonstrated by using this Monte Carlo plotting grid. The cluster size distribution as shown in Figure 37 follows a log-normal type of distribution, showing that the scattering-center size distribution within a random paint film is not that of the pigment itself, except at low pigment volume concentrations, where cluster formation is rare.
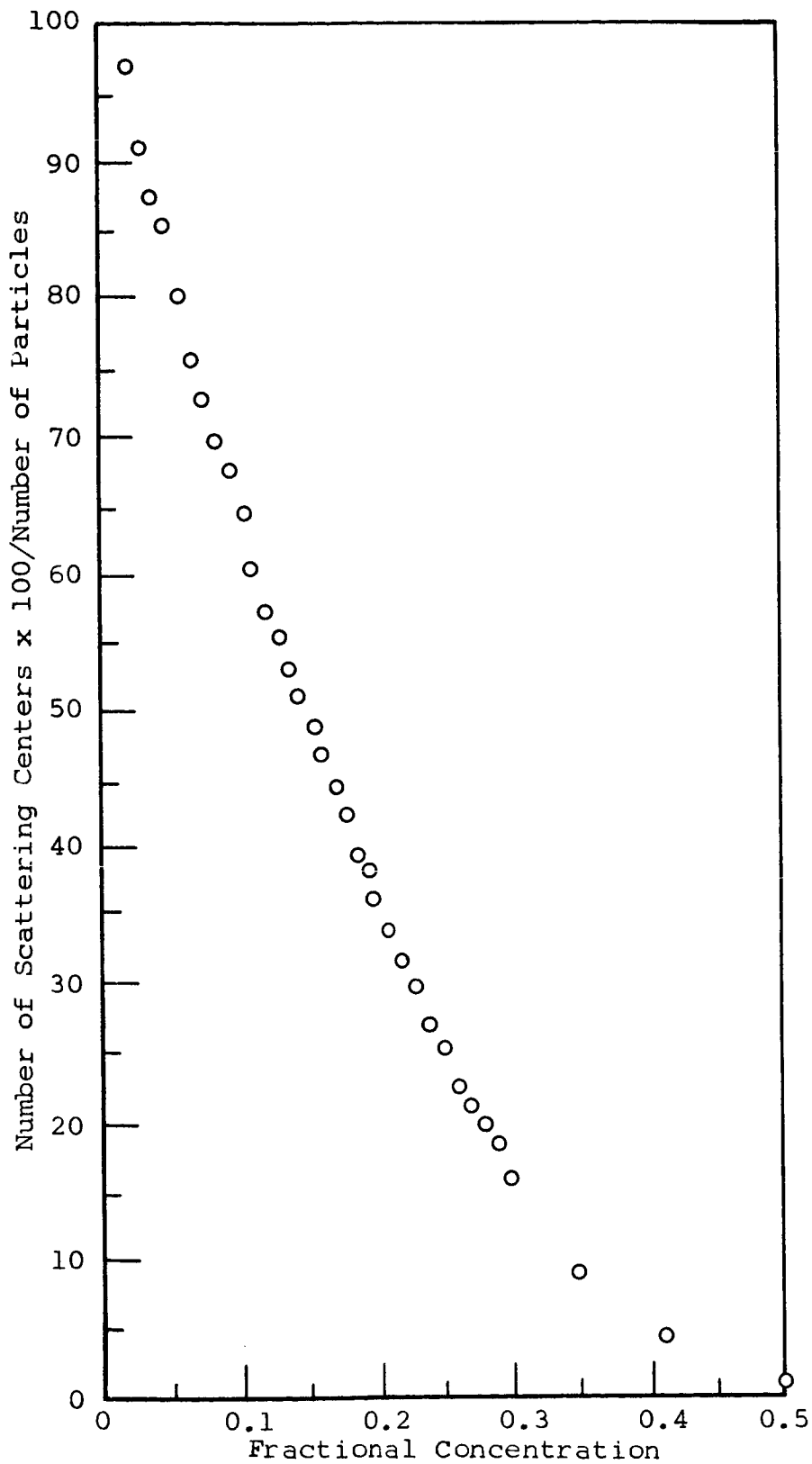
Figure 34

NUMBER OF SCATTERING CENTERS AT VARIOUS VOLUME CONCENTRATIONS
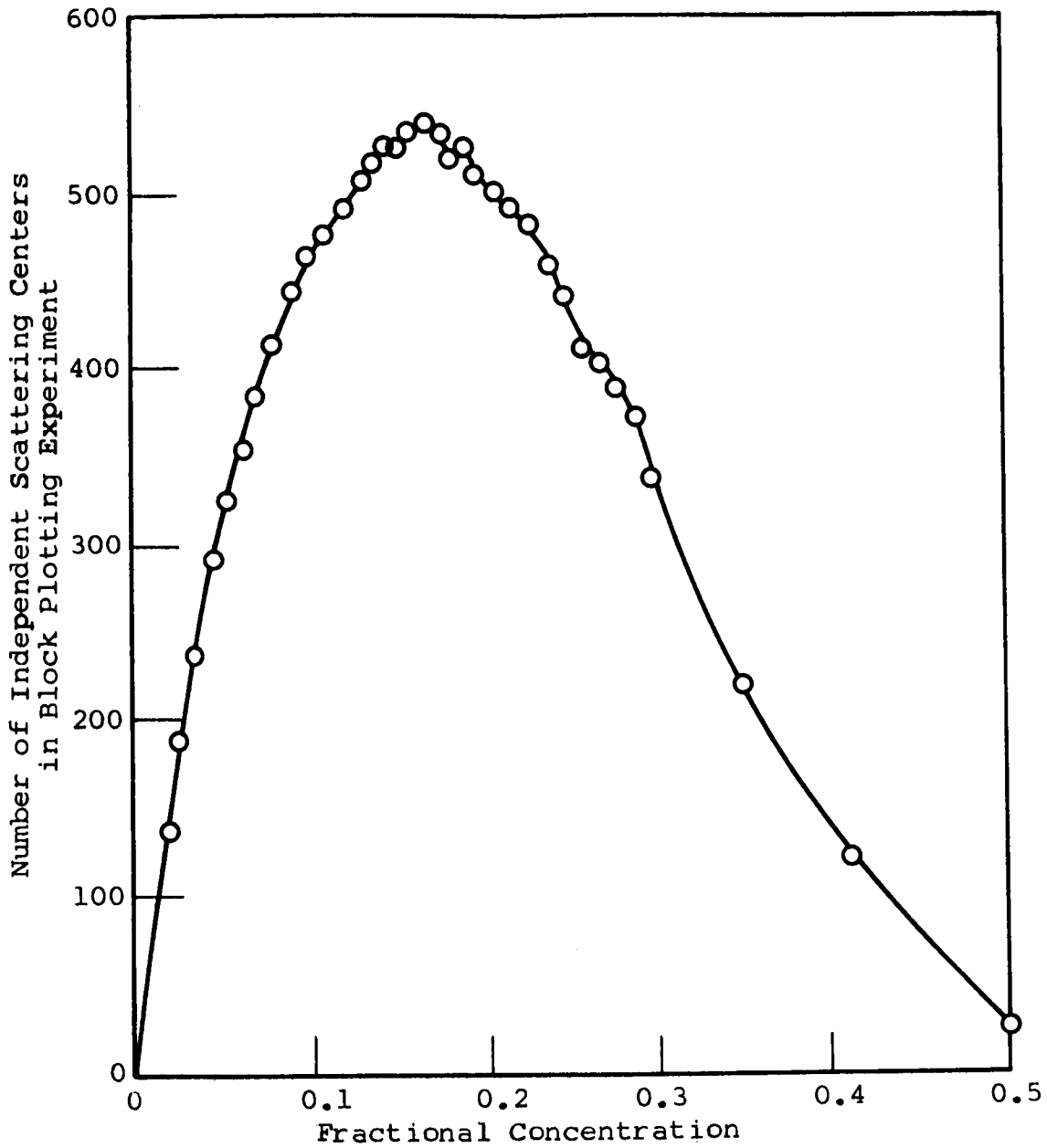FOR RANDOMLY DISTRIBUTED MONOSIZED PARTICLES

Figure 35
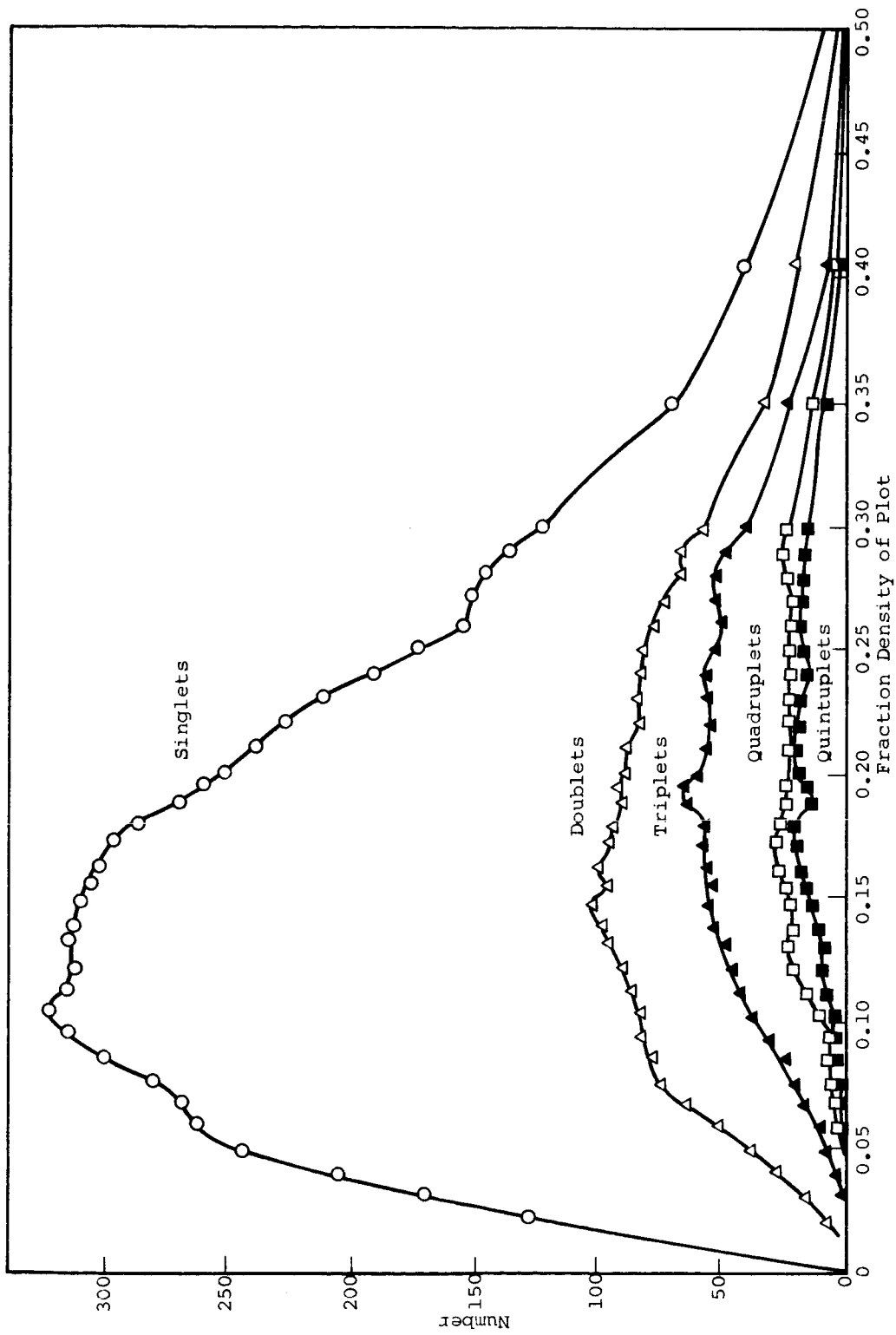
ABSOLUTE NUMBER OF SCATTERING CENTERS PER UNIT VOLUME

Figure 36

NUMBER OF DIFFERENT SIZED CLUSTERS AT VARIOUS VOLUME CONCENTRATIONS FOR RANDOMLY DISTRIBUTED MONOSIZED PARTICLES
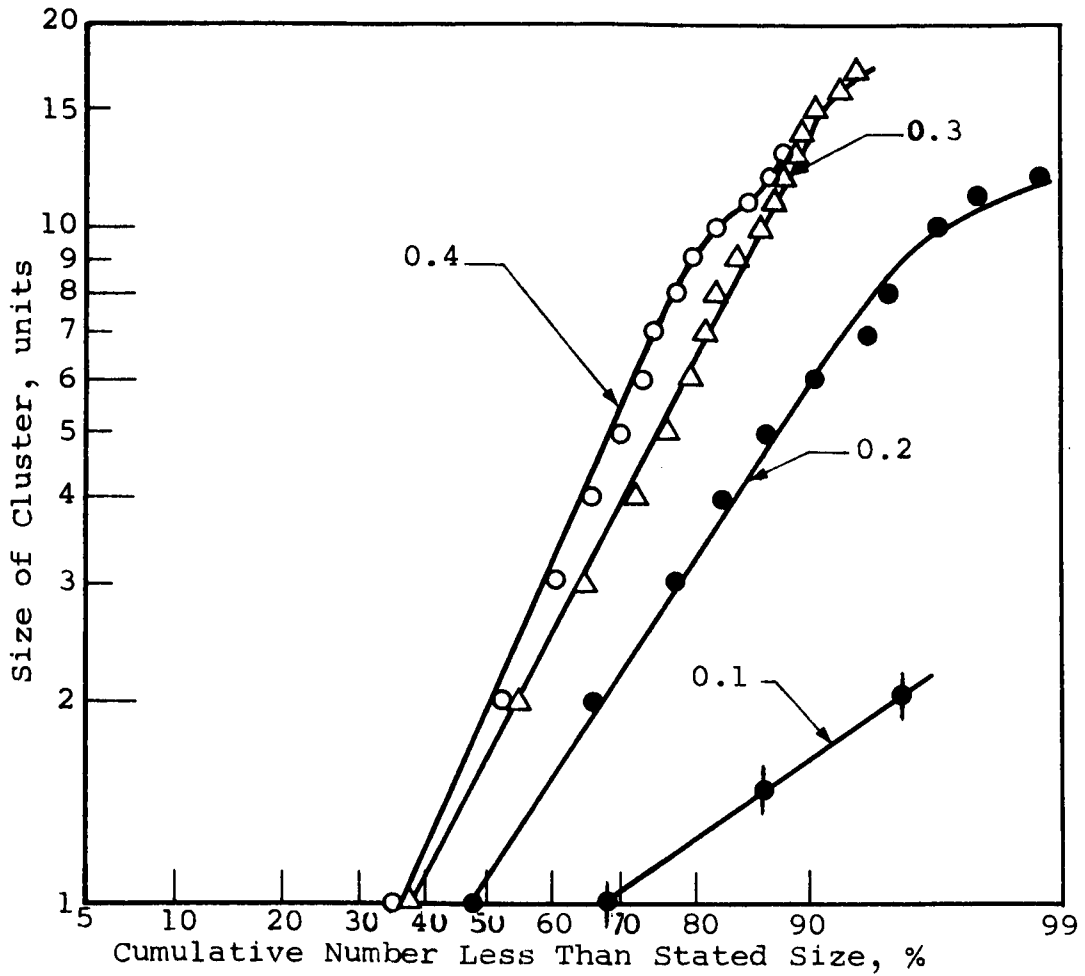
Figure 37

SIZE DISTRIBUTION OF CLUSTERS FORMED
AT VARIOUS FRACTIONAL CONCENTRATIONS

Thus, any experimental correlation of the scattering power of a paint film and its scattering-center size distribution must involve an experimental determination of scattering-center size distribution within the paint film rather than of particle-size distribution of the pigment before dispersion. In Figure 37 the indicated deviation from linearity for the larger clusters is probably due to the statistically small numbers of clusters of these sizes.

4. Edge Effects

In the original investigation of the number of scattering centers per unit area and in the experimental determination of the size distribution of clusters, the fact that clusters touching the boundary of the grid represented only partial clusters that possibly extended beyond the edge of the grid was ignored. For low equivalent volume concentrations, i.e., low density of coverage, the error involved in ignoring edge effects is negligible. For high equivalent volume concentrations, the error can be considerable.

A simple technique for calculating the correct size distribution of clusters is to eliminate from the data used to calculate the size distribution all clusters touching the boundary of the grid. This technique has the disadvantage that it rejects information available in the simulated field of view. Theoretically, one should be able to use partial clusters combined in pairs, using random-number tables to select mated pairs, to gain extra information on the cluster distribution. However, preliminary study of the problems involved in the recombination of partial clusters indicated that the preparation of an adequate procedure would involve more work than could be justified within the scope of the present investigation, and this subject was not pursued further. It should be noted that if many electron micrographs of composite materials have to be evaluated, the derivation of statistical techniques for recovery of information from the partial cluster distribution could be important because

of the expense involved in the preparation of electron micrographs. The corrected cluster size distributions were calculated by eliminating all clusters touching the grid boundary.

Techniques for calculating the true cluster density per unit area were investigated. All the techniques evolved can be illustrated by considering the 20% by volume grid (Figure 23).

The first technique considered was that of constructing on the grid system a new boundary that did not cut any cluster. Then the cluster density within the new boundary was calculated. The line for the new boundary passed equidistant between clearly independent whole clusters. A typical section of the boundary is shown in Figure 38. The calculated cluster density per unit of 100 squares using this new nonintersecting boundary was 7.18. The disadvantage of this technique is that information is discarded. In the case of the simulated 20% area grid, the total area enclosed by the new boundary is still sufficiently large that the number of clusters on which measurements are carried out is still relatively high. However, the usual type of electron micrograph would not contain such a high number of clusters, and the nonintersecting boundary area may reduce the information used to a relatively low level.

Another method for correcting for effects due to cluster interception by the boundary, and one that does not appear to have been described before, is to place small, known perimeters on the simulated field of view and measure the fluctuations in cluster density and cluster interception. Since cluster boundaries and cluster density vary because of the combined effect of random independent variables, both quantities should be distributed according to a Gaussian distribution.

To investigate the fluctuations in boundary interception and cluster density, the values of these two quantities in square areas of 100 units were investigated. Measurements were carried out on 90 squares. A typical set is shown in Figure 39.
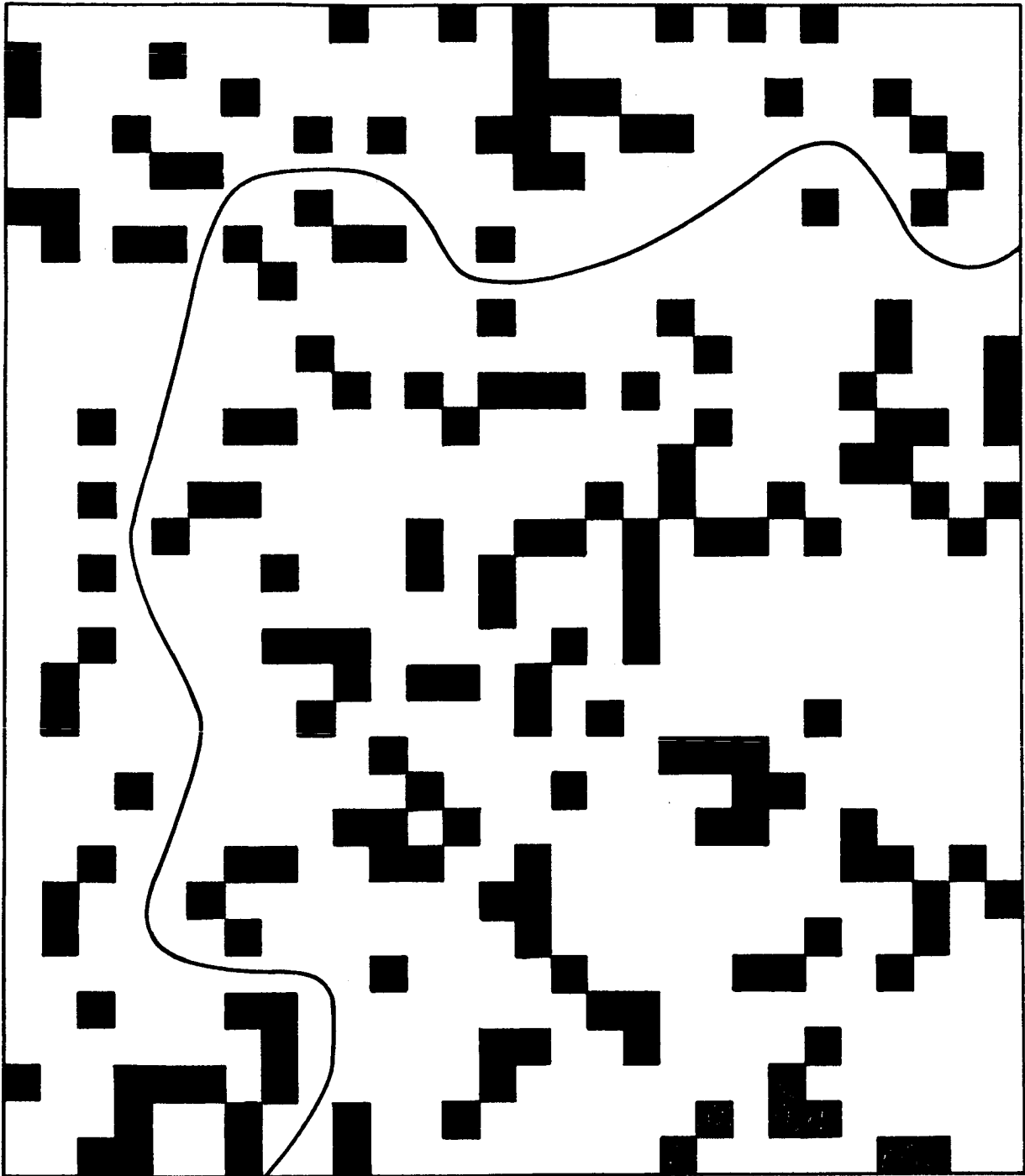
Figure 38

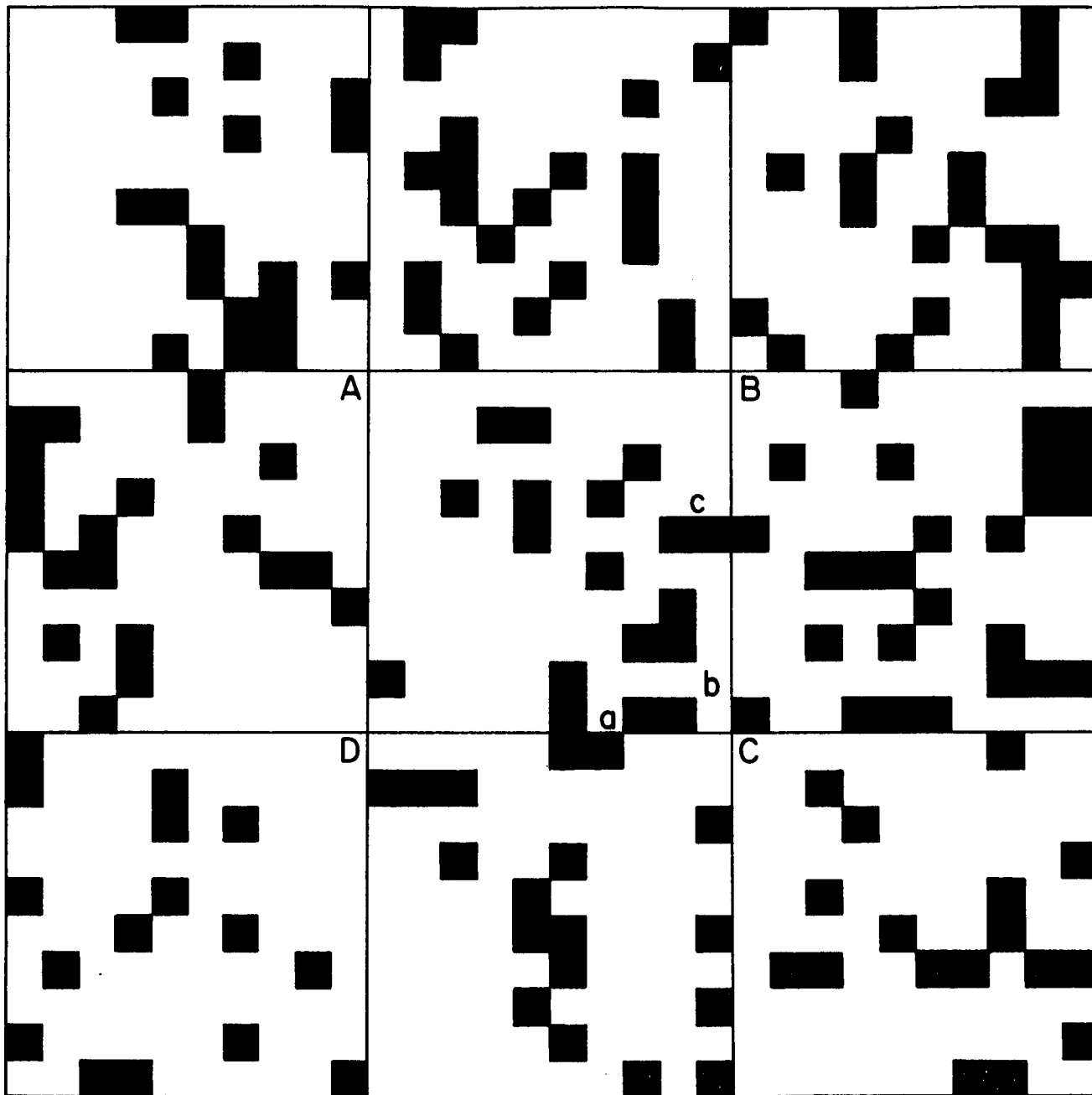CONSTRUCTION OF NEW BOUNDARY FOR 20% MONTE CARLO GRID PLOT

Figure 39

SCATTERING CENTERS IN A TYPICAL SUBUNIT OF 100 SQUARES

Consider the subsquare ABCD containing 100 units of area. This square apparently contains 10 clusters, but, in fact, two of them are fractions of the same cluster intercepted by the boundary. This square was chosen to demonstrate this possibility. Only four false counts of this kind were encountered in the 90 squares investigated, and this has a negligible effect on the number of clusters per square. Therefore, a square such as ABCD would be treated as containing nine clusters with two of the clusters crossing the boundary.

In Table 9, the distributions of the combined number of clusters and interceps are given. These are plotted on Gaussian scales in Figure 40. From this figure it can be seen that the expected value of the cluster number is 9 and the interception frequency is 3.8.

The fact that a cluster straddles the perimeter means that it is, on the average, counted twice. Therefore, the false count represented by particles crossing the boundary is half the interception frequency. Therefore, the calculated frequency of clusters for 100 unit squares is:

$$9 - \frac{3.8}{2} = 7.1$$

Thus, a simple technique for estimating the false count is to count the numbers of clusters at the boundary and subtract half this quantity from the total number of clusters. This is the method used to correct the estimates of the number of independent clusters per unit area in the analysis of the Monte Carlo plots considered here.

The cluster size distribution at 0.3 fractional coverage has been determined experimentally in two cases: (a) not correcting for and (b) correcting for clusters touching the boundaries of the plot. The data are presented in Table 10 and Figure 41. The corrected distribution is still essentially log-normal, and the largest correction is associated with the largest clusters. This is to be expected, since a large cluster has a greater probability of intercepting the edge of the plot than a smaller cluster.

Table 9

COMBINED CLUSTER DENSITIES AND INTERCEPTION DENSITIES OF 90 SUBSQUARES OF A TYPICAL MONTE CARLO PLOT OF 0.2 FRACTIONAL AREA

FLUCTUATIONS IN CLUSTER NUMBER IN SUBSETS OF 100 SQUARES
(90 Sets Examined)

Number of Clusters	Number of Sets Containing Stated Cluster Number	Percent Occurrence of Events Greater Than or Equal to Stated Number
5	4	100
6	6	95
7	13	89
8	23	74
9	20	49
10	12	27
11	8	13
12	–	–
13	4	4

FREQUENCY OF CLUSTER INTERCEPTIONS BY PERIMETER BOUNDARY
(Perimeter is That of Square Containing 100 Subsquares)

Number of Interceptions	Number of Perimeters with Stated Interception Number	Percent Occurrence of Interceptions Greater Than or Equal to Stated Number
0	3	100
1	10	97
2	17	85
3	17	67
4	17	48
5	15	29
6	4	12
7	6	8
8	1	1

Figure 40

NUMBER DISTRIBUTION OF CLUSTER AND INTERCEPT EVENTS

Table 10

CLUSTER DISTRIBUTION AT 0.3 FRACTIONAL CONCENTRATION

Number of Units in Cluster	Including Cluster Cut by Edge of Plot	Excluding Cluster Cut by Edge of Plot
1	121	111
2	56	46
3	38	33
4	23	21
5	14	11
6	9	8
7	6	6
8	13	12
9	8	8
10	6	5
11	4	3
12	3	3
13	3	3
14	1	0
15	5	4
16	4	3
17	3	0
18	2	1
19	0	0
20	0	0
21	0	0
22	4	3
23	4	3
24	0	0
25	1	0
26	1	1
27	0	0
28	0	0
29	1	1
30	1	0
31	0	0
32	0	0
33	1	1
34	0	0
35	1	1
36	0	0
37	0	0
38	0	0
39	0	0
40	1	1
41	0	0
42	0	0
43	0	0
44	0	0
45	0	0
46	0	0
47	1	1
48	0	0
49	0	0
50	0	0
51	1	1
52	0	0
53	1	1
54	0	0
55	0	0
56	0	0
57	1	0
58	0	0
59	0	0
60	0	0
61	0	0
62	0	0
63	0	0
64	1	1
65	0	0
66	0	0
67	0	0
68	0	0
69	0	0
70	0	0
71	0	0
72	1	1
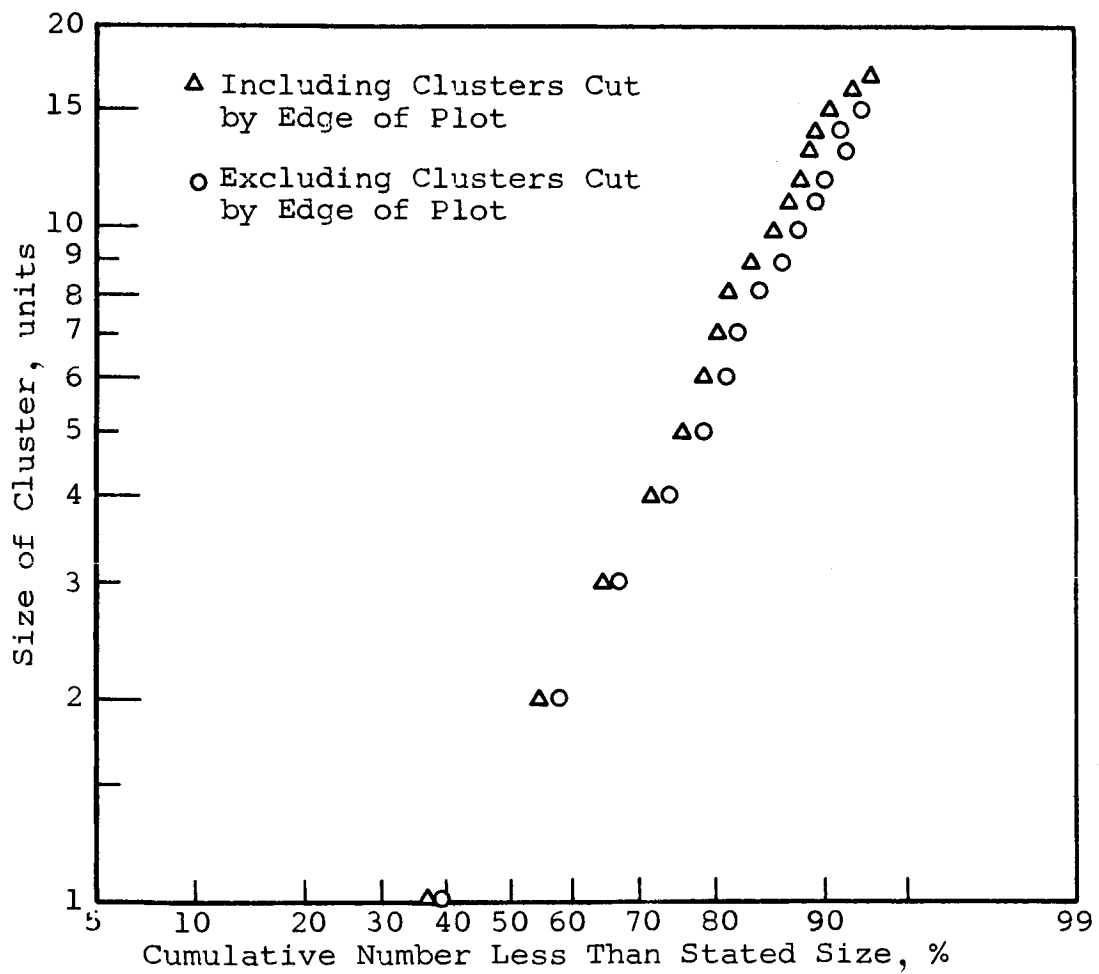
Figure 41

SIZE DISTRIBUTION OF CLUSTERS FORMED
AT 0.3 FRACTIONAL CONCENTRATION
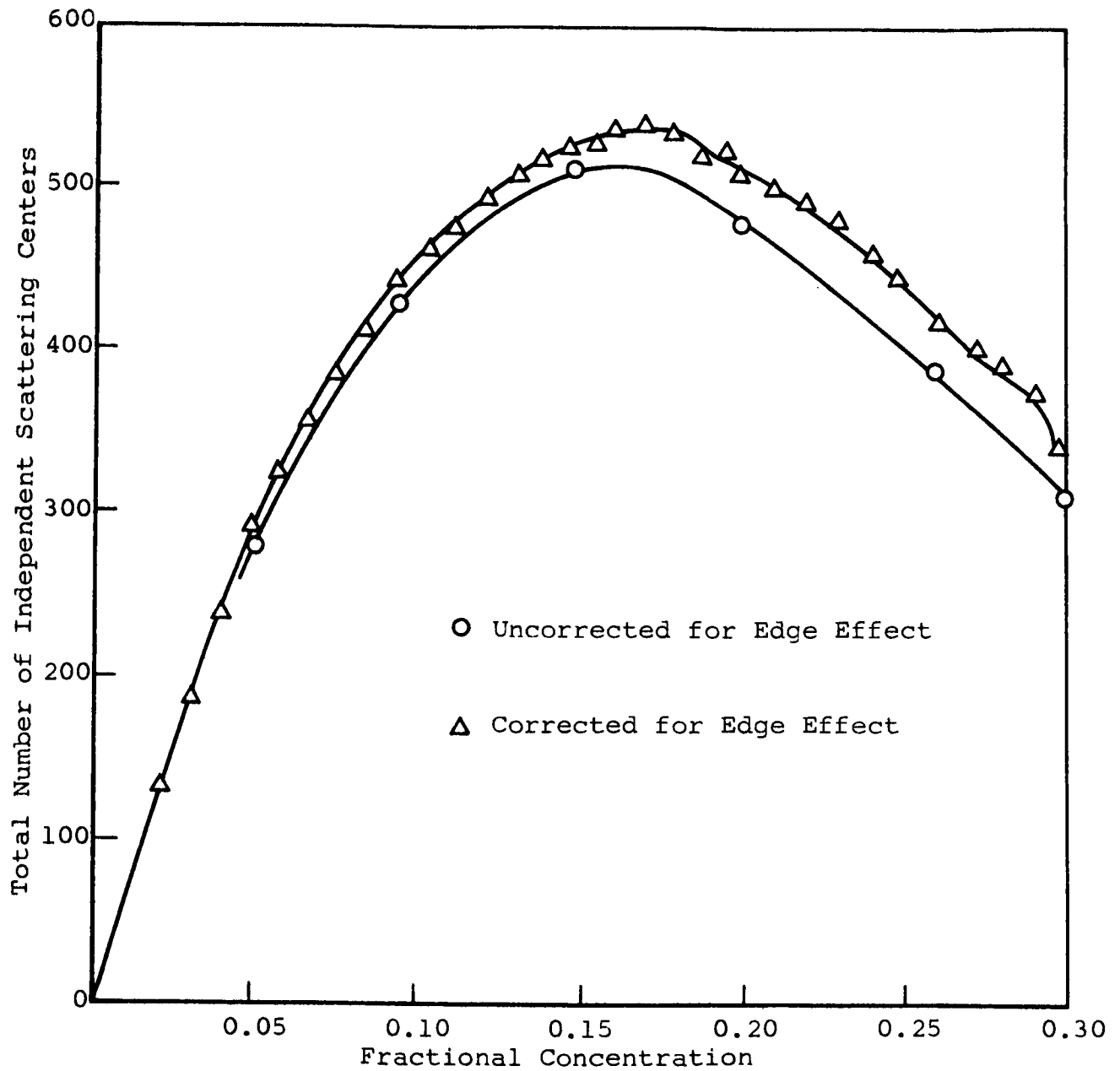
Figure 42

ABSOLUTE NUMBER OF SCATTERING CENTERS PER UNIT VOLUME

A plot of the total number of scattering centers against fractional concentration is shown in Figure 42 for edge-corrected and uncorrected plots. Since correction in this case is essentially exclusion of intercepted clusters, it is to be expected that the total number of scattering centers at a given concentration will be reduced.

B. Simple Model of Noncubic Pigment without Extender

In the simulation experiments reported in Section VA, the growth of cluster formation was simulated in two dimensions by using a two-dimensional grid-plotting experiment. Although the validity of the quantitative data on cluster formation deduced from these experiments is limited by the fact that clusters are growing in three dimensions, the qualitative deductions (such as the presence of a maximum in the total number of scattering centers) appear to correlate with known empirical data on the changes in opacity of a paint film at various solids concentrations.

A criticism of the simple cubic-pigment-particle model used in the first Monte Carlo experiment is that the particle shape assumed is too symmetrical and that results from the plotting experiment are not valid because real pigment particles have asymmetrical shapes. To explore the implications of this possible criticism, the following plotting experiment was carried out. A square grid containing 70 x 70 square subdivisions was marked out. On this grid particles consisting of two squares were plotted by using three random numbers.

The first two random numbers selected ranged between 1 and 70 to find a location on the plotting grid. The third random number was a single digit. If it was even, the particle was plotted with its left side lower corner on the coordinate and its longer side lying horizontally. If it was odd, the left side lower corner was agin laid on the selected coordinate but the long side was laid vertically.

In Figures 43 through 46 the resultant fields of view at approximately 5, 10, 15, and 20% coverage are given. The exact percentage is shown in the diagrams. The reason that cluster formation was not determined at exact fractional coverages was that these diagrams were prepared by plotting several 5% covered plots on translucent paper. (On a plane surface each 5% diagram has 7 independent positions. Therefore, if 4 diagrams are prepared, 42 different 10% diagrams can be prepared. However, the overlap losses vary from set to set.)

Many sets of 15 and 20% coverages can be drawn. In this research we studied one combination for each percentage coverage by using 5 diagrams. Apart from the advantage of the possible number of combinations using several 5% covered diagrams, these relatively low-density systems are easy to plot compared to the construction of the densely populated system at, for example, 20% coverage. We changed from a rectangular to a square plotting area in order to facilitate superpositioning of the separate grids.

The total number of scattering centers versus percent coverage is plotted in Figure 47. It will be observed that the growth of clusters again causes the number of independent scattering centers to reach a maximum in the region of 20% by volume. Comparison of Figure 47 with Figure 42 shows that the maximum shifted to slightly higher concentrations for the particles with a shape factor of 2:1. This phenomenon may not be real in the sense that statistical fluctuations between repeat Monte Carlo plotting experiments could demonstrate that the difference between it and 20% for the two differently shaped particles could arise purely from chance mechanisms.

Figure 48 presents the growth of the different sized clusters in the plotting experiment using particles of 2:1 shape factor. The results of the plotting experiments with the 2:1 shaped particles have important implications for paint reflectance studies.
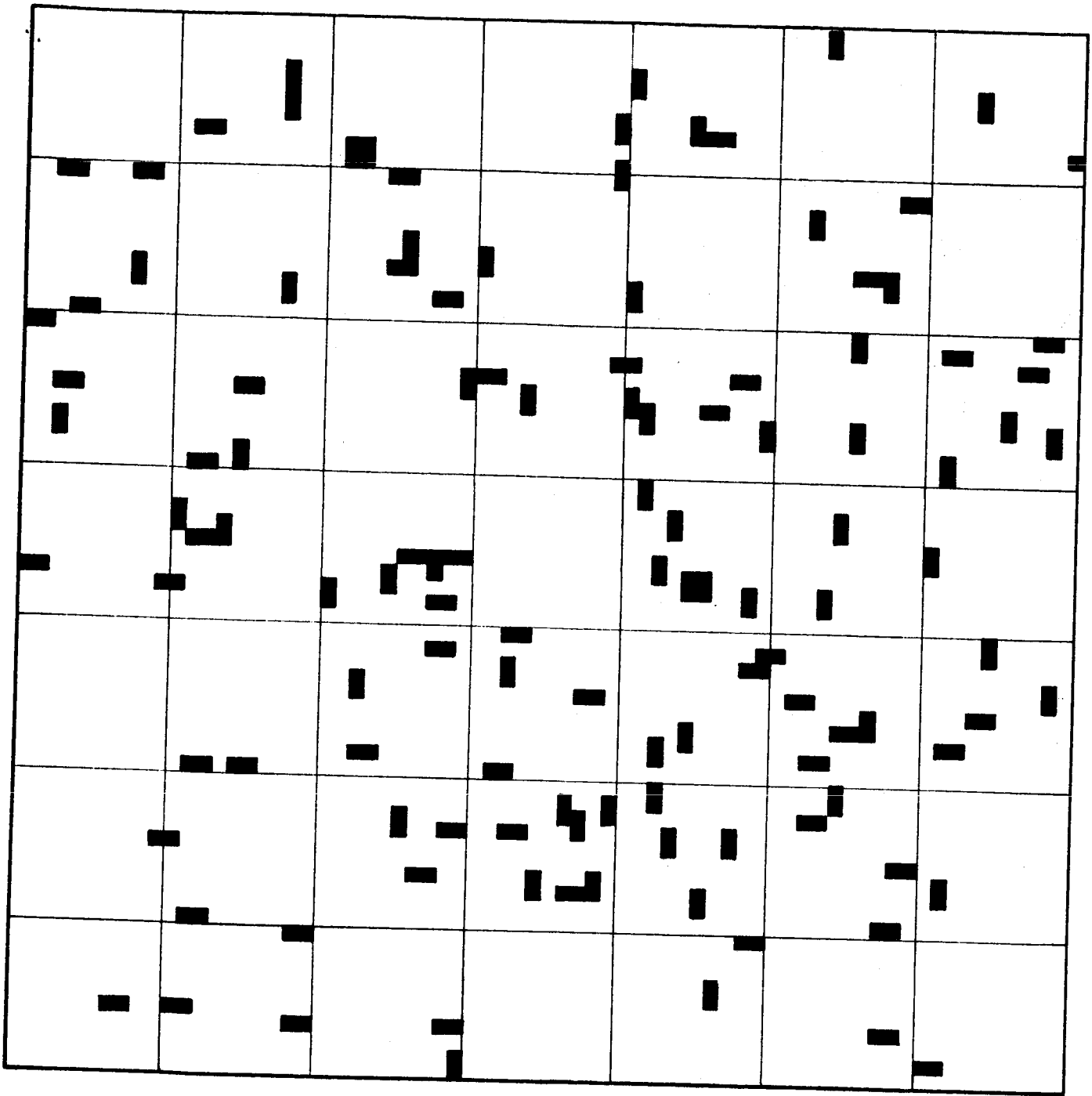
Figure 43

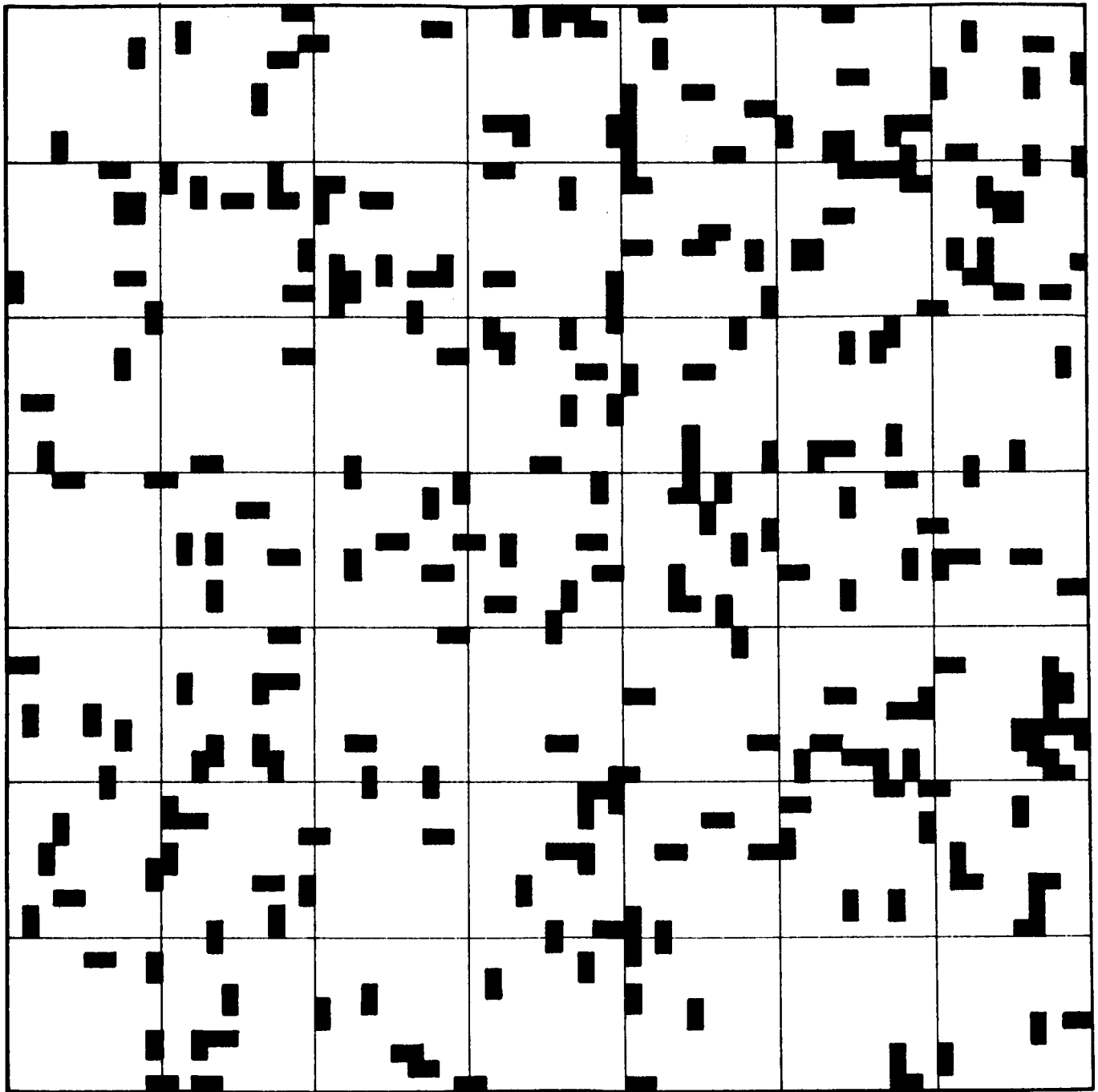5% COVERAGE BY PARTICLES HAVING 2:1 SHAPE RATIO

Figure 44

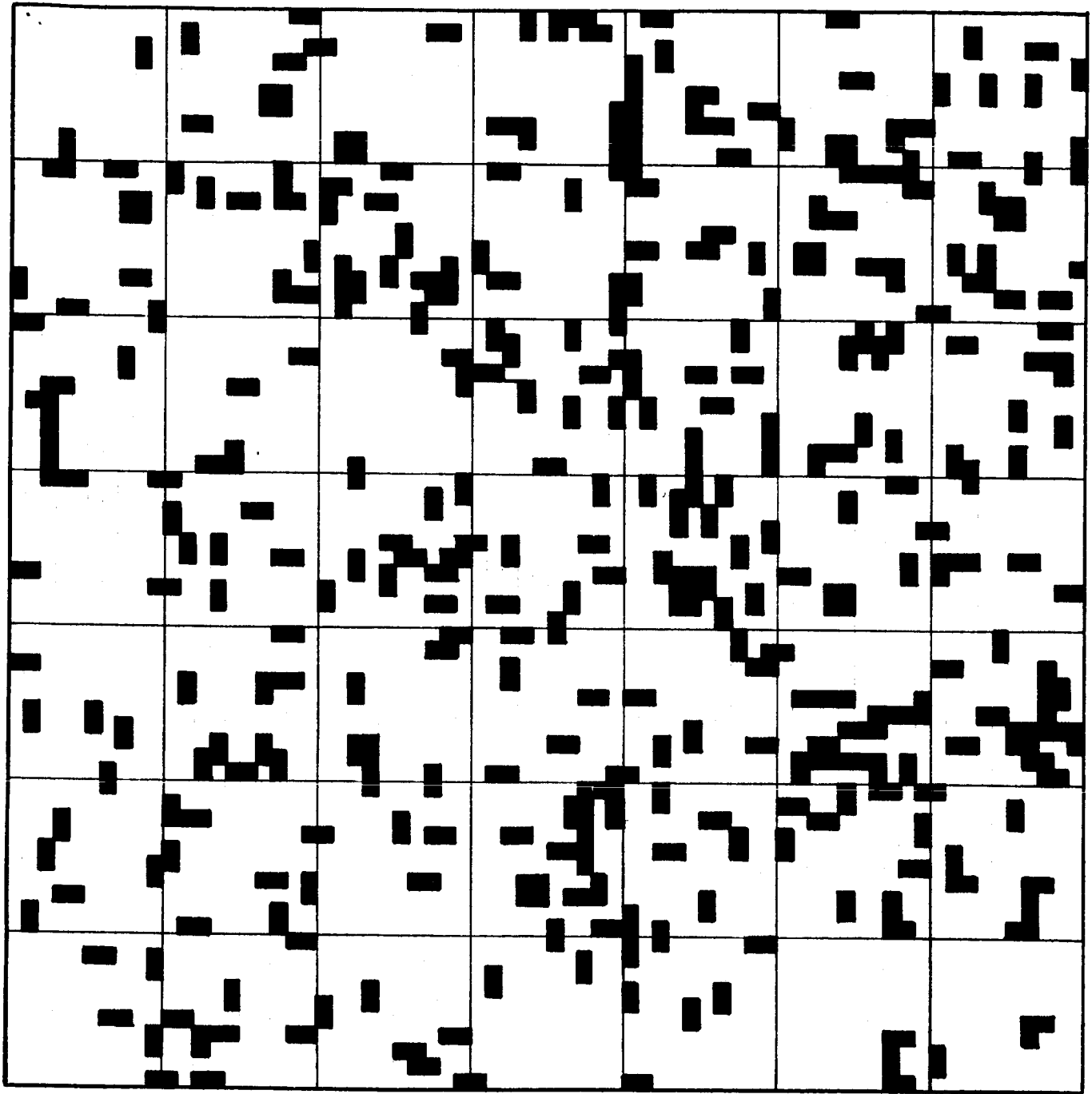10% COVERAGE BY PARTICLES HAVING 2:1 SHAPE RATIO

Figure 45

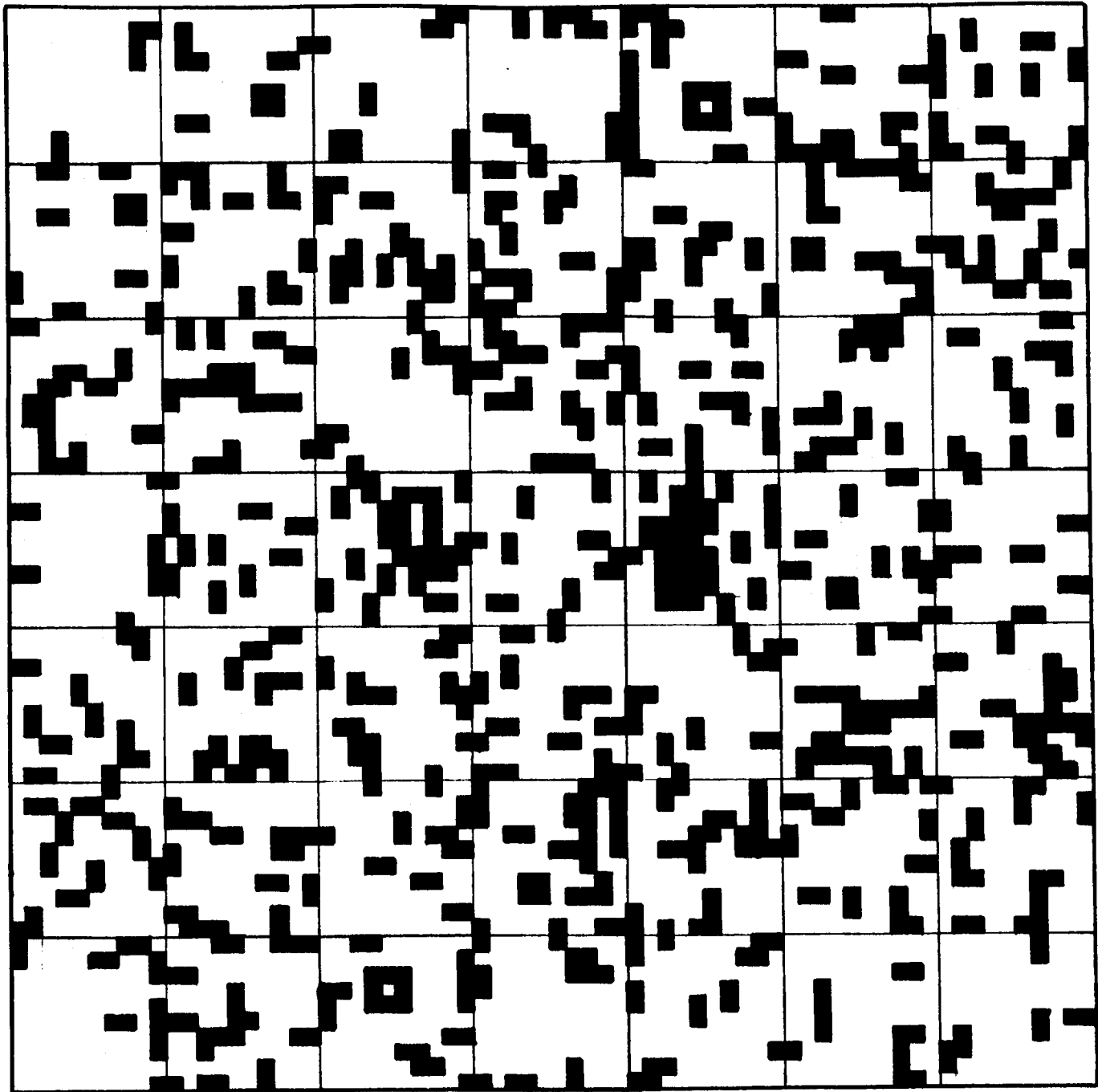14.8% COVERAGE BY PARTICLES HAVING 2:1 SHAPE RATIO

Figure 46
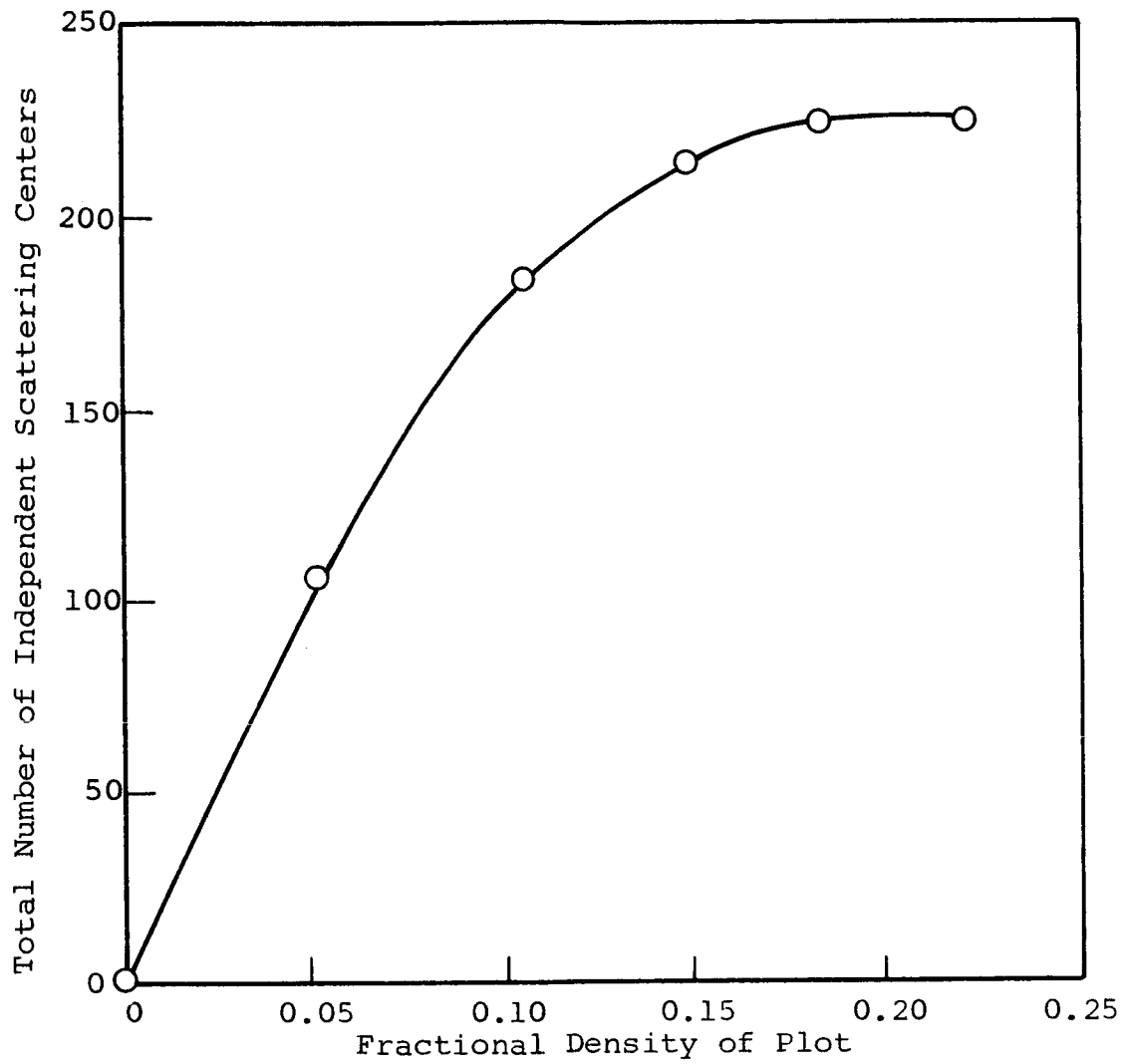
20% COVERAGE BY PARTICLES HAVING 2:1 SHAPE RATIO

Figure 47

ABSOLUTE NUMBER OF SCATTERING CENTERS PER UNIT VOLUME
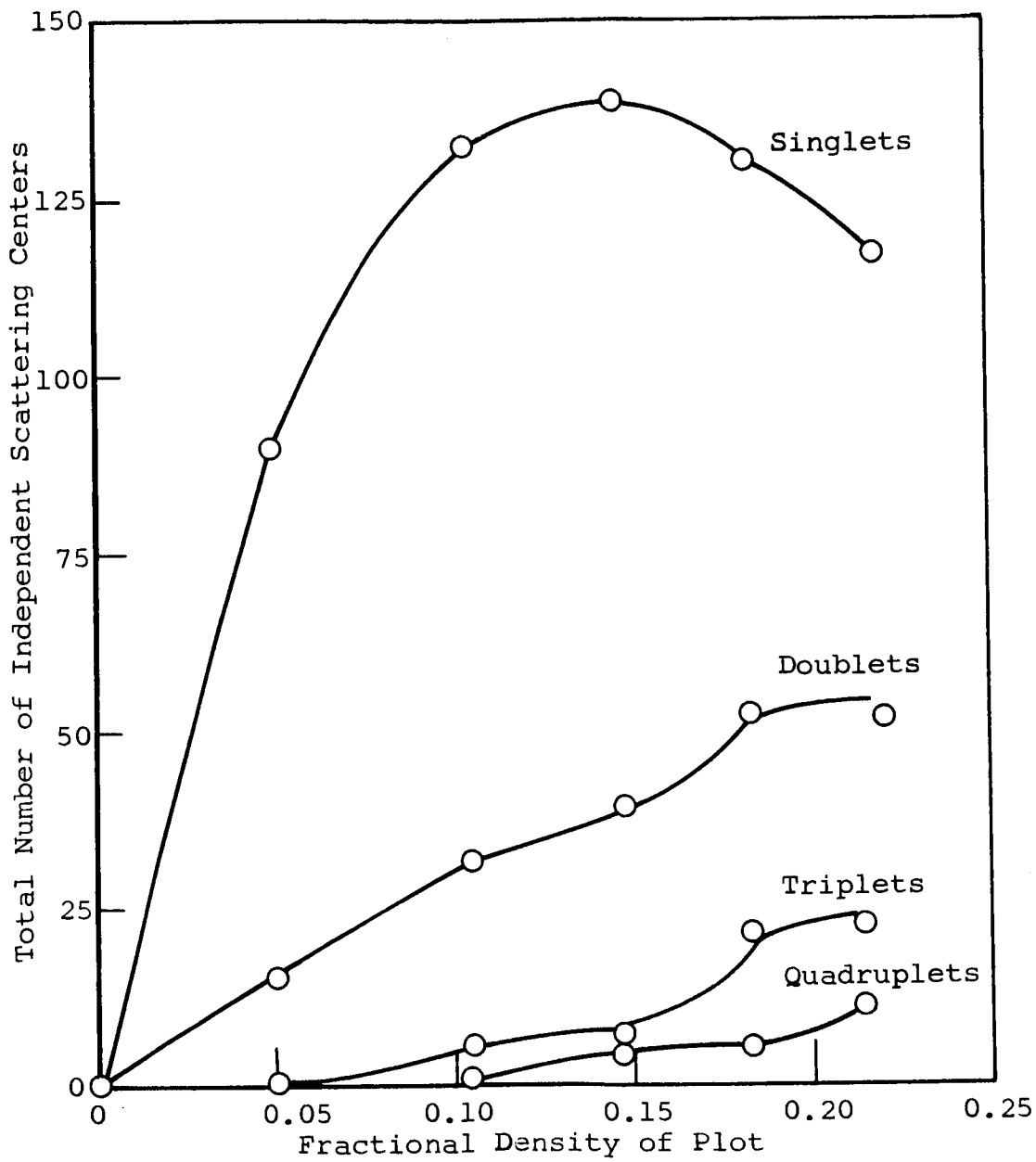FOR PARTICLES HAVING 2:1 SHAPE RATIO

Figure 48

NUMBER OF DIFFERENT SIZED CLUSTERS
AT VARIOUS VOLUME CONCENTRATIONS
FORMED FROM PARTICLES HAVING 2:1 SHAPE RATIO

First of all, irrespective of the significance of the small shift from 17 to 20%, these experiments confirm that cluster formation imposes a limit on the number of scattering centers achieved and that 20% by volume is the order of magnitude for pigment concentrations beyond which there is a loss in effective scattering power.

Secondly, the concentration at which the number of independent scattering centers starts to fall off is approximately the same for both the square model and the 2:1 particles and can be understood from examination of the structure of Figures 21 through 24 and the following qualitative reasoning. As long as the spaces between particles is several particles wide, the chances of a particle 2 diameters wide touching another particle is not much higher than the chances of a particle 1 diameter wide. For instance, consider a sphere of $\frac{n}{2}$-diameter radius such that if a small particle is placed within this sphere it can be considered to touch another particle if it at least touches the surface of the sphere. In one sense, the sphere can be considered an abstract model of an unpopulated region within a pigmented material, and in the following discussion it will be referred to as the location sphere. Now the chance that a center of a particle of diameter d will be located within the larger sphere so that it will touch its surface or extend beyond it is the ratio:

$$P_d = \frac{\frac{1}{6}\pi d^3 n^3 - \frac{1}{6}\pi d^3 (n-1)^3}{\frac{1}{6}\pi d^3 n^3} \qquad (48)$$

Thus:

$$P_d = 1 - \left(1-\frac{1}{n}\right)^3$$

It is important to notice that this relationship does not involve d, and this is why the relative locations within a paint film are not a function of particle size.

If we now consider the particle that has a shape factor of 2:1, this can be located in a larger volume in space and still

protrude through the surface of the location sphere to make
contact with a particle to form a cluster. For particles of
shape factor 2:1 with their long axis lying along the radius of
the location sphere, the probability of being in a position to
form a cluster is:

$$P_{d(2:1)} = 1 - \left(1-\frac{2}{n}\right)^3$$

However, only a fraction of the particles will lie along the
radius of the location sphere, and the probability of particles
occupying all possible orientations within the location sphere
will be:

$$P_{d(2:1)} = 1 - \left(1-\frac{a}{n}\right)^3 \tag{49}$$

where a is some number between 1 and 2.

From comparison of the probabilities expressed in Equations
48 and 49 it can be seen that the probability of cluster forma-
tion for the noncircular particle is higher than that for the
spherical particle (from spatial considerations evaluated in
isolation from other factors influencing cluster formation).
It can also be seen that the difference between them is small
when n is large but increases rapidly as n approaches a.

There is, however, a competing factor, which tends to
reduce the probability of cluster formation for particles of
shape factor 2:1 compared with particles of 1:1 symmetry. For
a given mass of particles, the number of points in space at
which a particle can occur for systems containing 2:1 particles
is half that for systems containing 1:1 particles. This means
that the effective value of n to be used in Equations 48 and 49
is larger for particles of 2:1 shape factor than for 1:1
symmetrical particles at a given volume concentration. There-
fore, we have two competing factors -- one tending to reduce
cluster formation and one tending to increase it for particles
of 1:2 shape factor. The competition between these two factors
could offer a qualitative explanation of the shift of the peak
for the maximum number of scattering centers toward the higher

volume concentrations for 2:1 shaped particles, should subsequent investigation confirm this shift.

This possible shift toward higher concentrations for achieving maximum number of scattering centers is not an argument for trying to achieve pigment particles with 2:1 shape factors, because the number of scattering centers schieved for a given mass of particles is always higher for particles of 1:1 symmetry. For instance, if both types of particles were measured by sieving techniques,[*] in which particles are classified by their minimum diameter, both types of particles would have the same measured particle size yet one set of particles would have a much higher number of scattering centers per unit mass. This suggests that it may not be possible to solve some problems associated with optical properties of paint films until quantitative methods of shape analysis are developed.

Thirdly, at the end of the discussion of the relation between Mie theory predictions of the scattering power of single particles and the optical properties of paint films (Section II), it was postulated that it may be advantageous to achieve maximum pigment surface per film thickness provided that the individual particles are still effective scattering centers. It might be argued that 2:1 or higher shape factors might be advantageous from the point of view that they have more surface per mass than a sphere. Again, this is a superficial argument and has no real meaning unless particle size is defined very carefully.

For example, consider the simple cubic model and the simple particle of 2:1 shape factor formed by fusing two cubes together over one surface. If the cube and the particle formed by fusing together have the same particle size, which they

---

[*] This is not possible for normal pigment particles at the current stage of size-analysis technology, but the fact that we are discussing a set of hypothetical measurements does not affect the validity of the points being made concerning particle size and paint film properties.

would have from sieving techniques, then the particle formed
from two cubes has less surface than the two cubes from which
it was formed, although it has more surface than a particle of
the same mass. Thus, when one dimension is identical for the
two particles, the cubical particles have more scattering
centers and more surface area per unit mass than do the particles
of 2:1 shape factor. This apparent paradox arises from the fact
that the property of interest is normally the surface area per
unit mass, whereas in discussing the properties of pigment
particles the property of interest is surface area for a given
particle size, which has to be defined carefully. Again, this
discussion underlines the need for knowledge of shape factors
in conjunction with accurate and well-defined particle-size
analysis.

It is possible to discuss the possible influence of dis-
persion on the optical properties of a paint film by using the
statistical considerations outlined in the foregoing paragraphs.
Consider a monosized pigment. If the particles are not well
dispersed in the paint film, this is equivalent to saying that
the units of pigment to be dispersed are not single particles,
but groups of particles containing 2, 3, 4 up to n particles.
A cluster of two particles can be considered to be a particle
of shape factor 2:1. The case of a cluster containing a number
of particles is more complex, because of the possible configu-
rations they can achieve in space. However, all clusters in
fact represent basic units of increasing particle-shape factor
as the cluster size increases.

From the statistical considerations given above, one would
anticipate that in a poorly dispersed pigment the concentration
of solids for maximum scattering centers is displaced toward
the higher concentration but that the total number of scattering
centers is low. Therefore, increasing the degree of dispersion
should increase the overall opacity and should shift the maximum
of the opacity/concentration curve toward lower concentrations.
This conclusion is based on tentative postulations and very

simple models, but its implications are sufficiently interesting to warrant investigation. If the conclusion proves to be a real description of the properties of a paint film, an interesting corollary to the hypothesis is that the location of the maximum in the concentration/maximum scattering centers curve will always be a function of the shape factor of a well-dispersed pigment.

It is pertinent at this point to discuss the relevance of the above speculations based on statistical reasoning. Even if all of the speculations proved to be irrelevant, this theoretical study has at least indicated the possible phenomena occurring within a paint film. Knowing these possible phenomena, we can design experiments efficiently so that the importance of the possible machanisms affecting the opacity of paint films can be either substantiated or eliminated.

C. Simple Model of Monosized Cubic Pigment with Extender

A simple modification of the original Monte Carlo plotting experiment can be used for exploring the possible role of extender particles in a paint film. Consider an idealized system in which equal quantities of equally sized pigment and extender particles are randomly dispersed. To simulate such a system we carried out the following transformations.

(a) A transparent piece of graph paper was placed on top of the 20% concentration plotted system. In a random-number table odd and even numbers occur equally. Therefore each particle was marked through onto the new graph paper in conjunction with a random-number table -- □ for even numbers and o for odd numbers. The result represented the system that would be obtained for equal numbers of pigment and extender particles. The ⊓ denotes pigment and the o extender particles. The fractional concentration of both extender and pigment was 10%.

The resultant transformation, corresponding to 790 particles plotted, is shown in Figure 49. The original data (for the pigment alone, Table 6) were obtained when 784 particles were plotted.
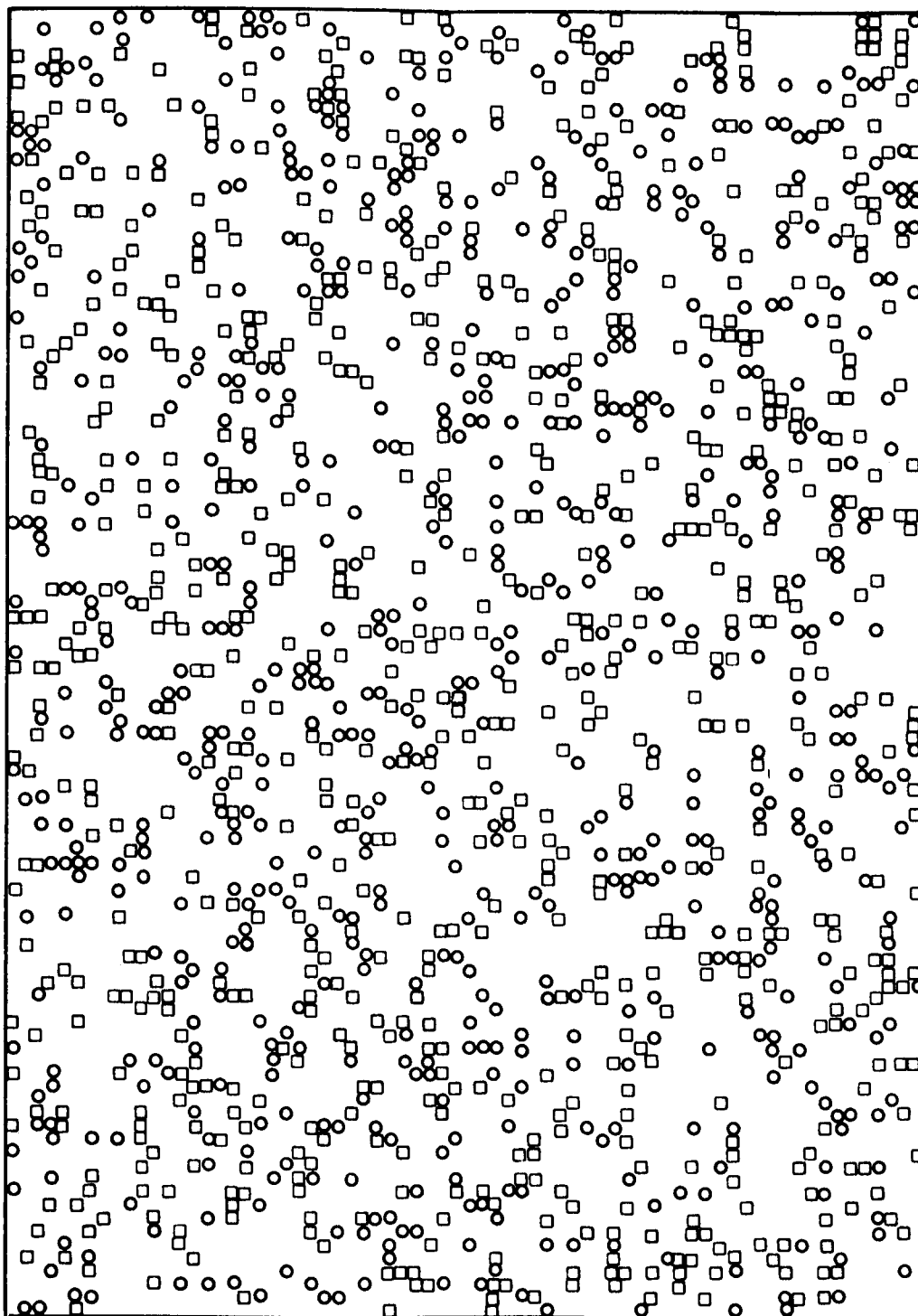
Figure 49

SIMULATED PIGMENT-EXTENDER SYSTEM: 10% PIGMENT, 10% EXTENDER

The number of particles plotted in each case is suffi-
ciently close for comparison of the number and the type of
scattering centers achieved for a fixed volume concentration
with and without extender particles. For direct comparison,
Table 11 lists the cluster distribution for pigment plus
extender (abstracted from Figure 49) and that for pigment alone
(from Table 6).

Table 11

DATA ON CLUSTER FORMATION AT 0.1 VOLUME FRACTION
OF IDEALIZED MONOSIZED PIGMENT
DISPERSED WITH AND WITHOUT THEORETICAL EXTENDER

Pigment	Number of Particles, N'	Number of Clusters									Number of Independent Scattering Centers, S
		Number of Units in Cluster									
		1	2	3	4	5	6	7	8	9	
Alone	784	315	86	43	15	7	6	4	–	1	477
Plus extender	790	387	75	45	15	6	1	2	1	–	532

(b) Plots having 30% pigment and 5% and 10% extender
respectively were constructed as follows. By using pairs of
coordinates chosen from random number tables, simulated extender
particles were placed in the 30% concentration plot (Figure 24).
In the event the location of an extender particle coincided with
a square occupied by pigment, the pigment particle was removed
and a record made of this event. After the required concen-
tration of extender had been placed in the grid, the displaced
pigment particles were relocated by random coordinates in free
spaces of the plot. These plots are shown in Figures 50 and 51.

For direct comparison of cluster growth, Table 12 lists
the cluster distribution for the pigment plus extender
(abstracted from Figures 50 and 51) and that for the pigment
alone (from Table 6).
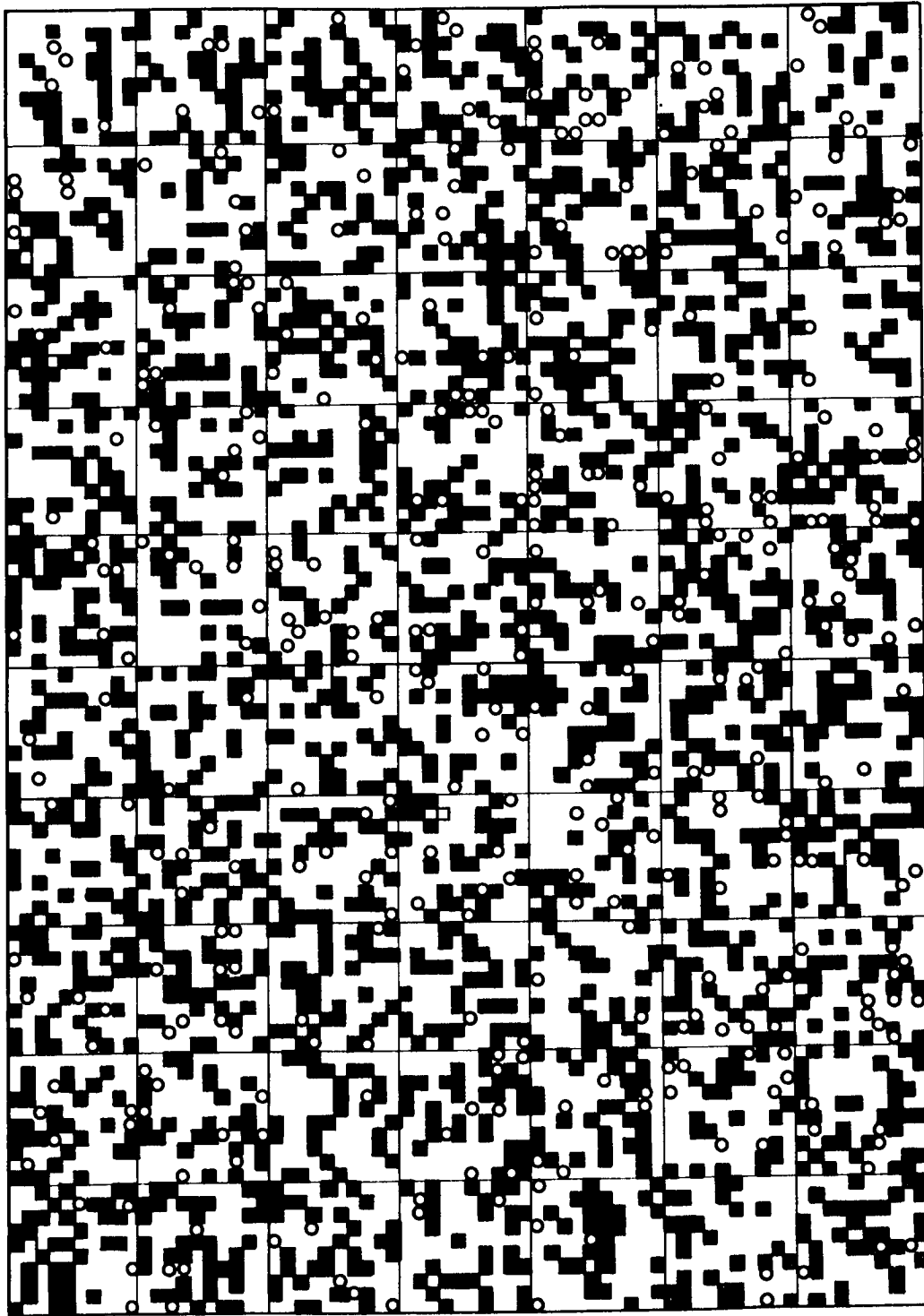
Figure 50

SIMULATED PIGMENT-EXTENDER SYSTEM: 30% PIGMENT, 5% EXTENDER

Figure 51

SIMULATED PIGMENT-EXTENDER SYSTEM: 30% PIGMENT, 10% EXTENDER

Table 12

DATA ON CLUSTER FORMATION AT 0.3 VOLUME FRACTION
OF IDEALIZED MONOSIZED PIGMENT
DISPERSED WITH VARIOUS CONCENTRATIONS OF THEORETICAL EXTENDER

Extender Conc., fraction	Number of Particles, N'	Number of Clusters									Number of Independent Scattering Centers, S
		Number of Units in Cluster									
		1	2	3	4	5	6	7	8	9	
0.0	2100	121	56	38	27	14	9	6	13	8	338
0.05	2100	125	51	37	25	18	9	10	12	7	351
0.1	2100	132	50	33	18	17	11	14	13	5	350

The data in Table 11 show that when 10% extender is present in equal quantities with the pigment, (a) there is an overall increase of 12% in the number of scattering centers achieved, (b) there is a 23% increase in the number of single-particle centers (these are probably the most effective in scattering the light), and (c) the overall number of scattering centers is as high as the total number achieved at any higher concentration with the pigment alone (Figure 35).

When cluster distributions for both plots (with and without extender) are plotted (Figure 52), both obey the log-normal distribution. Figure 52 also shows that when an extender is present, there is less probability that the larger clusters will occur.

On the other hand, when 10% extender or less is present with 30% pigment, (a) the increase in number of scattering centers is only 4% and (b) the increase in number of single-particle centers is less than 10%. These data are substantiated by Figure 53, which shows that at these relative concentrations the extender is not efficient at preventing the buildup of large clusters.
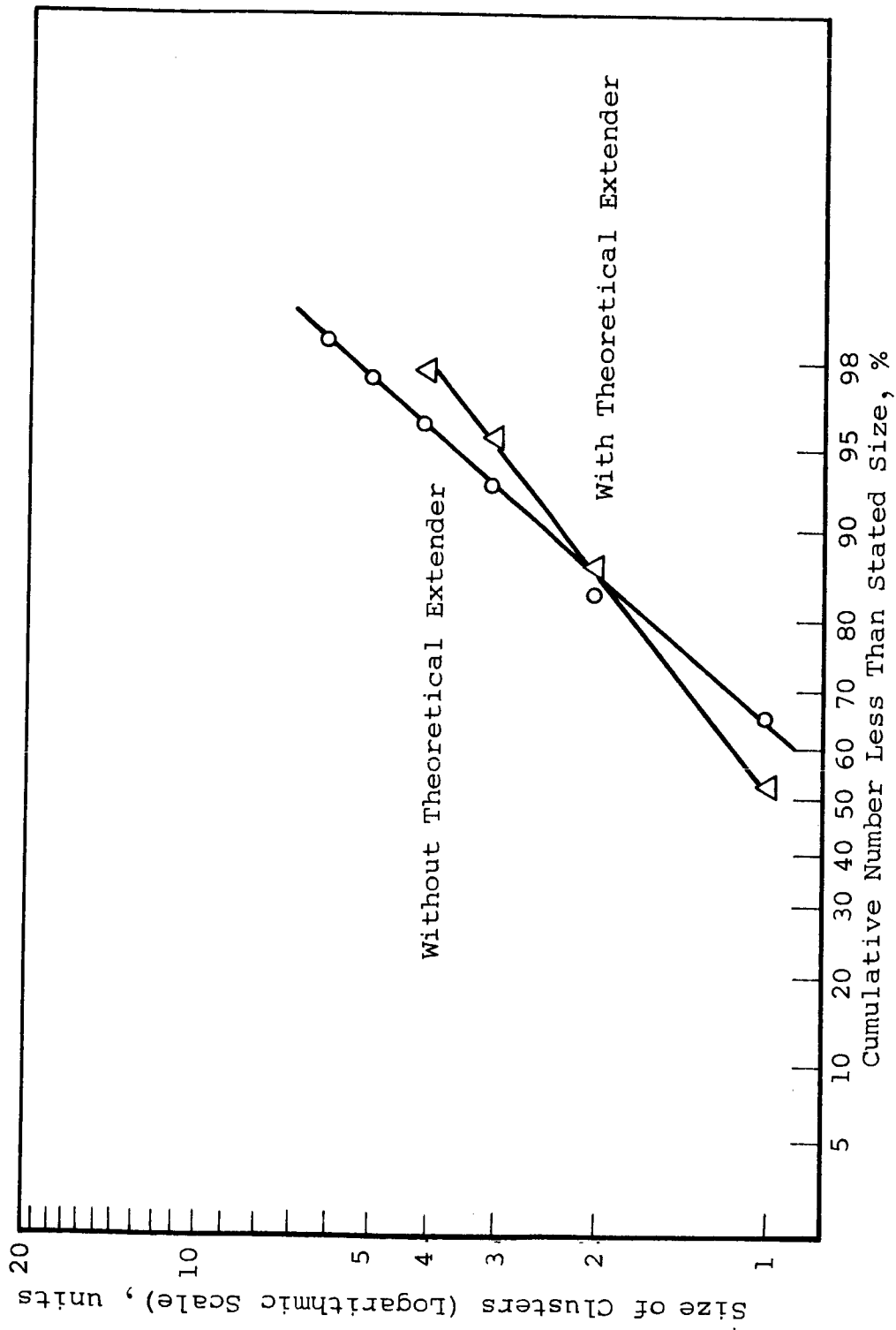
Figure 52

SIZE DISTRIBUTIONS OF CLUSTERS FORMED AT VARIOUS VOLUME CONCENTRATIONS
FOR IDEALIZED MONOSIZED PIGMENT DISPERSED WITH AND WITHOUT EXTENDER
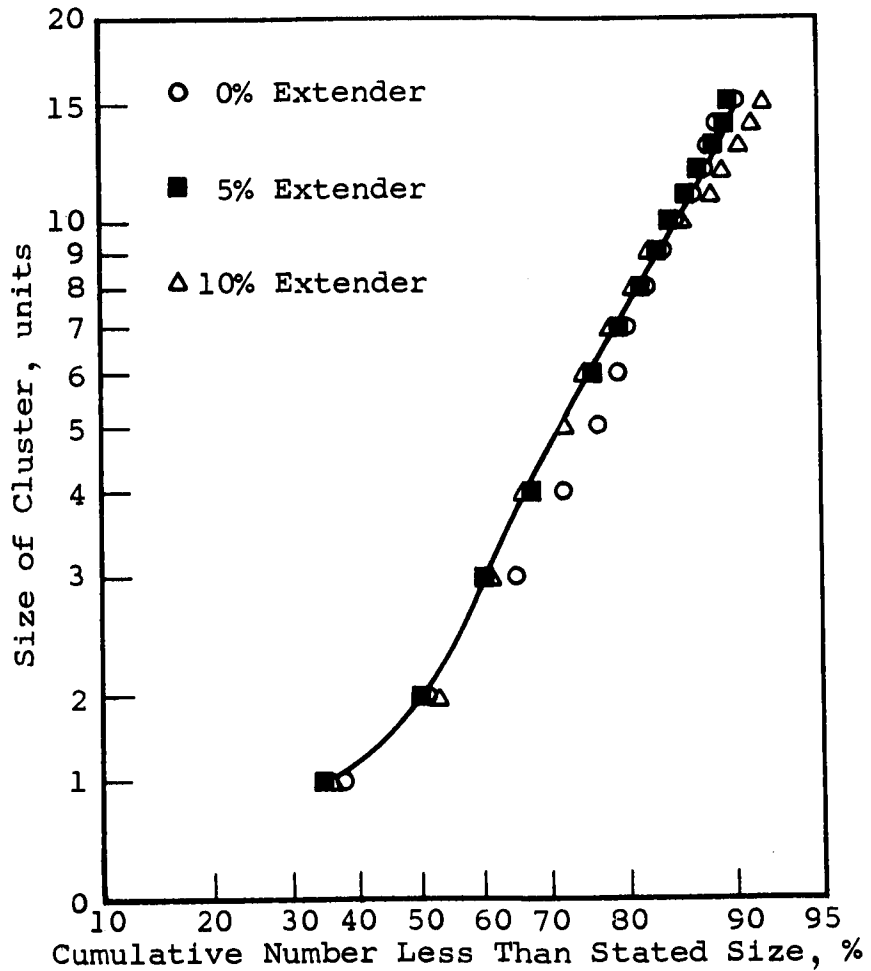
Figure 53

SIZE DISTRIBUTION OF CLUSTERS FORMED AT 0.3 VOLUME CONCENTRATION
FOR IDEALIZED MONOSIZED PIGMENT DISPERSED WITH VARIOUS CONCENTRATIONS
OF THEORETICAL EXTENDER

This simulation experiment strongly suggests that the extender has a definite role in light-scattering phenomena, i.e., in preventing pigment clusters by mechanical competition for possible positions. An extention to this conclusion is that most efficient use of pigment for scattering is to be gained from the use of a maximum quantity of free extender to compete for cluster sites.

Note than an encapsulated pigment would carry its own "built-in" extender; i.e., it would have a region surrounding it that another pigment particle could not occupy. Thus it could be a very efficient light-scattering center in a paint film. This aspect is discussed in Section D.

D. Partial Encapsulation of Pigment Particles

The role played by an extender in the light-scattering behavior of a paint film was discussed in Section C. It was concluded that the extender mechanically competes with the pigment for location within the film and thus depresses the buildup of clusters of pigment particles.

If all pigment particles were completely encapsulated with extender before they were randomized in the vehicle, formation of pigment-particle clusters would not be possible. Since it may not be feasible on economic or practical grounds to fully encapsulate each pigment particle, consider the advantage to be gained from partial encapsulation of pigment.

Consider the simple two-dimensional Monte Carlo plotting experiment described in Section A, in which square particles are randomly placed upon a flat grid. Suppose each particle is modified so that one face is coated with extender without altering the size or shape of the composite particle.

The possible configurations of two such particles are shown diagramatically in Figure 54. This figure shows that the probability of two cubes touching with a layer of extender between the pigment is 7/16, i.e., 0.437. Thus, approximately half the doublet clusters will be broken up into single scatterers by encapsulation of only 1 face in 4.
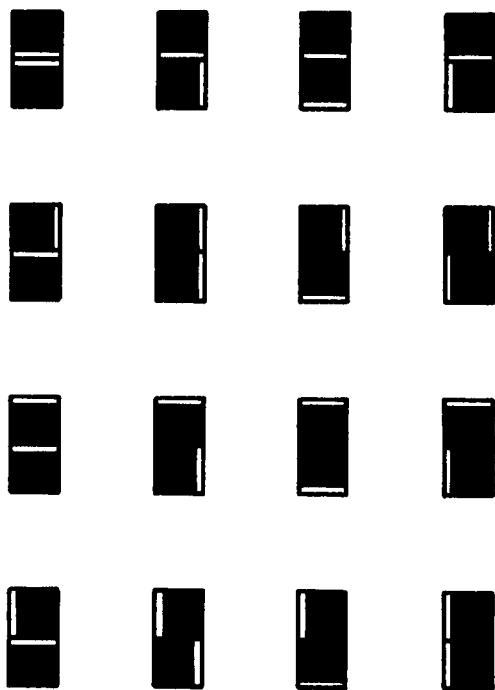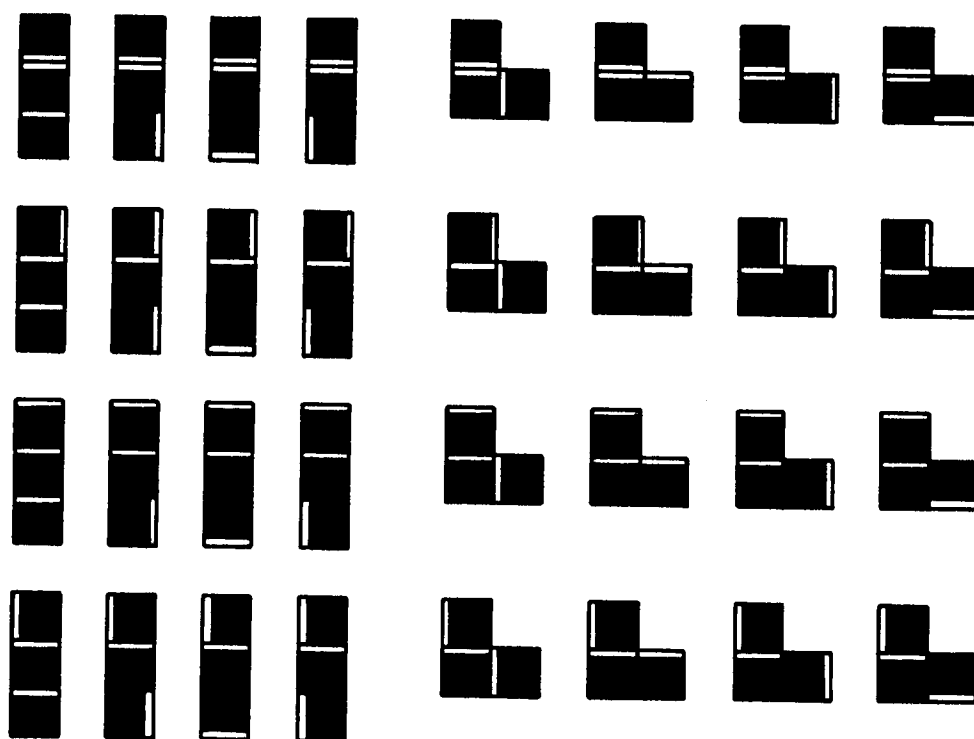
Figure 54

POSSIBLE CONFIGURATIONS
OF TWO PARTIALLY ENCAPSULATED PARTICLES

Figure 55 shows some of the possible configurations as a third particle is added to the doublet shown in Figure 55. In this case the probability of having an extender layer between at least two particles is 0.430.

As the clusters are allowed to grow, the number of possible configurations increases very rapidly to the point at which it becomes impractical to predict the probability of the pigment being separated by the extender layer. However, the effect of one-face coated particles on complex-cluster development has been demonstrated by using the clusters found in the 20% Monte Carlo plot (Figure 23). Each particle of a cluster was assigned a coated face by using random numbers 1 to 4 to represent the four faces of the square particle. Figure 56 shows the encapsulated cluster profile and the cluster development that would have resulted had partially encapsulated particles (1 face in 4) been used. For all six clusters examined, the use of partially encapsulated pigment would have produced a larger number of smaller clusters. In fact, the 6 clusters studied produced 33 smaller clusters.

The discussion has so far dealt entirely with a two-dimensional system using square particles. The transition to three dimensions is not simple and cannot be predicted from the above discussion. However, a study of the cluster break-up when the probability of a particle face being encapsulated is 1 in 6, thus simulating a three-dimensional cubic particle, has shown a similar significant decrease in cluster size and increase in cluster number. Figure 56 shows that 1/6 encapsulation of the particles in the clusters previously examined produces 19 smaller clusters.

The foregoing discussion strongly suggests that a significant increase in the number of dependent pigment scattering centers developed in a paint film of given pigment volume concentration can be achieved by less than complete encapsulation of pigment with extender.

Figure 55

SOME OF THE POSSIBLE CONFIGURATIONS
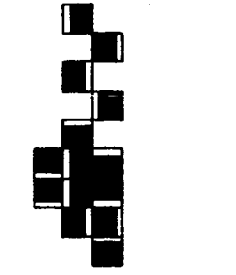OF THREE PARTIALLY ENCAPSULATED PARTICLES
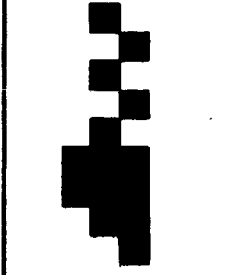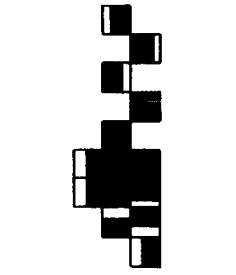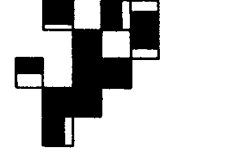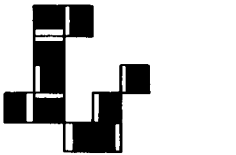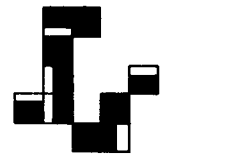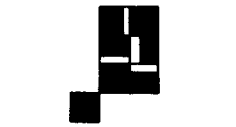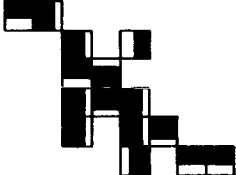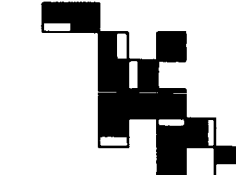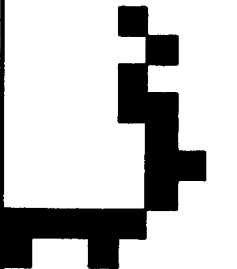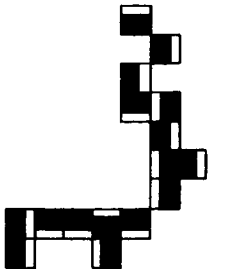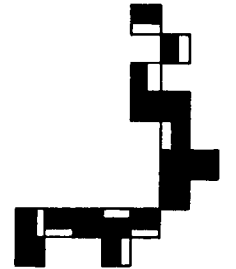
Cluster Profiles Using Unencapsulated Pigment	Cluster Profiles Using Pigment Encapsulated on 1 Face in 4	Cluster Profiles Using Pigment Encapsulated on 1 Face in 6

Figure 56

CLUSTER DEVELOPMENT USING PARTIALLY ENCAPSULATED PIGMENT

It appears that a relatively inexpensive method of partial encapsulation would be to suspend the pigment randomly in a thermosetting resin of the same refractive index as the vehicle to be used in the paint film. After the resin has set, the system would be milled to a predetermined size range to give roughly shattered pigment/resin composite particles. Provided the pigment/resin bond and the pigment and resin shatter strengths are all comparable, it is anticipated that the method will yield a partially encapsulated pigment suitable for use in highly reflecting coatings.

IX. RANDOM SCREEN MODEL FOR STUDYING PENETRATION OF LIGHT THROUGH PAINT FILMS

A. Introduction

If a section is taken through a paint film, it can be considered to define a screen in which the pigment cross section can be regarded as relatively opaque areas distributed at random in a transparent slab of material. On this basis, we decided to study the possibility of treating the transmission of radiation through a paint film as a series of radiation/screen encounters. The properties of the screens would be related to the pigment volume concentration of the paint film. It is possible to consider events at each screen to be independent of previous encounters, since diffraction effects would diffuse the light energy between encounters. As a first stage in developing this statistical model, the properties of random screens were studied.

B. Physical Properties of Random Screens

The first property of randomly imposed screens is the residual straight-through area, since this can be used to deduce important facts concerning the persistence of an incident plane parallel beam of light penetrating a paint film.

Consider an area, A, within which two laminae, or areas a_1 and a_2, can be placed at random (Figure 57). To define randomness in this situation, the position of the centroid of each subarea (a_1 and a_2) is specified by x and y coordinates, which are selected by using random-number tables. A fixed direction on the laminae permits random orientation; i.e., all directions are equally probable. If the whole of the area. A. is covered with N points equidistant from each other, the number of points within a_1 is:

$$N \cdot \frac{a_1}{A}$$

The number of points within a_2 is:

$$N \cdot \frac{a_2}{A}$$

If one point within A is selected, the chance that it lies within either area is:

$$\frac{a_1}{A} \quad \text{and} \quad \frac{a_2}{A}$$

The chance that one point will lie within both areas simultaneously is:

$$\frac{a_1 \cdot a_2}{A^2}$$

Figure 57

RANDOM LAMINAE WITHIN A DEFINED AREA
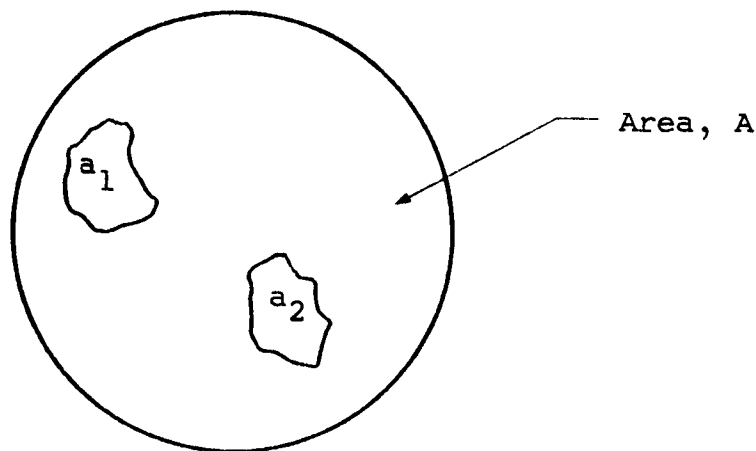
If many events are considered, the average number of points that will lie in both areas is:

$$N \frac{a_1 \cdot a_2}{A^2}$$

Therefore, the average overlap area over many events is:

$$\frac{a_1 \cdot a_2}{A^2} A$$

If A is taken to be unity and a_1 and a_2 are expressed as fractions of unit area f_1 and f_2, the fractional area of overlap for many events is $f_1 \cdot f_2$.

This discussion has proceeded in terms of many super-positions of two areas within a test area. Mathematically, an extended screen with many random apertures of average fractional area f_1, placed above another screen, contains many random apertures of average fractional area f_2, which is equivalent to many random superpositions of the two isolated areas.

Physically, the difference is that in the case of the two screens the average is for many events distributed in space, while in the case of the two areas the average is for many events distributed in time. Therefore, the average residual exposure for two random screens superimposed should be $f_1 \cdot f_2$. Similarly, for a series of n screens it should be $f_1 \cdot f_2 \cdot f_3 \ldots f_n$.

Two regular screens superimposed at random should be a close approximation to random screens placed on top of each other. Therefore, the following experiment was devised to test the reasoning given in the foregoing discussion. Consider the screen shown in Figure 58. This screen was chosen to fit the proportions of the wire openings in a 325-mesh screen. The width of the closed portions to the openings is 36/44. The basic unit of the screen is an open portion 44 units square, with opaque portions 36 by 80 units along two sides. Therefore, the fractional opening in the screen is:

$$\frac{44^2}{80^2} = 0.303$$

For two screens superimposed, the open area is 0.092, and for three screens, 0.028.

A master circular grid (Figure 58) containing 325 whole square openings was constructed on paper. The opaque portions were covered with India ink, and the openings were cut out with a scalpel. This master was copied by Xerography. The master was then superimposed at random on this copy, and the combination again copied by Xerography. The openings common to both screens could be seen clearly on this copy.
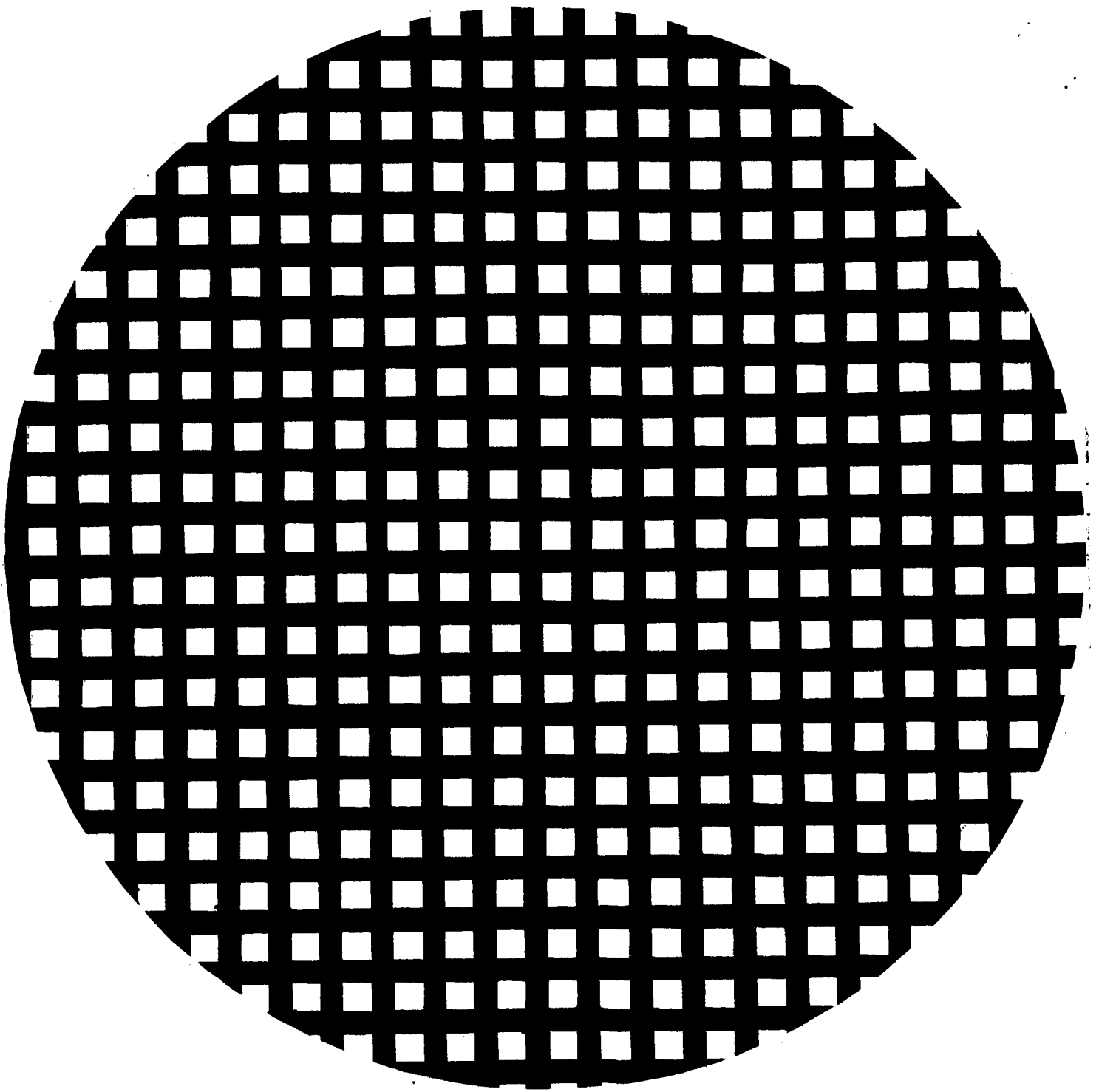
Figure 58

BASIC SCREEN (OPEN AREA, 0.303)

To measure the open area, the portions of the disk corresponding to the common open area were cut out with a scalpel. The loss in fractional weight of the disk represents the fraction of open area remaining. The experiment was repeated five times. The disks obtained by the two super-positionings are shown in Figures 59 through 63.

The result of superimposing the original master screen randomly on one of the double screens is shown in Figure 64. Again, the common open areas of all three screens were estimated by cutting away the appropriate portions of the reproduced disk and measuring the loss in weight. Similar experiments were carried out to simulate four, five, and six superimposed screens. Typical simulated systems for three, four, and five screens are shown in Figures 64, 65, and 66.

The experimental results are summarized in Table 13. The data show that the predicted and measured straight-through fractional areas agree within the limits imposed by experimental error and statistical fluctuations. This agreement indicates that the penetration of a light beam into a pigment can be predicted by considering the random screens formed by the pigment in the paint film.

It can be shown that the area ratio of solid to space exposed upon sectioning a composite body is the same as that of the solid to space in the composite body (ref. 26). Consider the general case of α percent solids. After n equivalent screens, the percentage area available for straight-through transitions is $(1-\alpha)^n$. Data for a few values of n and α are given in Table 14. It can be seen that for a paint of usual pigment volume concentration, the forward beam would not persist for more than a depth of a few pigment diameters even if diffraction effects were ignored. The spreading of the beam due to diffraction will enhance the decay of the forward beam. The general conclusion is that for penetration of a light beam into a normal paint film, the forward-directed beam is diverted after a depth of a few pigment diameters.
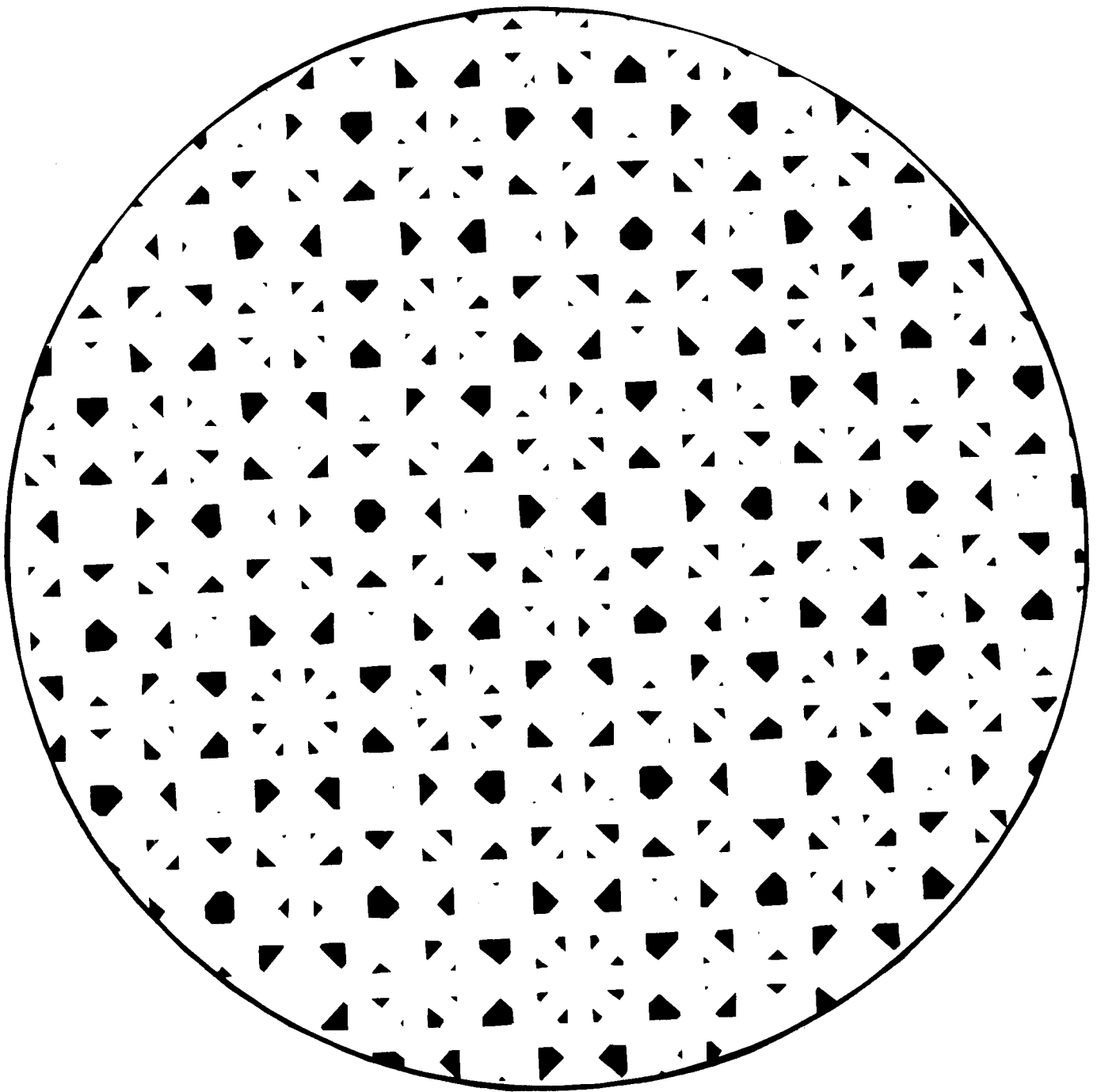
Figure 59

TWO RANDOMLY SUPERIMPOSED SCREENS (OPEN AREA, 0.098)

Figure 60

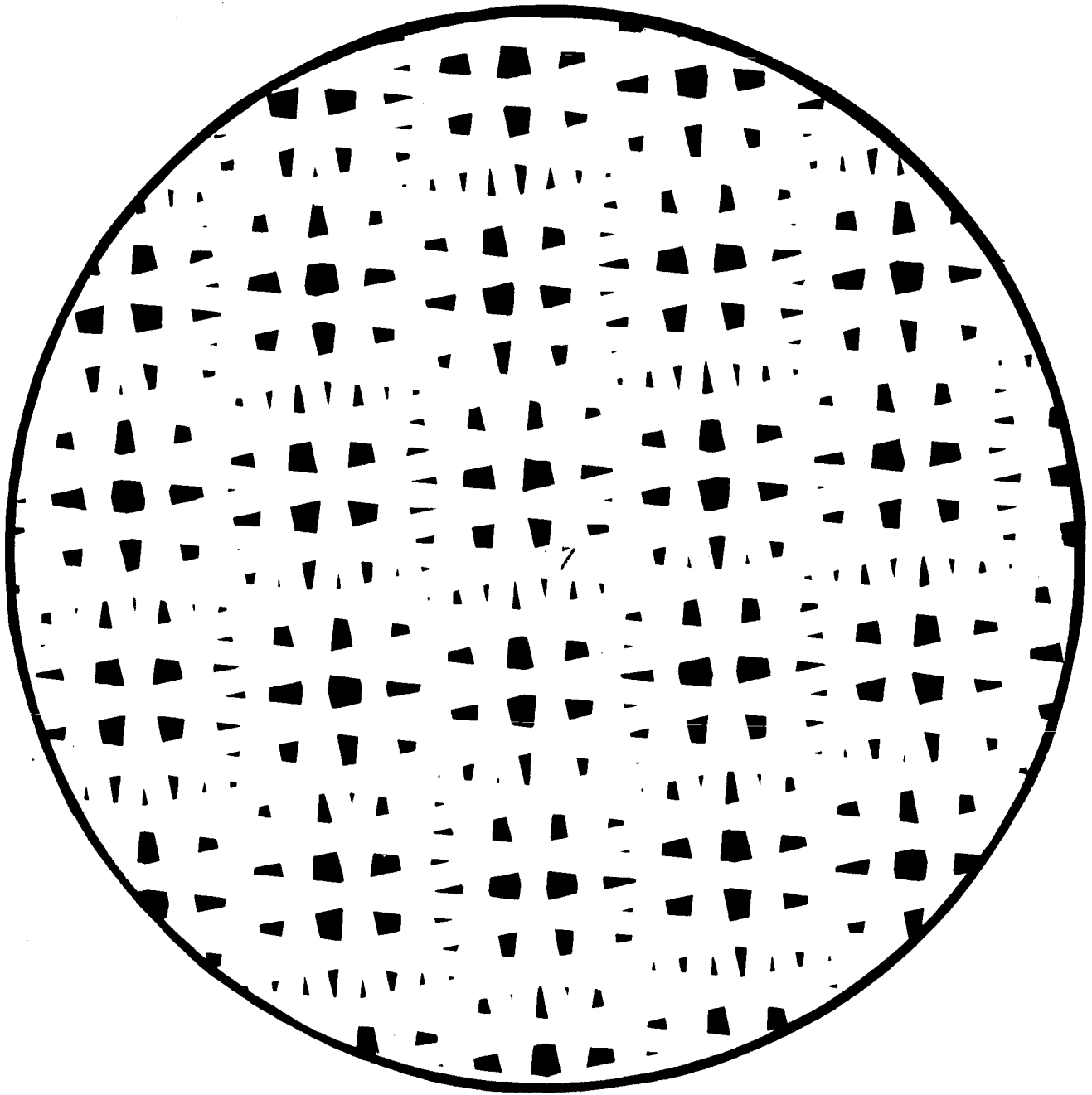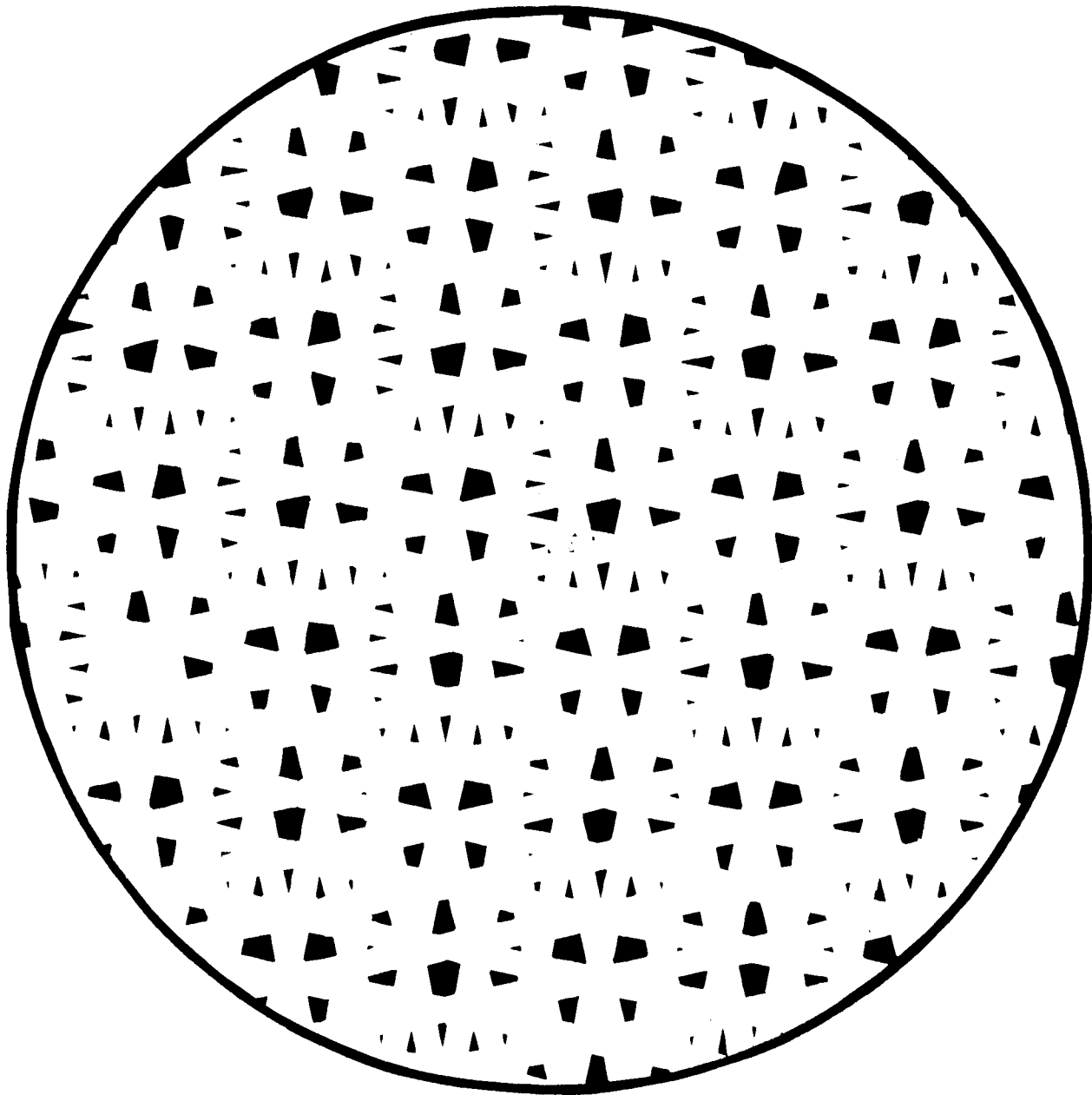TWO RANDOMLY SUPERIMPOSED SCREENS (OPEN AREA, 0.105)

Figure 61

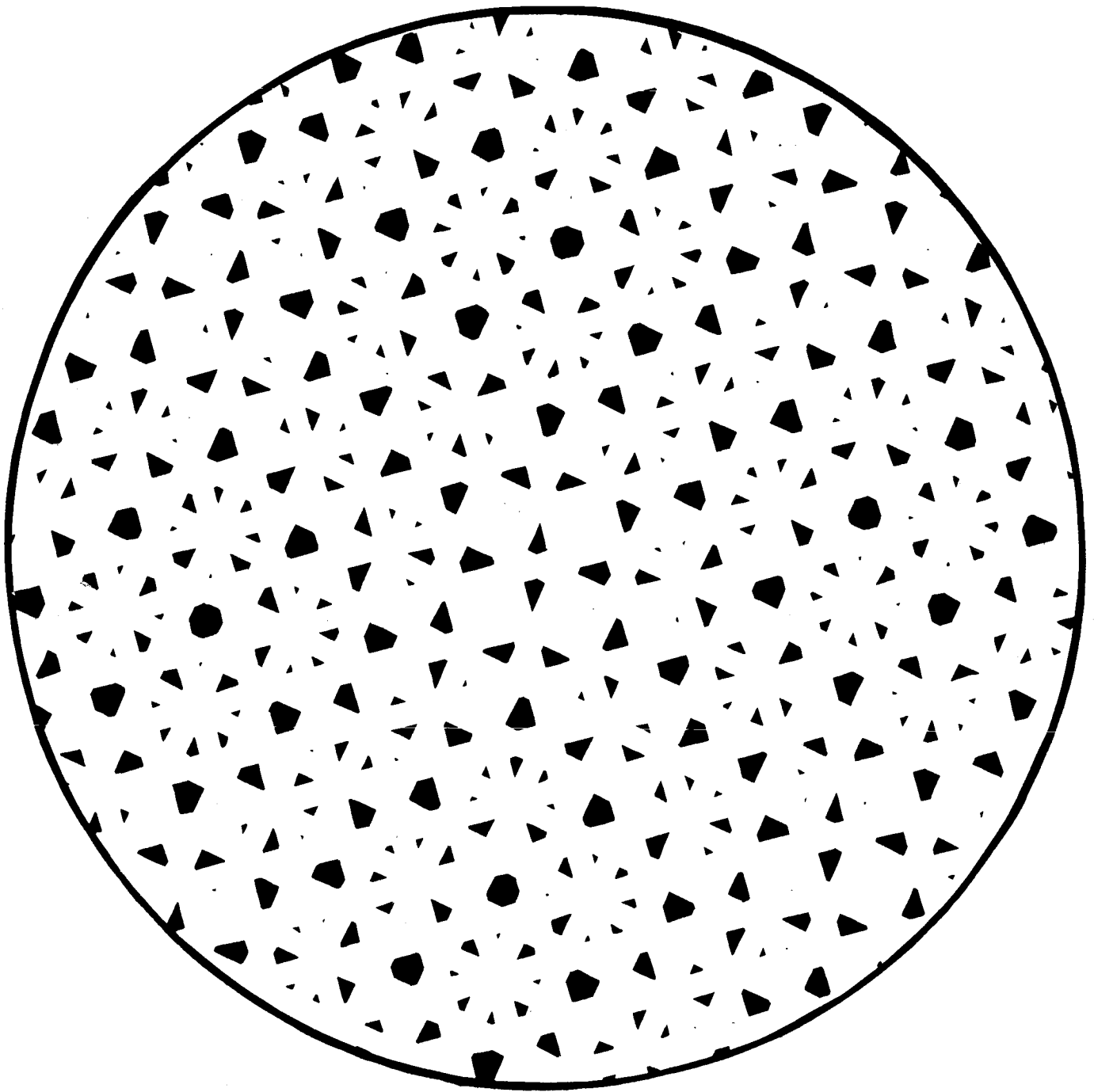TWO RANDOMLY SUPERIMPOSED SCREENS (OPEN AREA, 0.092)

Figure 62

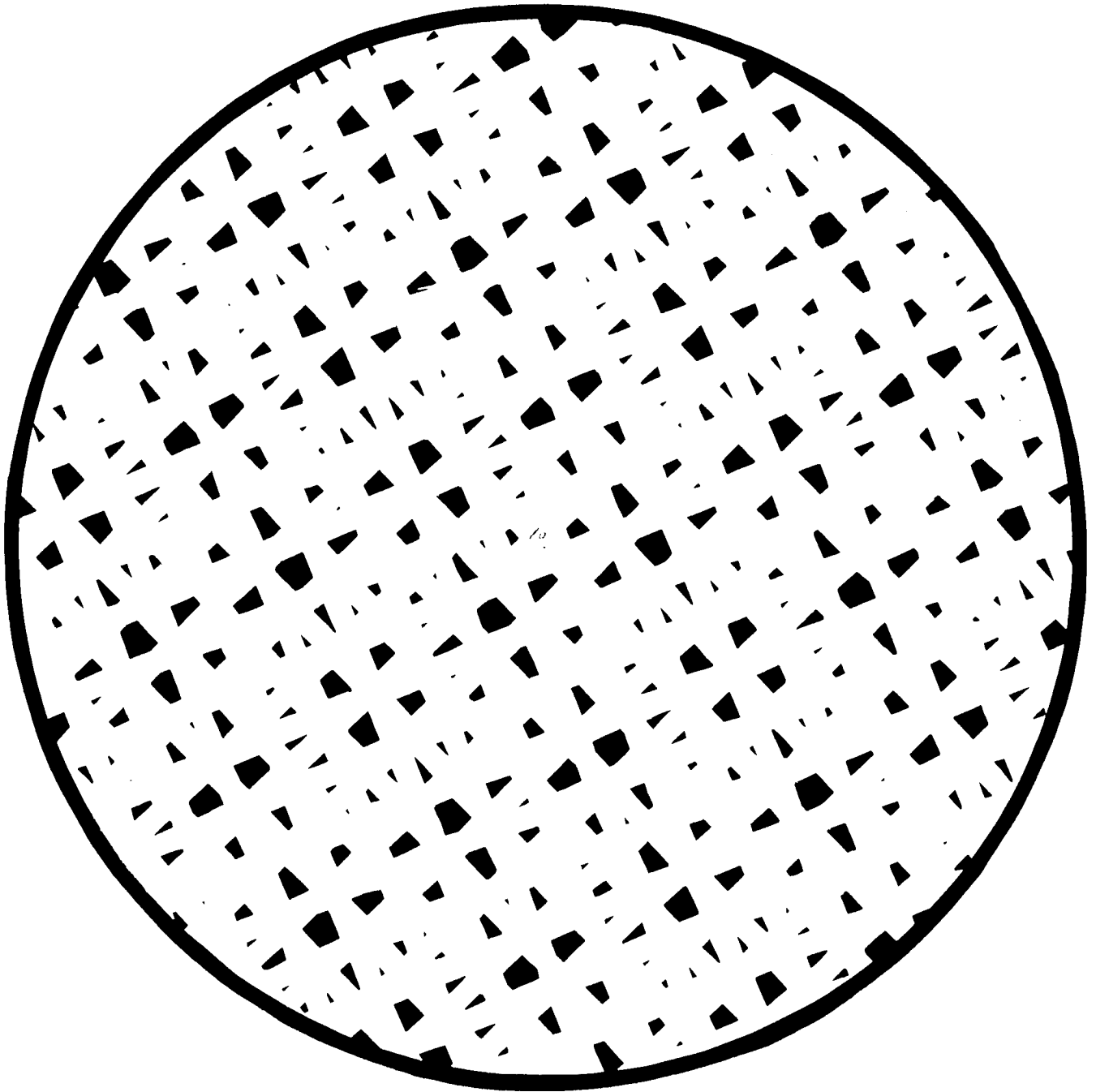TWO RANDOMLY SUPERIMPOSED SCREENS (OPEN AREA, 0.101)

Figure 63

TWO RANDOMLY SUPERIMPOSED SCREENS (OPEN AREA, 0.102)
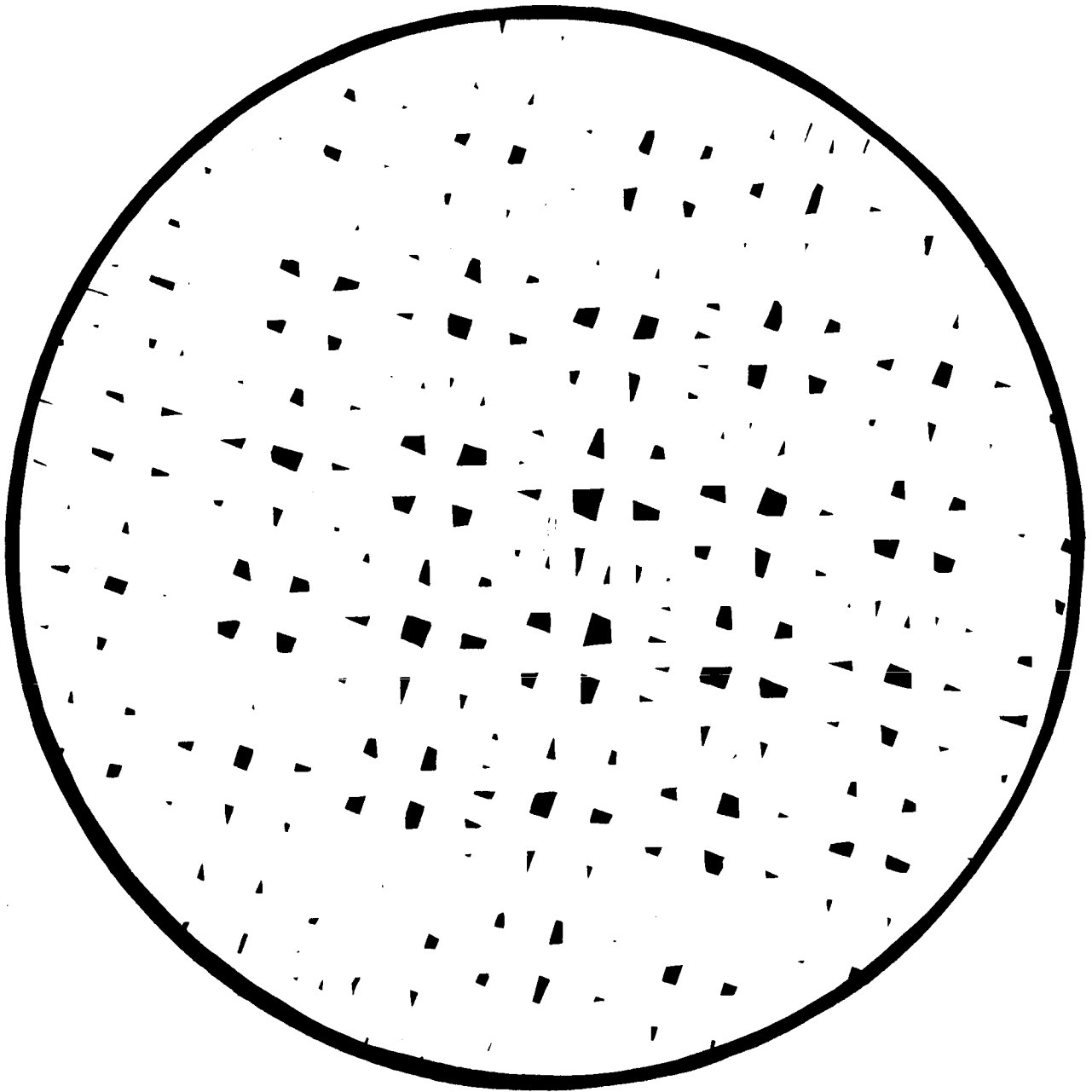
Figure 64

THREE RANDOMLY SUPERIMPOSED SCREENS (OPEN AREA, 0.03)
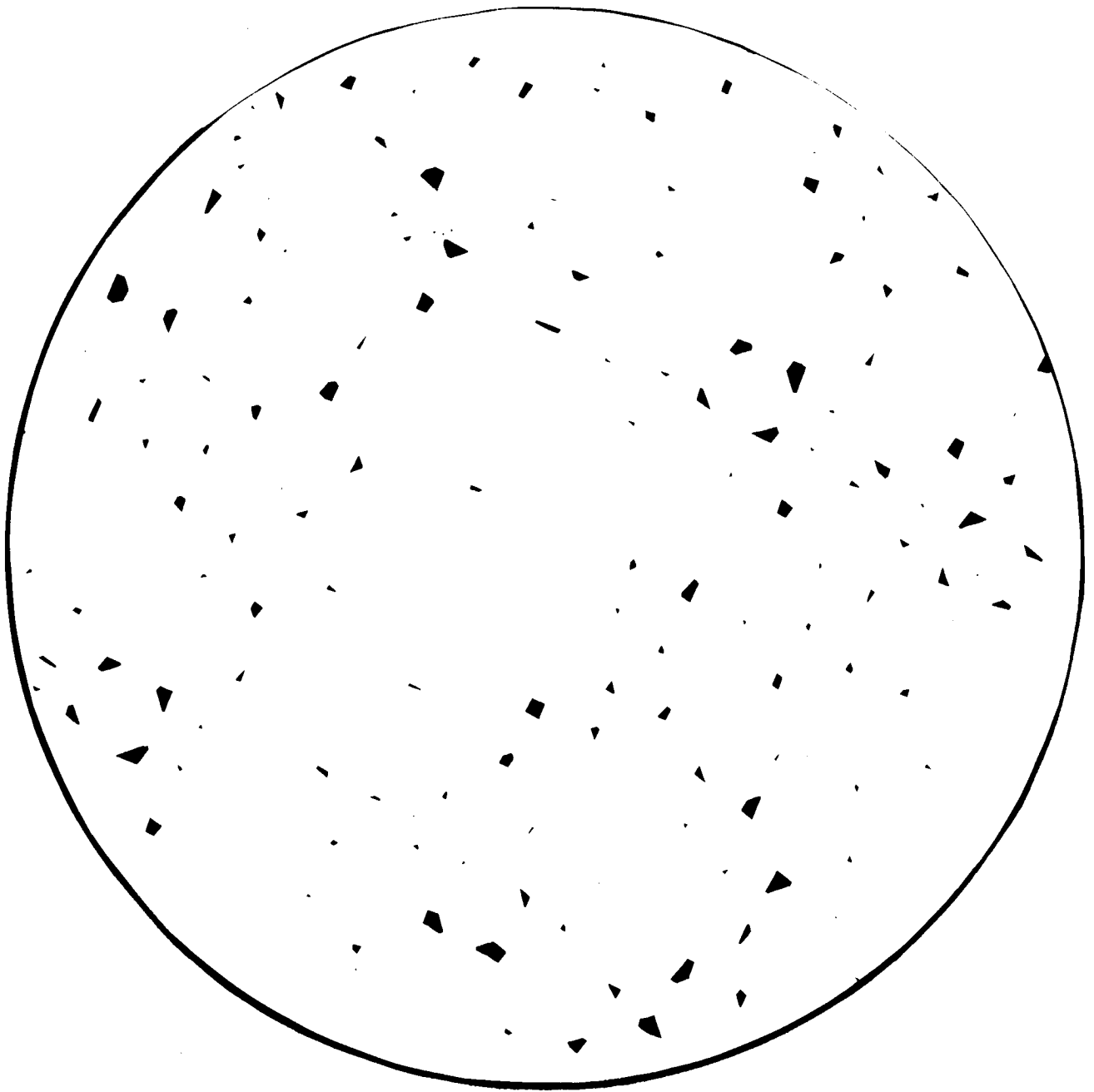
Figure 65

FOUR RANDOMLY SUPERIMPOSED SCREENS
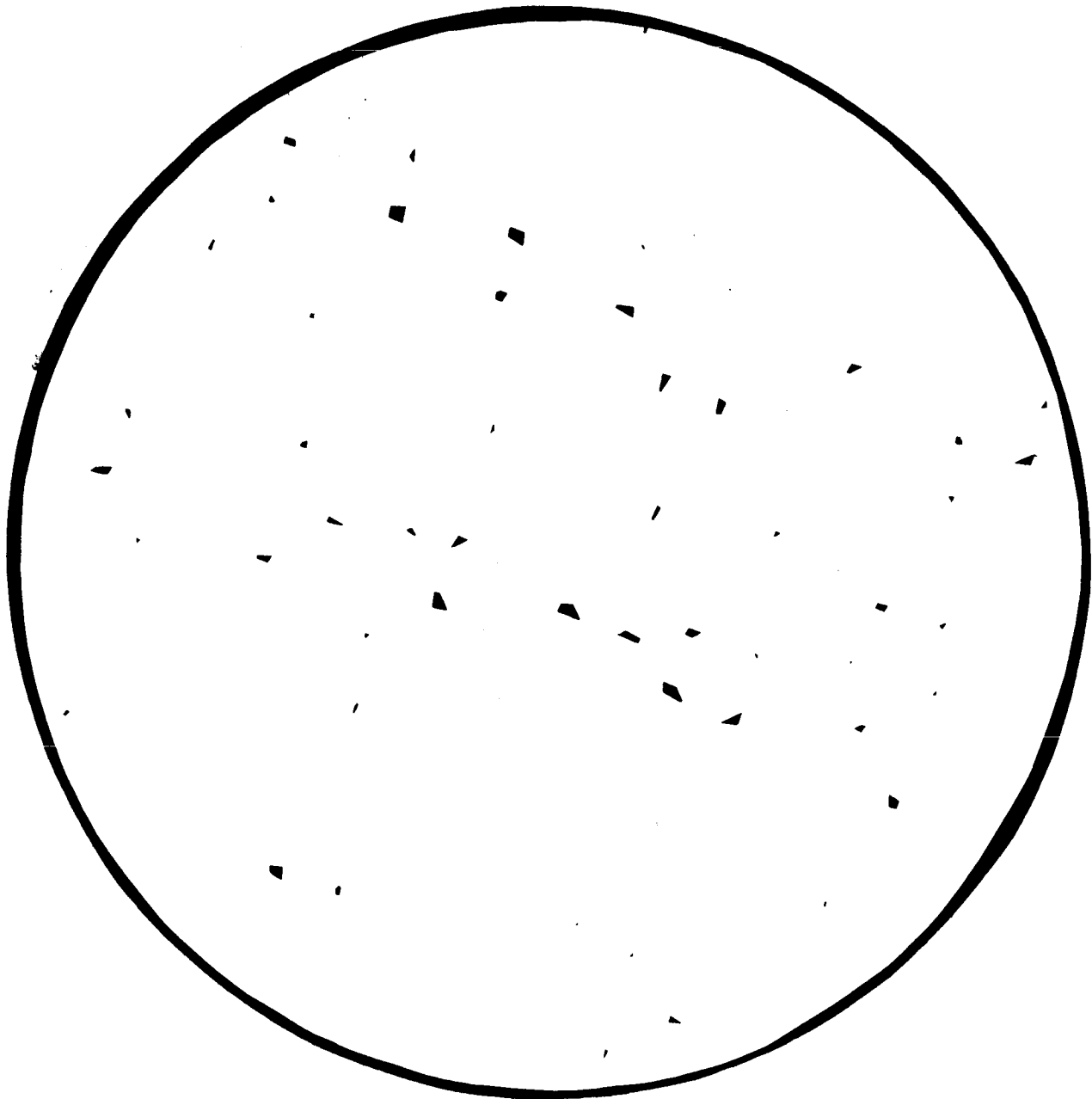
Figure 66

FIVE RANDOMLY SUPERIMPOSED SCREENS

Table 13

AVAILABLE STRAIGHT-THROUGH PATHS
IN RANDOMLY SUPERIMPOSED SCREENS
(Open Space in Original Screen, 0.303)

Number of Screens Superimposed	Straight-Through Fractional Area	
	Predicted	Measured
2	0.092	0.092
		0.102
		0.098
		0.101
		0.105
3	0.028	0.030
		0.028
4	0.008	0.012
		0.011
		0.007
		0.010
		0.008
		0.006
		0.014
5	0.002	0.003
		0.001
		0.001
6	0.0006	Too small to measure

Table 14

FRACTION OF SPACE AVAILABLE FOR STRAIGHT-THROUGH PASSAGE

α	Number of Equivalent Screens				
	3	4	5	6	7
0.50	0.125	0.062	0.031	0.015	0.007
0.40	0.216	0.130	0.078	0.047	0.028
0.30	0.343	0.240	0.168	0.118	0.083

C. Development of Random Screen Model

In the traverse of a multitude of photons through a paint film, the energy flow can be depicted pictorially as in Figure 67. It is pertinent to note that the arrows do not depict rays, but only the directional flow of energy. The use of arrows to depict energy directions and to symbolize encounters of energy with boundaries between media of different refractive indices is consistent with the procedure followed in advanced texts on wave optics theories. If it is preferred, the same type of reasoning based on the use of Huygen's secondary wavelets in the diagram would lead to the same result. It is not even necessary for the events shown to have a physical reality if they are adequate representations of energy flow, just as it is not necessary for a 3/4 child to be born before we can describe the average American family as having 1.75 children.

The situation shown in Figure 67 summarizes the information that at encounter 1 some of the energy is reflected and some transmitted. The reflected portion proceeds directly to encounter 2. The energy transmitted into the second medium at encounter 1 proceeds to encounter 3. Again, at encounters 2 and 3 there are partial reflection and transmission. The further sequence of events is suggested by the unbroken lines drawn in Figure 67.

Symbolically, the encounters of Figure 67 can be represented as shown in Figure 68. At encounter 1 the energy is separated into two parts, a reflected portion, R, and a transmitted portion, T. Each of these has associated with it a set of characterizing parameters: α, the directional function; Θ, the phase change with respect to the initial beam; S, a function of the absorption factor of the medium through which the energy is traveling and of the optical path length, P, between encounters; and β, the fraction of energy reflected or transmitted.
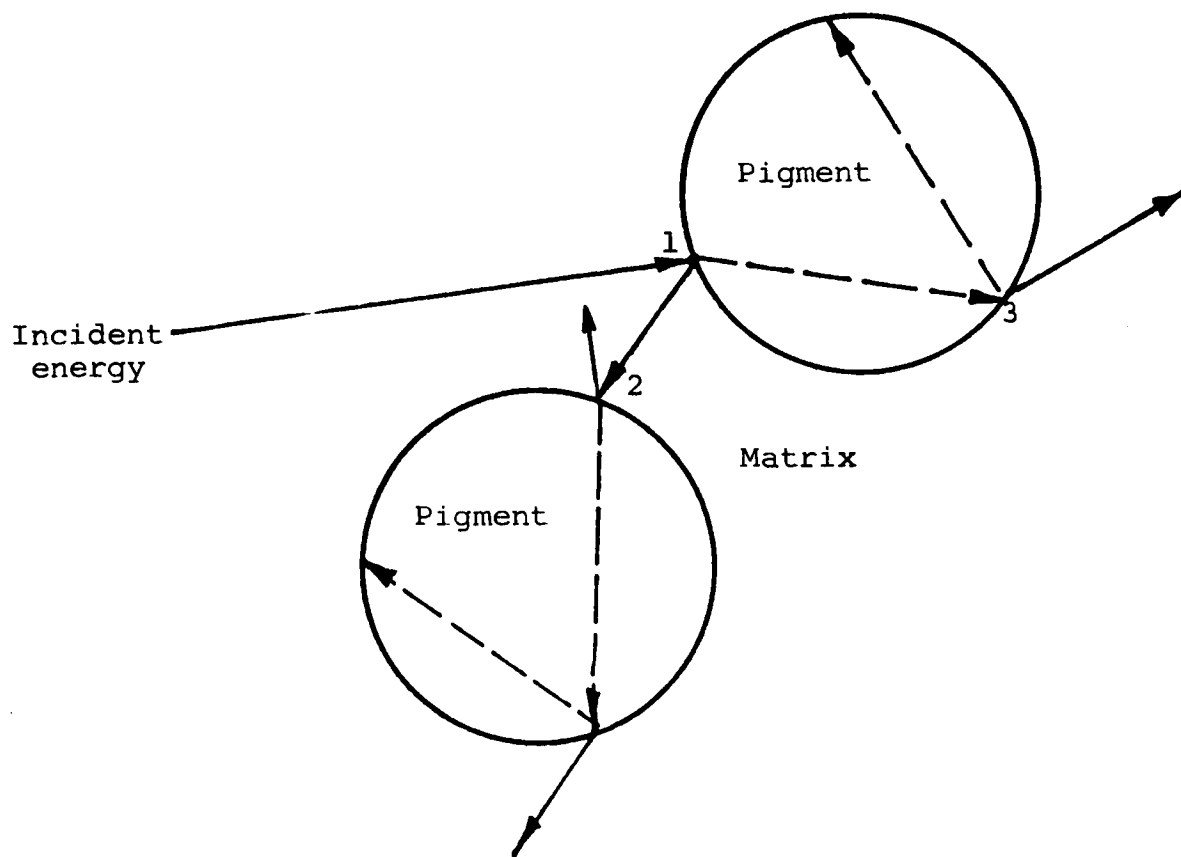
Figure 67

TWO-DIMENSIONAL REPRESENTATION
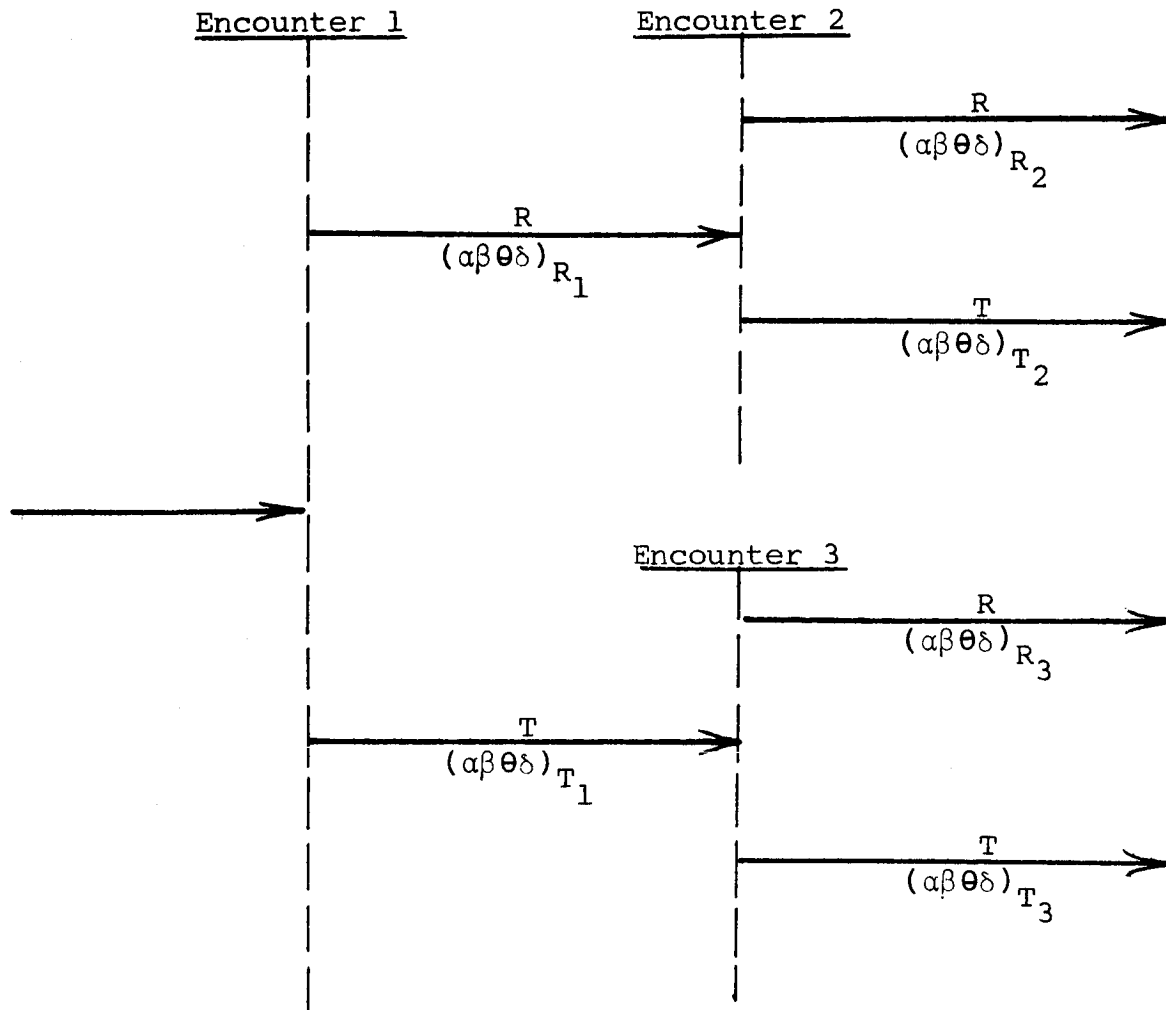OF ENERGY ENCOUNTERS IN A PAINT MATRIX

Figure 68

SYMBOLIC REPRESENTATION OF ENERGY/BOUNDARY ENCOUNTER

Now consider the energy incident on the surface to consist of random bursts of wave trains. As each wave train tries to penetrate the matrix, the orientation of the boundaries is completely at random. Therefore, all orientations are equally probable with respect to the incident direction. If a sufficiently large number of events is considered, it would seem reasonable to assume that half of the encounters reflect the energy forward and half backward. The reflection factor for determining the energy partition will have some average value taken over all individual values for all possible orientations. Let us assume that its value is a. Throughout the paint matrix the optical path length between energy/boundary encounters will vary between zero and an upper limit imposed by the characteristics of the paint matrix.

However, if enough events are considered, it would seem reasonable to assume that there is an average path length, d, between encounters. Again, the number of events experienced in a sequential path will vary for a given sequence, but for a given paint film there will be some average characteristic number of events that can be used for averaging the penetration of energy over many sets of events. If we consider the effects of many incident wave trains of the same frequency traveling through the paint matrix, the phase relationship between the many waves passing through a point chosen within the matrix will be distributed at random; i.e., all phase angles between 0 and 2π will be equally possible.

Consider first the simple case in which all amplitudes are equal. Let the amplitude of a wave be a, and let there be n waves passing through a point in space. If these motions were all in the same phase, the resultant amplitude would be na and the intensity n^2a^2, or n^2 times that of one wave. However, the phases are distributed purely at random. If the graphical method of compounding amplitudes were used, we would obtain a picture like that in Figure 69. The phases $a_1, a_2, \ldots$ take arbitrary values between 0 and 2π.
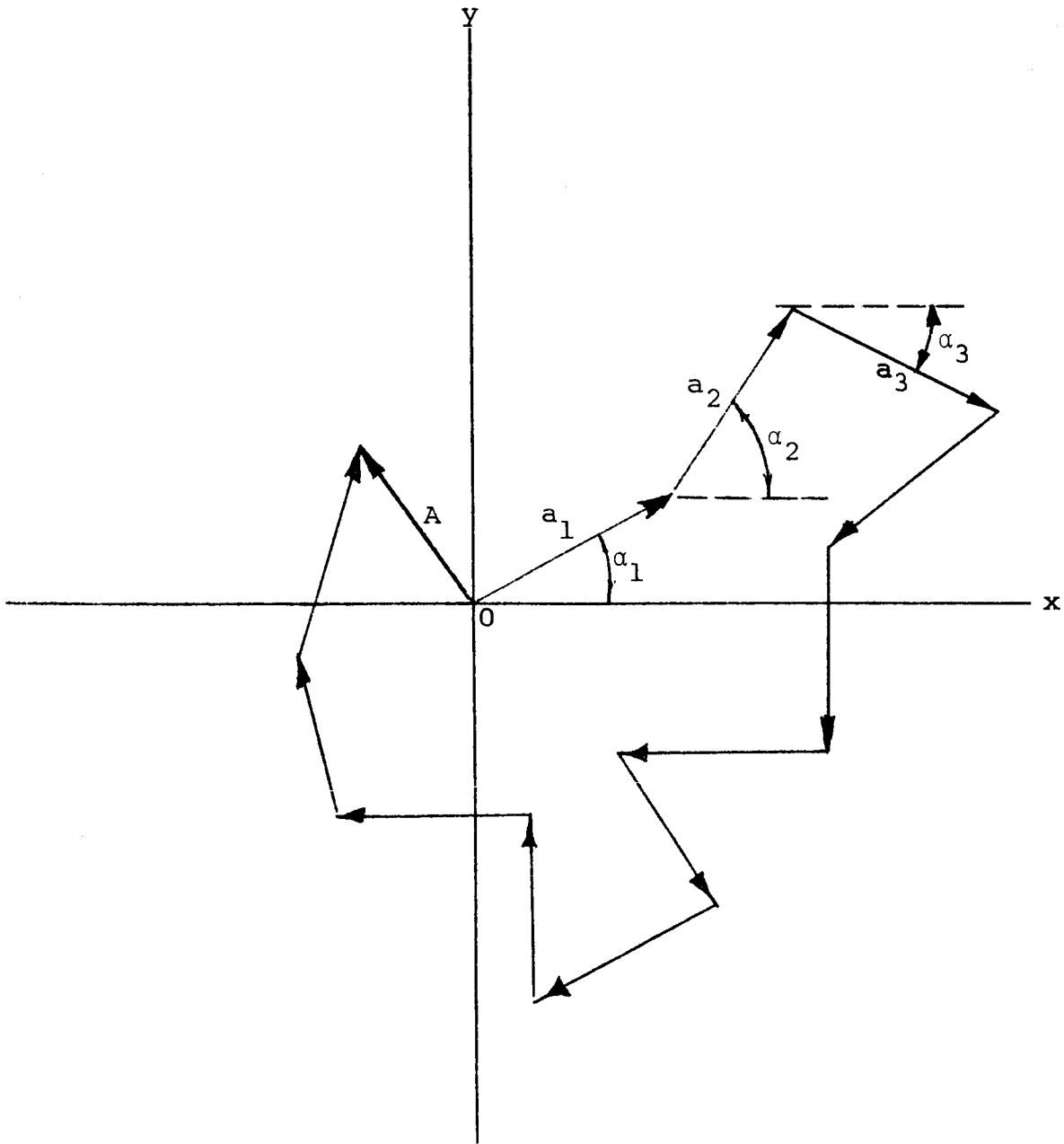
Figure 69

RESULT OF 12 AMPLITUDE VECTORS
DRAWN WITH THE PHASES AT RANDOM

The intensity due to the superposition of such waves can be determined by the square of the resultant A. To find A^2, we square the sum of the projections of all vectors a on the x-axis and add the square of the corresponding sum for the y-axis. The sum of the x projections is:

$$a(\cos \alpha_1 + \cos \alpha_2 + \cos \alpha_3 + \ldots + \cos a_n)$$

When the quantity in parenthese is squared, terms of the form $\cos^2 \alpha_1$ and others of the form $2 \cdot \cos \alpha_1 \cdot \cos \alpha_2$ are obtained. When n is large, the terms $2 \cdot \cos \alpha_1 \cdot \cos \alpha_2$ might be expected to cancel out, because they take both positive and negative values. In any one arrangement of the vectors this is far from true, however. In fact, the sum of these cross-product terms actually increases approximately in proportion to their number. Thus, we do not obtain a definite result with one given array of randomly distributed waves.

In computing the intensity in any physical problem, we are always presented with a large number of such arrays, and we wish to find their average effect. In this case, it is safe to conclude that the cross-product terms will average to zero, and we have only the $\cos^2 \alpha$ terms to consider. Similarly, for the y projections of the vectors $\sin^2 \alpha$ terms are obtained, and terms such as $2 \cdot \sin \alpha_1 \cdot \sin \alpha_2$ cancel. Therefore,

$$I \sim A^2 = a^2(\cos^2 \alpha_1 + \cos^2 \alpha_2 + \cos^2 \alpha_3 + \ldots + \cos^2 \alpha_n)$$
$$+ a^2(\sin^2 \alpha_1 + \sin^2 \alpha_2 + \sin \alpha_3 + \ldots + \sin^2 \alpha_n)$$

Since $\sin^2 \alpha_k + \cos^2 \alpha_k = 1$, we find at once that $I \sim \alpha^2 n$. Thus, the average intensity resulting from the superposition of n waves with random phases is just n times that due to a single wave.

The argument outlined above, which is taken from Fundamentals of Physical Optics, by Jenkins and White, can readily be extended to the case of n waves when a varies. However, now the average intensity would also be a function of the distribution of amplitudes.
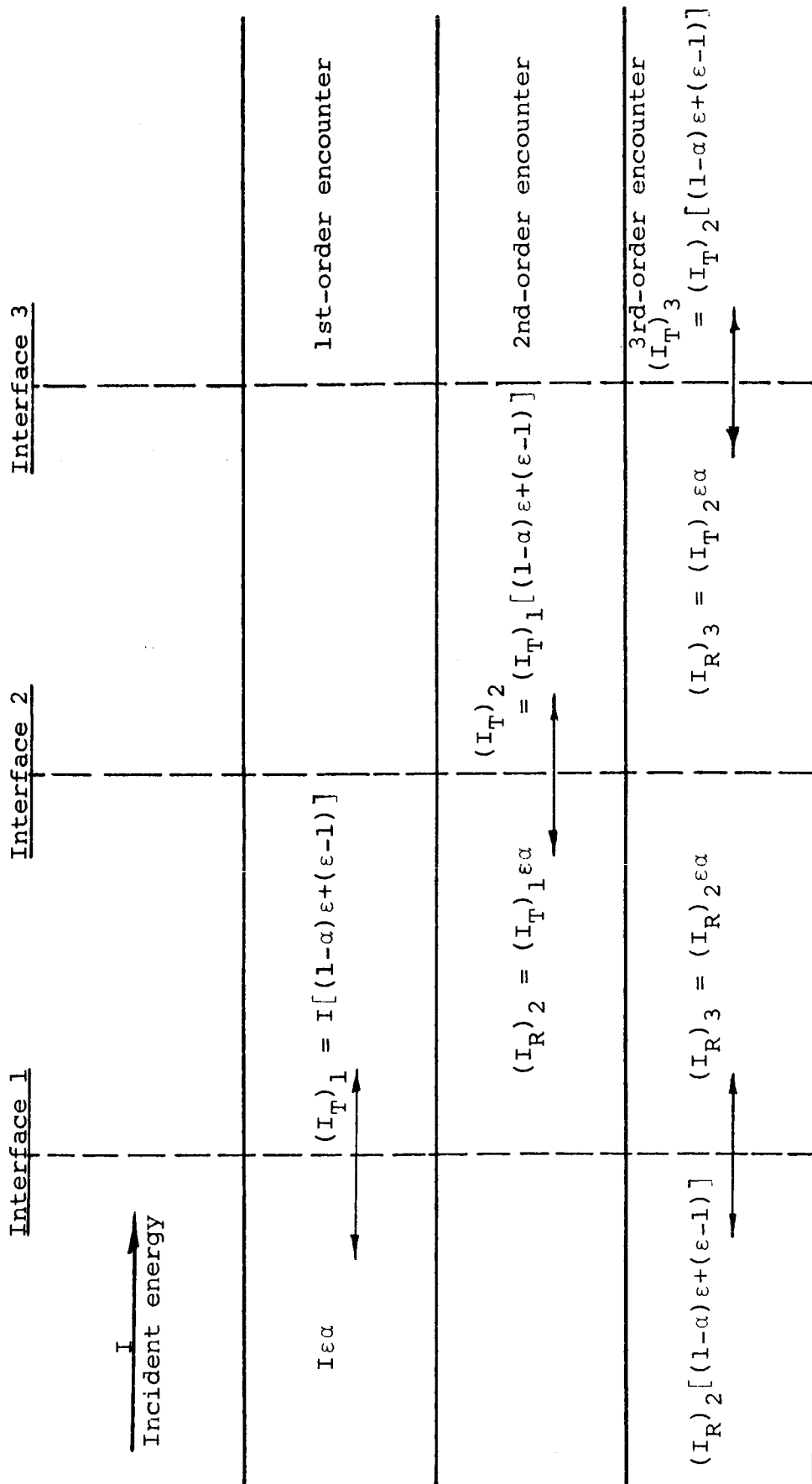
Figure 70

IDEALIZED SERIES OF ENERGY/BOUNDARY ENCOUNTERS

Therefore, for the purpose of judging the intensity of radiation at any point in the matrix, if we average over a sufficient number of events and wave trains, the effect of phase differences can be allowed for by straight addition of the intensities of the individual averaged energy flows.

By using these concepts of statistical averaging of many events, the flow of energy can be depicted as shown in Figure 70. We consider the flow of energy into a unit area of paint film. On the average, the amount of pigment encountered in a unit plane is the same as the fractional volume concentration of pigment (ref. 26). The amount of reflected incident energy, I, is $I\alpha E$, where E is the fractional volume of solids. The amount $I(1-\alpha)E$ is transmitted through the pigment, while $I(1-E)$ is transmitted through the vehicle. For simplicity, it is assumed that absorption is negligible, although it is possible to extend the model to allow for absorption.

The results of three successive encounters are shown in Figure 70. Pictorial representation of a high number of encounters is cumbersome, but the number of events shown is sufficient to illustrate the principle.

In order to develop a model of this amplitude, it is necessary to have terms for the number of screens needed to simulate the film of paint and to establish a correlation between the properties of the screens and the constituents of the paint film.

D. Average Track Length within a Randomly Distributed Paint System

If we create a model of a paint film in which we postulate the existence of physically equivalent screens, we have the problem of deciding the number of screens to postulate and the effect of varying the screen aperture.

The following considerations yielded a possible method of avoiding this problem. Let us calculate the average distance traveled by light energy between pigment/surface encounters. Consider first the simple case of a plane parallel beam of light entering the surface of a paint film that has a pigment volume concentration equal to α. At a distance L into the paint film, the proportion of the light beam that has not encountered a pigment film is:

$$- \frac{dI}{dL} = \alpha I$$

Therefore

$$I = I_0 e^{-\alpha} \frac{L}{d}$$

where I is the beam energy that has not yet encountered a particle.

The average track length can be calculated by integrating all the tracks at each depth before an encounter is registered. Thus,

$$\bar{L} = \frac{\int_{N_0}^{0} L\,dN}{\int_{N_0}^{0} dN}$$

where

dN is the number of tracks of length L

$\bar{L}$ is average track length.

But

$$N = N_0 e^{-\alpha L}$$

Therefore,

$$\bar{L} = \frac{1}{\alpha} \frac{\int_{N_0}^{0} \left[-\ln(N/N_0) \right] dn}{-N_0}$$

By integrating by parts,

$$\bar{L} = \frac{1}{\alpha}$$

This very simple result suggests that the average distance between pigment/surface encounters is the reciprocal of the pigment volume concentration. By a similar argument, the average track within the pigment is:

$$\bar{L}_p = \frac{1}{(1-\alpha)}$$

Implicitly in these formulas it has been understood that L is measured in units of particle diameters. Expressing both formulas in terms of average diameter of the pigment,[*] we have:

Any number of particle diameters between surface encounters $= N_v$

Average number of particle diameters for each residencies with a pigment $= N_p$

where $N_v = \frac{1}{\alpha}$ and $N_p = \frac{1}{(1-\alpha)}$.

We tested the accuracy of these formulas in the following way. Consider the Monte Carlo grid plot at 20% by volume coverage. From the formulas, the average distance between particle surfaces should be 5 diameters. However, since the average path is only a small number of diameters, the digitized nature of the model plot has to be taken into account. The reason for this can be understood from Figure 71. The theoretical calculation of the average track length is equivalent to the total integration of the decay curve by taking small increments like those shown as dN. The fact that the distances on the Monte Carlo plot are digitized is equivalent to estimating the area by the steps shown.

---

[*] In deducing the formulas, the pigment is considered to form a continuous network of non-reentrant surfaces.
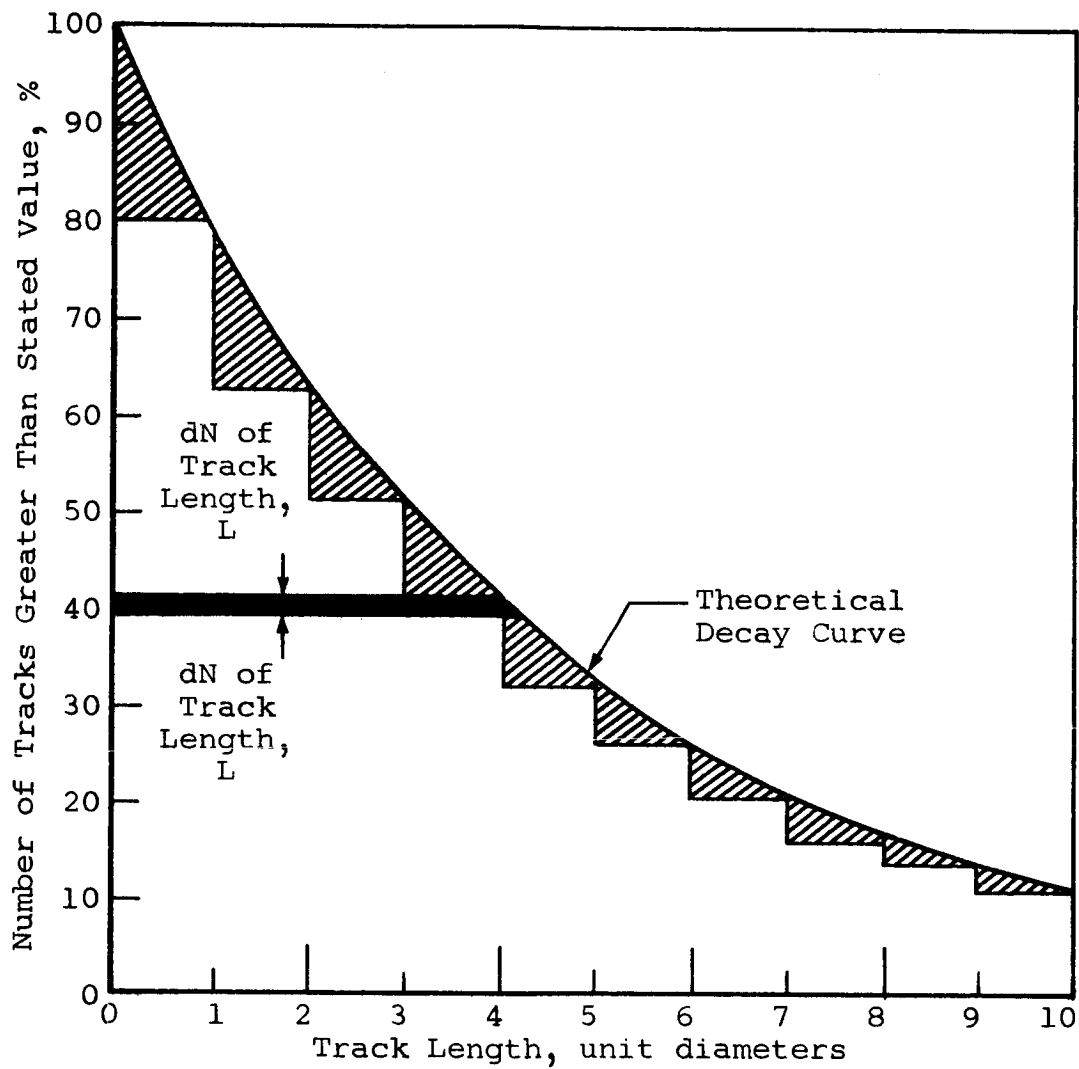
Figure 71

CALCULATION OF AVERAGE TRACK LENGTH

A set of tracks measured by going from particle to particle is shown in Figure 72. Their average value is 4.6. Since the properties of a random array should be the same in all directions, traveling from particle to particle in a fixed direction should be exactly equivalent to traveling in all directions from a fixed particle.

A set of randomly drawn lines was superimposed on the plot of 20% coverage, and the measured value for the average track was found to be 3.2 as estimated from 100 items of information. The reason for this short track length is that implicitly in the deduction of the formula for the average track length we assumed that each surface encounter was independent of the previous encounter. The spatial configuration of the clusters creates local regions of high probability for short track lengths. The structure of some of these clusters is shown separately in Figure 73. This structure arises mainly from the existence of reentrant surfaces on the cluster. Column II in Figure 73 was constructed by replacing clusters (column I) by circles of equal area with the center of the circles at the center of mass of the clusters.

Figure 74 shows the redrawn Monte Carlo plot for 20% coverage (Figure 23) in which each cluster has been redrawn as a circle of equivalent area. Between clusters the whole range of fractional paths is possible and reentrant surfaces have been eliminated.

Two sets of 100 tracks were measured on this diagram by using random lines. The average track length for the first 100 tracks was 4.8 and for the second 5.2. Thus, for this model, the expected value of 5 is achieved within the limits of statistical fluctuations. For an actual pigment having reentrant surfaces, the diagrams of Figure 73 suggest that conversion to spherical particles will increase the average track length between particle and will therefore reduce the probability of photon absorption.
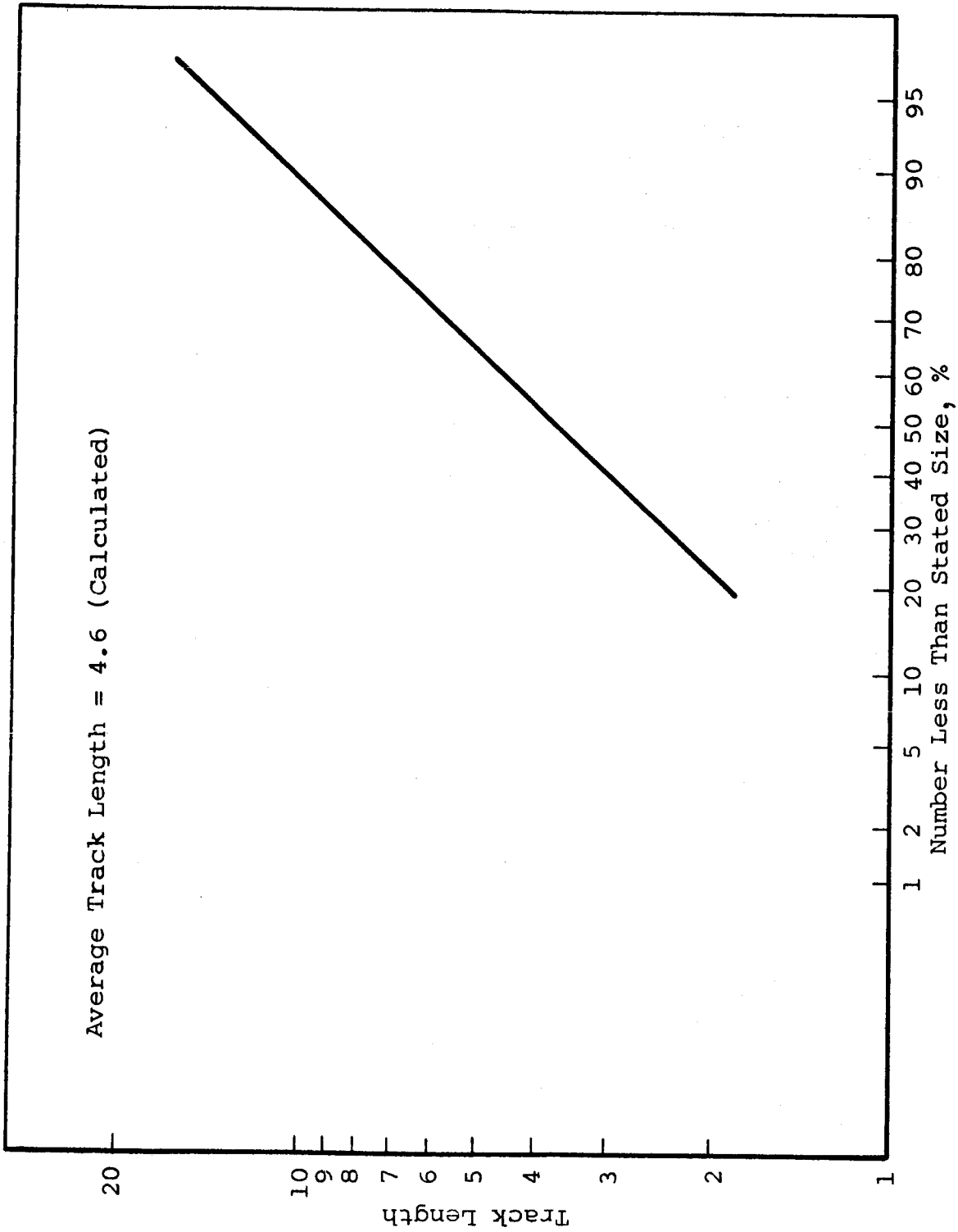
Figure 72

TRACK LENGTHS AT 20% SOLIDS CONCENTRATION

I II

Selected Cluster Regions
from the 20% Monte Carlo Plot
(Figure 23)

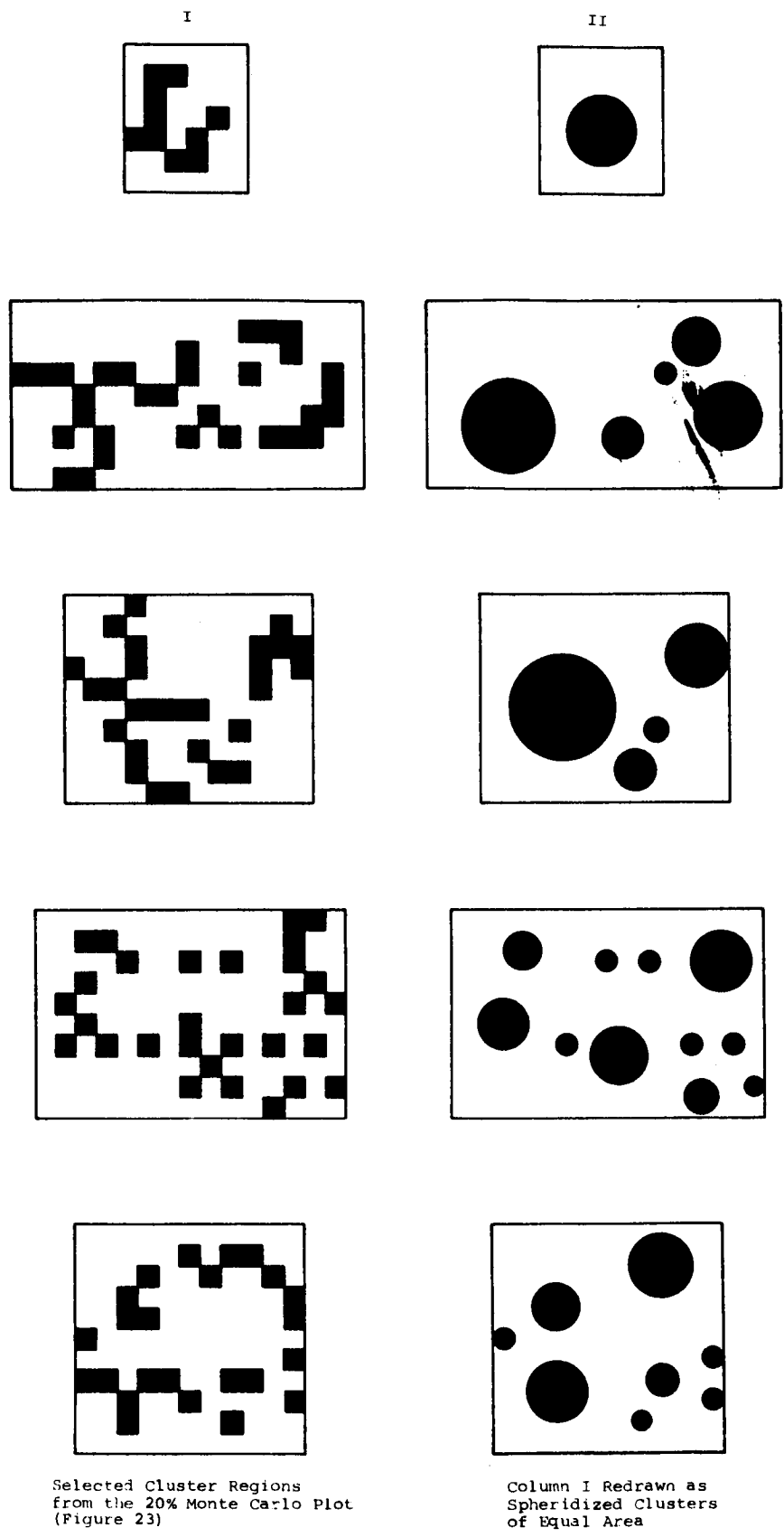Column I Redrawn as
Spheridized Clusters
of Equal Area

Figure 73

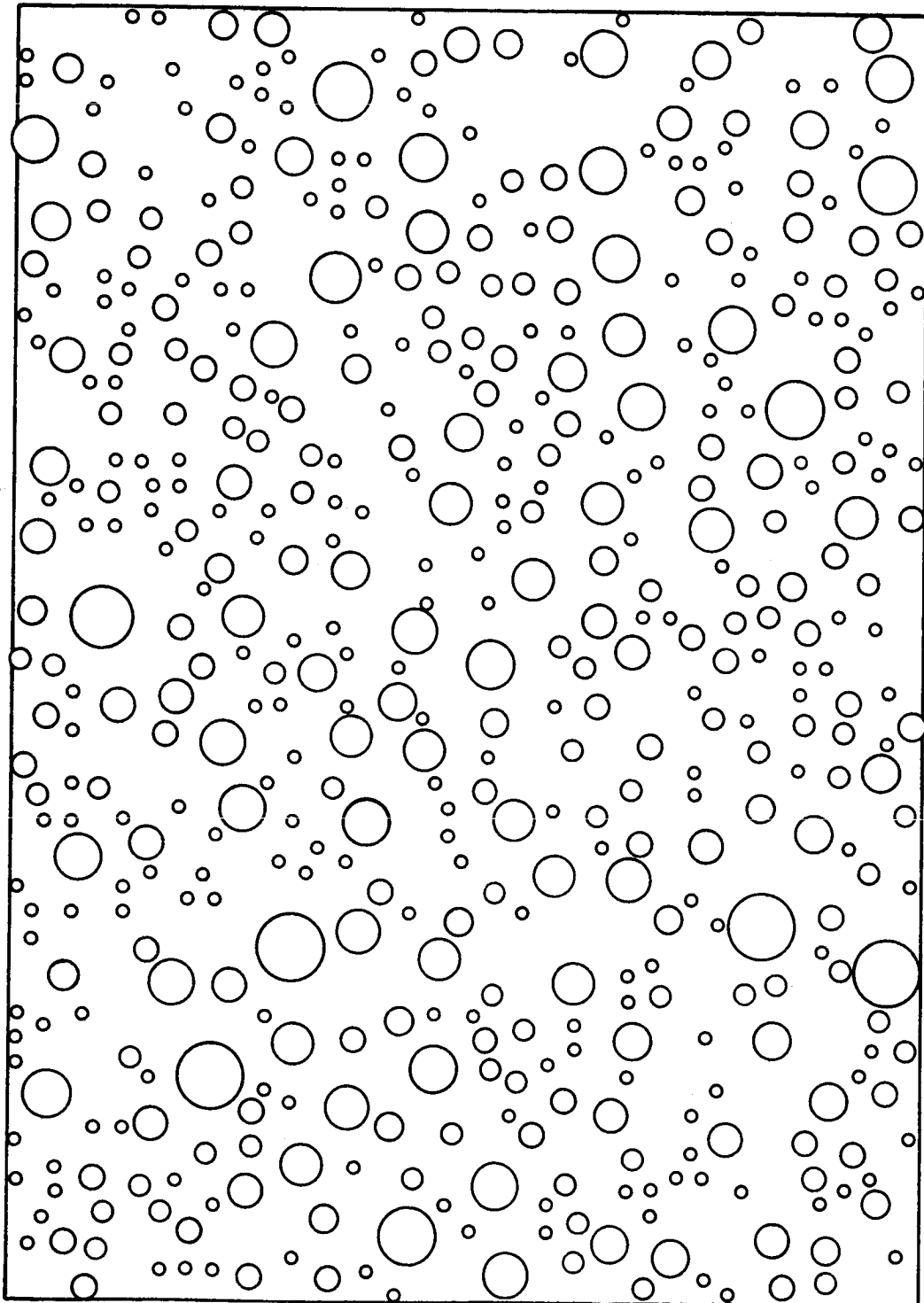ELIMINATION OF SHORT TRACK LENGTHS: TYPICAL CLUSTERS OF CUBIC AND SPHERICAL FORM

Figure 74

ELIMINATION OF SHORT TRACK LENGTHS: SPHERIDIZED 20% MONTE CARLO PLOT
(Conversion of Figure 23)

Figures 75 through 77 show sets of tracks measured on the Monte Carlo plots at densities of 5, 10, and 15%. Within the limits of statistical fluctuations, the average track lengths are as predicted from theory, i.e., $1/\mu$ diameters.

The successful prediction that the average track length within a randomly distributed pigmented film is the reciprocal of the volume fraction times the particle diameter indicates that a satisfactory model for a paint film consists of a series of translucent slabs of pigment material separated by the average track length. Each slab is a perfectly diffusing medium of thickness $1/(1-\mu)$. The total surface of the slabs is equal to the total surface of the pigment, so that probably the number of slabs is $S/2d^2k$, where S is the surface area/unit volume expressed in the same units as the average particle diameter, and k is a constant related to the spatial geometry of the particle and probably has to be determined empirically.

Treating the paint films as being constructed as a series of parallel slabs of perfectly diffusing material is equivalent to finding a physical basis for the Kubelka-Munk equations. The Kubelka-Munk theory postulates that the material can be treated as a perfectly diffusing material of given scattering and absorption power. This is difficult to accept physically, since a paint film is never large in terms of pigment diameter, so that the laws of statistical average cannot be applied without any qualification.

The treatment we have elaborated suggests that the reason statistically based laws can be applied to paint films is that the miriad of possible photon/track encounters represent a large statistical averaging system with respect to time, even though the paint film is statistically thin.
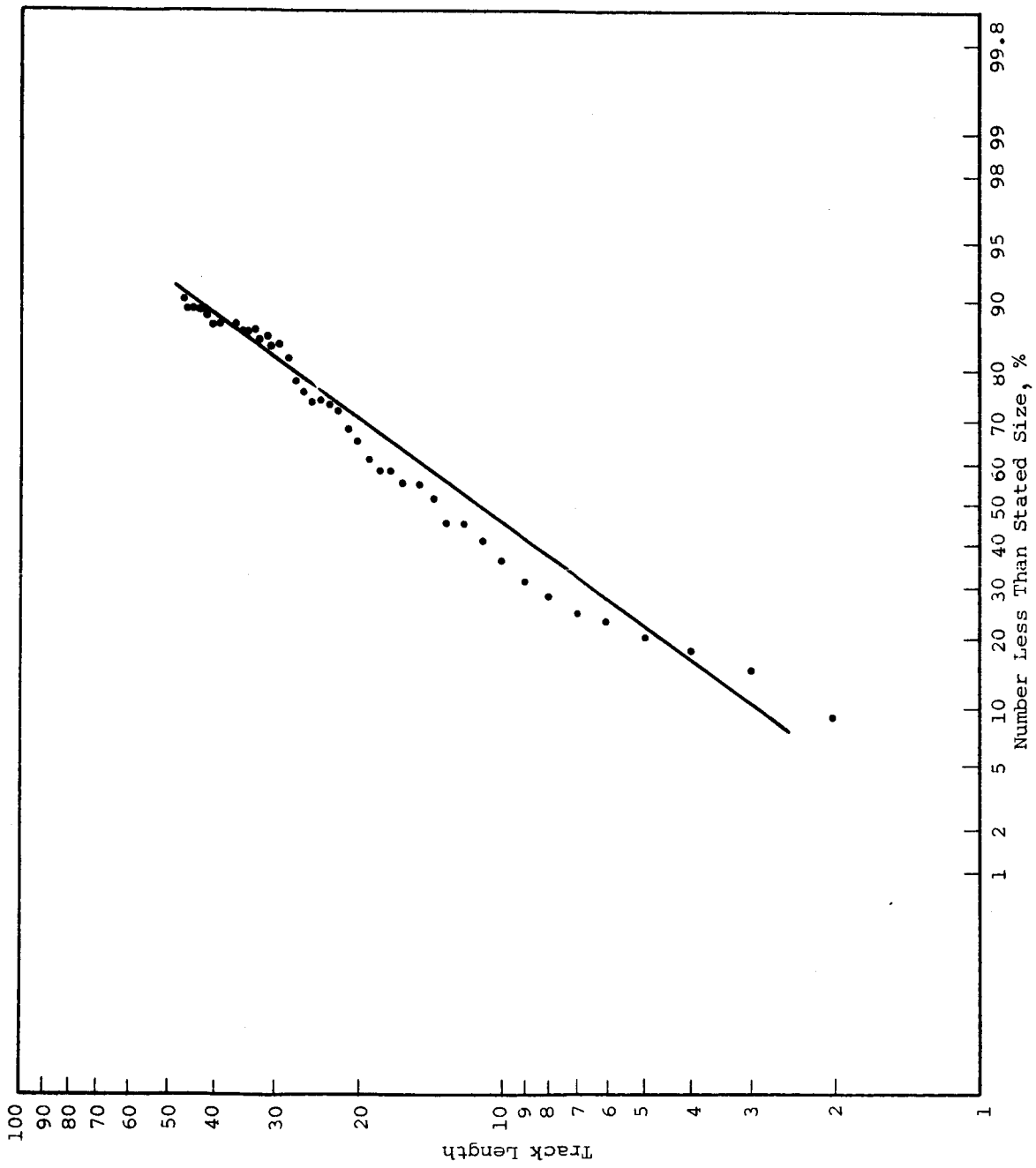
Figure 75

TRACK LENGTH DISTRIBUTION AT 5% CONCENTRATION
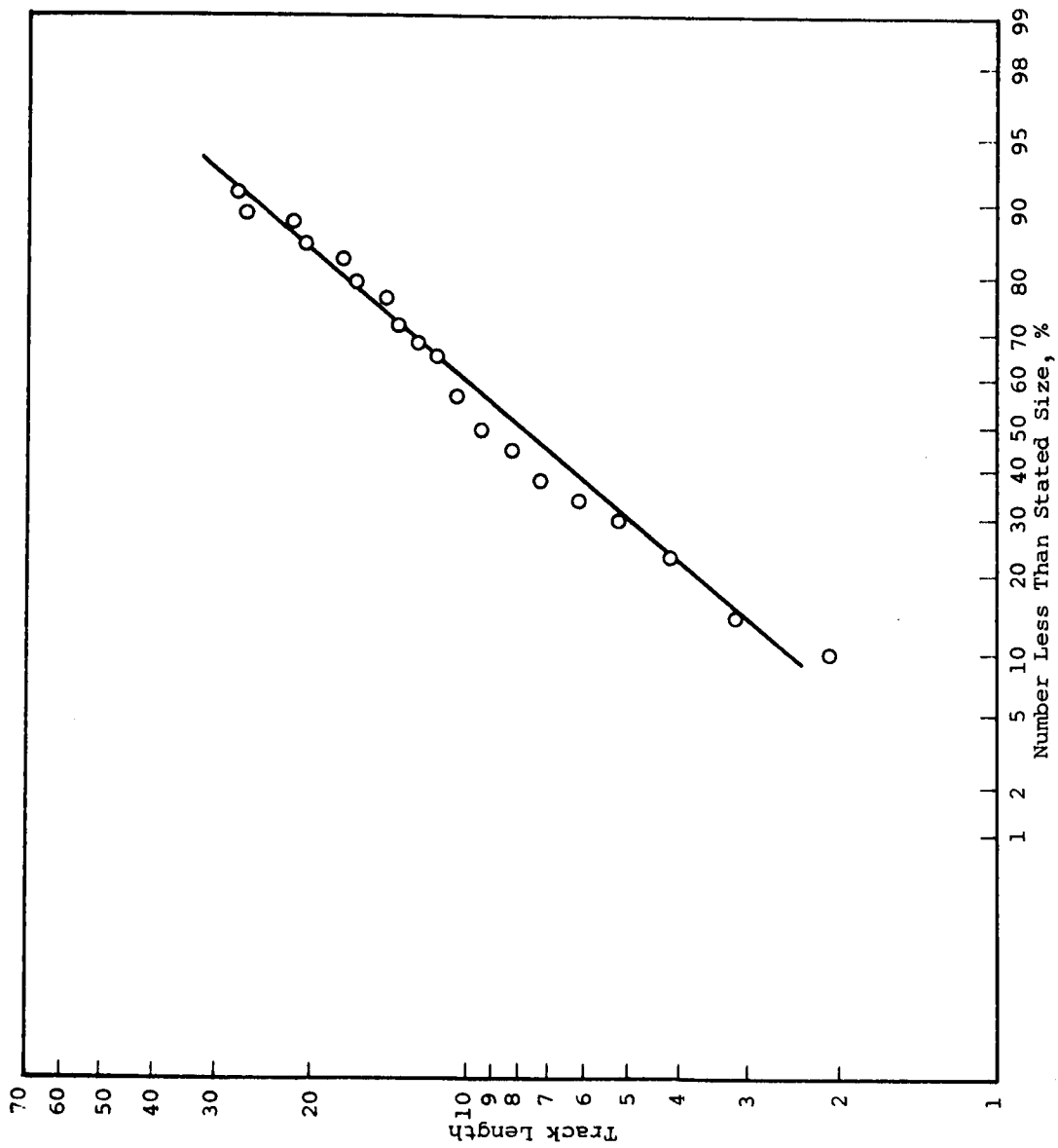
Figure 76

TRACK LENGTH DISTRIBUTION AT 10% CONCENTRATION
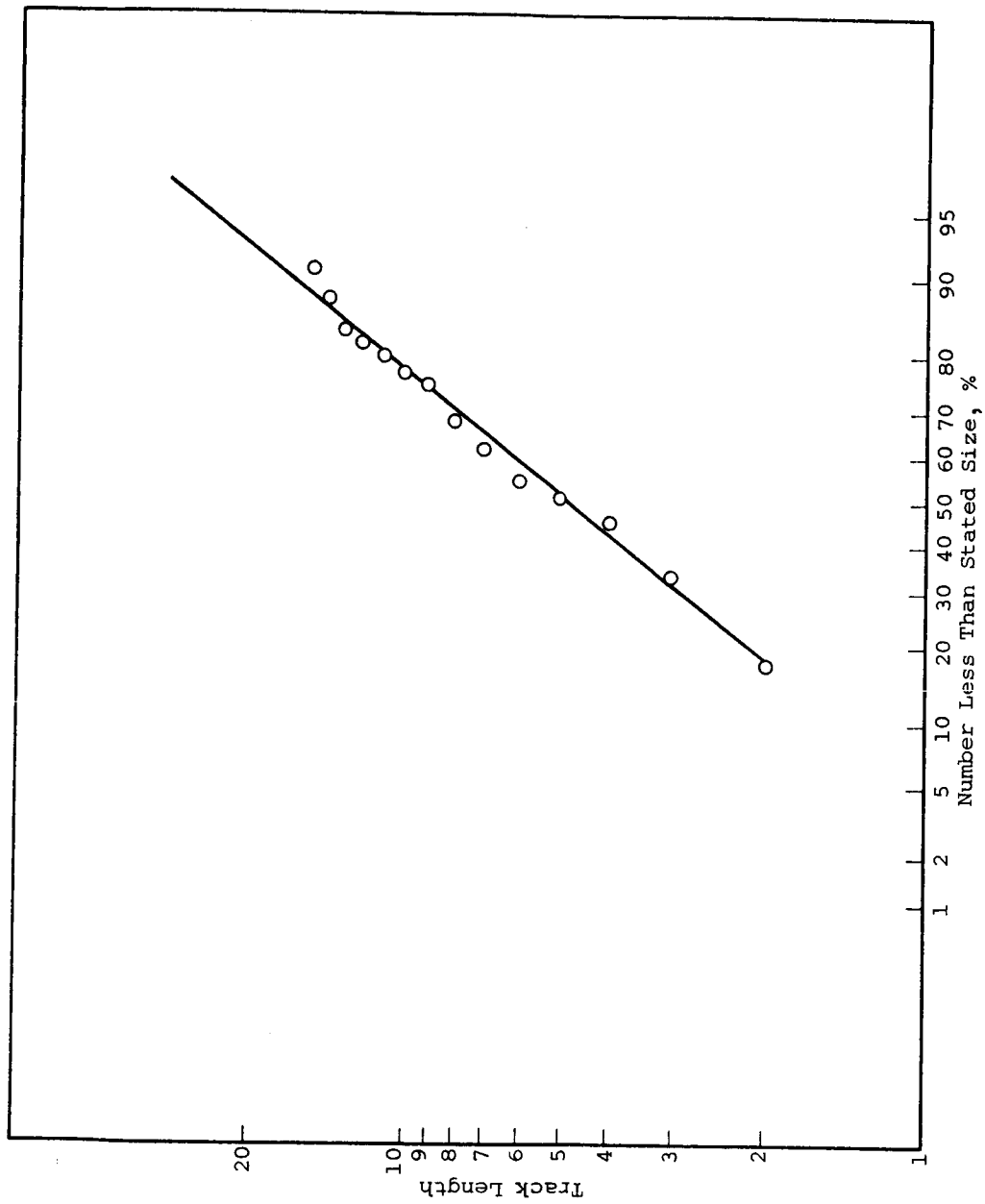
Figure 77

TRACK LENGTH DISTRIBUTION AT 15% CONCENTRATION

E. Comments on Theoretical Treatment of Paint Systems

The Kubelka-Munk theory for the transmission of radiant energy through a paint film is essentially the Lambert-Beer law with an added flux representing return flow of scattered light through the system of scattering centers. It is strictly limited because it postulates perfectly diffuse initial light and is applicable only to a system having perfectly diffusing physical boundaries. Duntley's theory extends the Kubelka-Munk analysis to the case of an initially directed beam entering a system having perfectly diffusing physical boundaries.

It is not possible to construct a theory for the general case of any boundary and type of light without extensive experimental studies of all possible systems. The Monte Carlo studies have established that the statistical basis of some of the well-known physical laws governing systems have specified boundary conditions, i.e., Lambert-Beer and Kubelka-Munk equations. It is reasonable to hope that extended physical experimentation combined with further Monte Carlo studies can form the basis of a general treatment of reflective properties of paint films.

X. IMPLICATIONS OF MONTE CARLO STUDIES OF RANDOM TRACKS ACROSS A CIRCLE FOR FILTRATION STUDIES

A. Concept of Randomness Applied to Fibrous Filters

Some filter systems are made by assembling an array of fibers in a random manner. The random intercepts drawn in Figures 78 through 81 can be considered as unit elements in a filter composed of randomly assembled fibers. Figures 78 through 80 show three simulated sets of 20 random lines drawn by using method A, and Figure 81 a set of 20 lines drawn by using method B (see Figures 10 and 11 and the discussion in Section III).

The fact that the two random arrays drawn by methods A and B can both satisfy the technical definition of randomness and yet have different physical properties indicates that technologists dealing with filtration theory may encounter difficulties arising from inadequate terminology. Apparently, similar fibrous mats that in a qualitative sense can be described as a random array of fibers may have been assembled in two different ways, which gave different types of randomness to the positions of fibers. The different types of randomness, unsuspected by the technologist, represent an uncontrolled variable in the experimental studies of filter performance and could cause unexpected differences in performance. The performance differences that could arise from "randomness" differences can be illustrated by the following considerations.

Two major mechanisms are used to capture particles passed through a filter: (a) direct obstruction to the passage of a particle by the pore system of the filter and (b) capture of the particle by single fibers when the particles impact onto the fiber. For both these mechanisms, random fibers assembled to form systems analogous to those constructed by method B will be more efficient, since in method B the pore distribution has smaller probability for larger apertures and has more fiber per unit area when captured by the second mechanism.
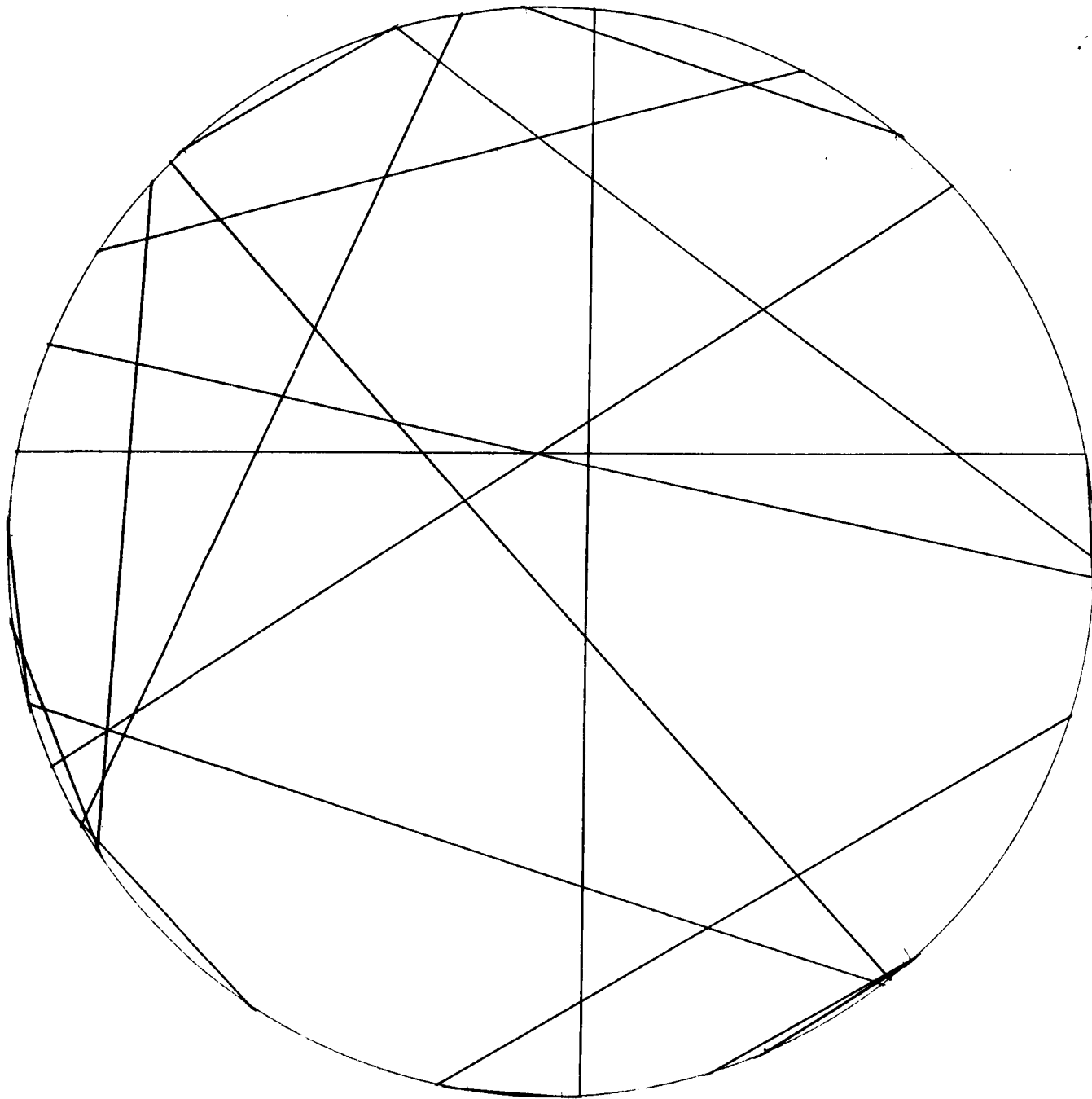
Figure 78

LINES DRAWN BETWEEN TWO RANDOM NUMBERS SELECTED ON THE PERIMETER OF A CIRCLE
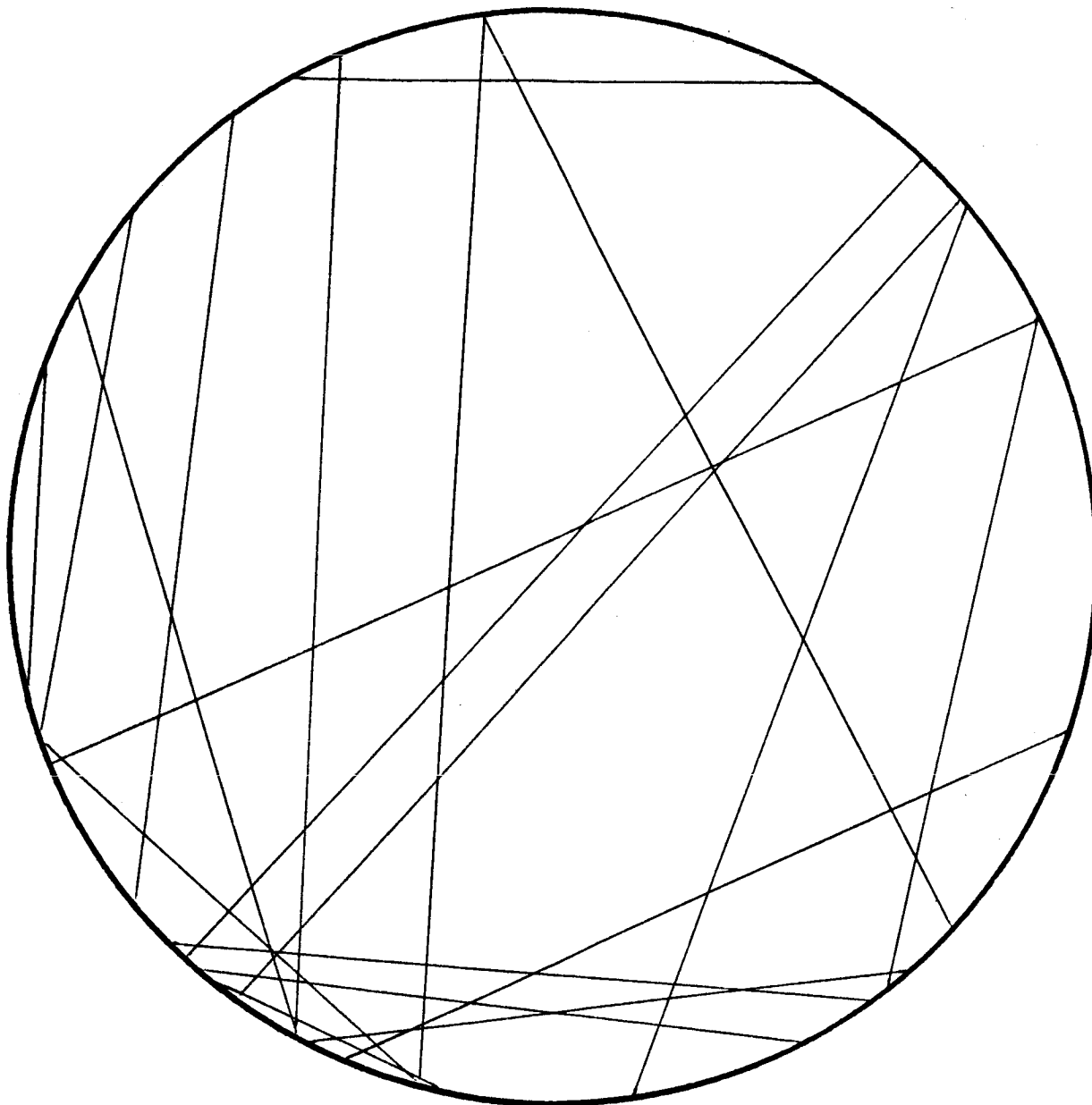
Figure 79

LINES DRAWN BETWEEN TWO RANDOM NUMBERS SELECTED ON THE PERIMETER OF A CIRCLE
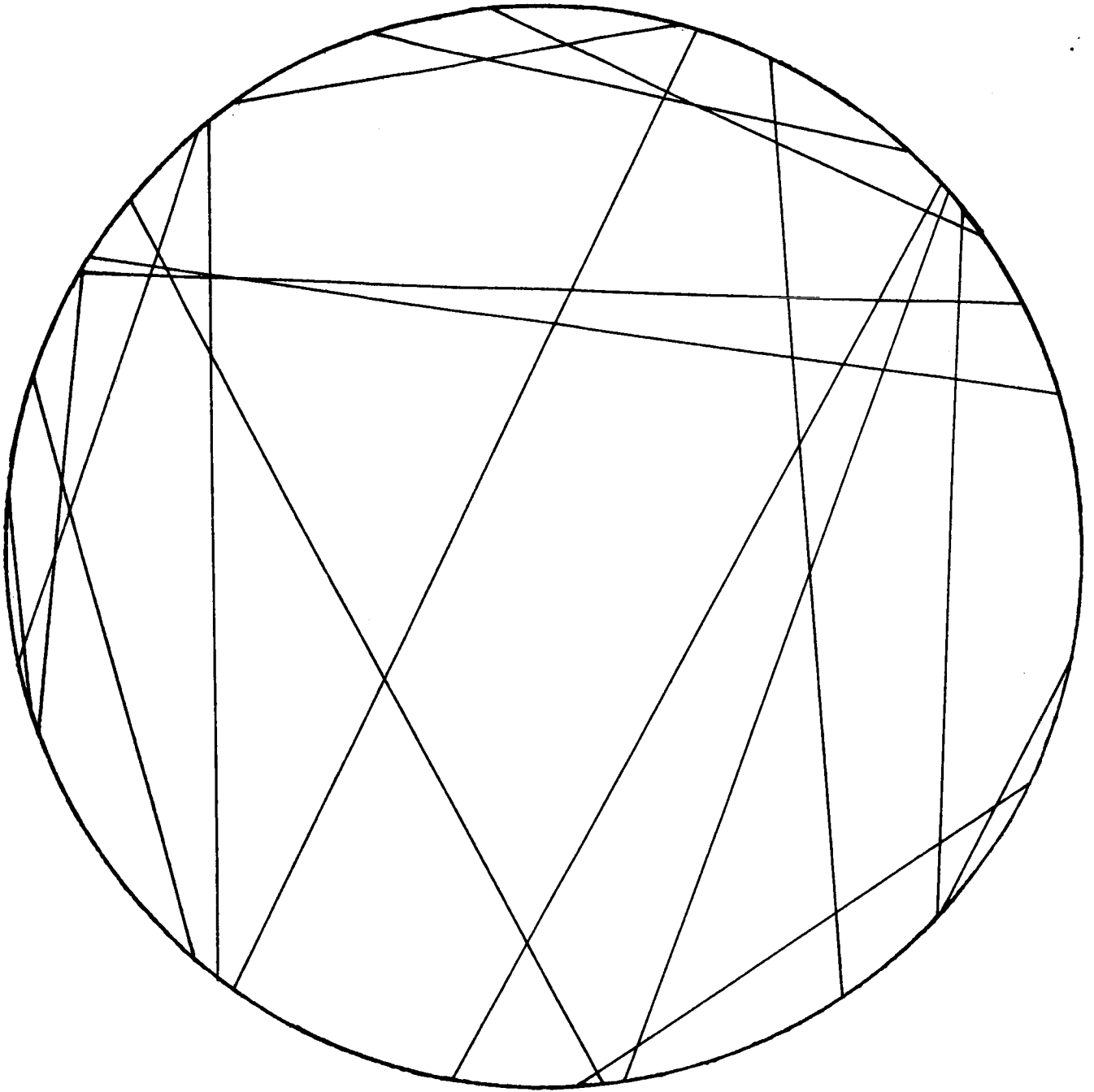
Figure 80

LINES DRAWN BETWEEN TWO RANDOM NUMBERS SELECTED ON THE PERIMETER OF A CIRCLE
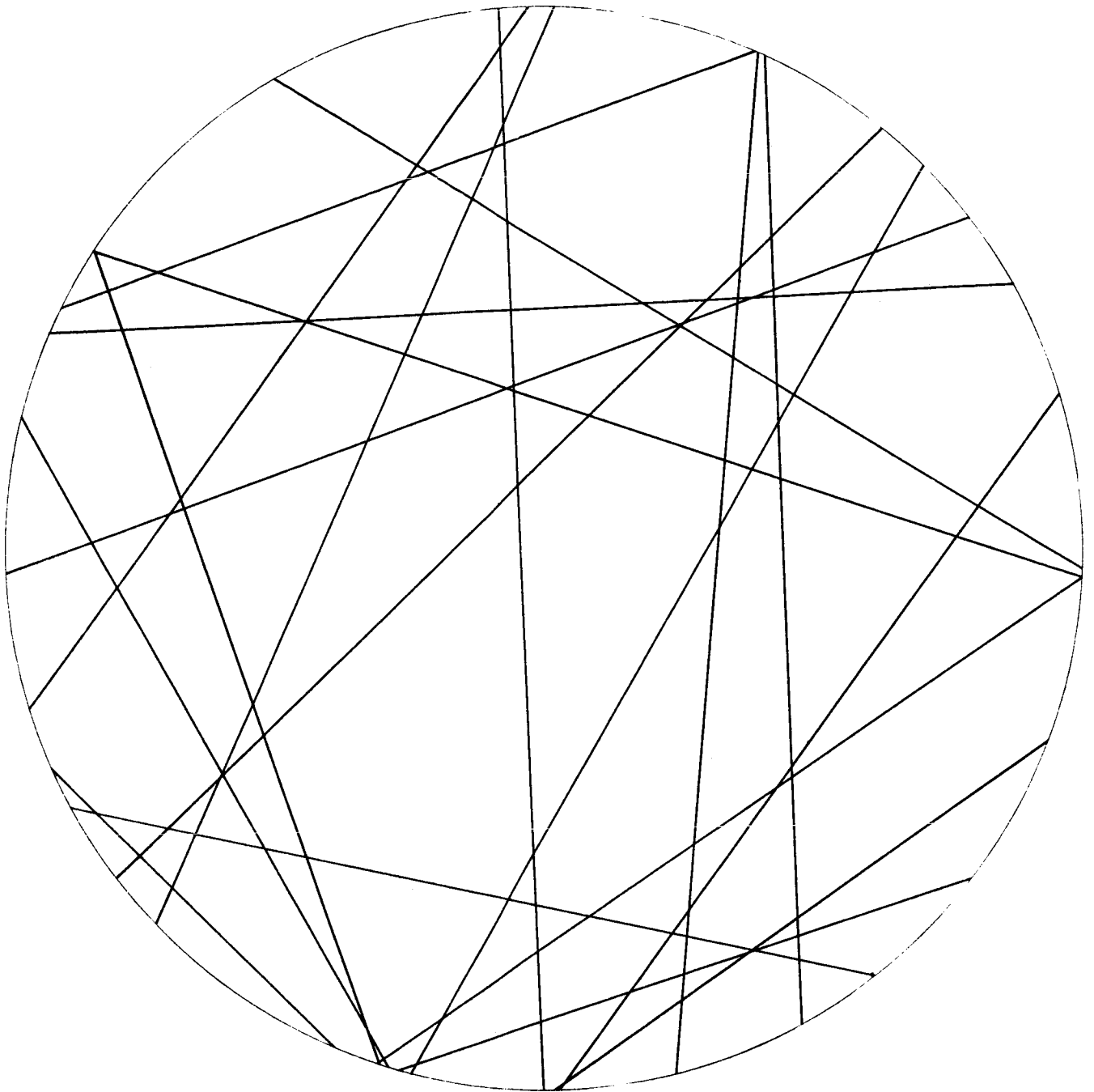
Figure 81

LINES DRAWN PERPENDICULAR TO RADIUS FOR RANDOMLY SELECTED ANGLES TO A FIXED DIRECTION

The effective pore-size distribution for the fiber simulation system in Figures 78 through 81 was measured by using the graticule shown in Figure 82. The largest circle that could be placed in any aperture defined by the random fibers was defined as the effective pore size for the passage of spherical particles through the filter.

The size distributions measured for the systems in Figures 78 through 81 are given in Figures 83 through 86, respectively. The number of apertures for systems drawn by method A were 70, 80, and 70; and the number for the system drawn by method B was 109. The pore structure was quite different for the system constructed by method B.

It can be seen that random track diagrams of the type shown in Figures 78 through 81 could be used to study dependence of the performance of filters on various random types of arrays of fibers. If it were desired to simulate fiber systems in this way, the effect of the fiber diameter can be taken into account by decreasing the radius of the circle considered able to pass through the simulated aperture by the magnitude of the fiber diameter.

If a filter mat is constructed by allowing relatively short fibers to fall into position, the randomness of the fiber system will be analogous to system B, since this corresponds to the equal probability of all points in the plane of imposition having a line through them. If, however, long fibers are assembled so that the density of fibers at the perimeter is uniform, the fibrous system is analogous to system A for a circular perimeter. From the estimated pore-size distribution measurements, it can be seen that the two systems would have different properties.

It may be possible to make major advances in filtration theory by considering the exact meaning of randomness in a fiber system and devising techniques for achieving a random system with optimum properties.
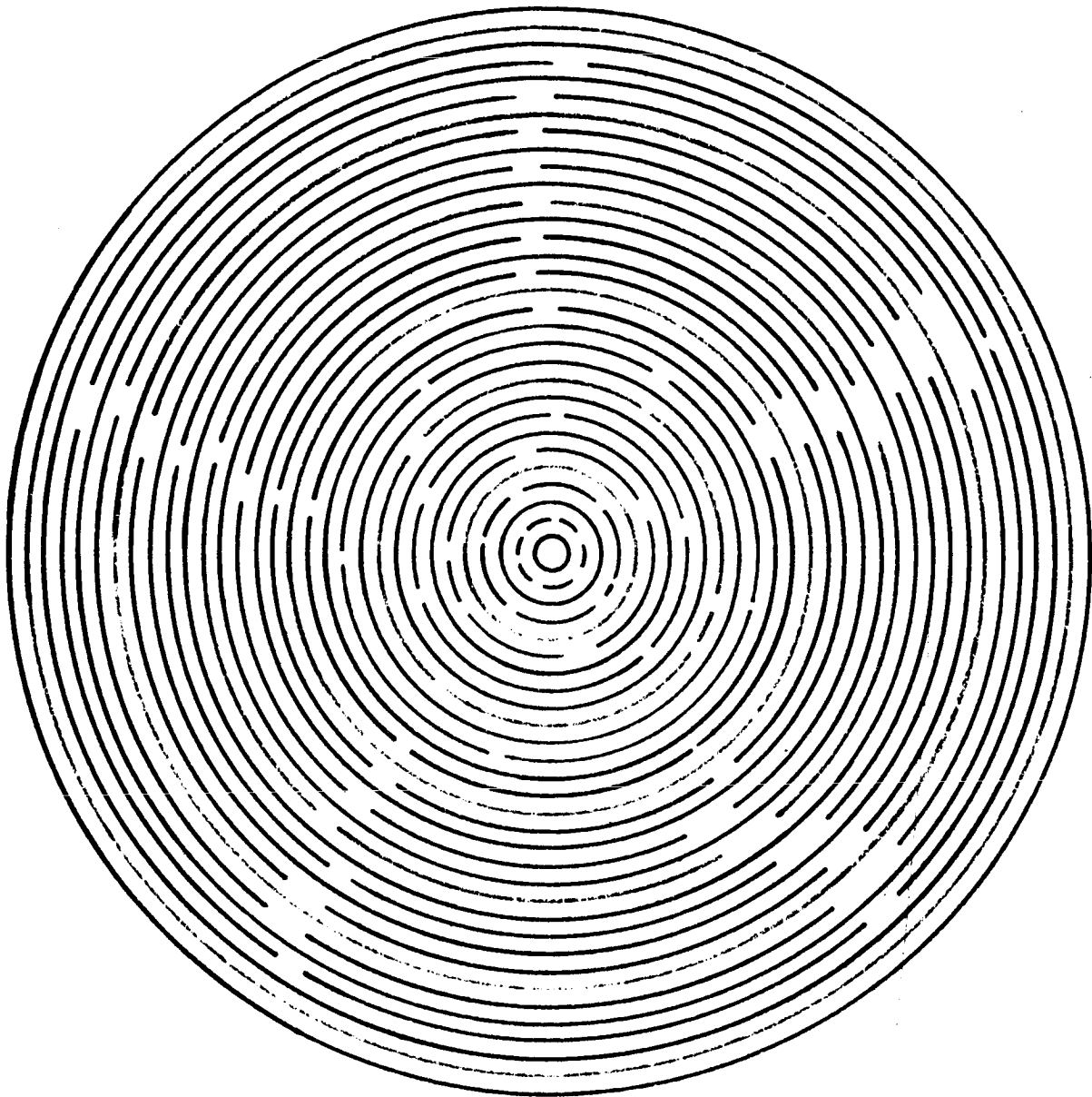
Figure 82

GRATICULE FOR DETERMINING PORE SIZE

Figure 83

PORE-SIZE DISTRIBUTION OF SIMULATED FILTERS
(Simulated in Figure 78)
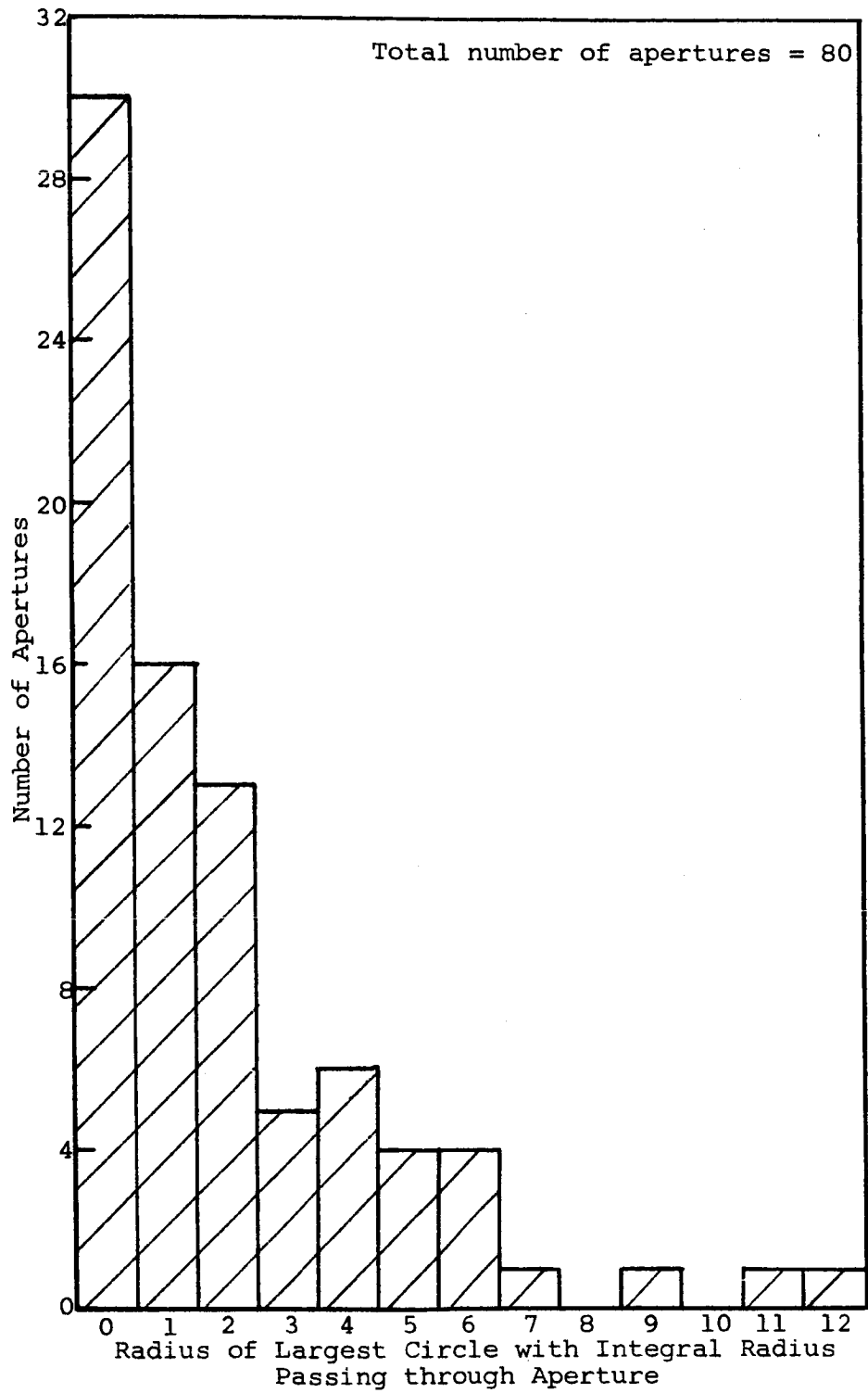
Figure 84

PORE-SIZE DISTRIBUTION OF SIMULATED FILTERS
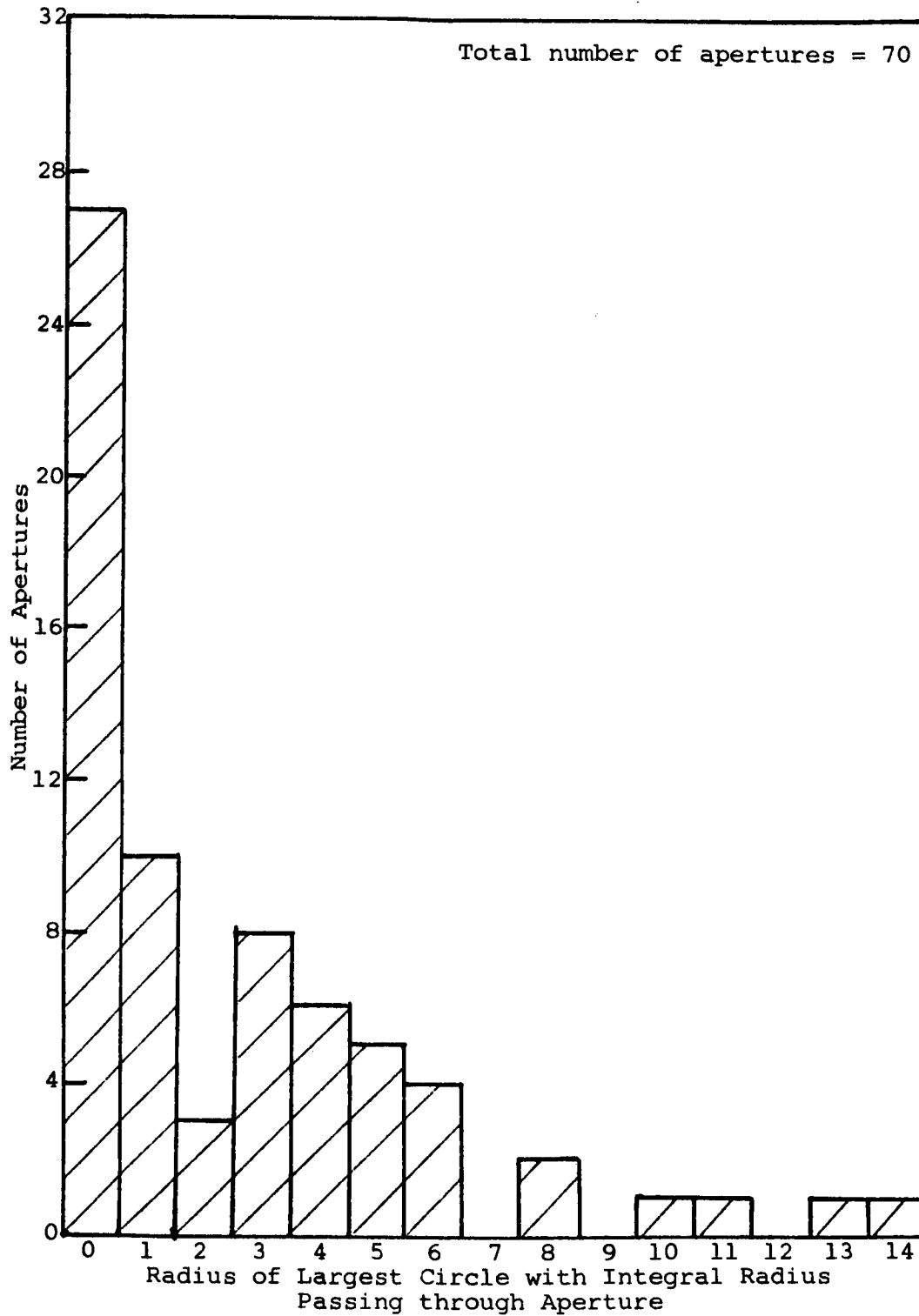(Simulated in Figure 79)
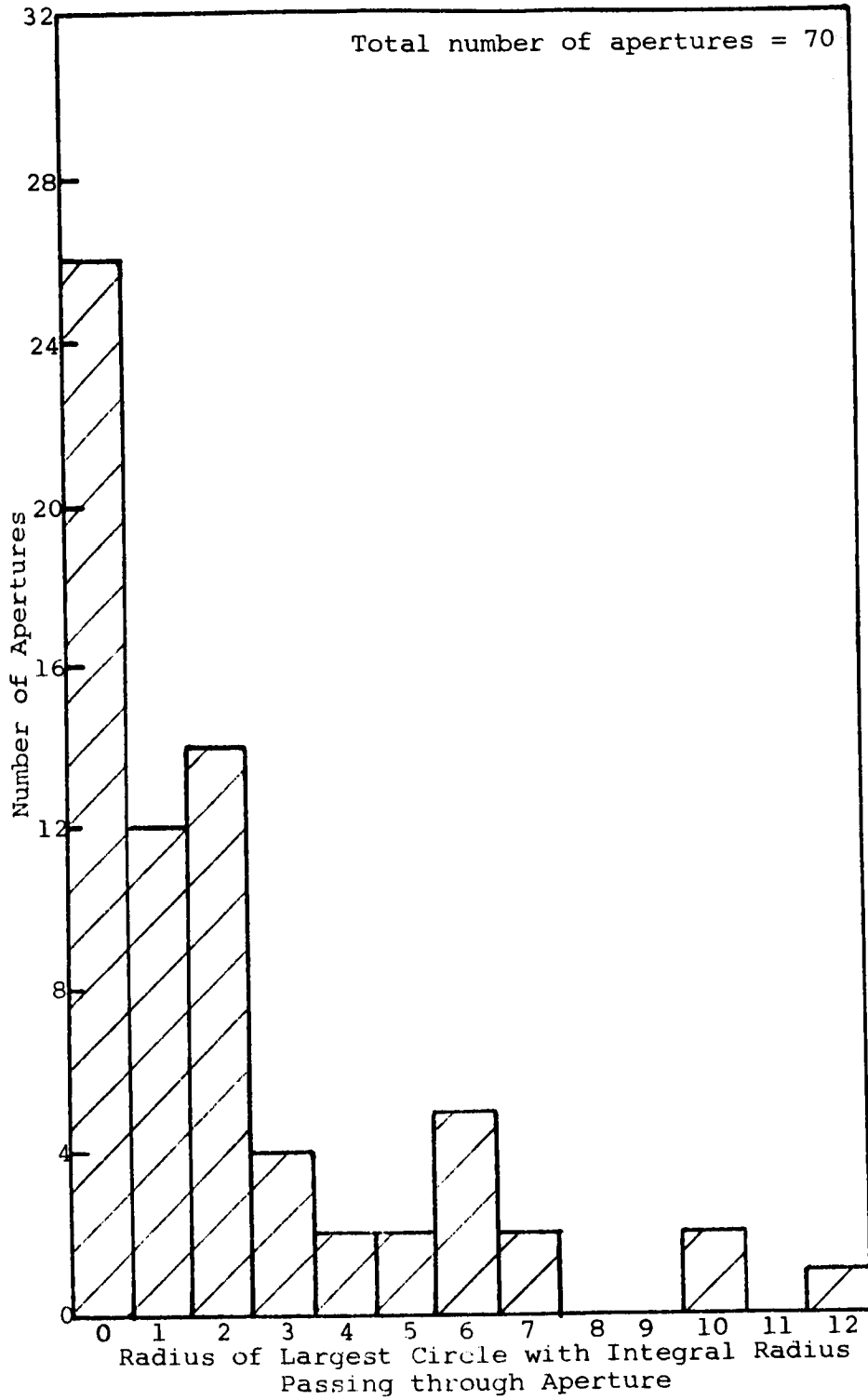
Figure 85

PORE-SIZE DISTRIBUTION OF SIMULATED FILTERS
(Simulated in Figure 80)
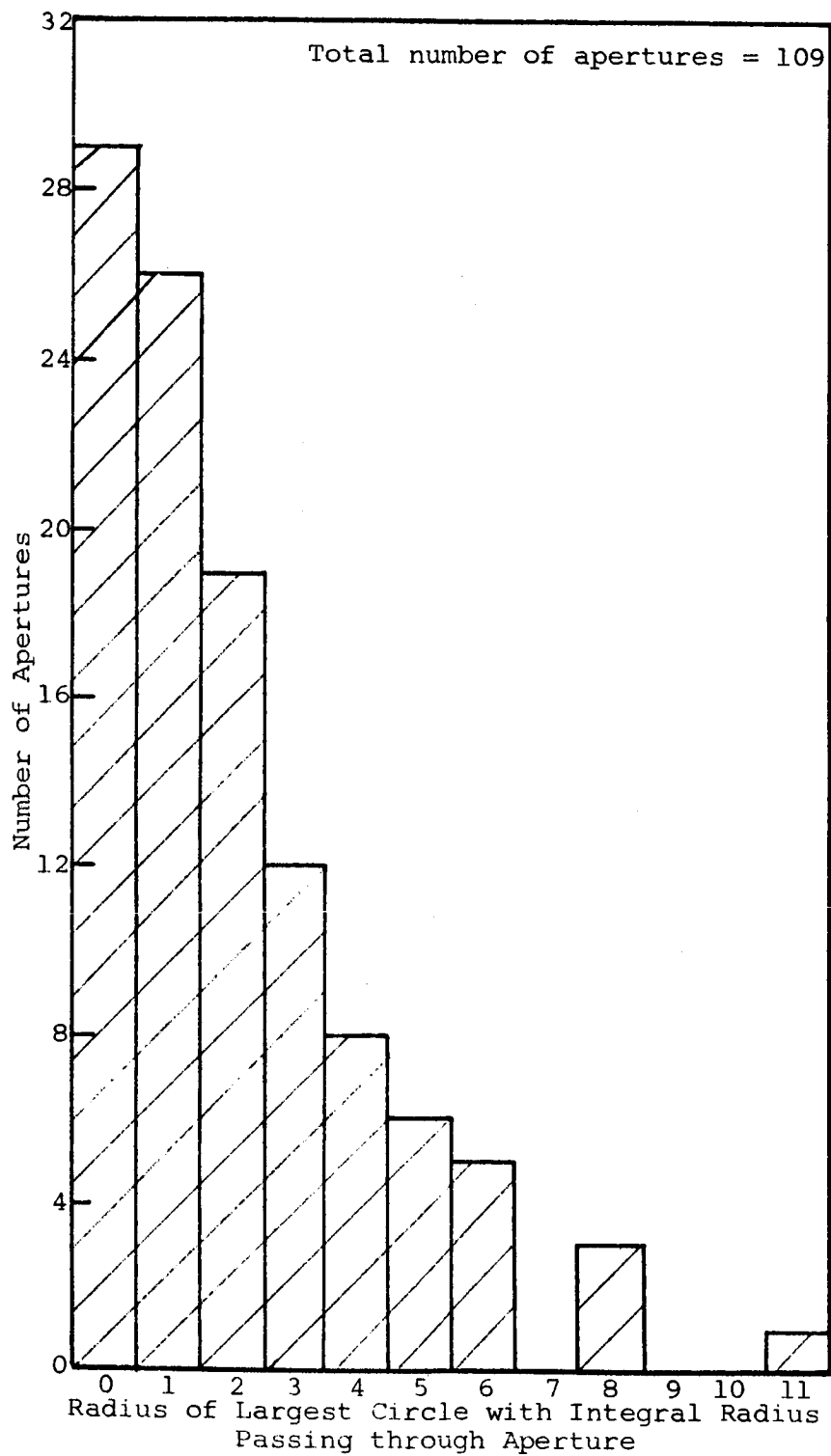
Figure 86

PORE-SIZE DISTRIBUTION OF SIMULATED FILTERS
(Simulated in Figure 81)

B. Use of Random Intercept Diagrams to Devise Monte Carlo Methods for Studying Aerosol Filtration

Prediction of the performance of any filtering device is complicated because of the many variables to be considered in constructing an appropriate theoretical system. Many workers have chosen to study the various factors that are known to influence filter performance in isolation. Thus, effects due to flow conditions and to electrostatic forces are studied separately. It is difficult to evaluate the usefulness of these studies for actual filtration systems because of the subtle way in which these variables interact. One way of studying the behavior of complex interacting systems is to construct an abstract model in which the major variables have been simulated and which can be used to predict the orders of importance of the various mechanisms by using the model as a basis for a Monte Carlo experiment. In a Monte Carlo routine a succession of events is simulated by using an abstract system, and the behavior of the model is studied as it undergoes these successive events.

Consider the system of Figure 78 to be a set of simulated fibers for a given filter system. To simulate particle capture, we now use a transparent sheet of paper on which a random set of particle profiles is simulated by using postulated characteristics of the distribution of particles in an airstream. This simulated set of particles can be placed on top of the fibers in many positions and the probability of capture simulated. In this way, the effect of the interaction of a random stream of particles encountering random fibers can be predicted. The effect of the fiber diameter can be simulated by drawing a dotted line at a distance of half a fiber width around the particle profile. This has been illustrated for several particles in Figure 87.
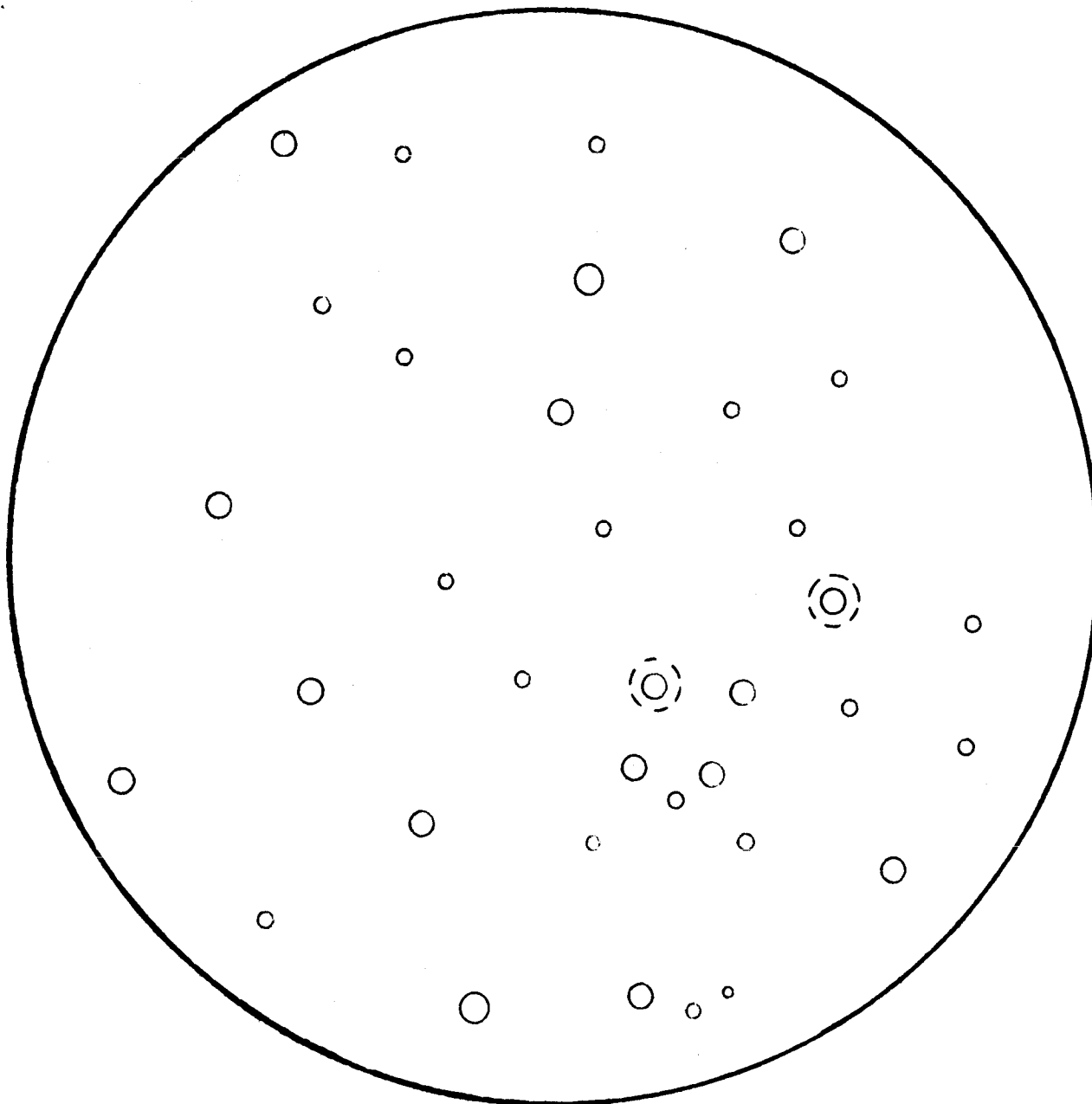
Figure 87

SIMULATED RANDOM ARRAY OF PARTICLES IN AN AIRSTREAM

Dotted line denotes encounter diameter.

It is useful to think of particles pursuing a random walk through the fibrous system. Thus, imagine that a composite filter consists of many sections like those in Figure 78 in series with each other. Imagine we wanted to predict how many filter sections would be required to capture all the particles in Figure 87. We could have a series of drawings like that in Figure 78, each of which could be placed on top of Figure 87 in many random orientations. The experiment could be repeated until all particles were captured. Each superposition of the simulated fiber system would be a step in the random walk of the particles through the filter.

The above concepts can obviously be extended to any system of fibers, either the regular pattern of a woven cloth or the orientation of the bristles on a brush filter. It is even possible to simulate the effect of rotary motion. For instance, in the systems shown in Figures 78 through 81, the fiber system could be rotated a definite distance to simulate the movement occurring for a given movement of airstream through the system, and thus the increased capture rate could be studied.

In conclusion, it can be stated that the use of Monte Carlo techniques for simulating random walk of particles through a filter system could be very useful for investigating capture efficiency of various fiber element orientations as well as effects of rotation of the filtering mechanisms.

XI. APPLICATION OF MONTE CARLO STUDIES TO METAL-FILLED CONDUCTING PAINT FILMS

In the development of microcircuitry, paints filled with metal particles have been developed so that at suitable volume concentrations the paint films can conduct electricity. The Monte Carlo plotting experiment can be used to gain an understanding of the development of conducting paths within paint films.

At the higher concentrations used in the Monte Carlo experiment it is difficult to locate the developing clusters within the general density of particles on the graph paper. The large clusters that developed at 27 to 40% by volume concentration are shown in Figures 28 through 32 (Section VIII). The extent and the configuration of the clusters are shown by the line traced through the individual particles. Smaller clusters have been omitted for clarity, and no attempt has been made to show all clusters on each of the five diagrams. In this system the properties of special interest in predicting electrical properties are the attainment of a continuous path through the unit volume and the number of paths existing at any higher concentration.

The maximum volume concentration considered is 50%, but higher concentrations can be considered by using the inverted plots of lower concentrations, i.e., by considering the particles as holes and the holes as particles. At 50% the plot is essentially comprised of two networks, from which it is possible to derive a very large number of unique continuous paths through the plot. Since the boundary conditions considered in Section VIII cannot be validly applied to a plot in which the cluster size is comparable to the plot size, further discussion is restricted to plots of up to 40% concentration.

The important parameter in conduction of electricity across a Monte Carlo plot is the extent of each cluster in the direction considered. Tables 15 and 16 list the measured spans of the clusters at various fractional concentrations in a horizontal and a vertical direction, respectively.

Table 15

HORIZONTAL SPAN LENGTH DATA FOR CLUSTERS

| Span | Number of Clusters at Specified Fractional Concentration | | | | | | | | | | | |
	.20	.21	.22	.23	.24	.25	.26	.27	.28	.29	.30	.40
1	274	270	258	143	117	104	82	78	70	61	45	55
2	113	106	101	102	108	101	94	93	86	84	70	22
3	53	53	53	52	51	55	57	56	55	49	43	11
4	24	25	29	28	28	25	21	20	23	20	21	6
5	15	17	18	21	22	23	26	18	16	17	18	7
6	13	12	13	12	9	10	11	14	12	13	14	9
7	7	8	8	10	12	12	11	11	11	10	5	3
8	3	4	6	7	6	6	8	7	9	9	13	2
9	1	2	2	2	1	1	2	4	3	4	4	1
10	1	2	2	2	3	3	3	5	6	5	9	3
11				1	1	2	2	3	3	3	3	0
12					1	0	0	1	2	2	1	1
13					1	1	1	0	0	0	1	0
14						1	1	1	1	1	1	0
15								1	0	0	0	0
16									1	1	1	0
17									0	0	0	0
18									0	0	0	0
19									0	1	1	0
20									0	0	0	2
21									1	1	1	1
37												1
56												1
57												1

Table 16

VERTICAL SPAN LENGTH DATA FOR CLUSTERS

Span	Number of Clusters at Specified Fractional Concentration											
	.20	.21	.22	.23	.24	.25	.26	.27	.28	.29	.30	.40
1	277	272	258	141	124	103	82	80	71	62	45	57
2	103	102	96	96	88	95	77	72	64	62	53	16
3	59	56	59	59	63	57	56	57	57	53	42	13
4	24	22	25	24	21	25	24	21	25	23	24	7
5	16	19	17	24	25	26	27	24	23	19	21	11
6	11	13	15	16	17	15	13	12	12	15	17	1
7	6	8	10	8	10	10	15	11	10	9	8	4
8	0	0	1	3	3	2	2	5	5	4	4	1
9	3	3	4	5	5	7	7	7	7	11	9	1
10	2	1	0	0	0	0	0	1	2	1	4	0
11		0	1	1	1	2	2	3	3	3	3	2
12		0	0	0	0	0	0	0	0	0	2	1
13		0	0	0	1	0	1	1	1	1	1	1
14		0	0	0	0	0	0	1	2	2	1	2
15		1	1	1	0	1	0	1	1	1	1	0
16					1	0	1	2	2	2	2	0
17					1	2	2	3	3	4	3	1
18								1	1	1	0	0
19								0	0	0	1	3
20								0	0	0	0	1
21								1	1	1	2	
22											0	
23											0	
24											1	
27												1
30												1
71												1
75												1

The data for fractional concentrations of 0.3 and 0.4 are presented in Tables 17 and 18 as cumulative percentage of clusters having spans larger than a stated size. These data are shown in Figures 88 and 89. The distribution of lengths can be anticipated from statistical properties of randomly distributed systems and, as shown in Figures 88 and 89, is the same in each direction.

In Table 19, the two sets of data from Tables 17 and 18 at 0.3 and 0.4 fractional concentration have been combined to form the best estimate of the equivalent linear path length distributions. These distributions, shown in Figure 13, describe projections in any direction provided that a sufficiently large number of clusters is considered.

Figure 90 can be used to study the properties of a paint film in the following manner. For two paint films of thickness n_1 and n_2 pigment diameters, the ratio of the probabilities of straight-through paths for the two films should be the ratio of the conductance of the two films. From the expected fluctuation in any given probability of occurrence, it should be possible to predict fluctuations in conductances of films of the same thickness and area and for films of different area. Figures 91 and 92 show the number of clusters that span up to six diameters at various volume concentrations.

Table 17

HORIZONTAL SPAN LENGTH DATA FOR CLUSTERS

	Cumulative Number at Specified Fractional Concentration, %	
Span	0.3	0.4
1	17.9	43.6
2	45.8	61.1
3	63.0	69.8
4	71.4	74.5
5	78.5	80.1
6	84.0	87.2
7	86.0	89.6
8	91.1	91.2
9	92.7	92.1
10	96.4	94.4
11	97.6	94.4
12	98.0	96.6
13	98.4	96.6

Table 18

VERTICAL SPAN LENGTH DATA FOR CLUSTERS

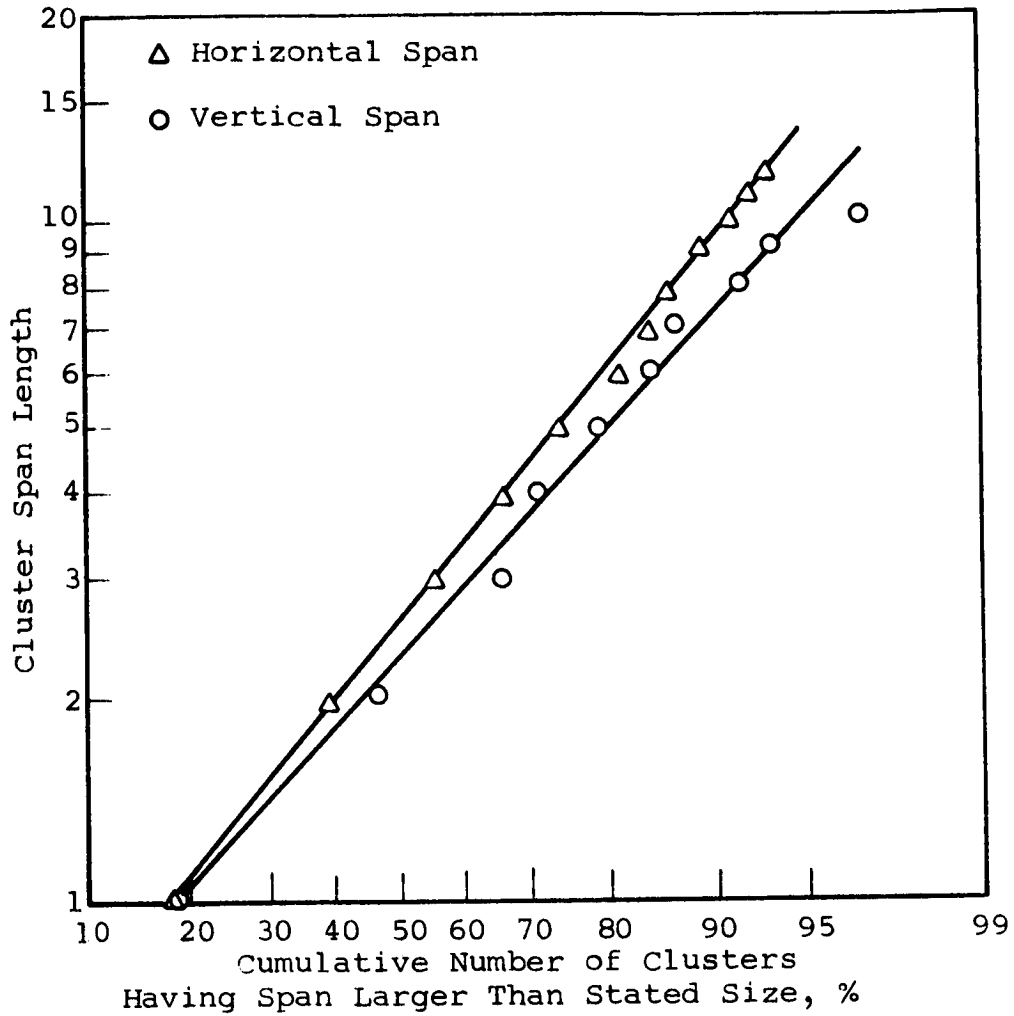|	Cumulative Number at Specified Fractional Concentration, %	
Span	0.3	0.4
1	18.4	45.2
2	40.1	58.8
3	57.4	68.1
4	67.2	73.8
5	75.8	82.5
6	82.8	83.4
7	86.2	86.5
8	87.6	87.4
9	91.4	88.0
10	93.0	88.0
11	94.2	89.9
12	95.0	90.5
13	95.5	91.2
14	95.9	93.0

Figure 88

NUMBER DISTRIBUTION OF HORIZONTAL AND VERTICAL CLUSTER
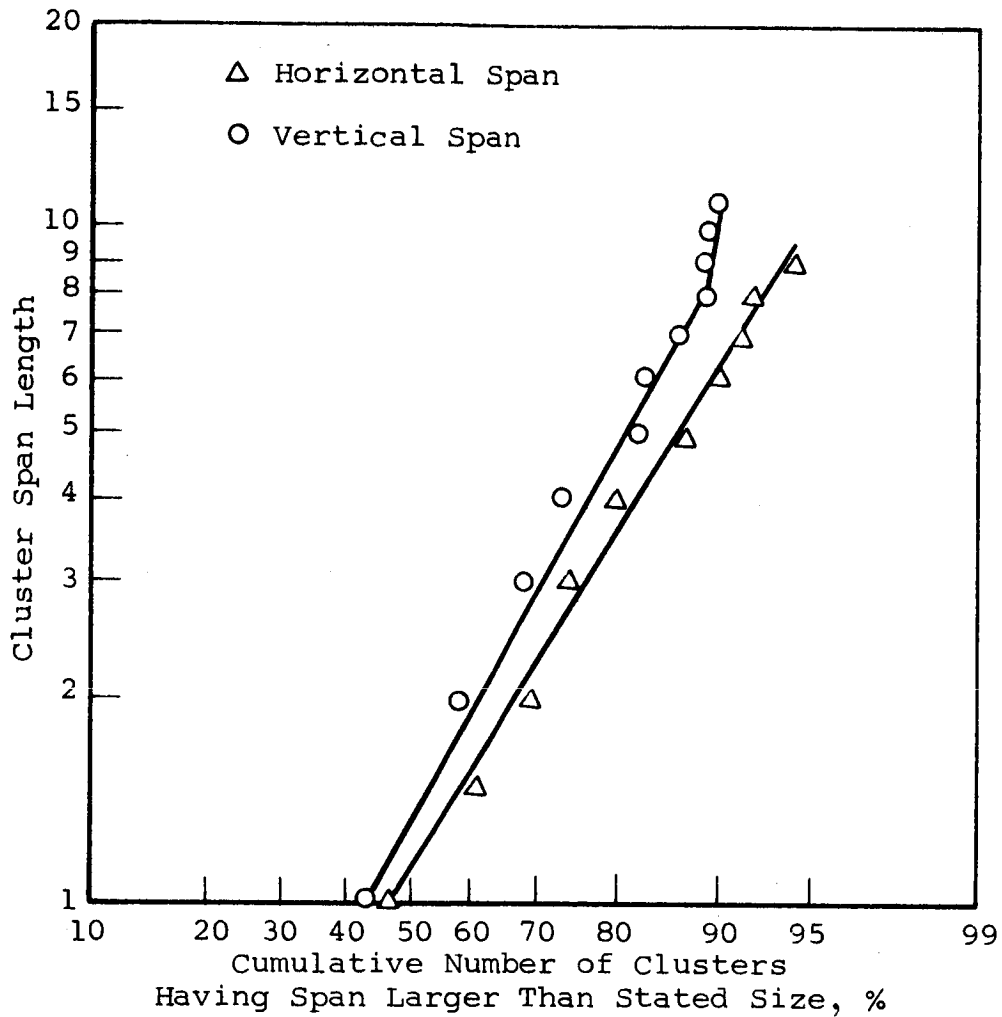SPAN LENGTHS AT 0.3 FRACTIONAL VOLUME CONCENTRATION

Figure 89

NUMBER DISTRIBUTION OF HORIZONTAL AND VERTICAL CLUSTER
SPAN LENGTHS AT 0.4 FRACTIONAL VOLUME CONCENTRATION

Table 19

COMBINED HORIZONTAL AND VERTICAL
SPAN LENGTH DATA FOR CLUSTERS

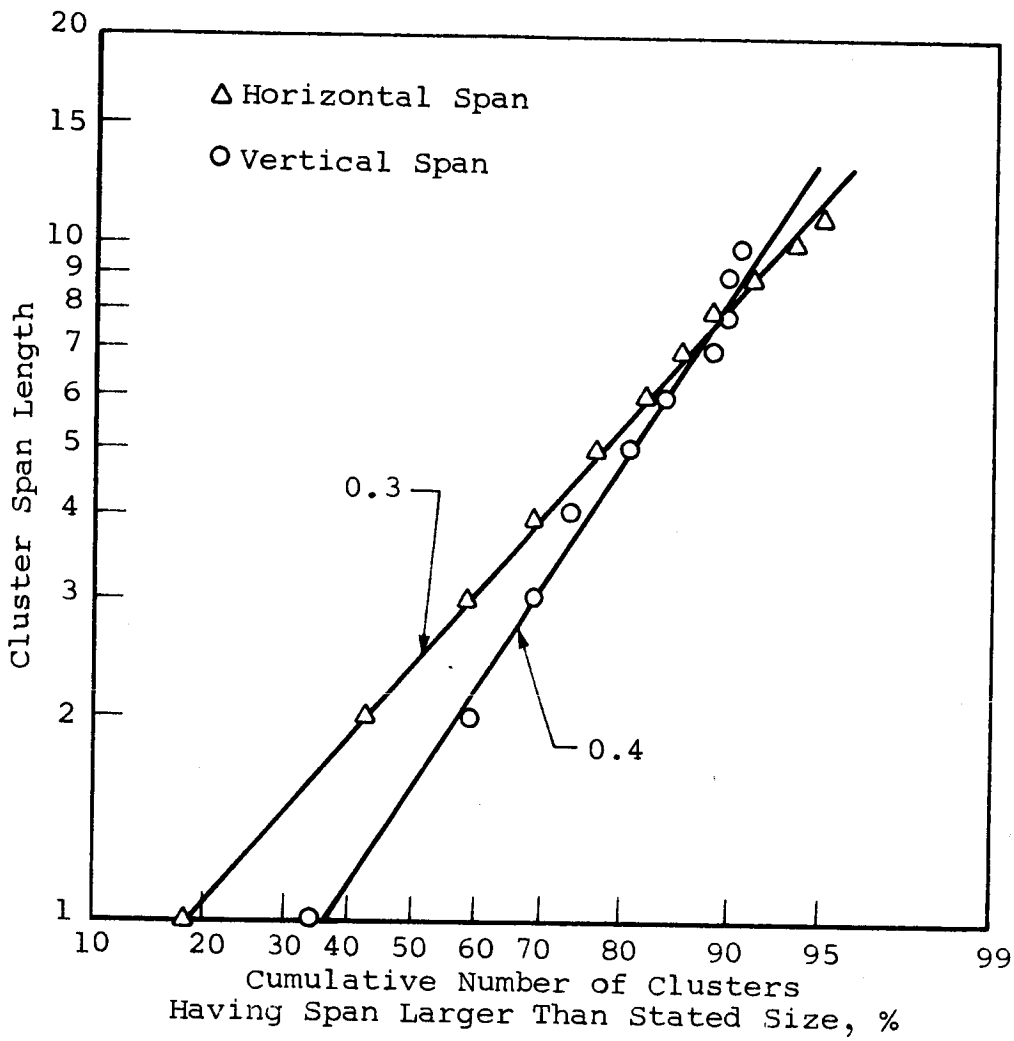| | Cumulative Number at Specified Fractional Concentration, % | |
Span	0.3	0.4
1	18.0	44.5
2	42.6	59.5
3	58.6	69.0
4	68.6	74.1
5	76.4	81.3
6	82.6	85.0
7	85.2	88.0
8	88.6	89.1
9	91.2	90.0
10	93.0	91.2
11	95.0	92.0
12	95.6	92.7
13	96.0	93.1
14	96.4	94.0
15	96.6	94.0
16	97.2	94.0
17	97.8	94.4
18	97.8	94.4
19	98.2	95.5
20	98.2	97.0
21	98.8	
22	99.8	
23	99.8	
24	100.0	

Figure 90

NUMBER DISTRIBUTION OF HORIZONTAL AND VERTICAL CLUSTER
SPAN LENGTHS AT VARIOUS VOLUME CONCENTRATIONS

Figure 91
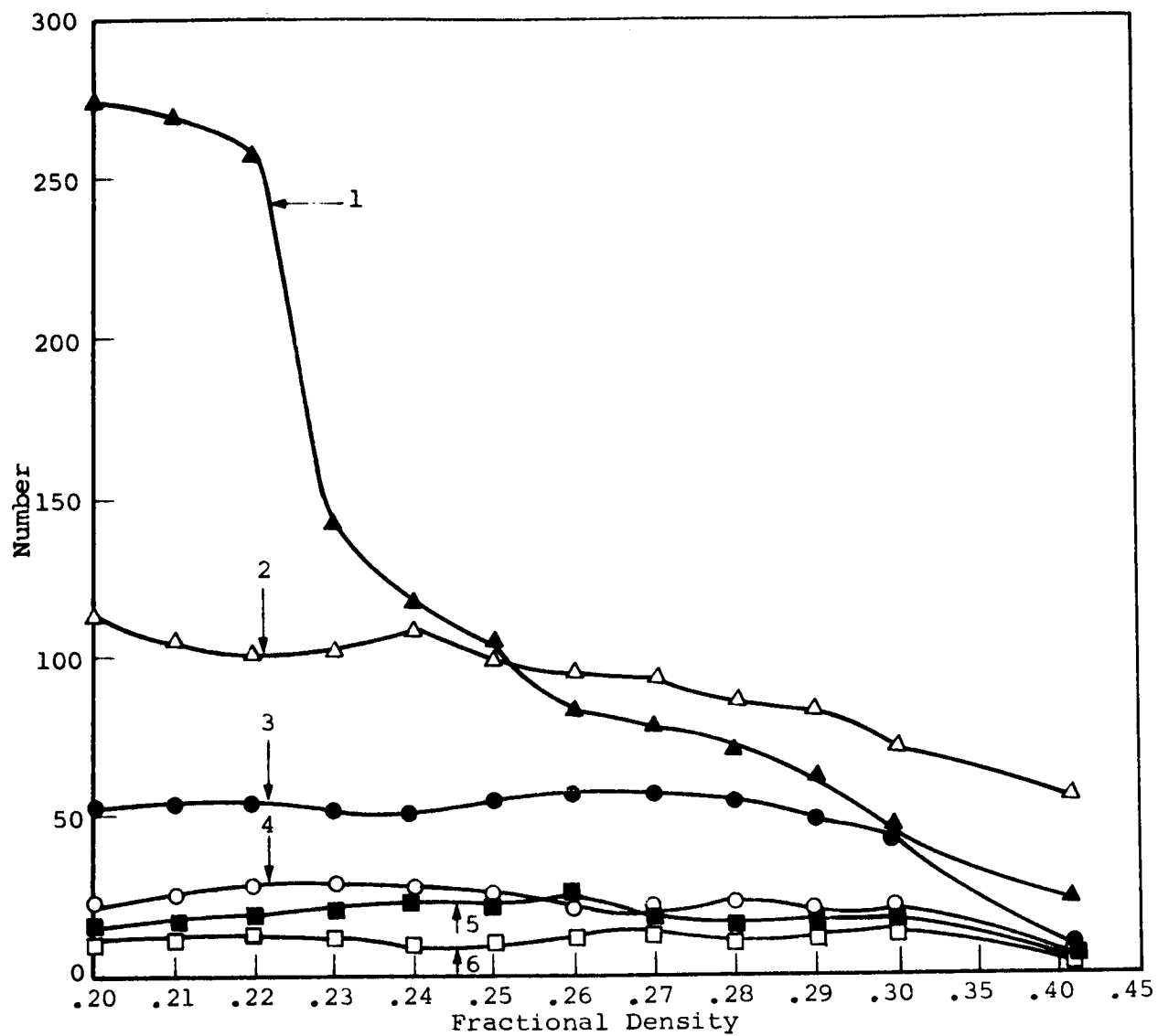
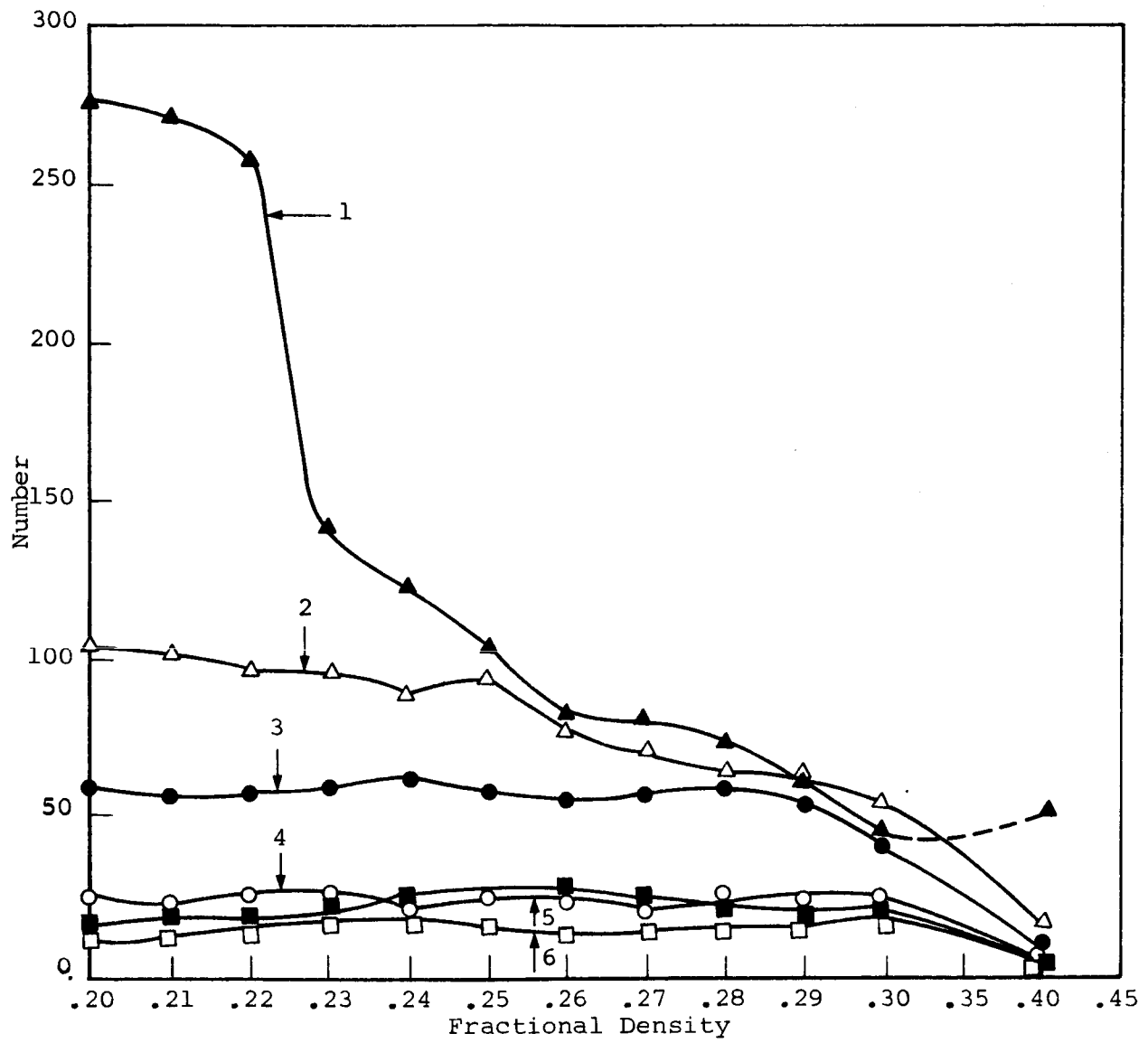DISTRIBUTION OF HORIZONTAL SPAN OF CLUSTERS EXPRESSED IN PARTICLE DIAMETERS

IITRI-U6003-19, Vol. 3

Figure 92

DISTRIBUTION OF VERTICAL SPAN OF CLUSTERS EXPRESSED IN PARTICLE DIAMETERS

REFERENCES

1. Mie, G., Ann. Physik, Vol. 25, 1908.

2. Andrews, C. L., "Optics of the Electromagnetic Spectrum," Prentice Hall, Englewood Cliffs, N.J., 1960.

3. Ditchburn, R. W., "Light," Interscience Publishers, Inc., New York, p. 28, 1961.

4. Heywood, H., "The Scope of Particle Size Analysis and Standardization," Symposium on Particle Size Analysis, published by London Institution of Chemical Engineers, p. 17, Feb. 1947.

5. Davies, C. N., "Survey of Scattering and Adsoprtion of Light by Particles," The Physics of Particle Size Analysis, Brit. J. Appl. Phys., Suppl. 3, Apr. 1954.

6. DeVore, J. R. and Pfund, A. H., J. Opt. Soc. Am., Vol. 37, No. 10, pp. 826-832, Oct. 1947.

7. Zerlaut, G. A., Kaye, B. H., and Jackson, M. R., "Investigation of Light Scattering in Highly Reflecting Pigmented Coatings," IIT Research Institute Report No. IITRI-U6003-16 (Quarterly Report), Contract NASr-65(07), pp. 19-27, Nov. 1965.

8. Zerlaut, G. A., Kaye, B. H., and Jackson, M. R., "Investigation of Light Scattering in Highly Reflecting Pigmented Coatings," IIT Research Institute Report No. IITRI-U6003-17, Contract NASr-65(07), pp. 14-20, Feb. 1966.

9. Millikan, R. A., essay in "Time and Its Mysteries," Collier Books, New York, p. 28, 1961.

10. Newman, A. C. C., "Particle Size in Relation to the Use of Pigments in Paints," Trans. Inst. Chem. Eng., Suppl., Vol. 25, p. 88, 1947.

11. Barnett, C. E., Ind. Eng. Chem., Vol. 41, p. 272, 1949.

12. Andreasen, A. H. M., Krebs, K., Dalsgaard-Pederson, N. Aa., Damradt-Petersen, D., and Kjaer, B., Trans. Inst. Chem. Eng., Suppl., Vol. 25, p. 4, 1947.

13. Strong, J., "Concepts of Classical Optics," Freeman and Co., London, p. 279, 1958.

14. Kendall, M. W. and Moran, P. A., "Geometrical Probability," Hafner Publishing Co., New York, 1962.

15. See, for example, the work of Cauchy, described in ref. 14.

16. See, for example, the work of Bates and Pillow, described in ref. 14.

17. Mason, G. and Clark, W., "Distribution of Near Neighbors in a Random Packing of Spheres," Nature, Vol. 207, No. 4996, p. 512, 1965.

18. Bonenali, R. F. and Brosilow, C. B., "Void Fraction Distribution in Beds of Spheres," AIChEJ, p. 359, July 1962.

19. Wise, M. E., Philips Res. Rept., 9, p. 25, 1954.

20. Herdan, G., "Small Particle Statistics," pp. 180-200, Butterworths, 1960.

21. McCracken, D. D., "The Monte Carlo Method," Sci. Am., p. 90, May 1955.

22. Van de Hulst, H. C., "Light Scattering by Small Particles", John Wiley and Sons, New York, 1957.

23. Steig, F. B., Jr., Off. Dig. Federation Paint Varnish Prod. Clubs, Vol. 29, No. 388, p. 439, May 1957.

24. Armstrong, W. G. and Madson, W. H., Ind. Eng. Chem., Vol. 39, p. 944, 1947.

25. Zerlaut, G. A., "Utilization of Pigmented Coatings for the Control of Equilibrium Skin Temperatures of Space Vehicles," Proc. Aerospace Finishing Symposium, Ft. Worth, Tex., Dec. 8, 9, 1959.

26. Rumpf, H., "Agglomeration," ed. Knepper, Interscience Publishers, p. 379, 1962.

DISTRIBUTION LIST

This report is being distributed as follows:

Copy No.	Recipient
1-50 plus 1 reproducible	Miss Winnie M. Morgan Technical Reports Officer National Aeronautics & Space Administration Office of Grants and Research Contracts Washington, D.C.
51	Mr. J. J. Gangler National Aeronautics & Space Administration Office of Advanced Research and Technology Washington 25, D.C.
52-54 plus 1 reproducible	Mr. D. W. Gates (M-RP-T) National Aeronautics & Space Administration George C. Marshall Space Flight Center Huntsville, Alabama
55	Mr. Gerhard B. Heller Deputy Director Research Projects Laboratory National Aeronautics & Space Administration George C. Marshall Space Flight Center Huntsville, Alabama
56	Mr. Conrad Mook Code RV National Aeronautics & Space Administration Washington, D.C.
57	Mr. William F. Carroll Jet Propulsion Laboratory California Institute of Technology 4800 Oak Grove Drive Pasadena, California
58	Mr. James R. Crosby Jet Propulsion Laboratory California Institute of Technology 4800 Oak Grove Drive Pasadena, California
59	Dr. Sam Katzoff, Assistant Chief Applied Materials & Physics Division National Aeronautics & Space Administration Langley Research Center Langley Station Hampton, Virginia

Copy No.	Recipient
60	Mr. Joseph C. Richmond National Bureau of Standards Washington, D.C.
61	Mr. James Diedrich, Mail Stop 7-1 National Aeronautics & Space Administration Lewis Research Center Cleveland, Ohio
62	Mr. Milton Schach Head, Thermal Power Section/Thermal Systems National Aeronautics & Space Administration Goddard Space Flight Center Greenbelt, Maryland
63	Mr. Carr B. Neel Head, Spaceflight Heating and Thermal Control Section National Aeronautics & Space Administration Ames Research Center Moffett Field, California
64	Dr. George Pezdirtz Chief, Spacecraft Materials Section National Aeronautics & Space Administration Langley Research Center Langley Station Hampton, Virginia
65	IIT Research Institute Division U Files
66	IIT Research Institute Editors, J. J. Brophy, J. I. Bregman, Main Files
67	IIT Research Institute S. Katz, Division C
68	IIT Research Institute B. Kaye, Division C
69	IIT Research Institute M. Jackson, Division C
70	IIT Research Institute V. Raziunas, Division U
71-85	IIT Research Institute G. A. Zerlaut, Division U